

**Development of a Self-Lubricating Plasma Sprayed Coating
for Rolling/Sliding Contact Wear**

David V. Niebuhr
B.S., California Polytechnic State University
San Luis Obispo

A dissertation submitted to the faculty of the
Oregon Graduate Institute of Science and Technology
in partial fulfillment of the
requirements for the degree
Doctor of Philosophy
in
Materials Science and Engineering

July 1997

The dissertation "Development of a Self-Lubricating Plasma Sprayed Coating for Rolling/Sliding Contact Wear" by David Niebuhr has been examined and approved by the following Examination Committee:

Paul Clayton, Thesis Advisor
Professor

Milton Scholl
Assistant Professor

David Atteridge
Professor

Roger Steele
Association of American Railroads, Ret.

Dedication

The completion of this dissertation is dedicated first and foremost to my dear wife Tina. Her encouragement and support allowed the completion of this 'book' with my sanity intact. Her love, dedication, and patience made the seemingly impossible a reality.

Also to my parents for their emotional support for the past 27 years of my life. They taught me the value of hard work and the power of a positive attitude.

Acknowledgements

The completion of this thesis was precipitated by the help of many people. Thanks must first be given to the Association of American Railroads for their ongoing financial support and willingness to see this project to completion.

Paul Clayton gets the gold star next to his name for his support and encouragement for the past several years. His guidance and wit kept this project on track and allowed for its timely completion.

Milt Scholl's technical expertise and accessibility were invaluable.

Dave Atteridge provided 99.9% of the philosophy found in a Ph.D.

Roger Steele provided a railroad expert's testimony to what all this really means.

Other individuals include Doug Davis for his help in machining and fixture design, Jack McCarthy for his SEM and TEM expertise, Andy² for their can-do attitude, CNC skills and "Yes I can make another dozen Amsler rollers." I also thank my fellow students and faculty for their help.

Table of Contents

Dedication.....	iii
Acknowledgements.....	iv
List of Tables.....	xi
List of Figures.....	xv
Abstract.....	xxv
1 Introduction.....	1
1.0 Objective.....	1
1.1 Preface.....	1
1.2 Literature Review.....	3
1.2.1 Friction.....	3
1.2.2 Wear.....	9
1.2.3 Fluid Lubrication.....	14
1.2.4 Solid Lubrication.....	15
Inorganic Compounds.....	16
Soft Metals.....	18
Polymers.....	21
Polymer Characterization.....	25
1.2.5 Current Wheel / Rail Lubrication Systems.....	26
1.2.6 Surface Engineering.....	28
Coatings.....	29
Thermal Spraying.....	30
Plasma Spraying.....	31
Plasma Fundamentals.....	31
Spray Materials.....	32
Plasma Spray Parameters.....	32
1.2.7 Solid Lubrication / Plasma Spray Application..	33
1.2.8 Background of Current Research.....	38

2	Experimental	64
2.1	Introduction	64
2.2	Materials	64
2.2.1	Spray Materials	64
	Graphite	64
	Nickel-Coated Graphite	65
	Gray Cast Iron	65
	Copper	66
	Polymers	66
2.2.2	Testing Material	66
2.3	Plasma Spray Equipment	67
2.4	Plasma Spraying Technique	69
2.4.1	General Procedure	69
	Surface Preparation	69
	Plasma Spray Procedure	69
2.4.2	Solid Lubricants	70
	Graphite	71
	Nickel-Coated Graphite	71
	Cast Iron Powder	72
	Copper Wire	73
	Copper Powder	73
	Polymers	74
2.4.3	Rail Coupons	75
2.4.4	Rail Steel	75
2.4.5	Parameter Optimization	76
2.5	Performance Evaluation	77
2.5.1	Amsler Machine	77
2.5.2	Amsler Machine Operation	78
2.6	Microstructural Evaluation	79
2.6.1	Metallography	79
2.6.2	Optical Metallography	80
2.6.3	Scanning Electron Microscopy	80
2.6.4	Image Analysis	81
2.6.5	Fourier Transform Infrared Spectroscopy	81

2.6.6	Focused Ion Beam	82
3	Results	98
3.1	Introduction	98
3.2	Graphite	99
3.2.1	Introduction	99
3.2.2	Graphite Powder	99
	Flat Coupons	99
	Amsler Rollers	100
	Early Work	101
	Aerodynamic Shield	101
	Dual Wire	102
	Synopsis	103
3.2.3	Nickel-Coated Graphite	117
	Initial Studies	117
	1 mm Coatings	118
	0.5 mm Coatings	119
	0.25 mm Coatings	120
	Low Volume Nickel-Graphite	121
	Repeatability Tests	121
	Synopsis	122
3.2.4	Cast Iron Powder	155
3.3	Copper	157
3.3.1	Copper Wire Feedstock	157
	Amsler Rollers	159
3.3.2	Copper Powder	161
	Amsler Tests	162
	Low Feed Wheel	163
3.3.3	Synopsis	163
3.4	Polymers	197
3.4.1	Initial Work	197
3.4.2	Nylon	199
	Neat Nylon / 1080 Steel Coatings	199

	Neat Nylon / 308 L-Si SS Coatings	200
	Solid Lubricants + Nylon / 1080 Steel	201
3.4.3	PTFE.....	201
3.4.4	UHMW.....	202
3.4.5	Surface Modification	204
3.4.6	Lubricated Tests.....	205
3.4.7	Polymer Reapplication.....	206
3.4.8	Interrupted Tests	207
3.4.9	Polymer Film Analysis.....	208
	Focused Ion Beam	210
3.4.10	Synopsis	210
3.5	Steel Coating Deposition On Full Scale Rail	248
3.5.1	Parameter Optimization.....	248
3.5.2	Large Scale Testing.....	249
4	Discussion	263
4.1	Introduction.....	263
4.2	Graphite.....	263
4.2.1	Introduction.....	263
4.2.2	Graphite Powder	264
	Flat Coupons	264
	Amsler Rollers	266
	Aerodynamic Shield.....	268
	Dual 1080 Wire.....	271
	Synopsis	273
4.2.3	Nickel-Coated Graphite	280
	Introduction.....	280
	Microstructural Characterization.....	281
	Wear Behavior of Nickel-Graphite.....	282
	Wear Mechanism.....	284
	Initial Work.....	287
	1 mm Coatings	288
	1 mm Coatings Part II.....	289
	0.5 mm Coatings	290

	0.25 mm Coatings.....	291
	Low Volume Coatings	292
	Repeatability.....	293
	Synopsis	293
4.2.4	Cast Iron.....	301
4.3	Copper.....	303
4.3.1	Copper Wire Feedstock.....	303
	Parameter Effects	303
	Flat Coupons	306
	Amsler Rollers	307
4.3.2	Copper Powder.....	310
	Amsler Rollers	310
	Normal Feed	311
	Low Feed Wheel.....	312
	Twin Wire Spraying.....	313
4.3.3	Synopsis	314
4.4	Polymers	315
4.4.1	Initial Work.....	315
4.4.2	Nylon	317
	Neat Nylon / 1080 Steel Coatings	317
	Neat Nylon / 308 L-Si SS Coatings	318
	Solid Lubricants + Nylon / 1080 Steel.....	319
4.4.3	PTFE.....	320
4.4.4	UHMW.....	321
4.4.5	Surface Modification	322
4.4.6	Lubricated Tests.....	324
4.4.7	Polymer Reapplication.....	324
4.4.8	Interrupted Tests.....	325
4.4.9	Polymer Film Analysis.....	329
4.4.10	Synopsis	331
4.5	Steel Coating Deposition on Rail.....	336
4.5.1	Parameter Optimization.....	336
4.5.2	Large Scale Testing.....	338

5	Conclusions.....	341
6	Synopsis.....	343
6.1	Future Work.....	343
6.2	Final Comments.....	344
	References.....	346
	Vita.....	370

List of Tables

Table 2.1.	Composition of standard carbon rail steel.	83
Table 2.2.	Composition of Class C wheel steel.	84
Table 3.1.	Spray parameters and results. Samples M1-M12.	104
Table 3.2a.	Spray parameters. Samples G1 through G8.	105
Table 3.2b.	Amsler test results. Samples G1 through G8.	106
Table 3.3a.	Spray parameters. Samples G9 through G19.	107
Table 3.3b.	Amsler test results. Samples G9 through G19.	108
Table 3.4a.	Spray parameters. Samples G20 through G23.	109
Table 3.4b.	Amsler test results. Samples G20 through G23.	110
Table 3.5a.	Spray parameters. Samples G25 through G27.	123
Table 3.5b.	Amsler test results. Samples G25 through G27.	124
Table 3.6a.	Spray parameters. Samples G28 through G33.	125
Table 3.6b.	Amsler test results. Samples G28 through G33.	126
Table 3.7a.	Spray parameters. Samples G34 through G37.	127
Table 3.7b.	Amsler test results. Samples G34 through G37.	128
Table 3.8a.	Spray parameters. Samples G38 through G41.	129
Table 3.8b.	Amsler test results. Samples G38 through G41.	130

Table 3.9a.	Spray parameters. Samples G50 through G54.	131
Table 3.9b.	Amsler test results. Samples G50 through G54.	132
Table 3.10a.	Spray parameters. Samples G42 through G45.	133
Table 3.10b.	Amsler test results. Samples G42 through G45.	134
Table 3.11a.	Spray parameters. Samples G46 through G48.	135
Table 3.11b.	Amsler test results. Samples G46 through G48.	136
Table 3.12.	Spray parameters and Amsler results. G55-G58.	156
Table 3.13.	Spray parameters and results C1 through C7.	165
Table 3.14.	Spray parameters and results C8 through C17.	166
Table 3.15.	Spray parameters and results C18 through C23.	167
Table 3.16a.	Spray parameters. Samples AC1 - AC10.	168
Table 3.16b.	Amsler test results. Samples AC1 - AC10.	169
Table 3.17a.	Spray parameters. Samples AC11 - AC14.	170
Table 3.17b.	Amsler test results. Samples AC11 - AC14.	171
Table 3.18a.	Spray parameters. Samples AC16- AC19.	172
Table 3.18b.	Amsler test results. Samples AC16 - AC19.	173
Table 3.19a.	Spray parameters. Samples AC30 - AC35.	174
Table 3.19b.	Amsler test results. Samples AC30 - AC35.	175
Table 3.20.	Spray parameters and Amsler test results for Kynar / steel coatings.	211
Table 3.21.	Friction coefficient as a function of load for several polymer / steel coatings.	212

Table 3.22.	Spray parameters and Amsler test results for nylon / steel coatings N1 - N15.	213
Table 3.23.	Spray parameters and Amsler test results for nylon / steel coatings N16 - N21.	214
Table 3.24.	Spray parameters and Amsler test results for nylon / steel coatings N22 - N29.	215
Table 3.25.	Spray parameters and Amsler test results for nylon / stainless steel coatings SS1 - SS7.	216
Table 3.26.	Spray parameters and Amsler test results for nylon + solid lube / steel coatings NS1 - NS8.	217
Table 3.27.	Spray parameters and Amsler test results for PTFE / steel coatings PT1 - PT8.	218
Table 3.28.	Spray parameters and Amsler test results for UHMW / steel coatings PE1 - PE6.	219
Table 3.29.	Spray parameters and Amsler test results for UHMW / steel coatings PE7 - PE10.	220
Table 3.30a.	Surface modification parameters for Amsler rollers coated with nylon. SM1 - SM10.	221
Table 3.30b.	Surface modification test results for Amsler rollers coated with nylon. SM1 - SM10.	222
Table 3.31.	Amsler test results for nylon coatings run under lubricated conditions.	223
Table 3.32.	Amsler test results for reapplied nylon coatings. RS1 - RS9.	224
Table 3.33.	Degradation stages of interrupted tests.	225
Table 3.34.	Steel coating optimization on rail, parameters and results.	250

Table 3.35a.	Spray parameters for steel and nylon / steel coatings applied to rail sections.....	251
Table 3.35b.	Performance results of large scale tests on coated rail steels.....	252

List of Figures

Figure 1.1.	The six stages of friction as defined by Suh.	41
Figure 1.2.	Plot of wear rate versus sliding speed for 60-40 brass rubbed against high-speed tool steel.	42
Figure 1.3.	The process of wear particle formation by the shear deformation.	43
Figure 1.4.	Schematic of a bond bridge produced when two solid surfaces are in contact.	44
Figure 1.5	The two types of geometry for lubricated surfaces: conformal and counterformal.	45
Figure 1.6.	Test bearings employing graphite reinforced polyimide (GFRPI) solid lubricant.	46
Figure 1.7.	Layer lattice structure of graphite.	47
Figure 1.8.	Structure of molybdenum disulphide. a) Schematic of MoS ₂ structure. b) SEM image of MoS ₂ lamellar structure.	48
Figure 1.9.	Mechanism of lubrication by lamellar solids.	49
Figure 1.10.	Graph of friction coefficient vs. ambient pressure for graphite and MoS ₂	50
Figure 1.11.	Mechanism of friction reduction by soft films on hard substrates.	51
Figure 1.12.	Effect of an indium surface film on the frictional characteristics of steel.	52

Figure 1.13.	The effect of load on the coefficient of friction of copper slid against copper.	53
Figure 1.14.	Wear of PTFE as a function of temperature.	54
Figure 1.15.	Molecular and crystalline structure of PTFE.	55
Figure 1.16.	Wear and film transfer mechanism of PTFE.	56
Figure 1.17.	Effect of counterface roughness on the wear of UHMW.	57
Figure 1.18.	Polymer wear process on excessively smooth and optimum roughness surfaces.	58
Figure 1.19.	Molecular structure of Nylon 11.	59
Figure 1.20.	'Lumpy' transfer mechanism of most polymers.	60
Figure 1.21.	Schematic drawing of attenuated total reflectance (ATR) crystal.	61
Figure 1.22.	Schematic drawing of a plasma-sprayed coating.	62
Figure 1.23.	Schematic drawing of the particle flux formed when wire and powder are injected into the plasma plume.	63
Figure 2.1.	SEM photographs of nickel-coated graphite particles showing morphology.	85
Figure 2.2.	Schematic drawing of Amsler rollers.	86
Figure 2.3.	Schematic drawing of plasma gun.	87
Figure 2.4.	Plasma gun set-up to spray Amsler rollers.	88
Figure 2.5.	Plasma gun showing powder and wire feed.	89
Figure 2.6.	Amsler rollers attached to rotatable shaft.	90

Figure 2.7.	Flat steel coupons attached to graphite bar.	91
Figure 2.8.	Portable grit blasting booth as attached to large rail section. a) Schematic drawing. b) Photo.	92
Figure 2.9.	Schematic drawing of aerodynamic shield #1.	93
Figure 2.10.	Schematic drawing of aerodynamic shield #2.	94
Figure 2.11.	Photo of track lab coupon and fixturing.	95
Figure 2.12.	Plasma gun and fixturing used to spray large rail sections. a) Close-up of gun. b) Overview.	96
Figure 2.13.	Amsler wear testing machine. a) Overview. b) Close-up of two mated rollers.	97
Figure 3.1.	Photomicrographs of graphite / steel coating M9 showing retained graphite particles.	111
Figure 3.2.	Photomicrographs of graphite / steel coating M8 showing retained graphite particles.	112
Figure 3.3.	Photomicrographs of graphite / steel coating M10 showing retained graphite particles.	113
Figure 3.4.	Photomicrographs of graphite / steel coatings showing retained graphite as injection distance increases. a) Sample M7. b) Sample M5.	114
Figure 3.5.	Photomicrographs of graphite / steel coating M2 showing lack of retained graphite.	115
Figure 3.6.	Photomicrographs of graphite / steel coatings. a) Sample G12. b) Sample G16.	116
Figure 3.7.	Photomicrographs of nickel-graphite / steel coating G25. a) 50x. b) 200x.	137

Figure 3.8.	Photomicrographs of nickel-graphite / steel coatings. (1 mm). a) G25. b) G27.	138
Figure 3.9.	Photomicrographs of nickel-graphite / steel coatings. (1 mm). a) G28. b) G33.	139
Figure 3.10.	Photomicrographs of nickel-graphite / steel coatings. (1 mm). a) G28. b) G29.	140
Figure 3.10.	Continuation. c) G30. d) G31.	141
Figure 3.10.	Continuation. e) G32. f) G33.	142
Figure 3.11.	Photomicrographs showing crack propagation through coating matrix. (G32).	143
Figure 3.12.	Photomicrographs of nickel-graphite / steel coatings. (1 mm). a) G34. b) G37.	144
Figure 3.13.	Photomicrographs of nickel-graphite / steel coatings. (1 mm). a) G34. b) G35.	145
Figure 3.13.	Continuation. c) G36. d) G37.	146
Figure 3.14.	Photomicrographs of nickel-graphite / steel coatings. (0.5 mm). a) G38. b) G41.	147
Figure 3.15.	Photomicrographs of nickel-graphite / steel coatings. (0.5 mm). a) G38. b) G39.	148
Figure 3.15.	Continuation. c) G40. d) G41.	149
Figure 3.16.	Photomicrographs of nickel-graphite / steel coatings. (0.25 mm). a) G50. b) G51.	150
Figure 3.16.	Continuation. c) G52. d) G53.	151
Figure 3.17.	Photomicrographs of nickel-graphite / steel coatings. (Low volume). a) G45. b) G44.	152

Figure 3.18.	Photomicrographs of nickel-graphite / steel coatings. (Low volume). a) G45. b) G42.	153
Figure 3.18.	Continuation. a) G43. b) G44.	154
Figure 3.19.	Photomicrographs of copper wire / steel coating C5. a) Depleted. b) Saturated.	176
Figure 3.20.	Photomicrographs of copper wire / steel coatings. a) C16 (no etch). b) C17 (etched).	177
Figure 3.21.	Photomicrographs of copper wire / steel coatings. (l= 25 mm). a) C6. b) C4.	178
Figure 3.21.	Continuation. c) C3. d) C1.	179
Figure 3.22.	Photomicrographs of copper wire / steel coatings (l= 45 mm). a) C15. b) C13.	180
Figure 3.22.	Continuation. c) C17. d) C10.	181
Figure 3.23.	Photomicrographs of copper wire / steel coatings. (l= 85 mm). a) C18. b) C20.	182
Figure 3.23.	Continuation. c) C21. d) C23.	183
Figure 3.24.	Photomicrographs of copper wire / steel coatings. (l= 25 mm). a) AC1. b) AC2.	184
Figure 3.24.	Continuation. c) AC3. d) AC4.	185
Figure 3.25.	Photographs of transferred copper material during wear testing. a) $P_o = 700 \text{ N/mm}^2$ b) $P_o = 1220 \text{ N/mm}^2$	186
Figure 3.26.	Photomicrographs of copper wire / steel coatings. (lA= 90°). a) AC11. b) AC12.	187
Figure 3.26.	Continuation. c) AC13. d) AC14.	188

Figure 3.27.	Photomicrographs of copper powder / steel coatings. a) AC16. b) AC17.	189
Figure 3.27.	Continuation. c) AC18. d) C21.	190
Figure 3.27.	Continuation. e) AC20. f) AC19.	191
Figure 3.28.	Photographs of debonded copper / steel coatings.	192
Figure 3.29.	Photograph of wear track showing debonded area (copper / steel coating).	193
Figure 3.30.	Photomicrographs of copper powder / steel coatings. (Low volume). a) AC30. b) AC31.	194
Figure 3.30.	Continuation. c) AC32. d) AC33.	195
Figure 3.30.	Continuation. e) AC34. f) AC35.	196
Figure 3.31.	SEM photograph of unmelted PTFE particles.	226
Figure 3.32.	SEM photograph of melted UHMW coating.	227
Figure 3.33.	SEM photograph of unmelted, non wetting UHMW coating.	228
Figure 3.34.	Photograph of nylon / steel coating wear process. Stage I.	229
Figure 3.35.	Photograph of nylon / steel coating wear process. Stage II.	230
Figure 3.36.	Photograph of nylon / steel coating wear process. Stage III.	231
Figure 3.37.	Photograph of nylon / steel coating wear process. Stage IV.	232
Figure 3.38.	Photograph of nylon / steel coating wear process. Stage V.	233

Figure 3.39.	Photograph of nylon / steel coating wear process. Stage VI.	234
Figure 3.40.	Photograph of nylon / steel coating wear process. Stage VII.	235
Figure 3.41.	SEM micrograph of nylon / steel coating wear process. Stage I.	236
Figure 3.42.	SEM micrograph of nylon / steel coating wear process. Stage II.	237
Figure 3.43.	SEM micrograph of nylon / steel coating wear process. Stage III.	238
Figure 3.44a.	SEM micrograph of nylon / steel coating wear process. Stage IV. (100x)	239
Figure 3.44b.	SEM micrograph of nylon / steel coating wear process. Stage IV. (1000x).	240
Figure 3.45a.	SEM micrograph of nylon / steel coating wear process. Stage V. (200x).	241
Figure 3.45b.	SEM micrograph of nylon / steel coating wear process. Stage V. (100x).	242
Figure 3.46.	SEM micrograph of nylon / steel coating wear process. Stage VI. (500x).	243
Figure 3.47.	FTIR spectra of an as-sprayed nylon coating showing characteristic peaks.	244
Figure 3.48.	FTIR resultant spectra of as-melted subtracted from as-sprayed.	245
Figure 3.49.	FTIR resultant spectra of as-worn subtracted from as-sprayed.	246
Figure 3.50.	SEM photograph of transferred nylon film.	247

Figure 3.51.	SEM photograph of 1080 steel coating on rail 200 slpm N ₂ / 30 slpm H ₂ , W.D.= 235 mm.	253
Figure 3.52.	SEM photograph of 1080 steel coating on rail 275 slpm N ₂ / 30 slpm H ₂ , W.D.= 235 mm.	254
Figure 3.53.	SEM photograph of 1080 steel coating on rail 230 slpm N ₂ / 0 H ₂ , W.D.= 235 mm.	255
Figure 3.54.	SEM photograph of 1080 steel coating on rail 230 slpm N ₂ / 50 slpm H ₂ , W.D.= 235 mm.	256
Figure 3.55.	SEM photograph of 1080 steel coating on rail 230 slpm N ₂ / 75 slpm H ₂ , W.D.= 235 mm.	257
Figure 3.56.	SEM photograph of 1080 steel coating on rail 230 slpm N ₂ / 100 slpm H ₂ , W.D.= 235 mm.	258
Figure 3.57.	SEM photograph of 1080 steel coating on rail 230 slpm N ₂ / 125 slpm H ₂ , W.D.= 235 mm.	259
Figure 3.58.	SEM photograph of 1080 steel coating on rail 230 slpm N ₂ / 30 slpm H ₂ , W.D.= 200 mm.	260
Figure 3.59.	SEM photograph of 1080 steel coating on rail 230 slpm N ₂ / 30 slpm H ₂ , W.D.= 250 mm.	261
Figure 3.60.	SEM photograph of 1080 steel coating on rail 230 slpm N ₂ / 30 slpm H ₂ , W.D.= 230 mm.	262
Figure 4.1.	Drawing of plasma plume showing dispersion of molten particles.	274
Figure 4.2.	Drawing of graphite particles captured by molten steel particles at l= 25 mm.	275
Figure 4.3.	Drawing of graphite particles captured by molten steel particles at l= 165 mm.	276

Figure 4.4.	Drawing of plasma plume showing path of travel for molten steel and graphite particles.	277
Figure 4.5.	Drawing of two wire interaction in plasma plume when wires are offset.....	278
Figure 4.6.	Drawing of two wire interaction in plasma plume when wires are too close.....	279
Figure 4.7.	Drawing of two mated Amsler rollers showing coating overspray.....	295
Figure 4.8.	Photograph of nickel-graphite / steel coatings showing edge effects.	296
Figure 4.9.	SEM photograph of removed wear track particles. Sample G46. a) SE imaging. b) BSE imaging.	297
Figure 4.10.	SEM photograph of removed wear track particles. Sample G48. a) SE imaging. b) BSE imaging.	298
Figure 4.11.	Photographs of removed wear track particles. Sample G48.	299
Figure 4.12.	Photographs of samples G46 and G41 showing effect of graphite volume fraction on rate of wear track particle removal.....	300
Figure 4.13.	Drawing of plasma sprayed coating surface showing texture conducive to retaining a polymer coating.	332
Figure 4.14.	SEM photograph of nylon / 1080 steel coating showing texture of interface.....	333

Figure 4.15.	SEM photographs showing surface texture. a) grit blasted surface. b) plasma sprayed steel coating surface.	334
Figure 4.16.	FTIR spectra of a nylon coating which was overheated.	335

Abstract

Development of a Self-Lubricating Plasma Sprayed Coating for Rolling/Sliding Contact Wear

David V. Niebuhr

Supervising Professor: Paul Clayton

The friction and wear that occurs between wheel and rail exacts millions of dollars out of maintenance budgets each year. Standard lubrication practices have been found to be unreliable in effectively lubricating curved track sections. Consequently, a method of reducing cost and increasing rail life is of significance to the railroad industry. Through the use of self-lubricating materials and thermal spray technology a composite surface coating was developed.

A 1080 steel coating provided a wear-resistant matrix, in which to incorporate solid lubricants. The 1080 steel coating was found to provide increased wear resistance and some friction reduction ($\mu=0.46$ vs. $\mu=0.5-0.7$ for uncoated rail). The reduced wear stems from the coatings resistance to degenerate into severe wear modes. The wear rate of uncoated rail steel can be an order of magnitude greater than that of a 1080 steel coating.

Three solid lubricant/steel coating systems were investigated; graphite incorporated into 1080 steel, copper incorporated into 1080 steel, and various polymers deposited over a 1080 steel coating. The structure of the coatings were evaluated by metallography and wear performance. Metallographic analysis included optical, SEM, and FIB. Polymer film analysis was performed

with FTIR. Wear testing and friction measurement were accomplished with the Amsler twin disk wear testing machine. Coatings were tested against class C wheel steel at 5% and 35% slide/roll ratios, with contact pressures ranging from 700 to 1315 N/mm².

The work identified unique wear mechanisms for each coating system. The friction reduction and durability of the graphite/steel coatings was good at low slide/roll ratios. The copper/steel coatings were unable to control friction and had limited life. The polymer/steel coatings, particularly nylon/steel, had excellent performance at a wide range of slide/roll ratios and contact pressures. The nylon / 1080 steel coatings were applied to rail sections for large scale and field testing.

Chapter One Introduction

1.0 Objective

Thermally sprayed self-lubricating coatings are investigated in this project. These coatings may have the potential to greatly improve the rail road industry with respect to operating costs. Friction and wheel/rail wear exact a large cost in maintenance budgets. Consequently, a method of reducing cost and increasing rail life concerns the industry. The emphasis of this project focuses primarily on friction control by means of thermally sprayed surface coatings. The reduction of severe sliding wear is also investigated. These new coatings will be developed to reduce friction and sliding wear at the wheel /rail interface. The applications of this work are potentially far reaching.

1.1 Preface

The wear and friction that occurs between wheel and rail costs the railroad industry millions of dollars each year. It was estimated that the North American Railroads were spending \$600 million annually for the replacement of deteriorated rails in the early 1980's.¹ A large portion of this spending was a direct result of severe wear. Plasma spray technology coupled with solid lubrication offers a potential, partial solution.

Plasma spraying involves forming an ionized gas of high temperature and velocity. This gas accelerates molten particles of metal or other material, to a substrate, to form a coating. The process allows for unique compositions not otherwise possible.

Surface coating allows for unique properties at the surface which may be undesirable in the bulk. Plasma spray is part of a larger family of thermal spray processes which have wide reaching industrial applications.

Long lasting composite coatings could reduce both wheel/rail wear and are renewable. Solid lubricants such as graphite, copper, or a polymer incorporated into or onto a steel coating may allow for friction reduction. Large frictional forces have been blamed for some low rail rollover derailments.² In addition to reducing friction and wear, plasma spray coatings may reduce or eliminate the need for trackside lubrication. Current trackside lubrication is unreliable and labor intensive to maintain. Plasma spray technology in the form of surface coatings has never been applied to the severe rolling / sliding contact conditions between wheel and rail. Although there is a high degree of uncertainty for success the work is justified by the potential benefits.

A 1080 steel coating was developed initially to provide reduced wear and act as a lubricant reservoir.³ It was believed this coating could provide better lubricant retention, thus reducing lubricant reapplication. The unlubricated steel coating provided some friction reduction. More importantly though, this coating had a wear rate an order of magnitude less than some uncoated rail steels.⁴

The scope of this current project was to combine solid lubricant materials with 1080 steel to form a self-lubricating composite coating. The friction reduction obtained from the 1080 steel coating suggested the addition of second phase solid lubricants could further reduce friction and wear. By dispersing a solid lubricant within the coating a potential lubricant reservoir was formed, which could renew itself as the coating wore. A solid lubricant film was also applied to the coating surface, to act as a barrier from steel on steel contact. When the coating was completely worn off it could be reapplied.

The development of this coating would involve testing and evaluating different solid lubricants in varying volume fractions. The different coatings would be evaluated as to their wear life and effect on friction reduction. This surface modification process could extend the life of tracks and reduce the frequency of track maintenance such as grinding.

This project draws from several disciplines. There has been some research into the wear of the wheel/rail interface. Plasma spray technology is its own field with many diverse applications. The theory of friction has spanned five hundred years and is still debatable. Lubrication, specifically solid lubrication, has been explored by the space industry and is now branching out to more common applications. The literature review attempts to cover the relevant topics which directly relate to this project.

1.2 Literature Review

The literature review focuses on subjects which were studied to understand the controlling mechanisms of the project. The theory of friction and sliding wear was reviewed to understand the nature of the interaction of two solids. The mechanisms of lubrication and solid lubrication were integral to the coating development. The types of solid lubricants are reviewed, with the emphasis on lamellar lattice structures (graphite, MoS₂), soft metals, and polymers. A review of coatings and plasma spray technology is also given. Lastly, a review of related plasma sprayed solid-lubricating coatings is presented.

1.2.1 Friction

Friction plays a large role in the interaction of the wheel and rail. Friction properties can change the performance of the train even when wear is ignored altogether. The doubts of the adequacy of friction were expressed in a practical way as early as 1812, when

the conventional design of wheel on track was questioned.⁴ Nonetheless, the worlds railways have operated within the limitations imposed by the friction available between smooth steel surfaces. The obvious need for friction is for traction and braking. On British Rail the limitations and unpredictability of friction are reflected by operational rules. When exerting traction a friction coefficient no greater than 0.22 can be relied upon, while for braking a friction of no greater than 0.095 can be expected.⁴ Given the importance and complexity of friction it has received much academic as well as industrial investigation.

Basic observations of friction have existed over five hundred years. The quantitative study of friction between two solids slid against each other is believed to have begun with the work of Leonardo Da Vinci.⁵ He was probably the first to report that frictional force is proportional to the load and independent of surface area.⁵ These two empirical laws are often associated with Amontons who rediscovered them in 1699.⁶ Amontons added that the frictional force was always equal to one-third of the normal load.⁷ He explained this result by assuming that irregularities on the surface of the two bodies interlocked. (These irregularities though had to be near macroscopic to be detected.) The motion needed to lift the bodies over the interlocking asperities was equivalent to the energy of the frictional force. Coulomb concurred with this theory of interlocking asperities but believed the frictional energy came from the whole surface being "lifted off" its asperities.

The idea of the entire surface moving up and down is incorrect. Surface asperities will deform plastically, and this is the suggested source of energy loss. The more recent view that friction had its origin in surface forces and was due to molecular cohesion between the solids was introduced by Ewing in 1892.⁸ Ewing considered that friction was due to the reaction of molecular forces following the molecular displacement. This theory received strong support from the work of Sir William Hardy on static friction in 1936. He considered that the friction could be explained in terms of the

surface fields of the solids. The results he obtained using lubricants were explained by assuming the lubricant caused a reduction of the molecular field of force at the surface of the solid.

Early theories of friction were based on empirical measurements and observations. The understanding of friction and its mechanisms is still a much debated issue. Friction experiments, which attempted to understand the components of friction, are often highly dependent on the experimental parameters. Even today an experiment's results will only be valid in its own window of parameters. Current theories and work have generally built on Bowden and Tabor's original friction model.

The publication of 'Friction and Lubrication of Solids' in 1950 provided the basis for modern studies of solid friction.⁹ Bowden and Tabor understood that in real surfaces there were many points of real contact and that asperities would push past each other by deforming rather than by displacing the bodies as a whole. Bowden and Tabor divided the total friction force resisting sliding into two components: a ploughing term F_p and an adhesion term F_a . It is believed these terms act synergistically since the sum of the individual components does not always equal the measured friction force.

The ploughing term (F_p) arises from the irreversible plastic deformation of surface asperities as they push past each other. The effect of ploughing is most easily observed when a hard material produces grooves in a mated soft material. Energy is dissipated through plastic deformation in metals. Polymers and rubbers dissipate energy through an internal hysteresis. Quantitative measurements of the ploughing term could only be made using simple models. For example, sliding wedges, cones, or spheres could simulate surface asperities. Bowden and Tabor postulated that in the absence of adhesion the contact pressure everywhere acted normal to the interface. If material pileup is ignored then μ_p (friction coefficient from ploughing term) is entirely dependent on

the geometry of the solids. The derivation of this is explained in detail elsewhere.⁹

The adhesion term is (F_a) is much more controversial. It is very difficult to measure the minute force of adhesion between solids. It is believed that adhesion arises when two asperities are pressed together in intimate contact.^{10,11} The junction is cold-welded. To break this “weld” the asperity of the softer metal must shear. Bowden and Tabor believed that the adhesion term was the product of the real area of contact and the shear strength of the interface. Thus, the F_a could approach the yield strength of the softer material. This simple idea did not take into account plastic flow at the interface. It is believed that the junction between asperities grew to increase the real area of contact when a tangential force was first applied to a junction before sliding began. This “junction growth” increased the true surface area of contact. In brief, the adhesion term can be said to attract the opposing surface, thereby increasing the overall contact and energy required to overcome this contact.

When the adhesion term was examined by energy considerations alone, the results were not consistent. The fundamental work to overcome adhesion forces is the surface energy, γ , which has a value of about 1 J/m² for metals. This value is too small to account for the observed frictional forces. There is a great deal not understood about adhesion and this has caused the term to be viewed as less significant. In addition, the friction theory is only that, a theory, and required some assumptions so that it could be explained mathematically. Even with its limits though, Bowden and Tabor provided the world with a fundamental understanding.

Real world friction experiments of metals have suggested a pattern of behavior. The sliding between most metal surfaces may not be a continuous process but may proceed in a series of intermittent jerks or “stick / slips”.^{12,13} The friction builds up to a maximum during the stick and falls rapidly during the slip. The

nature of this motion is dependent on the intrinsic properties of the metals and the measuring device. More important than the stick/slip nature of metallic friction is the relationship of friction to physical properties.

The behavior of friction is highly dependent on the relative hardnesses of the two surfaces sliding against one another and the sliding speed. One experiment suggested there are three possibilities: hard metal sliding on soft, soft metal sliding on hard, and like hardnesses.¹⁴ When hard metal is slid on soft a ploughed groove appears in the soft metal yielding a friction coefficient of roughly 0.9. When a soft metal is slid against a hard metal fragments of the soft metal are welded to the hard surface. The hard metal remains relatively undamaged. The friction coefficient was 0.7. This lower friction is due to a decrease of ploughing. All of these tests are done at slow sliding speeds to minimize heat buildup. If heat is a factor then the high temperature properties of the materials must be taken into account. These friction coefficients are observed for a particular test and again cannot be applied universally.

The last case, similar metals running against similar, is very dependent on the materials. If nickel or copper is run against its self the friction coefficient is very high (1-1.5). The surface is badly damaged, with ploughing and tearing evident over most of the wear track. Similar metals will form junctions of equal strength, thus when the junction is broken, material will be removed from both surfaces. Also, the junction will be work hardened making the junction harder than the bulk material. When the junction breaks material will be removed from the bulk, yielding a larger removed particle.

The sliding wear behavior of steel on steel is of the most interest to the railroad industry. Steel on steel does not behave like other similar materials.^{14,15} The friction coefficient is around 0.5 if severe wear is avoided. This behavior is attributed to the fact steel is a non-homogenous material. At the μm level the interaction

can be between ferrite, pearlite, or bainite. If pure iron or a homogeneous steel such as austenitic stainless are slid, they will behave much like other similar materials, with a large friction coefficient (>1.0) and wear rate.

Work by Suh¹⁶ investigated the friction behavior of hard and soft metals worn against one another. Figure 1.1 illustrates the six stages of friction incurred with sliding metals.¹⁶ In stage I the value of friction is controlled by plowing of surface asperities, it is largely independent of material combination, surface condition, and environment. In stage II the friction begins to rise because of an increase in adhesion. In stage III the slope of the friction curve rises due to the rapid increase in the number of wear particles entrapped in the contact zone. Stage IV is reached when the number of wear particles entrapped at the interface remains constant. Newly formed particles replace those that are lost from the system, this is generally the steady state for most metals during sliding. Stage V and VI occur under certain conditions, for example, when a soft metal is slid against a hard, stationary metal. The decrease in friction marks the potential for each surface to become highly polished and thus reduce the number of asperities formed.

The relation of soft and hard metal friction is of interest because a soft metal was proposed as a potential solid lubricant. The results of Suh's experiments appear to be specific to the sliding conditions and only deal with metals. Some general statements about the stages of friction can be applied to other systems, such as the low friction which occurs at the beginning of the test. This has been observed in 1080 steel plasma-sprayed coatings. This experiment approaches the friction model by looking at material properties, wear history, surface topography, and the contributions of adhesion and plowing term. This paper also illustrates how much information is yet to be learned about friction.

1.2.2 Wear

Wear is the progressive loss of substance from the operating surface of a body occurring as a result of relative motion at the surface.¹⁷ This removal can be the result of chemical processes or mechanical behavior of the material. These two classifications encompass all forms of wear. Chemical processes include solution wear, diffusive wear, oxidative wear, and corrosive wear.¹⁸ The latter two are more commonly seen when sliding contact occurs and a lubricating environment is present. The mechanical wear processes include abrasive wear^{19,20}, which is the result of hard particles rubbing against a surface. A simple model would be a shovel moving sand.

Fretting wear occurs when two surfaces have oscillatory relative motion of small amplitude.²¹ For true fretting the amplitude of the movement should not exceed $75 \mu\text{m}$.²² A good example is a steel pin vibrating while holding a gear or shaft in place. Erosion wear^{23,24} is a form of abrasive wear, but arises from the high kinetic energy of impinging particles. Particles are often contained within a fluid. Grit blasting to prepare a steel surface and abrasive deburring are forms of erosion.

Fatigue wear²⁵ is the result of cyclic loading and is a common problem in aircraft wings. Rolling contact fatigue occurs by cyclic loading combined with relative motion between bodies. For example, subsurface cracks are formed in rails due to the repeat loading of high tonnage wheels^{26,27} Sliding wear is the result of two surfaces being moved against one another.^{28,29} The mechanism involves plastic deformation, crack nucleation, and propagation in the subsurface. Brake pads pressed against rotors or drums are good examples of sliding wear. Sliding and fatigue wear are the two most common modes of wear failure in the rail road industry, and can be said to be the basis of this project. Given all the types of wear it becomes obvious how complex wear systems can become.

Early observations of wear, except abrasive wear, were explained in terms of the adhesion theory.³⁰ This theory is similar to the adhesion theory of friction explained by Bowden and Tabor.³¹ The wear of materials is a result of welding asperity junctions, which create a hemispherical wear particle near the junction when the weaker material fractures. The adhesive theory of wear was governed by Equation 1.³⁰

$$\text{[Equation 1.1.] } V = K (LS/3H)$$

where:

- V = wear volume
- L = applied load
- S = sliding speed
- H = hardness of material
- K = wear coefficient

The term K was the result of empirical observations. It is generally expressed as an order of magnitude, 10^{-4} to 10^{-3} for sliding metals and 10^{-2} to 10^{-1} for abrasive wear. This model does not account for microstructure or surface topography (roughness), nor does it take into account how different sliding conditions will effect wear. Also, this equation implies softer materials will wear faster than harder materials. There are some exceptions where softer metals have lower wear rates. The soft babbitt material used in automotive engine bearings has a lower wear rate than the opposing hardened steel crankshaft or camshaft. Another example is illustrated in Figure 1.2 showing how the wear rate of a high speed tool steel is greater than that of a softer 60-40 brass.³² The adhesive theory model of wear, given its limitations was revised.

The delamination theory of wear introduced by Suh provided the basis for the modern explanation of sliding wear.³³ The theory is based on the behavior of dislocations, subsurface void and crack formation, and shear deformation of the surface. The theory divides

the wear process into five events which lead to loose wear sheet formation.

Two surfaces which come into contact will transfer normal and tangential loads through their contact points. The softer material is deformed and fractures causing asperities; a smooth surface is generated between the two surfaces initially. The second event introduces plastic deformation in incremental steps as the surface is cyclically loaded. The deformation grows into the subsurface. The third event is the formation of cracks which nucleate below the surface as subsurface deformation continues. Crack nucleation does not occur very near the surface due to compressive stresses below the contact region. The fourth event is the propagation of cracks, which join other neighboring cracks to form a large network. Figure 1.3 illustrates the process of wear particle formation.³³ In the final event a critical crack network size is reached and material is removed. The size of the wear sheet is determined by the depth of subsurface crack growth. The wear rate thus is controlled by the crack nucleation rate or the crack propagation rate, whichever is slower. This theory aids to explain the microscopic events which occur during sliding wear.

Looking beyond Suh's model, the nature of solid wear is very complex. Physical damage and chemical attack often work in tandem, as well as different wear modes. Regardless though of the wear mechanism, the condition of the sliding surface strongly influences how the material will behave. Metals will usually be covered with a film of oxide, which is covered by a second film of adsorbed gases and oils.³² Polymer surfaces may contain water, and are commonly covered by mold release agents, oils, and gases.³⁴ These thin adsorbed layers are on the order of 10 nm. Despite their seemingly insignificant thickness, they play a large role in the wear behavior of materials. Just as oxides act as solid lubricants to reduce friction, so too will adsorbed films help reduce friction and wear. Oxide layers when worn away will reform. The speed at which they reform is controlled by sliding speed and temperature.

As sliding speed increases there is less time for the oxide layer to repair itself, but as temperature increases the rate of oxide formation is accelerated (assuming an oxygen environment). Polymers will form a continuous layer of adsorbed gases during the wear process. In a vacuum both metal and polymer can exhibit degrees of wear orders of magnitude greater than in ambient conditions due to absence of surface contaminants.

In wear of the wheel and rail there also exists a high degree of surface contamination. Adsorbed gases, oxides, and sulfides are amongst the many contaminants. Figure 1.4 is a schematic of two surfaces in intimate contact.³² The adsorbed films provide a boundary layer between the opposing metal asperities. Experiments have been performed to identify the effect of surface contamination to wear rate and friction coefficient. Lubricating oils placed on rail road tracks are altered to form a solid film of wear debris.³⁵ This solid film is believed to consist of organic matter, degraded lubricant, and wear debris. The tenacity of this film allows it to act as a type of solid lubricant between wheel and rail. Rain and organic material, commonly in the form of fallen leaves, aid to the corrosion wear of rails. Water and oil as lubricants can force their way to the subsurface. This may accelerate crack propagation that results from fatigue wear by generating hydrodynamic forces at the crack tips.

In the study of rail wear and attempting to assess different levels of wear damage Bolton and Clayton simulated wheel /rail wear in the laboratory using the Amsler wear testing machine.³⁶ Three distinct wear modes were defined in this work, and are referred to throughout this thesis. Type I wear is the mildest form resulting in debris of both oxide and metal particles in a constant proportion. This mode approaches true oxidative wear, where material is removed by the progressive growth and breakdown of a continuous oxide film, when contact pressure and creep values remain low. Type II wear was characterized by completely metallic debris showing a much smaller mean particle size but a wider range

of particles sizes as compared to Type I. In addition there is metal transfer and a rougher surface topography. Type III wear is the severest and is marked by prominent score marks on both the wear surface and on the debris. There is localized evidence that material has been gouged out of the surface. This form of wear is unacceptable in any application and marks a rapid degradation process.

The general theories of both adhesive³⁷ and delamination³³ wear are difficult to apply to wheel and rail wear in curves. For example, most wear theories do not deal with combined rolling and sliding. Also these wear theories assume plastic flow is limited to thin surface layers or asperities.^{38,39} Full scale wheel /rail wear testing by Jamison⁴⁰ confirmed previous data⁴¹ that wheel rail wear is a synergistic effect of stress and creepage. When a critical combination of the two is reached wear is greatly accelerated. Jamison also showed that humidity had a definitive effect on wear rate, with low humidity (< 25%) increasing mild wear by a factor of 6 to 10, over high humidity (> 50%) wear.

The wear processes of sliding are very complex. Since no fundamental first principles exist only empirical data is available. The sliding wear behavior of metals has been well documented. However, the wear process varies greatly depending on operating conditions, thus even a carefully controlled laboratory experiment must be viewed conservatively with respect to reproducibility in the field. The literature on sliding wear behavior of coatings, specifically plasma sprayed steel coatings is much more limited. The literature that does exist is again specific to the coatings application, and must be re-evaluated for each new experiment.

1.2.3 Fluid Lubrication

Lubrication is accomplished between two sliding solids by adding a gaseous, liquid, or solid lubricant at the sliding interface in order to reduced friction and wear, and to carry away wear debris and heat.⁴² The three main types of fluid lubrication are hydrodynamic (or thick film), thin film, and boundary. In hydrodynamic lubrication the shape and relative motion of the surfaces cause the formation of a fluid film which has sufficient pressure to separate the surfaces. As there is no physical contact between surfaces the friction is purely viscous and is directly dependent on the area of the film, the rate of shear, and the viscosity of the lubricant. The shear strength of the film will determine how effective the load is carried, by its ability to support the opposing surfaces. Thin film (or mixed lubrication) occurs when part of the load is carried by fluid pressure and the rest is borne by contacting surface asperities.⁴³ These surface asperities are lubricated with a molecular thick film.

Thin film lubrication occurs when the motion of the two bodies being lubricated is insufficient to create hydrodynamic conditions. When sliding speed or viscosity are insufficient for the fluid to carry any load, sliding between surface asperities occurs, this is known as boundary lubrication. To discern between boundary and thin film lubrication regimes the load ratio is used. This consists of the load carried by the fluid pressure over the load carried by the asperities. Full boundary lubrication occurs when this ratio approaches zero.⁴⁴ The asperities are thus only lubricated by surface films of liquids, gases, or solids.

The most common lubricants for wheel/rail applications are greases. Greases consist of three components: a fluid, a thickener, and additives.⁴⁵ The fluid is the base of the grease and generally consists of mineral oils for most industrial applications. Mineral oils are stable over a wide range of temperatures. Thickeners generally consist of metallic soaps; lithium, barium, and aluminum

compounds to name a few. Thickeners act as a sponge to maintain the consistency of the individual ingredients. The additives can include rust inhibitors, extreme pressure anti-wear agents, and solid lubricants, such as graphite, PTFE, or MoS₂. Solid lubricants increase the lubricity of the grease, and are generally added in volumes of at least 5%.⁴⁶ Greases provide an inexpensive means of controlling friction and wear.

The two types of geometry for lubricated surfaces are conformal and counterformal, and are illustrated in Figure 1.5.⁴² Counterformal geometry closely approximates the rolling /sliding contact of wheel and rail, where the contact patch at any given time is very small. This small area of interaction is described by Hertzian contact theory. Hertzian contact theory uses mathematical models to describe the state of stress at the contact of two elastic solids.⁴⁷ A subsurface stress distribution exists as a result of rolling contact. This stress distribution is a function of loading conditions but independent of material. The theory is a powerful tool in the study of rolling contact fatigue in rails.^{48,49}

Boundary lubrication dominates the interaction of wheel and rail, as thick film lubrication would deteriorate rapidly under the extreme pressure, temperature, and rolling /sliding contact. The conventional grease lubricants provide adequate protection when adherence to the rail is achieved. Several questions arise however, regarding economics, ease of application, durability, and degree of control. These questions prompt the experimentation with solid lubricants.

1.2.4 Solid Lubrication

A solid lubricant is a thin film of a solid interposed between two rubbing surfaces to reduce friction and wear.⁵⁰ Solid lubricants serve a wide range of functions. They are used exclusively in space where no atmosphere exists. Other common uses exist where severe pressure, temperature, or chemical reactivity would prohibit the use

of an organic liquid. Solid lubricants should not only reduce wear but have a low wear coefficient themselves. Applications vary from jet engines to compressor pumps. Figure 1.6 illustrates a state of the art solid lubricated bearing.⁵¹

There exist several classes of solid lubricants. These include the inorganic compounds, metal films, and solid organic compounds. The solid lubricants used in this research were the laminar lattice compounds, soft metals, polymers. Each of these fall into the above classes respectively. The relevant materials to this project will be discussed in detail, this will include the structure and lubricating mechanism of the material.

Inorganic Compounds

The first class are the inorganic compounds. This class is subdivided into three categories. The first is the layer lattice or laminar solids. These materials, which include graphite and the dicalcogenides (MoS_2 , WS_2 , etc.), are some of the most common solid lubricants. The other two classes include miscellaneous soft solids and chemical conversion coatings which are discussed in detail elsewhere.⁵⁰

The materials in the laminar solids class have crystal lattices in layers. Like most solid lubricants they possess anisotropic properties because of their layered crystal structure. These materials lubricate because strong covalent bonds are difficult to break while the weak bonds between layers easily break and reform. This allows shear to be accommodated by sliding the laminar plates parallel to each other.⁵² Figure 1.7 illustrates the layer lattice structure of graphite.⁵³ Figure 1.8a is a schematic of MoS_2 molecules, and Figure 1.8b is a scanning electron microscope image of the MoS_2 structure.⁵³ These materials are able to withstand high temperatures and are generally inert.⁵⁴ Not all layer lattice structures act as solid lubricants, boron nitride and mica for example can be abrasive under sliding wear.⁵⁵ Mica rubbed against

itself can exceed friction coefficient values of 100 at low loads.^{56,57}

In the case of graphite the mechanism of interplanar sliding is thought to be quite likely since distance between lamellar planes is quite large, 3.4 Å for the simple hexagonal lattice of graphite where hexagonal planes of carbon atoms are stacked on top of one another. Figure 1.9 is a schematic of the mechanism of lubrication by lamellar solids.⁵⁸ This simple picture is somewhat clouded by actions of absorbed oxygen and water and atomic disorder on the bonding energy between lamellar planes.^{59,60}

Graphite is unique in that it requires an absorbed film in order to lubricate effectively. This absorbed film exists between the carbon planes. It is thought that oxygen and water absorb on the surface of graphite lamellae and suppress bonding between lamellae. The absorbed film can be water or oxygen, which is abundant in nearly all systems.⁶¹ In a contaminant-free vacuum graphite is a very poor lubricant. An example of this is illustrated by a graphitized carbon brush which would last 500 to 1000 hours in air when rubbed against a metal spring.⁶² This same brush would degrade in only a few minutes under vacuum. When the vacuum tested brush was examined, it was noted that the layers were of random orientation during heavy wear. Graphite lubricates best when its layers are parallel to the surface. The layers can then slide past one another, much like a deck of cards. It has been postulated that the absorbed contaminant or interplanar lubricant appears to be, at least in part, one of enabling a graphite film to become oriented on both surfaces.⁶² The absorbed contaminants also aid in the interplanar shearing ability of the graphite film.

Graphite gives limited protection when applied as a rubbed film, as it has poor adhesion to most surfaces. It has been postulated that neither graphite or MoS₂ is hard enough to become imbedded in the surface. Widely accepted views believe the adhesion of a solid lubricant plays a decisive role in the mechanism

of solid lubrication.^{63,64} Continued lubrication requires a continual replenishment of the graphite.

Generally graphite is bonded or used with carrier materials, with grease being the most common. Graphite makes an excellent additive to greases because its degree of subdivision is very high.⁴⁶ The grease acts as a carrier and supply and the graphite acts to provide lubrication when the grease film fails. Graphite is stable in air to 350° C, at which point it sublimates to form CO or CO₂. Graphite is inexpensive and commercial powders are readily available. These include plain graphite and graphite encapsulated in a thin metal shell.

MoS₂ is the most common dicalcogenide, which is the family of materials with the MS₂ structure.⁶⁵ MoS₂ is a similar lubricant to graphite, but has some superior lubricating properties. MoS₂ generally has a higher tolerance to load and sliding speeds.^{66,67} A film of MoS₂ rubbed onto a surface from a powder becomes oriented in the wear track in the same manner as graphite.⁶⁸ Its lubricity does not depend on the presence of an absorbed contaminant. In fact, an increase in humidity from zero to sixty percent has shown a reduction in lubricity.⁶⁹ Figure 1.10 is a good illustration of the effect of ambient pressure, which is a correlation of contamination, on the friction of graphite and MoS₂.⁴⁶

There is evidence to suggest that an interplanar absorbed film of sulfur develops during wear giving MoS₂ its low shear force.⁷⁰ A contaminant may interfere with this sulfur layer reducing its resistance to friction. Sliding speed does not appear to affect the coefficient of friction, but as with most solid lubricants, high sliding speeds reduce wear life.⁷¹ MoS₂ is stable in air to 350° C much like graphite. However, for both materials, the particle size and environment are influential in their thermal stability. MoS₂ powders tend to be manufactured in finer sizes than those of graphite. This is due to the fact most MoS₂ is used as a grease additive.

Soft Metals

The second category are the metal films. Soft metal films have been used for many years in the metal forming industry. The coating of a die or workpiece with a continuous film of another metal fulfills a number of purposes. For one, the adhesion between die and workpiece can be reduced. In the absence of other lubricants a metal film reduces friction, provided the shear strength T_s of the lubricant metal remains below K , the bulk metal shear strength of the workpiece.⁷² Copper, gold, and silver films on steel have yielded $\mu = 0.1$ at room temperature.⁷² The films must be well bonded to the surface and thick enough to coat the entire workpiece. If the film was too thick though it would be scraped off. Generally thin metal films were targeted at $1 \mu\text{m}$ in thickness.

Thin metal coatings have also been used for cutting tools and cylinder liners. Rhodium and chromium are hard metals which show very little wear when slid against other metals.⁷³ Thin films provide a means of reducing surface wear on other metals. Chromium's hard oxide film is not easily broken down because of the hard chromium surface underneath. The oxide limits the number of intimate metallic connections achieved. Figure 1.11 illustrates the mechanism of thin metal film protection for sliding wear.⁷⁴ Indium is a soft metal similar to lead in its mechanical properties.

Figure 1.12 illustrates how a thin film of indium greatly reduces the friction coefficient over unlubricated and oil lubrication conditions.⁷⁵ This figure also illustrates how at higher loads the friction coefficient is reduced. It is thought that the contact area is controlled by the hard substrate.⁷⁶ The amount of contact area will determine the asperity interaction and subsequent friction between the two bodies. If the friction coefficient is large, severe galling of the softer material may occur. Lubrication with metal films is especially useful in vacuums, where the lack of oxygen allows repeated transfer of the metallic film between sliding surfaces.⁷⁷ Another example involves the impregnation of silver, BaF_2 and CaF_2

in chromium carbide to achieve a high temperature lubricating film.^{78,79}

The use of metal films coupled with deposition by plasma spraying was limited to high temperature applications.¹⁶⁹ No specific rolling / sliding applications were found, but the mechanisms of why soft metals lubricated in metal forming and surface coating seemed translatable to wheel / rail lubrication. In the application of wheel / rail contact the metal film would be expected to deform over the sprayed coating as it was exposed during wear. The premise being the increased ductility and reduction of shear would lower the friction. The metal forming industry has extensive research into metal as lubricants. Most materials are unsuitable on the large scale for economic or toxicity reasons, with gold and lead being good examples.

Oxide films are a subcategory of metal films. Nearly all metals will have some form of an oxide film, with this film acting as a solid lubricant in some cases. This subject has been widely studied. One such experiment indicated that the friction levels of some metals were an order of magnitude greater when tested in a vacuum with the oxide removed.^{80,81} At high temperatures the oxide film plays a significant role in reducing friction and wear.⁸² A good example of the effect of the oxide film is shown in Figure 1.13.⁸³ This figure illustrates how copper will have low friction provided the oxide layer is unbroken. This can only occur at small loads (< 1 gram). Once the oxide is broken the friction increases dramatically. Copper, because of its soft, ductile nature, will have a high friction when rolled against itself.

Although oxide layers can act as solid lubricants, in most cases oxides are poor solid lubricants because they are brittle and generally harder than the metal. When the oxide layer is broken and particles are retained in the contact zone, wear will be accelerated. Iron oxide, fortunately, is a better than average solid lubricant. Scale formed on iron at high temperatures is of a layered structure; the outermost oxygen-rich Fe_2O_3 layer and the intermediate layer

Fe_3O_4 are brittle, but the FeO layer adjacent to the metal is capable of some limited deformation.⁸⁴ FeO becomes softer than iron at temperatures above 900°C . This is due to the transformation of ferrite to austenite.⁸⁵ Alloying elements greatly influence the oxide structure. Thus, no generalizations can be made as to the subsequent oxide behavior of different steel alloys.

Polymers

The third class of lubricants are the solid organic compounds. These include polymers, soaps, and waxes. Soaps and waxes are used under light loads as they have low thermal stability and are incapable of supporting appreciable loads. Polymers offer excellent wear under moderate loads and speeds. Wear properties stem from surface film formation and the inherent relative softness of the polymer. The surface morphology (roughness, hardness, etc.) of the counterface has a strong influence on the tribology of polymers. Most polymers are more effective when worn against a hardened counterface than when worn against themselves.⁸⁶ When a polymer is slid against another polymer the cohesively weaker polymer is worn preferentially, forming a transfer film on the cohesively stronger polymer. The wear mechanism is similar as that observed with hard and soft metals.⁸⁷ Polymers have poor adhesion to most surfaces and require specialized application. For example, Teflon™ requires a high temperature cure to become adhered to a surface when it is applied as a thin film.

Friction properties are excellent for materials such as Polytetrafluoroethylene (PTFE) or Teflon™ and polychloroethylene. PTFE has the ability to form oriented films on its own surface as well as transferring films onto the mating counterface.⁸⁸ PTFE has specific wear behavior as a function of sliding speeds and temperature. Reduced friction and wear is present at a wide range of sliding speeds. When a critical sliding speed is reached the transfer morphology changes from a thin uniform film to thicker

fragments of bulk material, causing a large increase in wear.⁸⁹ PTFE exhibits a large increase in wear when its melting temperature is reached, beyond which wear rate falls to the pre-melting temperature wear rate.⁹⁰ This phenomena is illustrated in Figure 1.14.⁹⁰ The friction coefficient shows little effect by temperature, unlike the “critical” temperature and sliding speed for wear.

The wear behavior in oscillatory and unidirectional contact has been investigated extensively.⁸⁸ The results vary between experimental parameters, with the wear behavior being similar with respect to temperature and sliding speed dependence. When PTFE was filled with a solid lubricant such as graphite or MoS₂ the friction was found to be no different than for unfilled PTFE.^{91,92} However, in another experiment the opposite was true and depended on the amount and size of the added solid lubricant.⁹³ This illustrates how complex these systems can become. Figure 1.15 illustrates the molecular and crystalline structure of PTFE.⁹⁴

The mechanism of film transfer in PTFE is unique amongst polymers, except for high density polyethylene (HDPE) and ultra-high molecular weight polyethylene (UHMW). In a vacuum it was observed that strong adhesion occurred between PTFE and a metallic surface.⁹⁵ The cause for this adhesion was believed to be an interfacial chemical reaction between the fluorine and carbon in PTFE and the opposing metallic surface.⁹⁶ PTFE in contact with a hard counterface loses material as a series of laminae, which yields low friction but a large wear rate.^{97,98,99} This phenomenon is illustrated in Figure 1.16.¹⁰⁰ PTFE has seen widespread use because of its unique wear, friction, and non-reactive properties.

Polyethylene is the most widely used thermoplastic today.¹⁰¹ It is available in a wide variety of grade formulations and properties. Its uses range from ice cube trays to injection molded components. Ultra high molecular weight polyethylene (UHMW) is a linear chain with a molecular weight of 2-5 million grams/ mole. Long chains of methylene (CH₂) groups make up the structure. UHMW has coefficients of friction ranging from 0.15 to 0.3. Its

outstanding abrasion resistance and high impact strength make it useful for bearings, gears, bushings, and other sliding components.¹⁰² UHMW has been used for bio-medical applications in the fabrication of load bearing joints.^{103,104} The degree of polymerization generally determines the end use. Chains are bonded to each other by weak hydrogen and Van der Waals secondary bonds.¹⁰⁵ Deformation occurs as chains slide past one another. In a highly oriented UHMW specimen Youngs Modulus can exceed that of steel in the direction parallel to the chains.¹⁰⁶ This strength is the result of strong covalent bonding between CH₂ groups. Because of its long chains UHMW requires heating well above its melting point to reduce its viscosity to that of a slightly melted nylon, which is on the order of water.¹⁰⁶

The wear behavior of UHMW is similar to that of PTFE. Figure 1.16 illustrates the wear mechanism. This behavior is believed to be caused by a “smooth molecular profile” or the absence of side groups and kinks in the polymer chain.¹⁰⁷ The initial friction of UHMW and PTFE, effectively the static coefficient of friction, is about 50% higher than the dynamic coefficient of friction.¹⁰⁸ This is believed to be caused by the extra force necessary to initiate a transferred surface film.

High counterface hardness, (700 Vickers) is employed and widely accepted for polymer systems. The counterface should have sufficient hardness to prevent roughening by contamination (sand, dirt, etc.) which would lead to an increased wear rate of the polymer.¹⁰⁹ Surface roughness has an effect on the wear rate of all polymers. Figure 1.17 illustrates the effect of counterface roughness on wear rate.¹¹⁰ The wear rate reaches a minimum at a certain surface roughness, which varies from polymer to polymer, and is strongly influenced by loading conditions.^{111,112} Figure 1.18 illustrates the mechanism of polymer wear on both a smooth and very smooth counterface.^{113,114} If the counterface is too smooth than the transferred polymer will not adhere to form a lubricating film. A slightly abraded surface acts as a physical anchor for the

polymer, allowing for a high integrity transferred film. An excessively rough surface will cause a rapid wear rate and accelerated failure.^{115,116,117}

The understanding of how film transfer and counterface roughness effects wear is important in the development of self lubricating coatings. The system will be open, in that the coated rail would transfer material to fresh wheel steel. The surface roughness would vary depending on the stage of wear of the wheel. In the laboratory, observations of closed systems give evidence to the nature of transferred films and the effect of surface roughness. The polymer film coating system mimics a pure polymer vs. a hardened counterface. Thus, the observations in the literature of pure polymers will be similar, if not identical.

Nylon is a polymer from the class known as polyamides. Polyamides are produced by condensation polymerization reactions between an organic diacid and a diamine.¹⁰² The amide linkage consists of carbon, oxygen, nitrogen, and hydrogen. This connects a series of CH₂ or methylene groups. The number of carbon atoms in a single mer is used to describe the nylon type. For example Nylon 11, used in this research, has 10 methylene groups plus a carbon atom in the amide group before repeating itself.

The melting temperature of nylon is generally dependent on the number of methylene groups. When the number of amide groups is odd the melting temperature is larger due to the line up of amide linkages. As each mer becomes longer, by the the addition of methylene groups, the melting temperature will asymptotically approach that of polyethylene.¹⁰⁶ The molecular weight of nylons range from 11,000 to 34,000 grams/mole. The structure of nylon 11 is illustrated in Figure 1.19.¹¹⁸ Bonding between amide groups occurs when the amide hydrogen and carbonyl oxygen line up from adjacent chains. This bonding is fairly strong, and resists chain sliding to a greater degree than UHMW. Like UHMW, the upper service temperature is low 110°-180° C, with UHMW being only 95° C.¹¹⁹

When nylon is overheated, the excess thermal energy will break the methylene bonds causing the chain to become reactive.¹²⁰ The broken bonds may react with an adjacent chain, causing a pseudo-cross linking.^{102,121} This altered structure embrittles the nylon, reducing wear resistance. Nylon should display typical “lumpy” transfer during wear, in that, unlike PTFE, large particles are transferred to the opposing surface and vary greatly in size. This mechanism is common to most polymers and is illustrated in Figure 1.20.¹⁰⁰ MoS₂ and graphite when added to nylon have been shown to reduce both wear and friction in sliding tests against a steel counterface.¹⁰²

There exist many different solid lubricants each with its own unique properties and applications. This project attempts to utilize readily available lubricants which can be integrated into or onto a developed 1080 steel plasma sprayed coating. The lubricants need sufficient durability and spray-ability to be practical.

Polymer Characterization

The field of polymer bulk and film analysis relies on many analytical techniques. These include nuclear magnetic resonance, which is related to the spin of the nuclei, and differential scanning calorimetry, which measures thermal transitions. Fourier transform infrared spectroscopy (FTIR) is another analytical technique which has been used extensively in studying polymer surfaces and degradation.¹²² FTIR spectroscopy is based on the absorption process and involves measuring the amount of energy that passes through or is reflected off a sample and comparing this amount to that transmitted or reflected from a perfect transmitter or reflector, respectively.¹²³ Fourier Transform algorithms increase the speed and accuracy of data acquisition.

The absorption of radiation over the wave numbers 4000 to 400 cm⁻¹ causes stretching and vibrations of bonds in polymer molecules.¹²⁴ The motions for any specific functional group are

essentially independent of the rest of the molecule. This allows different bonding vibration, stretching, and rotation to be isolated and examined. For example, the degree of crystallinity can be examined on polyethylene by comparing the amount of methylene rocking vibration at 720 cm^{-1} to the amount of vibration at 1303 cm^{-1} of a pure, 100% amorphous polyethylene sample. The IR spectra for many bulk polymers is amazingly simple given the complexity of the molecular chains. The simplicity occurs because a large number of individual vibrations have virtually the same frequency.¹²⁵ FTIR uses interferometry in the course of generating the spectra. In FTIR the detector monitors the entire IR spectra coming from the sample at any one time.^{126,127} Older IR methods would scan the spectrum over time. As a result spectral resolution and data manipulation has improved tremendously.

Polymer surface analysis has inherent problems not seen in bulk analysis. Surface contamination and degradation by the incident beam may distort the spectra. Attenuated total reflectance (ATR) is probably the most widely used method of analyzing polymer surfaces.¹²⁸ Figure 1.21 illustrates the structure of an ATR crystal.¹²⁸ In ATR a polymer sample is attached to a crystal such as ThBr or AgCl that is transparent to IR. An IR beam is directed into the crystal, and after penetrating the polymer sample ($1\text{-}5\ \mu\text{m}$), is reflected. Some of the IR frequencies are absorbed by the surface, and the attenuated reflected beam is directed to the detector where it is recorded. The ATR spectrum represents a normal absorption, the same that would have been obtained from a thin film. ATR is particularly useful for studying surface coatings in situ. The ATR surface penetration is extremely small, thus information obtained may not be characteristic of the bulk polymer.

1.2.5 Current Wheel / Rail Lubrication Systems

Friction and wear reduction of the wheel/rail interface, in a curved track, is currently accomplished through the use of trackside and vehicle born lubrication systems. The trackside lubricator is a

device designed and operated to provide a controlled and consistent supply of lubricant to the area of contact between wheel and rail.¹²⁹ These systems have been around since the early 1930's. The designs are simple, generally involving a reservoir of lubricant and a mechanical pumping system.

Trackside lubrication systems are designed to apply a set quantity of grease onto the track upon demand. The lubricators are activated each time a train passes. The weight of the train, specifically a wheel, activates a pump. The pump will apply lubricant from the reservoir to the track and sometimes the wheel. The intended target of the lubricant is the gauge face. It is undesirable to retain lubricant on the rail head as a loss of adhesion between wheel and rail may occur.

These systems though simple, have weaknesses. They are inefficient, in that only a fraction of the grease applied adheres to the intended location. This encourages overapplication of lubricant to ensure that critical areas are coated. An investigation in the early 1970's in which 18 curved sites were examined, showed that, although each curve was equipped with a lubricator, there was little evidence of lubricant.¹³⁰ The grease itself brings up environmental concerns; where will the residual grease eventually settle and what long term impact will it have on the environment? This is especially important in high traffic areas where large quantities of lubricant are applied. In addition, the mechanical nature of the lubrication system requires frequent maintenance, which can be difficult for remote locations. This mediocre performance has prompted new and improved lubricators to be developed.

New, intelligent rail lubricators have been developed which use electronics to substitute for more complicated and less reliable mechanical components.¹³¹ The pumps of older, mechanical lubricators were located inside the grease reservoir. This made a messy job when maintenance was required. Newer systems, both electronic and mechanical, separate the pump into a "clean chamber."¹³² There are many advantages to the newer systems. For

one they are self-lubricating and have fewer moving parts, which equates to longer service life. In addition, adjustments to the delivery rate or mechanical components at or near the rail are rarely required. The electronic lubricators offer diagnostic features which will shut the unit down when the pump clogs, the unit is out of grease, or there is insufficient power to operate.

Trackside lubricators are the current method of controlling friction and wear. The use of a liquid lubricant with solid lubricant additives is the current practice. A plasma sprayed coating with a solid lubricant reservoir would reduce and possibly eliminate the need for trackside lubricators. The nature of solid lubricants and the films they form offer potential improvements for lubrication in the railroad industry.

1.2.6 Surface Engineering

Thermal spray coatings fall under a broader category of surface engineering. This encompasses any surface treatment which will modify the working surface of a material. Generally, the properties required at the surface may not be needed or wanted in the bulk material. Surface engineering falls under two categories: surface treatment and surface coating.¹³³

In surface treatment the microstructure is physically changed by thermal treatment and /or alloying. Some of the more common methods to increase wear resistance include ion implantation, flame hardening, and nitriding.¹³⁴ All of these methods involve minimal material addition and rely heavily on the inherent properties of the treated material.

The surface coating process involves the application of material to the bulk component. Hardfacing is the most common treatment in industrial applications, and involves the deposition of a hard wear-resistant material to the surface.¹³⁴ This can be accomplished by welding , spraying, or by a combination of the two. Materials include primarily carbides and cobalt or nickel base

superalloys, but may also include iron base alloys.¹³⁵ Thermal spray is but one of many techniques used in surface modifications.

Coatings

The structure of a coating is unique compared to that of a material created by other means, i.e. casting, forging, sintering, etc. A thermally sprayed coating is the product of millions of tiny particles or splats, which build up layers to create the bulk coating. The molten particles flatten upon impact with the substrate due to their high kinetic energy. This build up of flattened particles creates a substrate-parallel, lamellar structure. Figure 1.22 illustrates schematically the morphology of a typical coating.¹³⁶ The bulk of the coating consists of dense, solidified large and small particles. In addition, porosity and unmelted particles are present, and are generally considered undesirable.

Porosity occurs when voids between impacted particles are formed. Unmelted particles upon impacting the surface will not flatten, and create unusual geometries within the coating. Porosity has been blamed for lower fracture strength and ductility in some coatings.¹³⁷ The formation and cause of porosity has been studied in detail. Parameters which effect porosity include: powder size, powder injection angle, and traverse rate.¹³⁸ It has been demonstrated that by maximizing molten particle velocity, high quality coatings with porosity volume fractions less than 1% can be produced.¹³⁹ Post deposition heat treatments can reduce porosity. Hot Isostatic Pressing (HIP)¹⁴⁰ and tempering¹⁴¹ allow plastic deformation to close voids. Heat treatment also allows diffusion to occur at the interface, which enhances the metallurgical bond, and thereby improves coating adhesion.

The coating structure is a combination of metallurgical and mechanical bonding. The metallurgical bonding results in diffusion between molten particles upon impact of the substrate. The effect is minimal as the cooling rates are very fast. The mechanical

bonding is responsible for the bulk coating strength, combining the strength of the individual splat and the cohesion between splats.¹⁴² Adhesion is the most critical at the interface between coating and substrate. The dynamics of particle interaction at the substrate are very complex. Attempts have been made to correlate single particle morphology, both in flight and after impact, to the spray parameters of the system.¹⁴³ Residual tensile stresses in coatings reduce the cohesive bonding. Post deposition heat treatments have increased cohesive strength by alleviating stresses.¹⁴⁴ Good cohesion is critical to the performance of any sprayed coating which undergoes loading during service.

Substrate preparation is paramount to avoiding delamination or debonding of the coating. Substrate preparation has been based on empirical results, mainly trial and error. In general a rough surface is desirable to maximize the substrate surface area. The roughness (as equated to R_a value) of the substrate has been correlated to the final coating surface roughness.¹⁴⁵ An ideal surface roughness is desired for the polymer/1080 steel coating system of this research. Ideal is defined as a coating with a large number of random peaks and valleys within its structure. Coating roughness has been increased by high current, low primary gas flow rate, smaller working distance, and larger powder size.^{146,147} Coating roughness varies greatly depending on the composition of feedstock and spray parameters.

Thermal spraying

Several types of thermal spray techniques exist, all of which operate on the principle of heating and accelerating particles to form coatings. Techniques include: twin wire arc, detonation-gun, HVOF, and plasma.

Twin wire arc consists of oppositely charged combustible wires.^{148,149} A high velocity gas jet propels the molten particles onto a substrate. This system can be hand held and portable, making

the deposition of coatings possible outside of the laboratory. The detonation-gun or D-gun™ propels particles out of a long barrel via the ignition of gases.^{150,151} The particle velocity of 800-1000 m/s is the highest of the thermal systems. This high velocity allows for very high integrity, low porosity coatings to be produced.

High velocity oxygen fuel (HVOF) combusts an organic fuel, such as kerosene, and oxygen to form a supersonic velocity flame.^{152,153} The system combines high speeds with relatively low temperatures (3000° C) to form dense coatings. Recent improvements in the HVOF system have allowed high bond strength coatings to be created which exhibit the metal working properties similar to that of wrought material.¹⁵⁴ The last system is plasma spraying and the focus of this research.

Plasma Spraying

Plasma Spraying is one of the most versatile and rapid methods of applying coatings, with the number of applications of this technology ever increasing.¹⁵⁵ There are two basic plasma spraying techniques, air plasma spraying (APS) and vacuum plasma spraying (VPS).^{156,157,158} VPS is performed in inert or a low pressure atmosphere. This technique allows for increased particle velocities and lower oxide content. APS allows for better control of substrate temperature and is less cumbersome. A background of air plasma spray is necessary to understand the coating deposition process used in this research.

Plasma Fundamentals

A plasma is formed when a gas flowing between a tungsten cathode and a copper anode is ignited by a high frequency spark. The anode and cathode are energized with DC current, and power output can range from 30 kW for small systems to the 200 kW OGI system,

and beyond. Some applications use radio frequency plasmas instead of DC current.^{159,160}

Plasma is essentially an ionized gas, it contains electrons, ions of the plasma gas, and un-ionized molecules of the plasma forming gas.¹⁶¹ Electromagnetic radiation (photons) is also present and permeates the plasma filled space. If the gas has a high degree of ionization, particle motion will produce localized magnetic fields.¹⁶² The plasma gas is generally argon or nitrogen. Diatomic gases release energy through ionization and molecular recombination.¹⁶³ A secondary gas, commonly hydrogen or helium, can be added to increase the enthalpy and thermal efficiency of the system. The secondary gas will increase plasma velocity by broadening the thermal pinch effect.¹⁶⁴

Once the plasma is formed, it expands creating the plasma jet which exits the water-cooled anode. The plasma can reach temperatures of 30,000° K and can be sub or supersonic. The plasma jet can melt any known substance, which allows a wide variety of powders to be codeposited. Powders or wire feedstock are introduced into the system at the exit region of the nozzle. The feedstock materials become molten particles whose temperature and size greatly effect the resulting coating. Powders are the most commonly sprayed materials, but with the advent of high energy systems, wire can be sprayed just as efficiently.¹⁶⁴ Figure 1.23 illustrates the interaction of material as it is injected into the plasma plume.¹³⁶

Spray Materials

The high temperature of the plasma jet allows a wide range of materials to be deposited. The materials most commonly sprayed include metals, ceramics, and organics. A wide range of metals can be deposited in the form of wire or powder. Nonmetallic compounds, including carbides, nitrides, and borides, are common for hardfacing applications. Organic polymers can be deposited over wide

parameters and in very small thicknesses. Care must be taken to avoid thermal degradation.

Plasma Spray Parameters

Plasma spray parameters are critical in most applications. The synergistic relationship of gas flow rates (amount of gas introduced into the system), substrate distance, and plasma enthalpy all determine coating quality. An ideal coating would have a density near the equivalent to its constituents. Research to increase coating density focuses on parameter optimization and attempting to understand the inter-relationships of parameters.^{165,166,167} Real world coatings have oxide (air plasma spray), inclusions, and porosity with a wide range of particle sizes.

Particle behavior is very dependent on the thermal conditions of the plume. If the particles are not fully molten then the interparticle bonding will be poor. If particles are overheated then the substrate becomes a molten surface, with particles impacting and bouncing back. This bounce back yields inconsistent geometry which leads to higher porosity and bonded coating particles. If the plume is too hot, the smaller desirable particles will vaporize and be lost from the system. Working distance and plume velocity determine how long a particle is heated in the plume, thus directly affecting the particles behavior. Only through experimentation can an acceptable set of plasma parameters be attained.

The effects of the parameters on final coating properties are very system and material dependent. The performance of a 1080 steel coating was optimized by understanding the need to idealize particle size and distribution.³ Understanding the effects of plume temperature, gas flow, etc. lead to educated guesses of what may or may not work. Ultimately, trial and error is the only pragmatic approach to creating the optimum self-lubricating plasma sprayed coating.

1.2.7 Solid Lubrication / Plasma Spray Applications

Plasma spraying is a very diverse field with a great number of applications. Plasma spraying a solid lubricant to form a self-lubricating coating has previously been done by Ford Motor Co. in the automotive industry¹⁶⁸ and by NASA^{169,170} in the aerospace industry. Its application in the railroad industry as a friction and wear control mechanism has never been attempted. The literature available does offer some information as to the mechanisms of the coating process.

Self lubricating bearings, a predecessor to plasma sprayed or other composite solid lubricant coatings, were first introduced in 1927. These bearings utilized retained or "buried" graphite in a metal binder consisting of iron, bronze, etc.¹⁶⁸ To retain the graphite the bearing had to be heated to at least a thermoplastic state. This enabled the graphite to be impregnated within the bearing structure. These bearings were crude and did not demonstrate reduced friction unless significant wear was achieved to expose the graphite. The near molten state of the metallic binder did not allow for a controlled heat treatment. Self lubricating bearings have come a long way and are found in many industries, especially the aerospace field.

Newer bearing structures extend beyond metallic binders. Ceramic binders are frequently used for high temperature applications. These utilize high temperature lubricants such as lead oxide or calcium fluoride. Lower temperature bearings can use a polymeric binder coupled with graphite, MoS₂, or other dicalcogenides. These bearings can be used over a wide range of loads, temperatures, and environments. Often a bearing will be tailored for its specific application.

Sliney¹⁷¹ investigated solid lubricated bearings which consisted of a barium fluoride-calcium fluoride eutectic composition impregnated into a porous nickel or nickel/nickel chromium alloy. The load carrying capacity was shown to be much

greater for the nickel-chromium matrix as it had a higher yield strength. These coatings were intended for use at high temperatures (600-1000° C) and moderate loading (34 MPa) during sliding in air or a reducing hydrogen atmosphere. It was found with the addition of silver friction reduction was possible at temperatures less than 400° C. This material was recommended for use as a retainer material in ball bearings, sleeve bearing material, or possibly as a sliding contact seal material. It was realized that this solid lubricant material would be suitable for plasma spray deposition.

The plasma spray technique allowed for quick deposition of a lubricant film, while only minimally heating the substrate. Plasma spray allows for deposition of a combination of materials which are not amenable to surface heat treatment. Sliney¹⁷² also evaluated plasma sprayed solid lubricant containing coatings. The impregnated bearings discussed previously were structurally weaker and less dimensionally stable than a coated dense metal part. These coatings were developed to be used for aerospace applications where both low and high temperature lubrication was necessary. The coatings consisted of a nickel-chromium matrix, calcium fluoride, and silica glass. The glass is a special formulation to provide high temperature oxidation protection to the nickel-chromium matrix. The coating process involved plasma spraying a nickel and chromium bond coat. An excess thickness of lubricant coating was then plasma sprayed and finish ground to a mean thickness of 0.025 cm (0.010 in.). A high volume of silver (30%) was added to the lubricant coating to reduce low temperature (< 400° C) friction.

Performance was evaluated using a pin on disk machine in both vacuum and a dry nitrogen atmosphere. It was found that a coarse microstructure created local friction fluctuations which were undesirable under conditions of low velocity sliding and small area contact geometry; this suggests a more homogenous fine-grained structure would be desirable. The friction coefficient of the coating with silver remained at 0.2 over the range of 0 to 870° C. As the coating was multi-component it could be modified to meet specific

applications. Through plasma spraying, a composite material was created that would be difficult to produce by other means.

A solid lubricant film would be unlikely to have the durability required for wheel/rail interaction due to large loads and slide/roll ratios. A composite coating provides an alternative. A wear resistant matrix incorporating a solid lubricant has been the focus in the automotive industry, work by Sliney,¹⁷² and in this project.

A study by Solomir evaluated the performance of several plasma spray coated piston rings.¹⁷³ The piston rings and cylinder block were made of gray cast iron. Controlling wear became increasingly difficult given new performance requirements of marine engines. This experiment explored several wear resistant alloys both with and without a solid lubricant incorporated in the matrix.

Full scale testing of piston rings would involve installation into an actual engine. For over twenty coatings this would be time and cost prohibitive. The alternative involved spraying coatings onto gray cast iron rollers for testing in the Amsler twin disk wear testing machine. The bottom roller was made of the same grade gray cast iron as the cylinder wall. In the Amsler test two rollers were loaded against one another. They rotated in the same direction but at different speeds- yielding a slip or creep ratio. The amsler allowed for accelerated testing. The results showed a coating of blended alloys with 20-30% free graphite had the lowest wear (<1 mg when others were > 400 mg) and a friction coefficient of 0.10. The coating was tested at a load of only 500 N and 10% creep. These mild conditions would allow even uncoated cast iron to perform exceptionally well.

This experiment was of special interest because it employed the use of the Amsler machine to evaluate the wear performance of its coatings. The same equipment has been used in the current program. Evidence that graphite matrix coatings perform well under light loading conditions is illustrated in this ring experiment and also in the current research project. The Amsler however, does not

represent conditions in an internal combustion engine. Nevertheless, the coating performance results are of interest.

Ford motor company also used plasma spray to produce self lubricating coatings. They have patented their process for coating a cylinder wall.¹⁶⁸ This process involves plasma spray coating the cylinder wall with a low friction, high durability material. The material is a mix of wear resistant compounds such as, silicon carbide and intermetallics of nickel, chromium, vanadium, etc. The material also includes metal encapsulated solid lubricants of graphite, CaF_2 , and MoS_2 . The engine block may then be made from another material with better heat transfer properties. This idea also reduces the extensive design required to ensure near elastohydrodynamic lubrication on every surface inside the engine. The process can be performed using lubricant cored wire¹⁷⁴ or a solid lubricant powder.

Ford uses a metal encapsulated solid lubricant powder in lieu of plain powders. Solid lubricant powders have several advantages. The lubricant is encapsulated resulting in less degradation while in the plasma jet. Powder spraying relies on the particles being partially melted to adhere to the substrate. Graphite will never melt, thus metal encapsulation provides a means of retention not otherwise possible. The increased density by encapsulation gives better control of particles in the highly turbulent plasma jet. The metal used to encapsulate the solid lubricant will include an alloy which is adherently compatible with the cylinder bore wall metal and has a hardness between 20-30 Rc. The wear resistant particles and lubricant powders will be retained at a near equal distribution. The coating is applied to a thickness of 40-250 μm . Excess material is honed away to produce a final coating thickness of 25-175 μm .

The cored wire deposited using twin wire arc follows the same principle as the powders. Lubricants and wear resistant materials are carried by molten metal drops to the substrate. The coating, independent of spray process, which is formed on the cylinder wall has a certain degree of porosity. As solid lubricants are worn away

local porosity increases. This porosity acts as an oil reservoir, promoting fluid lubrication. This coating can be applied directly to the cylinder wall or to a liner, which is inserted into the block during engine assembly.

Plasma sprayed nickel-graphite coatings were evaluated by Ghouse.¹⁷⁵ These coatings were made from nickel-graphite powder only as opposed to being an additive. The coatings were tested using a disk on flat plate machine. The friction coefficient was 0.1 at a 100 mg load and increased to a maximum of 0.2 at a 10 kg load. This mild testing is difficult to compare to the severe wheel/rail environment. The mild steel used as comparison had a friction coefficient of 0.35 at a load of 10 kg.

The experiments with solid lubricants have always been application driven. This gives information regarding mechanisms and processes, but rarely can direct comparisons be made. The current project is based on empirical results. Each iteration is dependent on previous findings. The research plan involves a systematic evaluation of three types of solid lubricants. The unique characteristics of this project dampen the direct usefulness of the literature, but the basic understanding given by the literature as to predicting how certain materials behave is invaluable.

1.2.8 Background of current research.

The literature review is useful in the evaluation and optimization of coatings in this project. The path of research is based heavily on coatings work done at OGI. McMurchie provided the fundamental parameters for producing 1080 steel coatings which had good wear resistance.³ The scope of the project had been to reduce friction and wear and possibly provide a lubricant reservoir. This was the rationale for expanding the research to include solid lubricants.

Early work by McMurchie involved the plasma spraying of cored wire and music wire. Both of these were similar in composition to

the 1080 spray steel wire used currently. Early coatings had poor durability and often debonded. Through mostly trial and error the parameters and materials required to create a durable coating were narrowed to an acceptable envelope.

Evaluation techniques by McMurchie for the 1080 steel coatings involved metallography, image analysis, and observation in a scanning electron microscope. The coating's performance, both friction coefficient and durability were assessed using the Amsler twin disk wear testing machine. Coating evaluation was expanded for the current project to yield greater understanding of the coating structure and degradation.

Wear testing each coating at every possible parameter was time prohibitive. Single splat analysis³ allowed for observation of individual particles. A glass slide was passed through the plume to collect a thin layer of coating. By observing the individual splats assessment of potential coating quality became possible. The individual splats ideally would be flattened upon impact with the glass slide or substrate. Uniform splats and distribution of mostly small with some large particles indicated optimum parameters had been achieved. Deviations required adjustment of various plume parameters such as working distance or gas flow rates.

Ultimately a high quality 1080 steel coating was developed that provided some degree of friction reduction (0.45 vs. 0.7-0.9).³ This coating had a wear rate an order of magnitude less than an uncoated rail steel. Parameters for reproducing this coating were established. The objective of the current research was to incorporate a solid lubricant into this coating to further reduce friction and wear. This coating must reduce friction in order to replace conventional grease lubrication.

To create the composite coatings the Plazjet hypersonic plasma system was used in conjunction with wire and powder feeders. A large part of the project involved developing parameters to produce predictable structures. The goal was to produce coatings with varying volume fractions of solid lubricant. The coatings can

then be characterized on the basis of wear performance and friction reduction. Optimizing plasma spray parameters was an ongoing process.

All work stemmed from ongoing analysis so that a final product could be achieved in the least amount of time. The rail road industry required a durable surface coating be created that could reduce friction and survive the hostile rolling / sliding contact of wheel and rail. In essence this project was the marriage of industrial end use demands and thorough academic analysis to yield a product which was both practical and useful while being well understood and documented.

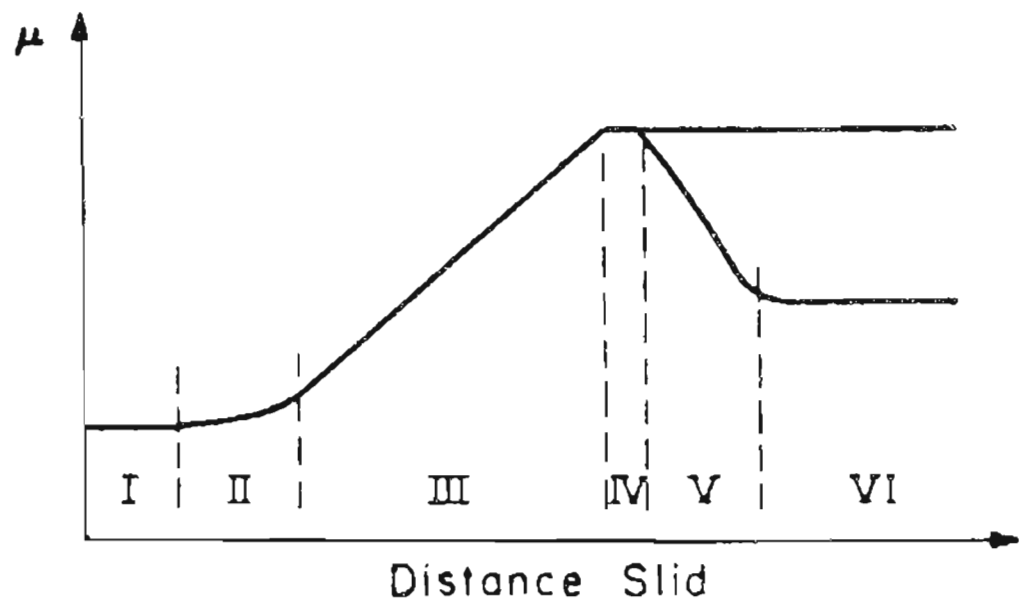


Figure 1.1. The six stages of friction as defined by Suh.¹⁶ Stage I, ploughing by surface asperities. Stage II, increase in adhesion between bodies. Stage III, rapid increase in number of wear particles. Stage IV, wear particles generated equals number lost. Stage V and VI, reduction of friction due to varying material behavior.

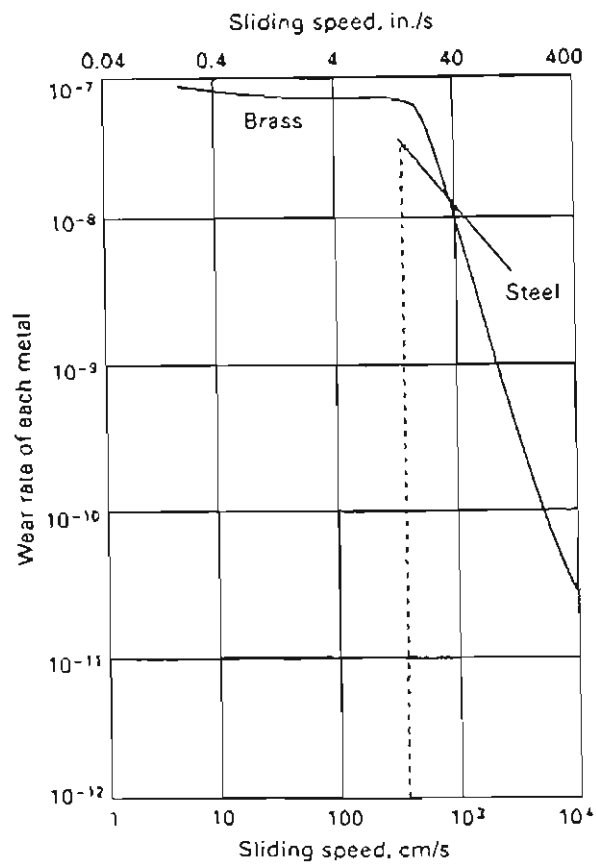


Figure 1.2. Plot of wear rate versus sliding speed for 60-40 brass worn against high-speed tool steel in which brass hardness differs from steel hardness. ³²

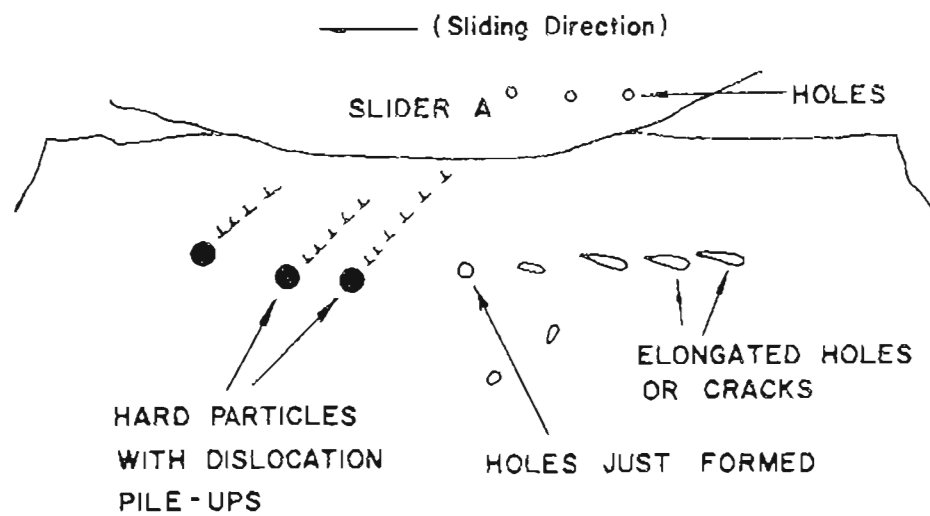


Figure 1.3. The process of wear particle formation by the shear deformation of voids. The elongated holes form cracks which network together to form loose wear sheets. ³³

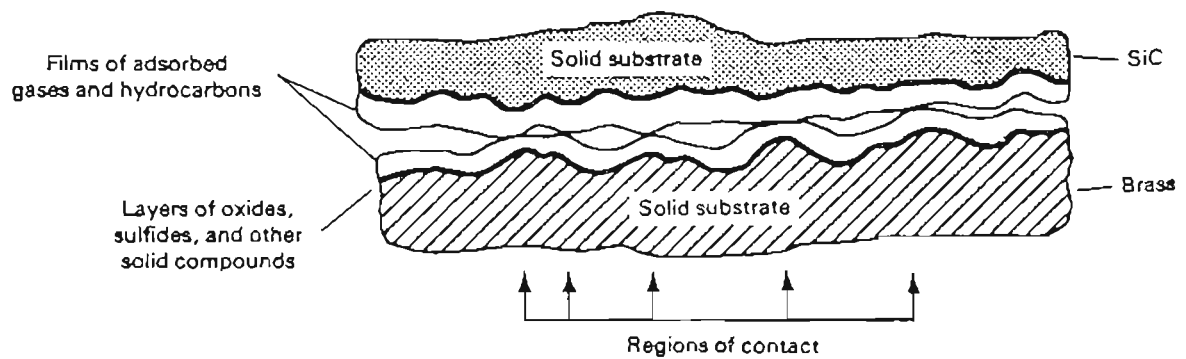


Figure 1.4. Schematic of a bond bridge produced when two solid surfaces are in contact with each other. When two rough surfaces are brought together, actual contact occurs only in a few isolated regions. ³²

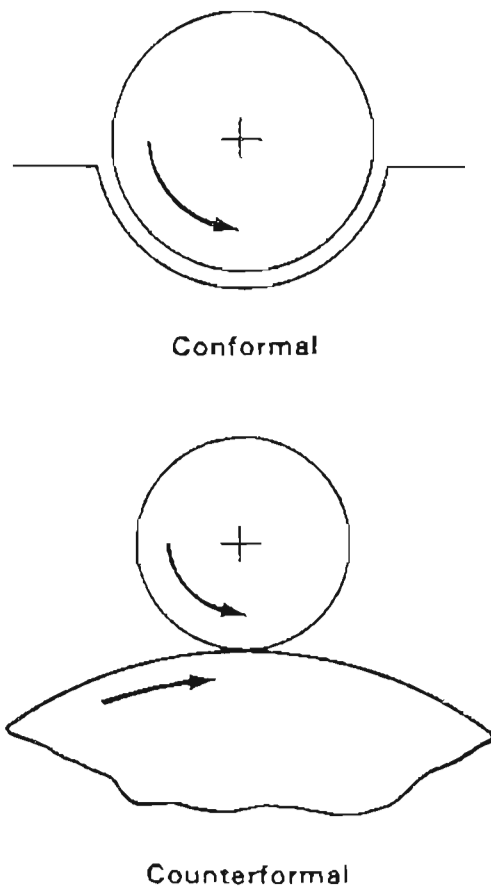
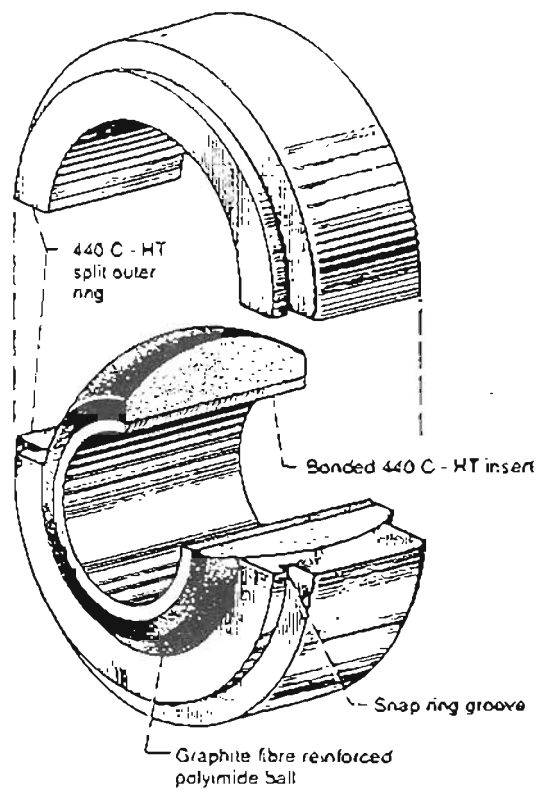
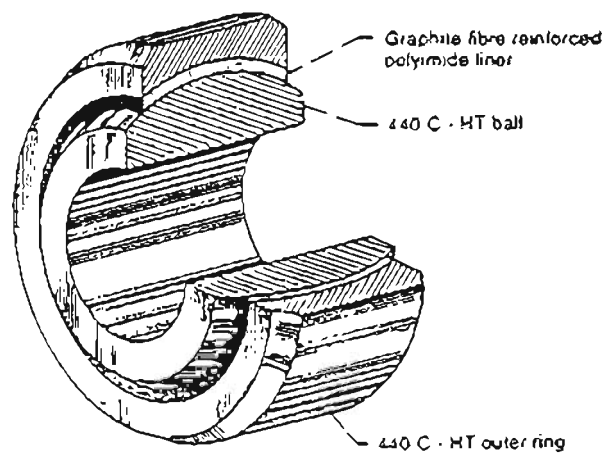


Figure 1.5. The two types of geometry for lubricated surfaces: conformal and counterformal. Counterformal geometry closely approximates the rolling / sliding contact of wheel and rail. ⁴²



(a)



(b)

Figure 1.6. Test bearings employing graphite reinforced polyimide (GFRPI). a) Bearing design featuring GFRPI ball. b) Bearing design featuring a steel ball and a GFRPI liner bonded to a steel outer ring. ⁵¹

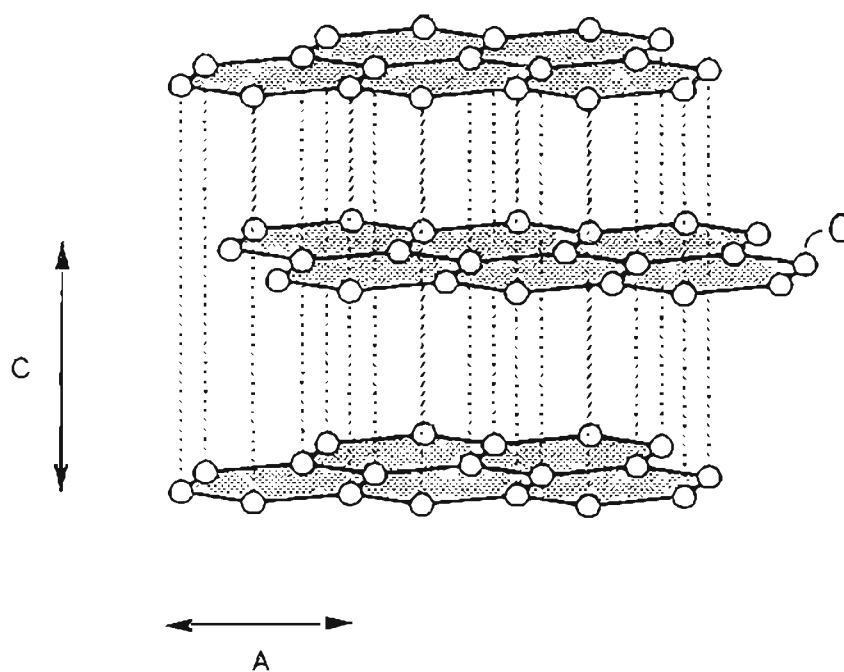
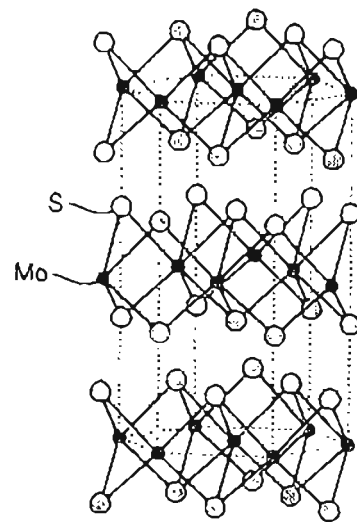
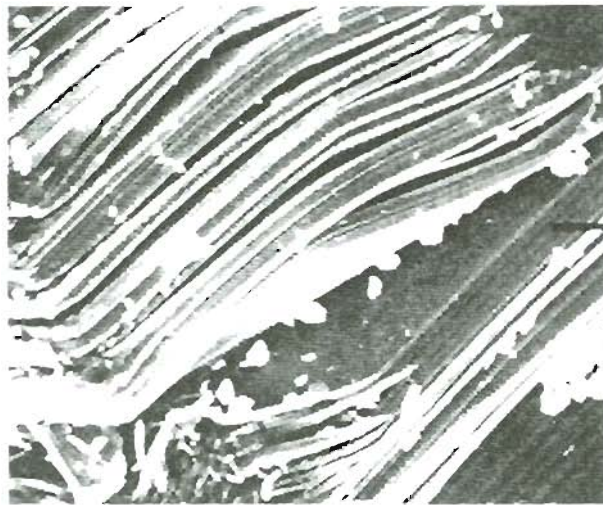


Figure 1.7. Layer lattice structure of graphite. $a = 1.4 \text{ \AA}$,
 $c = 3.4 \text{ \AA}$. 53



(a)



5 μm

(b)

Figure 1.8. Structure of molybdenum disulphide. a) Schematic drawing. b) SEM photograph of the layered MoS_2 structure. Layers are on the order of $1 \mu\text{m}$ thick. ⁵³

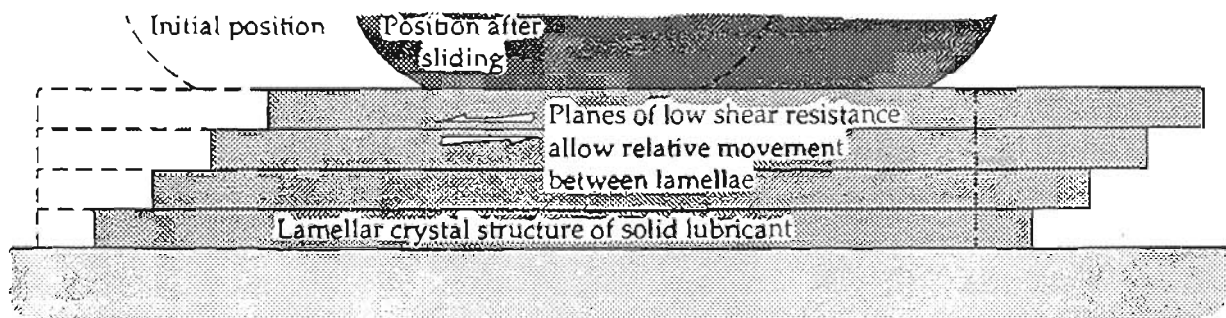


Figure 1.9. Mechanism of lubrication by lamellar solids. The lamellae slide over one another at relatively low shear stresses. 58

Friction Coefficient vs. Ambient Pressure

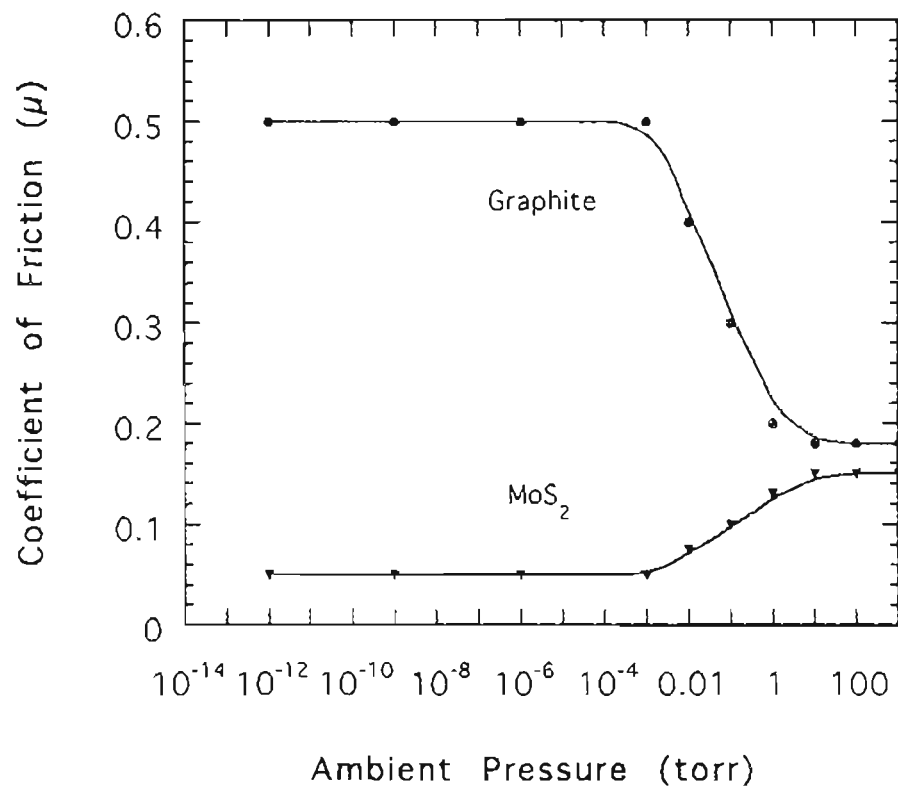


Figure 1.10. Graph of friction coefficient vs. ambient pressure for graphite and MoS_2 . At low pressures graphite friction is high due to lack of adsorbed gases. MoS_2 lubricates better when contaminants and gases are absent.⁴⁶

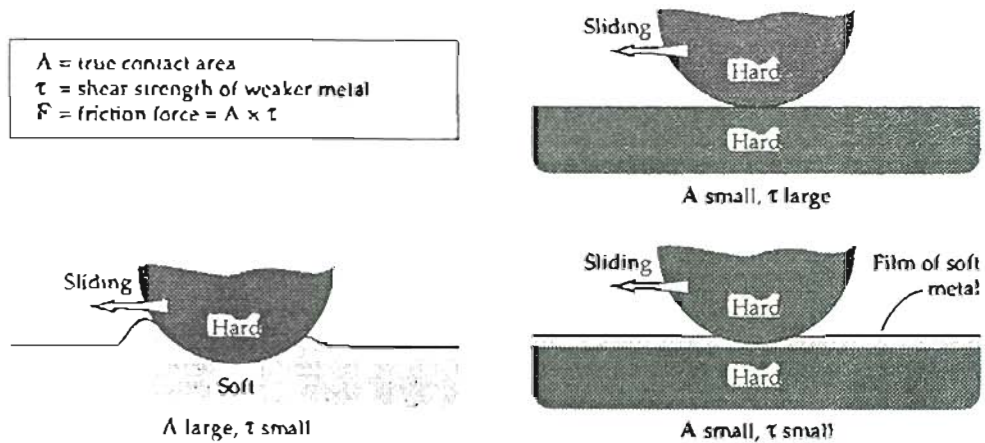


Figure 1.11. Mechanism of friction reduction by soft films on hard substrates. The soft material has a large asperity contact area. The hard substrate has a reduced contact area, and subsequently reduced friction. ⁷⁴

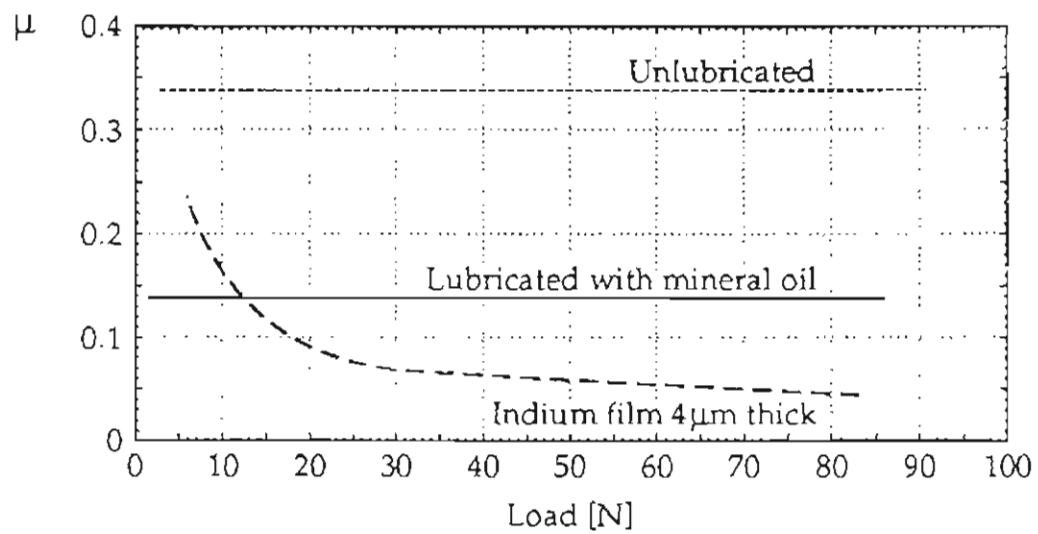


Figure 1.12. Effect of an indium surface film on the frictional characteristics of steel. A thin film of soft metal applied to a hard substrate decreases friction by reducing asperity contact area.⁷⁵

Friction vs. Load for Copper on Copper

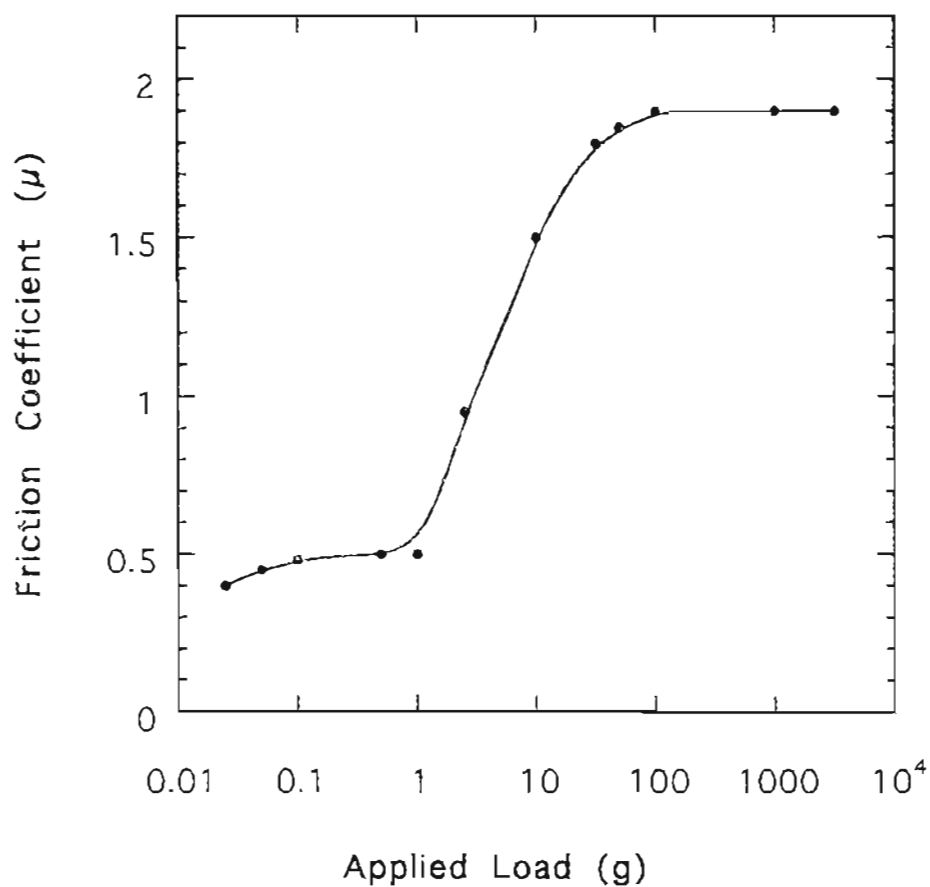


Figure 1.13. The effect of load on the coefficient of friction of copper slid against copper. At a load of 1 gram the oxide layer is broken, creating metal on metal contact. ⁸³

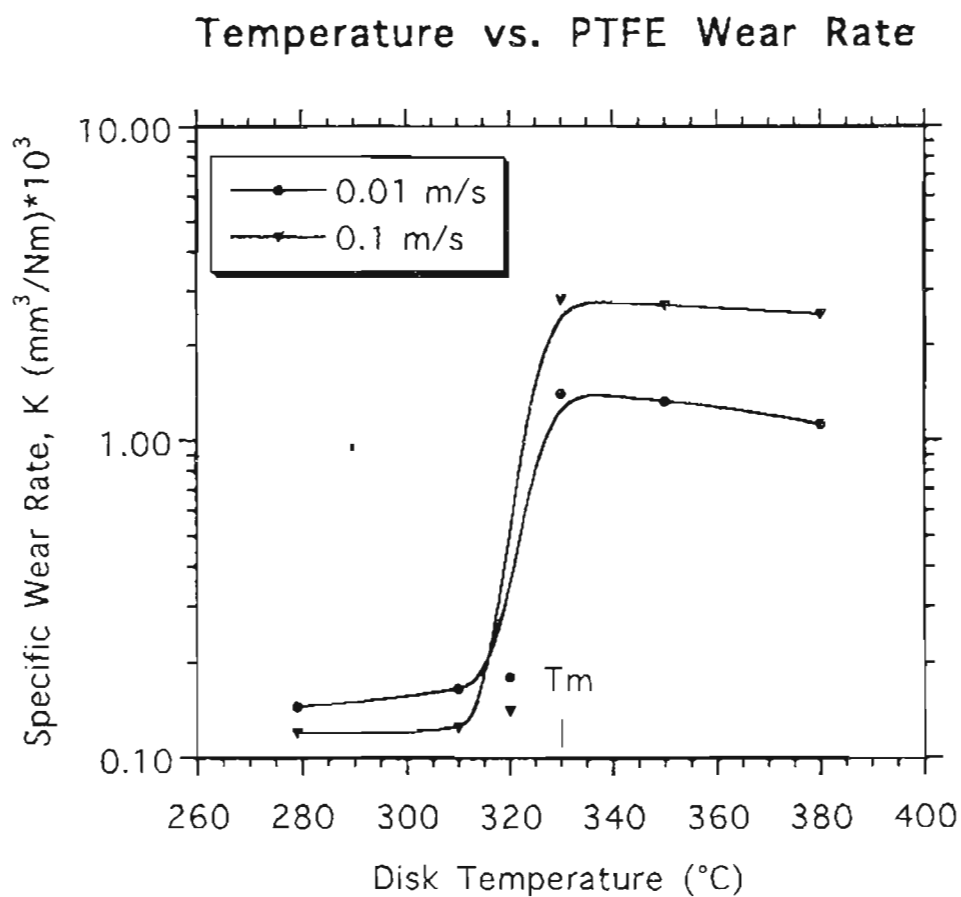


Figure 1.14. Wear of PTFE as a function of temperature. The wear increases rapidly around the melting point, 320°C .⁹⁰

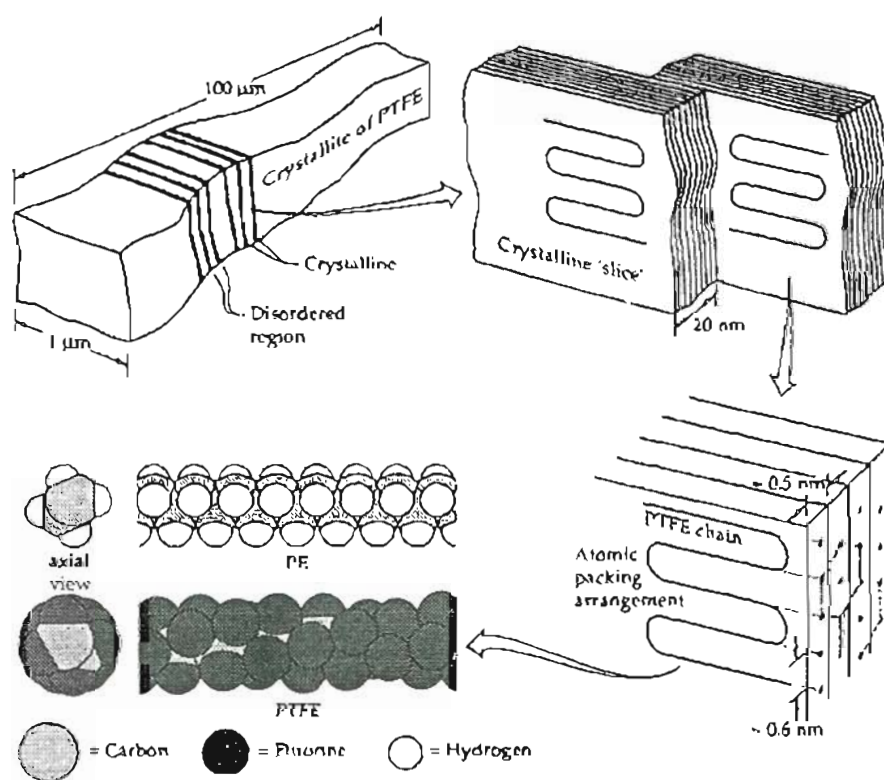


Figure 1.15. Molecular and crystalline structure of PTFE. 94

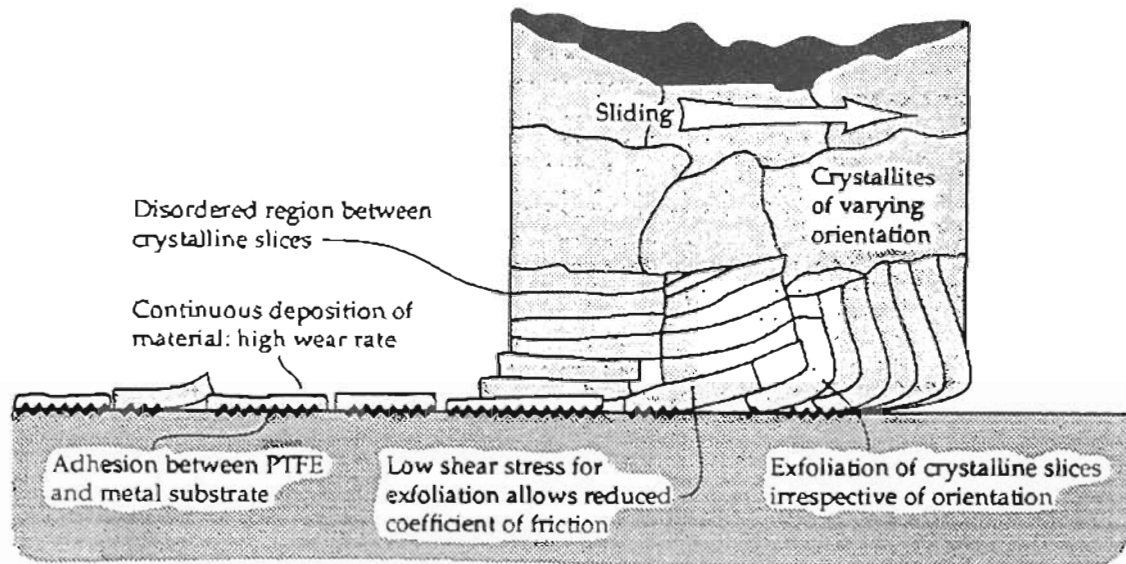


Figure 1.16. Wear and film transfer mechanism of PTFE. The block of PTFE loses material in a series of laminae which results in low friction but a high wear rate. ¹⁰⁰

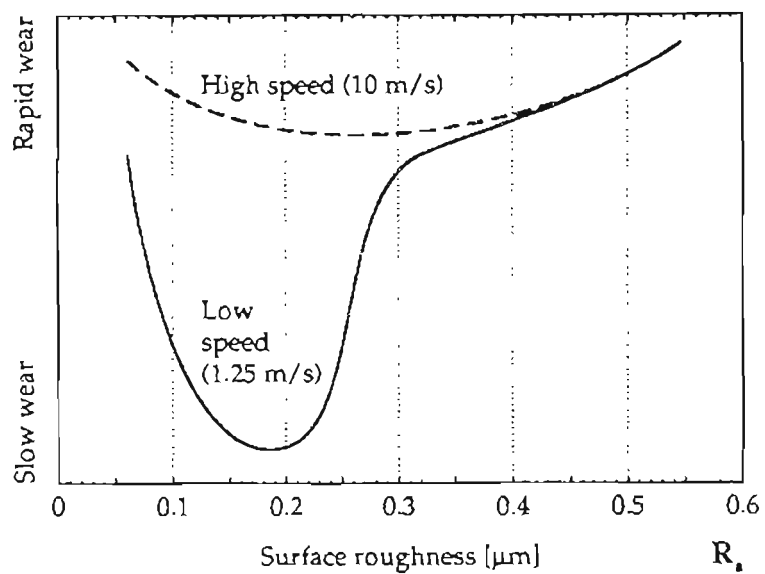


Figure 1.17. Effect of counterface roughness on the wear of UHMW. This figure illustrates the existence of an optimal surface roughness for low wear. 110

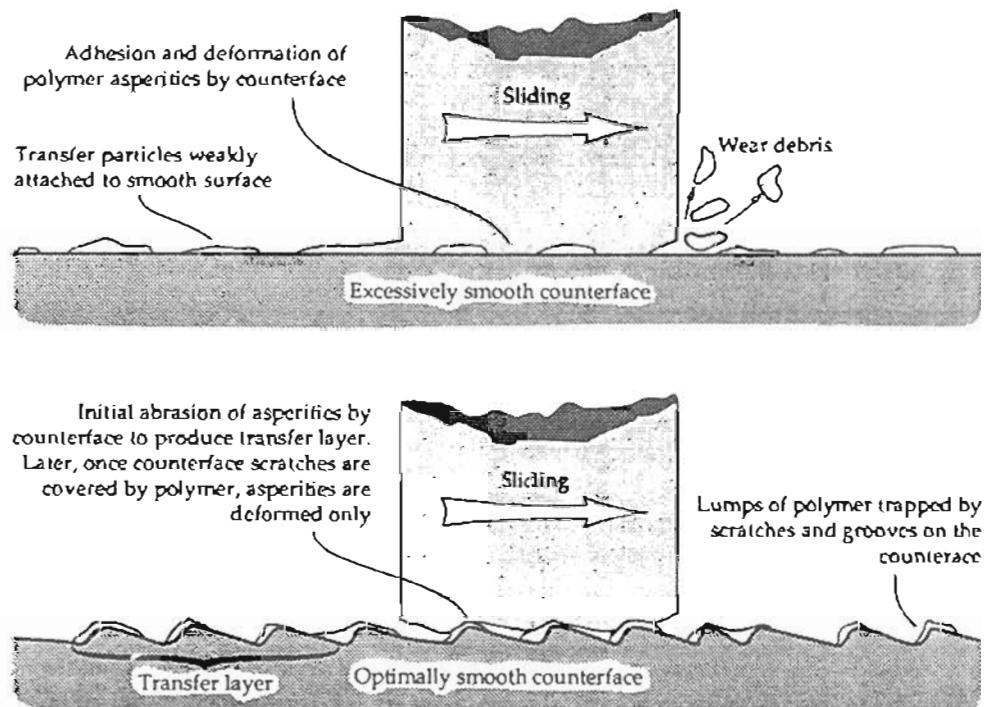


Figure 1.18. Polymer wear process on excessively smooth surface and on a surface with optimum roughness. The optimum roughness would benefit a closed system where a polymer film would have a chance to form. ¹¹³

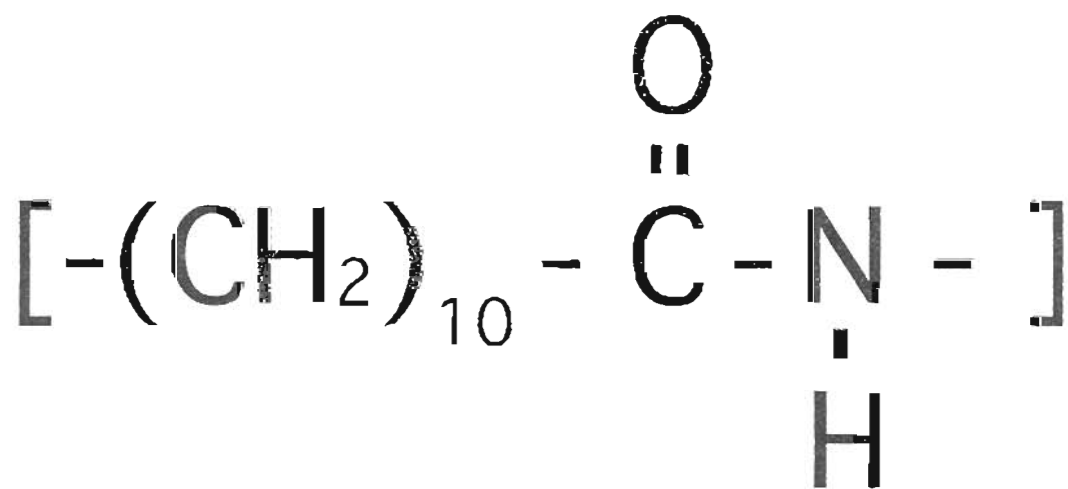


Figure 1.19. Molecular structure of Nylon 11. One mer consists of 10 methylene groups and one carbonyl group. ¹¹⁸

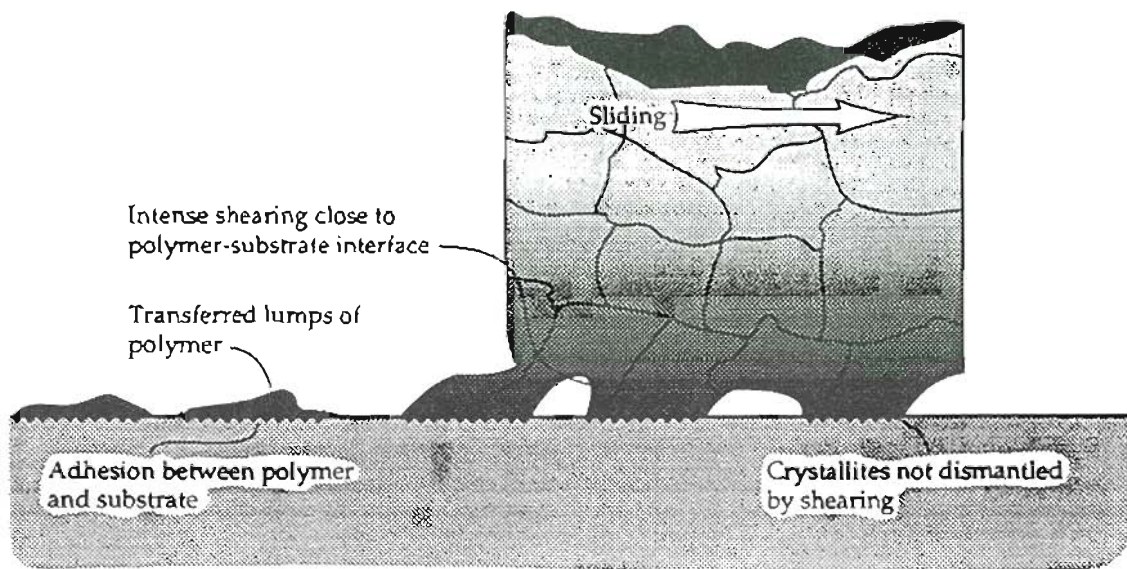


Figure 1.20. 'Lumpy' transfer mechanism of most polymers during sliding wear caused by random crystal orientations. The 'lumps' are on the order of $1 \mu\text{m}$ in diameter. ¹⁰⁰

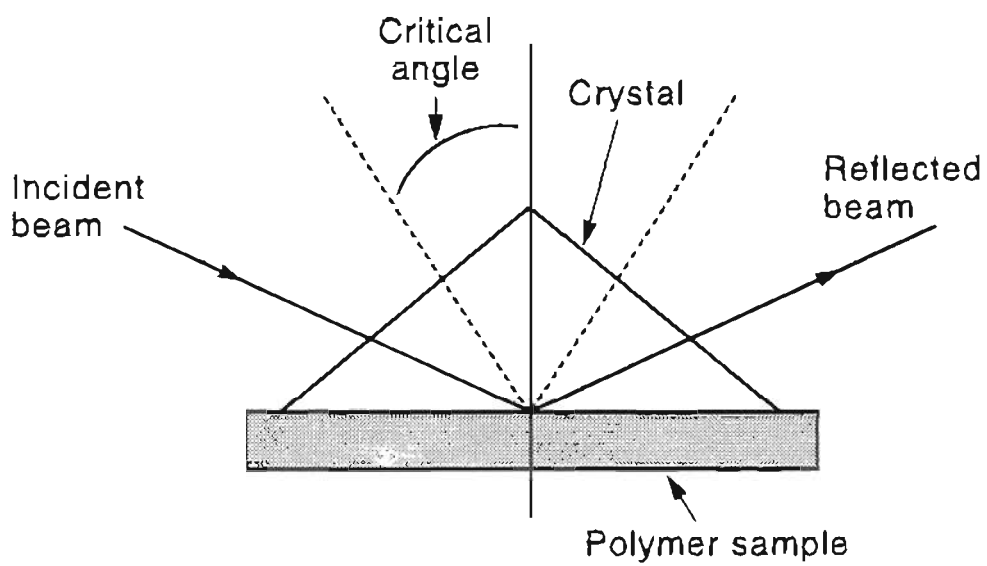


Figure 1.21. Schematic of attenuated total reflectance (ATR) crystal used in conjunction with FTIR analysis of in situ polymers. ¹²⁸

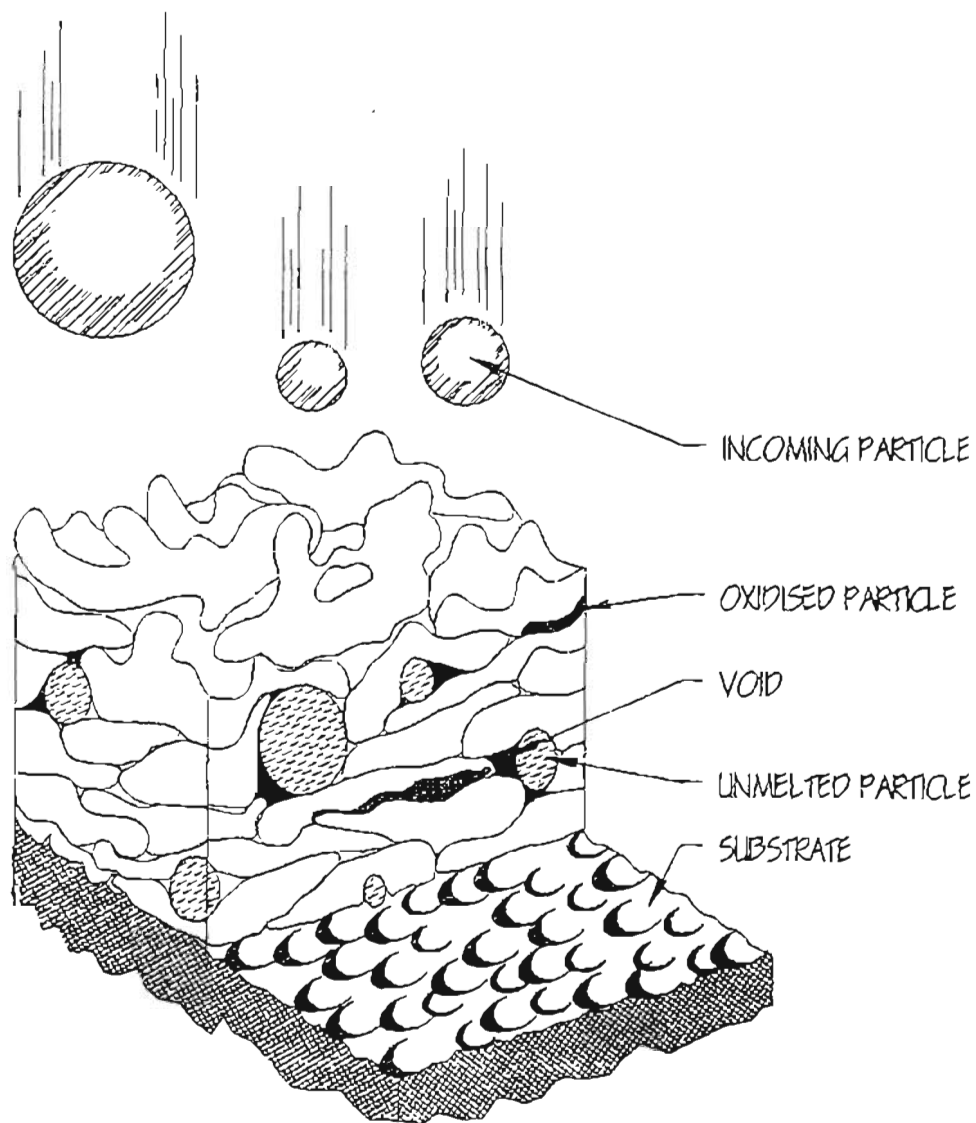


Figure 1.22. Schematic of a plasma-sprayed coating. The structure consists of solidified particles, porosity, unmelted particles and impurity inclusions.¹³⁶

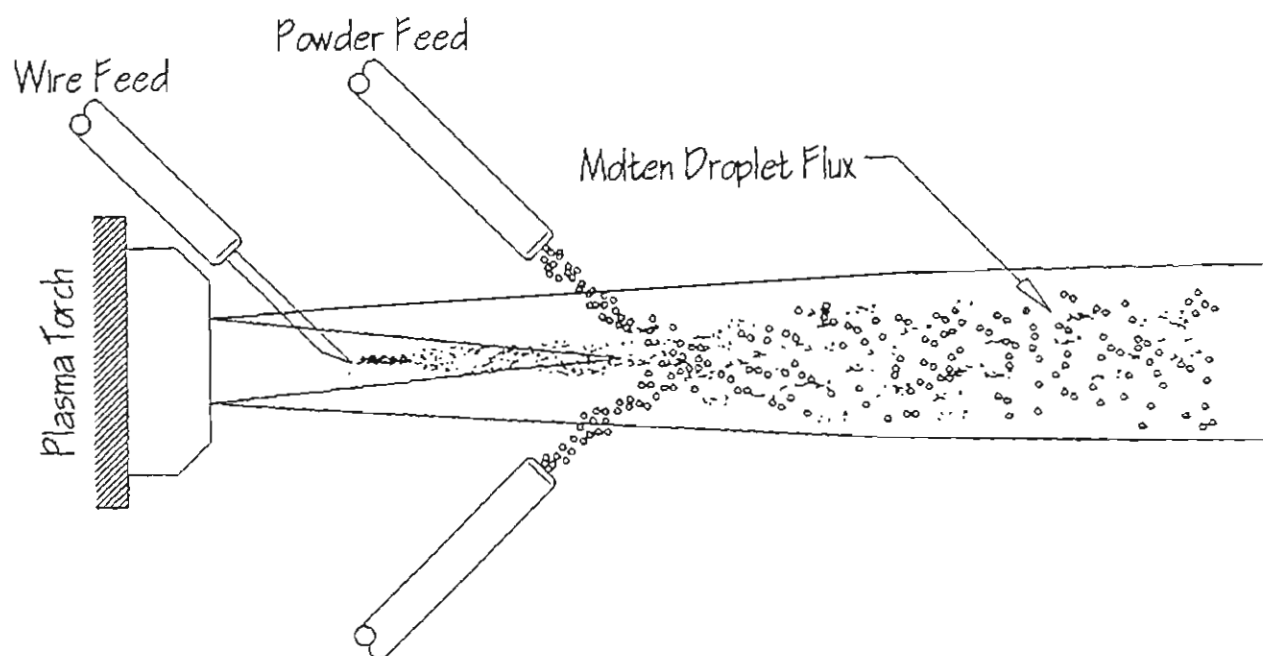


Figure 1.23. Schematic drawing of the particle flux formed when wire and powder are injected into the plasma plume. 136

Chapter Two Experimental

2.1 Introduction

The experimental procedure to produce steel coatings with or without a second phase lubricant is presented. This includes a description of the coating materials and plasma spray equipment. The operation of the equipment and method of coating deposition is also presented. Coating evaluation included microstructural characterization and wear performance, which consisted of durability and friction behavior. The procedures for coating evaluation are described in detail.

2.2 Materials

2.2.1 Spray Materials

The steel coating material consisted mainly of 1.6 mm (0.0625 in.) 1080 spraysteel wire. 308 L-Si stainless steel wire (1.6 mm) was used in a limited number of polymer / steel coatings. The vast majority of coatings were formed by the deposition of 1080 steel plus a solid lubricant powder or wire. Second phase lubricant powders included graphite, nickel-coated graphite, and copper. Overlay lubricants, which resided on the surface of the coating versus being dispersed in the coating, included several polymers.

Graphite

An exhaustive search of commercially available graphite powder was performed. Two forms of graphite were available. The first was a high purity graphite flake powder. This powder was very fine ($< 50 \mu\text{m}$), with a particle morphology consistent with thin shavings. This fine graphite powder was used for a limited number of experiments. The other type of graphite powder was too coarse ($> 1 \text{ mm}$) and had low purity. This coarse powder was not used for any experiments. The bulk of the plain graphite used was produced in-house. Solid graphite bars were machined using a lathe, and the turnings collected. Feed and spindle speeds determined the size and shape of the resulting graphite particles. Graphite particle size was targeted at 1 mm before post-processing. The particles were sieved using a shaker and several screens of decreasing size to separate the powder. This process allowed large friable particles to break apart into smaller stable particles. Better than 90% of the rough graphite particles ended up $500 \mu\text{m}$ or less.

Nickel-Coated Graphite

Two samples of commercial nickel-coated graphite were obtained. The first powder was 25% graphite by weight and 57% by volume. The second powder was 37% graphite by weight and 70% graphite by volume. Both powders were nominally $100 \mu\text{m}$ in size. The 70% volume graphite powder was used due to commercial availability. The density of the 70% graphite powder was 1.42 g/cm^3 . Figure 2.1 is an SEM photomicrograph showing the morphology of the nickel-coated graphite powder.

Gray Cast Iron

Gray cast iron powder was obtained. The graphite volume fraction was nominally 30%. The powder size was on the order of

350 μm . Attempts were made to manufacture cast iron powder in-house through the use of lathe and mill turnings from cast iron bar stock. The turnings were collected and ball milled to reduce particle size. Ball milling was performed at room temperature, and in an attempt to embrittle the turnings, in a liquid nitrogen atmosphere.

Copper

High purity 1.59 mm (0.0625 in.) OFC Copper wire was used. Later experiments employed a 100 μm OFC copper powder. Both wire and powder are readily available commercially.

Polymers

Several sprayable polymer powders were employed. The primary materials included nylon 11 (herein referred to as nylon), nylon 11 blended with solid lubricants, ultra high molecular weight polyethylene (UHMW), UHMW blended with solid lubricants and PTFE (Teflon™). Torlon and Kynar were used as secondary polymers in that they were only used for a small number of experiments. All of the polymers were available commercially.

Powder properties were adjusted through mixing of different materials. The ratios reflect weight proportions not volume. Nylon was mixed with fine graphite powder in proportions of 4:1. Nylon was also mixed with MoS_2 powder in proportions of 2.5:1. Both graphite and MoS_2 additives were < 25 μm in size. UHMW was also mixed with graphite and MoS_2 . Two powders were made, with the proportions being 4:1 for the UHMW plus graphite and 2.5:1 for the UHMW plus MoS_2 . PTFE was sprayed as pure powder but was also mixed with nylon. The three batches of PTFE plus nylon included mixtures of (%) 75-25, 50-50, and 25-75.

2.2.2 Testing Material

Lab test substrates used for spraying consisted of flat mild steel coupons, cold-rolled round steel blanks, and specimens for Amsler testing. The mild steel coupons were 75 mm x 25 mm and 6 mm thick. The Amsler rollers were machined from standard carbon, 300 BHN rail head. Several different rails were used, all of which were similar in composition and hardness. The geometry of the Amsler roller is shown in Figure 2.2. The mating Amsler roller was machined from class C wheel steel. The average compositions of standard carbon rail steel and a class C wheel steel are listed in Table 2.1 and 2.2, respectively. Round doughnut-shaped blanks were machined from stainless or mild steel. The outer diameter was the same as an Amsler roller but without the top hat profile.

Full size steel coupons were obtained for full scale testing in the AAR track lab and at the FAST testing facility. The geometry of the coupons was similar to a rail head but without the web or foot. Sections of both head hardened and 300 BHN premium rail steel were also obtained, in both new and worn condition.

2.3 Plasma Spray Equipment

The plasma spray system consists of an energy source, gas source, plasma gun, and a control system. The energy source consists of two DC 100 kW rectified power supplies wired in series. The maximum power output of the power supplies was 200 kW at 400 V and 500 A. For this research only nitrogen and hydrogen were used as plasma gases. The plasma gun employs a thoriated tungsten cathode and copper anode. These are contained in a water cooled brass gun assembly. Figure 2.3 is a schematic of the plasma gun illustrating the water and gas flow paths. A high output pump circulated 26.5 liters per minute (lpm) through the gun. The gases and power were regulated with a mass flow control system. The whole plasma system was contained in a sound deadened room. A

water curtain backdrop collected any overspray, while a high volume fan removed any residual powder or particles.

Secondary equipment to the basic plasma system included wire and powder feeders, sample cooling fixtures, and sample holding fixtures. The wire feeders were similar to those used in conventional MIG welders. Two wire feeders were available, making twin wire spraying possible. The wire feed rate was controlled at each individual feeder. Wire was delivered through conduit cable to fixturing on the gun. The tip of the conduit cable contained a 1.9 mm i.d. ceramic insert to guide the wire in a true direction. The powder feeder allowed for controlled delivery of 25-900 μm powders. The volume of powder as well as the powder velocity were adjustable.

A fixture attached to the gun held the wire feed conduit and powder feed tubing. The fixture allowed for variable injection sites and angles. Wire, powder, or both could be fed at 90 or 45 degrees normal to the plume. The powder or wire could be injected as close as 10 mm or as far downstream as 165 mm. Current fixturing could accommodate two wire feeders and two powder feeders. Powders are generally fed diametrically opposed to ensure the bulk remains in the center of the plume. A photograph of the plasma gun and traversing table ready to spray Amsler rollers is shown in Figures 2.4a and b. Figure 2.5 is a closeup of the plasma gun itself showing wire and powder feed tubes.

To prevent overheating, a pair of gas nozzles delivered cooling gas to the surface of the specimen. The cooling gas was predominantly CO_2 , though dry compressed air was also used. The cooling fixturing changed with specimen size. This simply consisted of using different shaped cooling tubes to deliver gas to a given geometry, either round amsler rollers or flat steel coupons.

The fixture to spray Amsler rollers consisted of a steel bar attached to a variable speed motorized chuck. The steel bar was the same diameter as the Amsler roller center hole. Steel tubing protected the exposed bar from metal overspray. Figure 2.6 illustrates Amsler rollers ready to spray. Flat coupons to be

sprayed were attached to a graphite rod which was machined flat on two sides. The rod was suspended from the chuck. The rod accommodated one to four flat coupons, and is illustrated in Figure 2.7.

2.4 Plasma Spraying Technique.

2.4.1 General Procedure

Although different parameters, materials, and combinations thereof were employed in this research the basic method of applying a coating, from surface preparation to post processing, remained constant. The technique varied slightly for coating application to large rail specimens.

Surface Preparation

Surface preparation consisted of degreasing the surface of the material using an organic soap and water. Amsler rollers were grit blasted using a standard grit blasting system. The grit blasting gun had an exit orifice size of 7 mm with the system air pressure being 80 psi. Grit consisted of steel shot and 500 μm alumina (Al_2O_3) particles. The samples were washed in acetone to remove any residual contamination.

Rail sections required that a form fitting, portable grit blast booth be constructed. The booth surrounded the rail to prevent grit from escaping and provided a grit reservoir. A schematic and photograph of the booth showing its configuration are shown in Figure 2.8a and b, respectively. The steps of the surface preparation were modified to cleaning with Al_2O_3 (alumina) followed by surface roughening with steel shot. This was again followed by a thorough acetone rinse. These processes were done immediately prior to coating deposition.

Plasma Spray Procedure

The mass flow control unit fed primary gas into the gun and a high frequency spark ignited the gas. Secondary gas was then introduced, and gas flows were adjusted to the desired rate. At this point the coating material, wire or powder, was fed into the plume. The plume was traversed manually across the specimen at speeds varying between 0.20 and 0.25 meters per second. Application of the polymers required a traverse speed of 0.50 to 0.75 meters per second. The number of passes was adjusted to give the desired coating thickness. All coatings were sprayed with a minimum of 0.1 mm 1080 steel before second phase lubricants were added. The amount of time the sample was traversed upon was also recorded. The specimen was cooled with compressed CO₂ gas or air directed at the specimen's surface.

Gas flow defines the rate of delivery of the primary and secondary gas. The units are in standard liters per minute (slpm). The working distance is the length in mm from the anode opening to the substrate. Injection distance is the measure in mm from the opening of the anode to the point at which powder or wire entered the plume. Injection angle was the angle normal to the plume at which wire or powder entered. Powder gas flow was the rate of carrier gas from the powder feeder. Powder feed rate was defined as the RPM of the feed wheel within the powder feeder.

The gas flow and working distance are abbreviated as: primary gas (slpm)/ secondary gas (slpm)/ working distance (mm). For this research the primary gas was nitrogen and the secondary gas was hydrogen. 230 slpm N₂ / 30 slpm H₂ / 235 mm were the standard parameters for spraying steel onto Amsler rollers.

2.4.2 Solid Lubricants

Each second phase lubricant required optimization of spray parameters. This included varying the parameters defined above.

For each type of lubricant the exact spray technique is defined. The second phase lubricants were graphite, cast iron, nickel-coated graphite, and copper. The overlay lubricants were various polymers, with or without solid lubricants. The exact spray parameters for each test are presented in the results section.

Graphite

Early coatings with graphite were sprayed on flat coupons. A variety of gas parameters and injection sites were attempted. The injection distance ranged from 25 mm to 165 mm. The materials included a graphite powder made in-house and a commercially obtained graphite flake. Gas flow rates varied between 200 slpm N₂ and no secondary gas to 270 slpm N₂ / 110 slpm H₂. The working distance was 225 mm. The powder feeder RPM varied between 10 and 15.5. Powder feeder carrier gas varied between 40 and 85 L / min.

Amsler rollers were spray coated based on the results of the coupons. Gas parameters varied from 200 slpm N₂ and no secondary gas to 250 slpm N₂ / 100 slpm H₂. The working distance was again 225 mm. Powder feeder RPM ranged from 10 to 18 and the powder carrier gas flowed from 28 to 57 L / min. Powder injection distance varied from 5 mm to 85 mm at 45 or 90 degrees. Coating thicknesses were targeted between 0.5 mm and 1 mm. Some tests employed two 1080 steel wires injected at the standard 15 mm and 35 mm. One or two powder injector tubes were used. Multiple rollers and a witness sample were sprayed at each parameter.

An aerodynamic shield was introduced to increase graphite deposition efficiency. The shields were manufactured from a solid piece of graphite. The shields were free standing from the other fixtures. Two shields were made, the second shield iteration was equipped with backside cooling tubes. The first iteration is illustrated in Figure 2.9, and the second iteration in Figure 2.10.

Nickel-Coated Graphite

Nickel-coated graphite powder was co-sprayed with 1080 steel wire. The spray conditions were similar to those used to spray graphite, except an aerodynamic shield was not used. Preliminary samples were sprayed to fine tune the system. Amsler rollers plus a round witness sample were sprayed at varying parameters. These early tests confirmed the parameters were acceptable. The gas parameters remained at 230 slpm N₂ / 30 slpm H₂. The working distance was increased to 235 mm. Powder injection via two tubes was at 45 degrees with an injection distance of 25 mm. Powder feeder gas flow rate varied between 37 and 45 L / min. Powder feed rate (RPM) and coating thickness became the primary variables.

With the basic parameters established several test matrices were performed to determine the effect of coating thickness and graphite volume fraction. The matrices included coatings which were 0.25 mm, 0.5 mm and 1 mm. Powder feed rate varied between 5.0 RPM and 18.5 RPM. Graphite was dispersed in the entire coating matrix in two sets of tests. The remainder of the tests were done with graphite dispersed in only the top 30% of the coating. A set of coatings was produced using a low feed wheel in the powder feeder. The wheel allowed 60% of the powder to flow at a given RPM, as compared with the original powder feed wheel. The low feed wheel permitted reduced volume fractions (< 5%) of graphite to be deposited.

Cast Iron Powder

Cast iron powder was deposited with 1080 steel wire onto Amsler rollers. The variables were similar to the nickel-coated graphite coatings. The gas parameters were 230 slpm N₂ / 30 slpm H₂, with a working distance of 235 mm. The injection distance was 15 mm for the first powder and 85 mm for the second, both at 45 degrees. The powder feed rate varied between 2 and 10 RPM, and the

powder carrier gas flowed between 25 and 31 L /min. One of the coatings was sprayed with two 1080 steel wires.

Copper wire

Copper wire and 1080 steel were initially sprayed onto flat steel coupons for metallographic examination. These early tests encompassed the spraying of more than twenty steel coupons. Within these tests several variables changed, the wire feed rate, wire injection distance, and the wire injection angle. Wire feed rate ranged from 1.4 kg/hr to 4.8 kg/hr. The wire injection distance was between 15 and 85 mm at 45 degrees. The gas parameters remained constant at 230 slpm N₂ / 30 slpm H₂. Working distance was 225 mm or 235 mm.

Based on the microstructural information from the coupons, Amsler rollers were sprayed with copper wire and 1080 steel. Gas parameters were held at 230 slpm N₂ / 30 slpm H₂, with a working distance of 235 mm. The wire feed rate again varied between 1.4 kg/hr and 4.8 kg/hr. The injection distance was 10 to 110 mm with a feed angle of 45 or 90 degrees. The optimum wire feed speed varied depending on injection distance. Two rollers and a metallographic blank were sprayed for each test. Copper was distributed throughout the matrix and the target coating thickness was 0.75 to 1 mm.

Copper Powder

Copper powder was codeposited with 1080 wire. The gas parameters remained at 230 slpm N₂ / 30 slpm H₂, with a working distance of 235 mm. Powder feeder RPM was the main variable, which only varied from 0.5 to 3.0. The injection distance remained constant at 15 mm at 45 degrees. Two different sized injection tubes were used. The standard size tube had an exiting diameter of 1.9 mm and required a gas flow rate of 45 L /min. The large tube had

an exiting diameter of 6.5 mm and required a gas flow rate of 26 L /min. The standard tube size was used for all the work with graphite and polymers. Multiple coupons were sprayed to evaluate the microstructure. Amsler rollers were sprayed given the results of the coupons. The same range of variables were used.

The low feed wheel was used to produce low copper volume fraction coatings. The powder feeder RPM for the low feed wheel varied between 1 and 3. The standard powder injection tubes (1.9 mm) were used. Powder gas flow rate remained constant at 31 L / min. The other variable ranges were the same.

Polymers

Polymers used a unique set of parameters, unlike the other lubricant materials. The polymers were overlaid on the 1080 coating as opposed to being dispersed within it. The polymer coatings were very thin, ranging from 25 to 75 μm . The gas parameters were developed through early work on polymers over rail steel. The ideal polymer deposition parameters were 200 slpm N_2 / 50 slpm H_2 , with a working distance of 255 mm. These were the standard parameters for all polymer coatings. Injection distance was generally 65 mm at 45 degrees. Carrier gas rate varied slightly between 23 and 30 L / min. Some polymers were sprayed on flat plates for macro-evaluation.

Amsler rollers were sprayed with 1080 steel as done in early work on 1080 steel coatings. The coatings were sprayed to nominal thicknesses of 0.25 mm, 0.5 mm, and 0.7 mm. The rollers were sprayed in blocks of five. The samples were allowed to cool to room temperature. The polymer coatings were applied as layers. A jet of dry compressed air dwelled on the samples for 30 seconds between layers. The number of layers were adjusted to give the desired polymer coating thickness.

A wide variety of polymers were used as described earlier. Nylon and UHMW were sprayed neat or mixed with a solid lubricant of

either MoS₂ or Graphite. Teflon was sprayed neat and mixed with nylon. Torlon and Kynar were sprayed neat. Neat simply means unmixed or pure, without any additives.

2.4.3 Rail Coupons

Steel coupons (SAE 4340 steel) with a similar profile to a standard carbon rail steel head were coated with a 1080 steel coating or a polymer / 1080 steel coating, for larger scale testing. The parameters were generally the same as those used to spray steel coatings on Amsler rollers and flat steel coupons. Gas parameters did change for the latter samples, specifically an increase in the secondary gas flow rate from 30 slpm H₂ to 75 slpm H₂.

A fixture was created to hold the coupon and allow it to be rotated during the spraying operation. The entire surface could not be coated in only one pass. Thus, the sample was rotated about the rail head while the gun was traversed across the length of the rail. Figure 2.11 illustrates a coupon and holding fixture, ready to spray. Three iterations of rotation were required to coat the entire width. Surface preparation techniques followed those outlined earlier. The sample was cooled with dry compressed air as opposed to CO₂. The entire width of the coupon was coated. The coating thickness was deposited uniformly on the first sample. Later samples feathered the coating thickness at the ends. Coating thickness ranged from 0.25 mm to 1 mm at the center tapering off to nothing at the edges.

2.4.4 Rail Steel

Varying length rail sections were spray coated with 1080 steel and a polymer for full scale rolling load and FAST track implant testing. The size, shape, and weight required new fixturing to be created. Figures 2.12a and b illustrate the fixturing used to spray large rail specimens. The gas parameters for 1080 steel

changed to 230 slpm N₂ / 75 slpm H₂, with a working distance of 235 mm. The traverse speed varied between 0.20 and 0.25 meters per second. Application of the nylon was again at a traverse speed of 0.50 to 0.75 meters per second. The polymer was deposited at the standard 200 slpm N₂ / 50 slpm H₂, 255 mm working distance.

The method of coating the rail was similar to that used for the rail coupons. Uniform deposition required traversing in the length of the rail coupled with rotation about the rail head. The rotation was iterated to allow the center of the plume to impinge at each location during the coating process. The smaller samples, i.e. track laboratory coupons and rolling load machine sections, required only three iterations of rotation. In these samples the focus was on the top of the rail, with little emphasis on the gage face. The working distance remained within 10 mm during the sample rotation. The large twelve foot rail required 5 iterations of rotation to fully cover top to gage face. In addition the working distance had to be modified when the gage face was coated. This was accomplished by interrupting spraying and moving the gun fixture to the new working distance. This event required spray interruption for less than 45 seconds. All of the rail samples were cooled with air during both steel and polymer deposition.

2.4.5 Parameter Optimization

Parameters were optimized for depositing the 1080 steel coating on the rail head surface. Two inch sections of rail were coated at various gas flow rates and working distances. The nitrogen gas flow rate varied between 200 slpm and 275 slpm, the hydrogen between 0 and 125 slpm, and the working distance from 200 to 250 mm. The samples were cooled with compressed air impinging on the surface. Each sample was sectioned, mounted, and polished through 0.05 μm alumina. The sample microstructures were analyzed with the scanning electron microscope using back

scattered electron imaging. Porosity and oxide content were evaluated qualitatively.

2.5 Performance Evaluation

Plasma sprayed coatings were evaluated in the laboratory with the Amsler machine, a large scale rolling loading machine, and in the field with full scale train cars. The Amsler machine is described in detail. Descriptions of the large scale tests are presented in the Discussion section with the results of those tests.

2.5.1 Amsler Machine

The coating performance was tested in the lab under dry and lubricated rolling/sliding conditions on an Amsler twin roller test machine. Figure 2.13a is an overview of the Amsler wear testing machine. Figure 2.13b is a close-up of the Amsler machine showing two rollers mated, and ready for testing. The Amsler machine is a twin roller dynamometer capable of mechanically measuring friction coefficients over a range of creepage. Creepage also known as slip, is defined as the percent difference in surface speed between the mated rollers. The amount of creepage or slip can be calculated from Equation 2.1.

$$[\text{Equation. 2.1.}] \quad \text{Slip} = \{ 2 (1.104 D_2 - D_1) \} / [1.104 D_2 + D_1]$$

D_2 is the diameter of the bottom roller, and D_1 is the diameter of the top roller.

The Amsler has two shafts with the lower shaft rotating at a speed 1.104 times faster than the top shaft. The machine has two running speeds 200 RPM and 400 RPM. The cylindrical specimens, further referred to as Amsler rollers, are fixed on the end of each shaft. These two rollers mated against one another produce controlled rolling/sliding contact. By varying roller diameter the creepage can be varied from 0-100% under loads up to 2500 N.

Pressure was applied to the specimens with a coil spring. The contact pressure is calculated using Equation 2.2, the Hertzian contact formula.

$$\text{[Equation 2.2.]} \quad P_o = 0.418 [LE/R]^{0.5}$$

P_o is the maximum contact pressure, E is Young's modulus, L is the load per unit contact width, and $R = [R_1^{-1} + R_2^{-1}]^{-1}$ where R_1 and R_2 are the upper and lower roller radii. All tests were run with a contact width of 5 mm. It is noted that the modulus for the coatings is unknown as the coatings are composite in nature. The modulus for steel was subsequently used as an estimate.

The friction coefficient is related to the amount of pendulum deflection in the Amsler. A pendulum, of specific weight is attached to the shaft holding the lower roller. The value of the coefficient of friction was calculated from Equation 2.3.¹⁸¹

$$\text{[Equation 2.3.]} \quad \mu = 2.75d / LG$$

In equation 2.3, d is the amount of pendulum deflection in N·m, as read from the Amsler itself, L is the load (Newtons), and G is the radius of the lower roller. The constant 2.75 was determined by counter weights added to the pendulum.

2.5.2 Amsler Machine Operation

Performance was measured in terms of test cycles and average and final friction coefficient. One cycle was defined as a complete revolution of the bottom roller. The coating durability was defined as the number of cycles before the coating failed by debonding or surface wear, or the friction coefficient increased beyond 0.3-0.5. Virtually all of the wear tests were run uninterrupted to evaluate the change in friction coefficient over the number of revolutions. However, a wear rate was calculated for some samples requiring

test interruption. Roller wear rates were measured by removing the rollers from the machine at set intervals and weighing them. Wear rate was calculated from the slope of the weight loss vs. revolutions curve.

Wear tests were all performed at 200 RPM unless otherwise noted. A jet of dried compressed air impinged on each roller to prevent overheating. The cooling jets were eliminated for lubricated tests. The bottom rollers were cleaned with soap and water and rinsed with acetone prior to testing. The bottom rollers were always uncoated wheel steel. The bottom roller diameter was altered to change the amount of slip. The top rollers were plasma spray coated rail steel and were targeted at a constant 35 mm. The coatings were tested as-sprayed. Tests were run to failure or to a reasonable length (generally no greater than 20,000 revolutions).

Water and grease lubricated tests were performed on nylon and 1080 steel coatings. In the water lubricated tests a constant flow (approximately 2 drops per second) was maintained onto the top roller. For the grease lubricated tests a set amount of lubricant was applied to the sample at given intervals. 0.4 cc of lubricant were applied initially, followed by 0.2 cc at each interval. Interval duration and type of lubricant are noted in the test results.

The test parameters used in the Amsler wear test consisted of the number of revolutions (length of test), contact pressure, load, and slip (creep). The parameters for the individual tests are presented in the results section.

2.6 Microstructural Evaluation

2.6.1 Metallography

Steel coupons were sprayed early in the research to provide a metallographic record of spray parameters. Later, when Amsler rollers were sprayed with a specific coating, a witness sample was often included to provide a metallographic record. Metallographic specimens were taken from transverse and longitudinal sections of

the witness sample. For Amsler wear tests of interest a transverse or longitudinal section was taken from the wear track.

Metallographic sections were cut from the coating and substrate with a slow speed saw. Steel coupons, being less fragile were cut, with a high speed abrasive saw. The specimens were mounted in Epomet epoxy resin. Attention was paid to edge retention and edge rounding during polishing. The samples were polished through 0.05 μm alumina (Al_2O_3) abrasive. Graphite and nickel-coated graphite steel coatings were polished dry through 600 grit papers to retain the graphite particles.

2.6.2 Optical Microscopy

The coating microstructures were observed optically using a Nikon Epiphot inverted microscope. Magnifications ranged from 50x to 400x. The coatings were observed as polished except for the copper containing coatings. These coatings were swab etched with 2% nitric acid in ethanol (Nital). Etch time was generally between 2 and 5 seconds.

2.6.3 Scanning Electron Microscopy (SEM)

Sprayed coatings were observed in the scanning electron microscope at magnifications up to 10,000x. Secondary electron (SE) imaging was utilized to examine surface topography. Backscattered electron (BSE) imaging was used to enhance the phase contrast and to locate compositional variations.

Energy Dispersive X-ray detection (EDS) allowed for the identification of coating composition. EDS detects the specific elemental x-rays being emitted from a sample. Both qualitative and quantitative information can be extracted from a sample. Elements with atomic numbers below 12 are more difficult to detect due to their weak characteristic x-rays. EDS can detect thin films, but

caution must be used as electron interaction will yield information about the subsurface that may skew the results.

Surface films which formed on both the coated (top) roller and the wheel (bottom) roller during wear testing of nickel-graphite containing steel coatings and polymer / steel coatings were examined. The coatings were examined for the presence of certain elements, primarily carbon. Only qualitative data was collected, no attempt was made to determine the exact amount of transferred material.

2.6.4 Image analysis

Computer-based image analysis was performed to measure volume fraction of the second phase lubricant material. Image analysis was performed at 100x, 200x, or 400x depending on the coating thickness. The procedure for each field involved capturing an image and doing a histogram modification, which increased the contrast between constituents. This image was then sharpened to give clearer boundaries between components. Thresholding allowed assignment of gray scale range to each field element. For example, graphite is black, whereas the steel matrix is white and gray. By assigning a gray scale value to the black areas and another to the gray and white areas, the graphite can be separated. The pixels which are contained in the black areas are counted, thus giving a volume fraction of graphite. Images for quantification were taken only from areas which had both matrix and second phase lubricant particles. Thirty fields were found to give good statistical results. Quantification was performed on the nickel-coated graphite and copper containing steel coatings.

2.6.5 Fourier Transform Infrared Spectroscopy

Fourier Transform Infrared Spectroscopy (FTIR) was performed on various polymer films. Samples were cut from as-sprayed and as-tested Amsler rollers. Polymers were melted onto flat shim

stock in an air furnace at 210° C. Flat shim stock was also plasma sprayed with polymer coatings at various states of heat input. Both attenuated total reflectance (ATR) and specular reflectance (SR) modes were utilized. The FTIR spectra were downloaded to a PC based system for analysis.

2.6.6 Focused Ion Beam

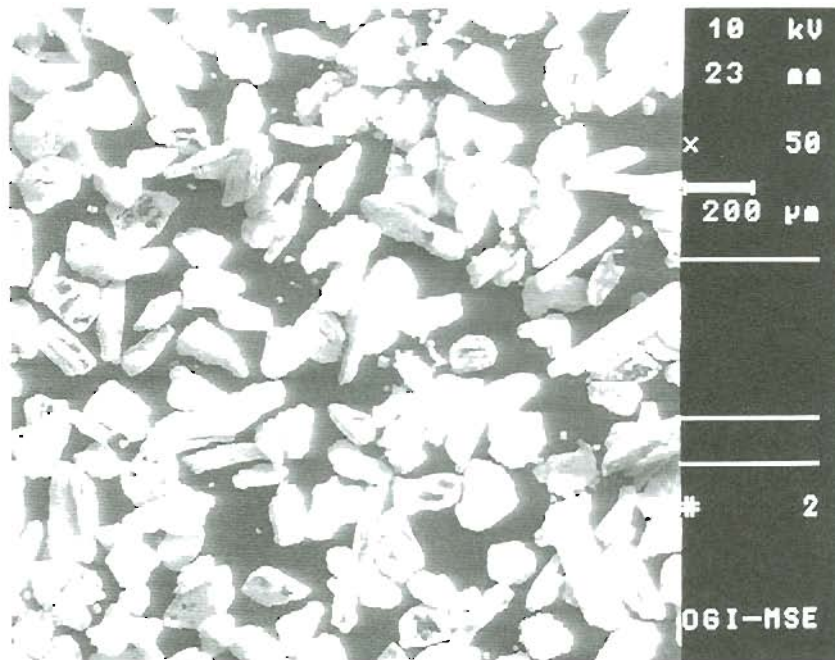
The FEI 610 focused ion beam (FIB) was used to cut small sections in polymer coating surfaces. This was performed to measure the very thin surface film which transferred from polymer / steel coated top roller to the bottom roller during wear testing. Cutting small canyons allowed a transverse section of film and substrate to be observed. Polymer coatings were sputter coated with gold-palladium. Transverse sections of spray coated rail (top) rollers and worn wheel (bottom) rollers were examined. Canyons were cut from the coating surface to the steel interface. Microcross-sections were examined in the SEM using secondary electron and backscattered electron imaging.

Table 2.1. Composition of standard carbon rail steel used to machine Amsler rollers. Average hardness equaled 31.4 Rc.

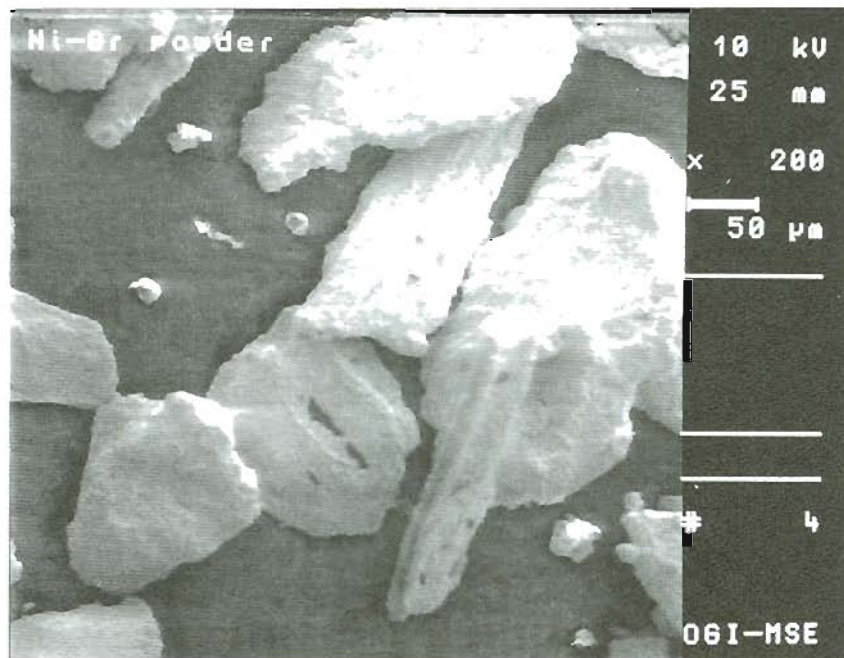
Steel	C	Mn	Si	Cr	Ni	Cu	S	Al
X-95	0.730	0.927	0.283	0.173	0.117	0.223	0.029	0.002
X-244	0.787	0.86	0.25	0.21	N/A	0.21	0.006	0.011

Table 2.2. Composition of Class C wheel steel. Wheel steel was machined into Amsler rollers. Average hardness equaled 30.4 Rc.

C	Cr	Mo	Mn	Si	S	Cu	Ni	V
0.66	0.036	0.014	0.684	0.528	0.022	0.089	0.029	0.009



(50x)



(200x)

Figure 2.1. SEM photomicrograph illustrating the morphology of nickel-coated graphite particles used to produce nickel graphite / 1080 steel coatings. SE imaging, 50x, 200x.

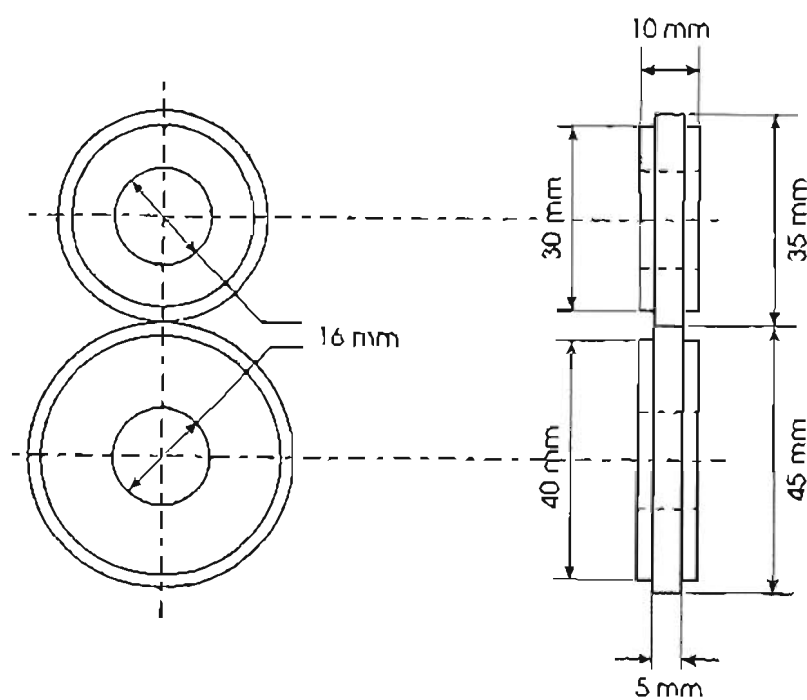


Figure 2.2. Schematic drawing of mated Amsler rollers showing dimensions.¹³⁶ The 35 mm roller is the as-sprayed dimension of a rail steel roller. The wheel steel roller is machined to 45 mm to yield a slip ratio of 35%.

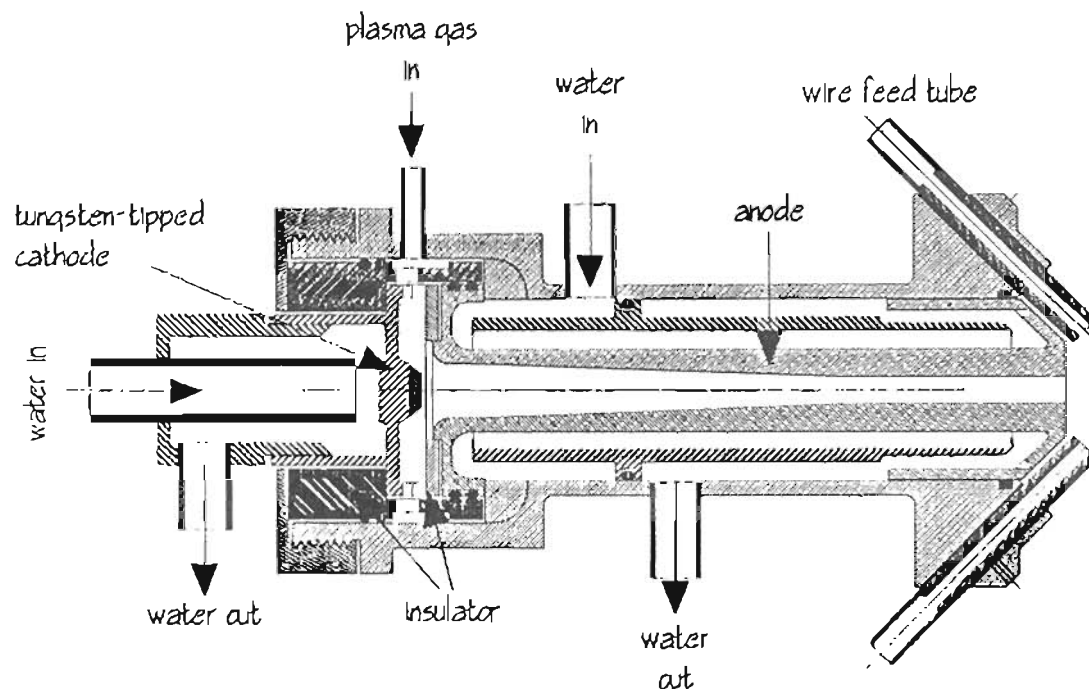
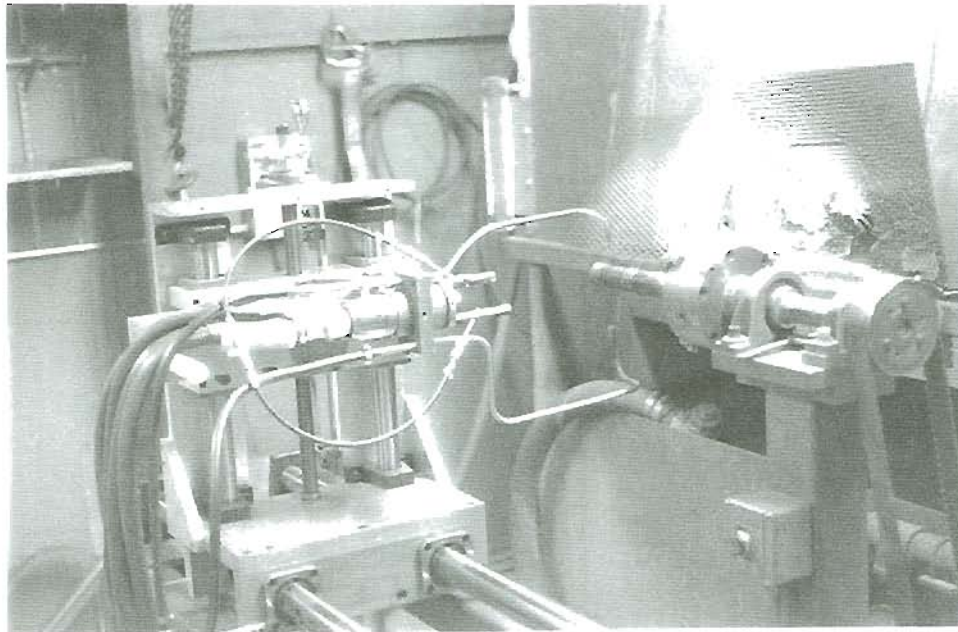
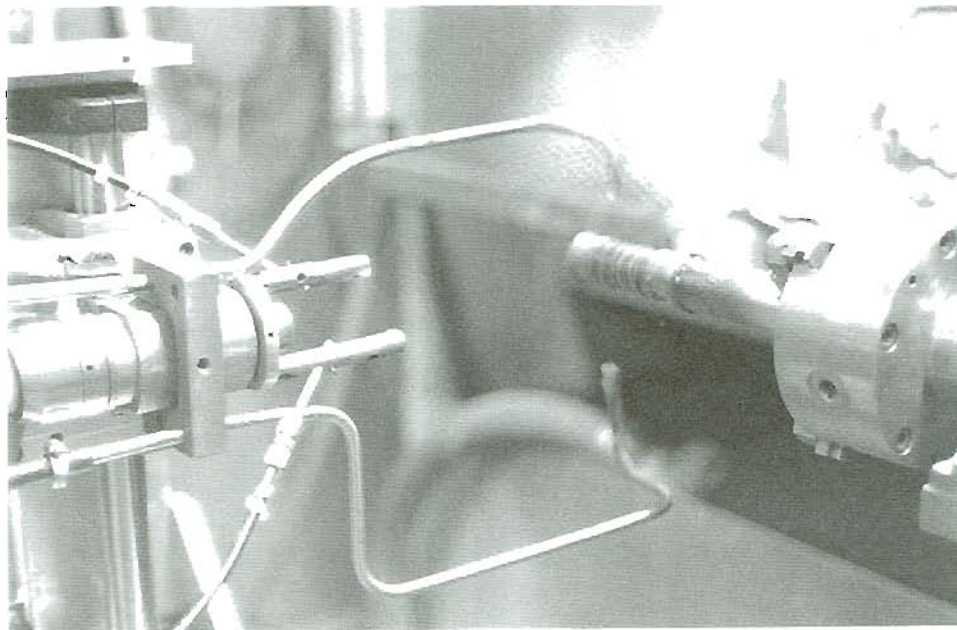


Figure 2.3. Schematic drawing of plasma gun illustrating the location of the tungsten cathode and copper anode.¹³⁶ This drawing also illustrates the flow path of plasma-forming gas and cooling water.



(a)



(b)

Figure 2.4. Photograph illustrating plasma gun set-up to spray Amsler rollers. a) Overview of plasma gun, traverse table, and Amsler holding fixture. b) Closeup of plasma gun and backside cooling tubes.

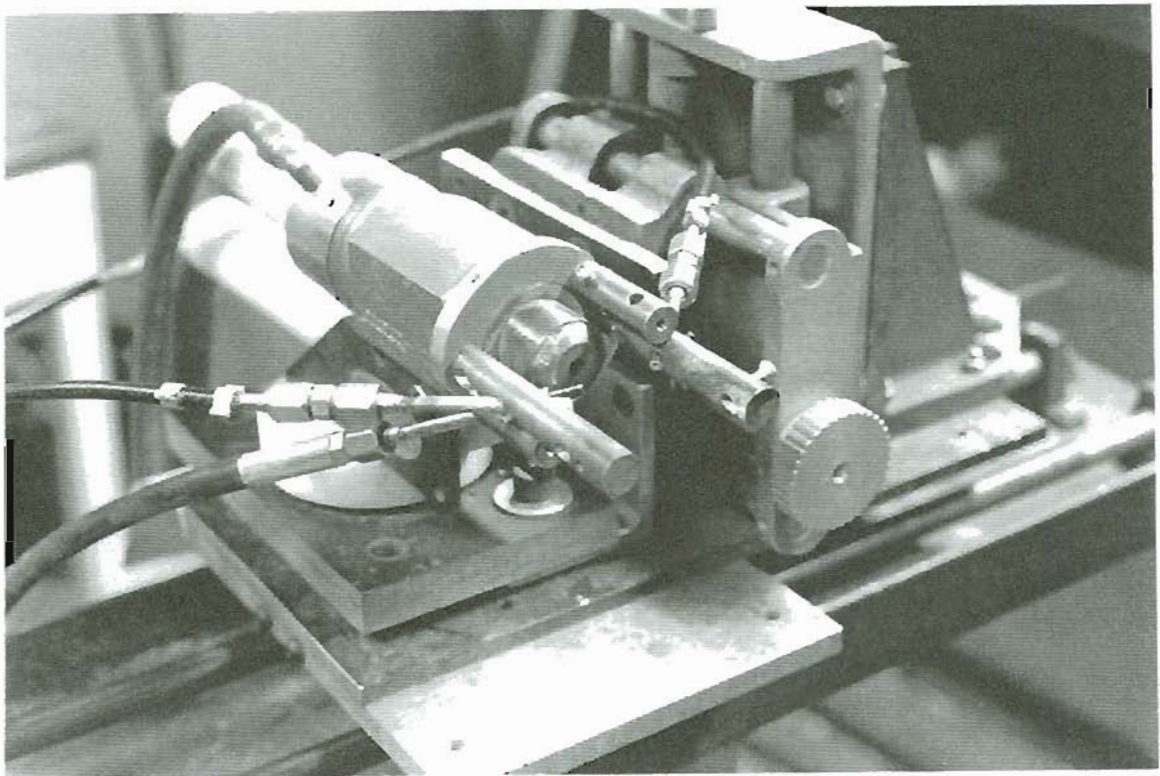


Figure 2.5. Photograph illustrating close-up of plasma gun showing powder and wire feed. Note: powder feed tubes are diametrically opposed to ensure smooth flow into the plasma stream.

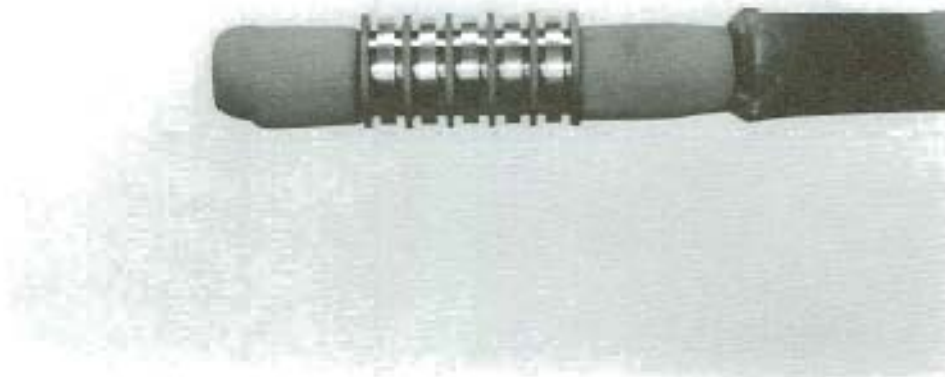


Figure 2.6. Photograph illustrating Amsler rollers attached to rotatable steel shaft. Surface preparation has not been done.

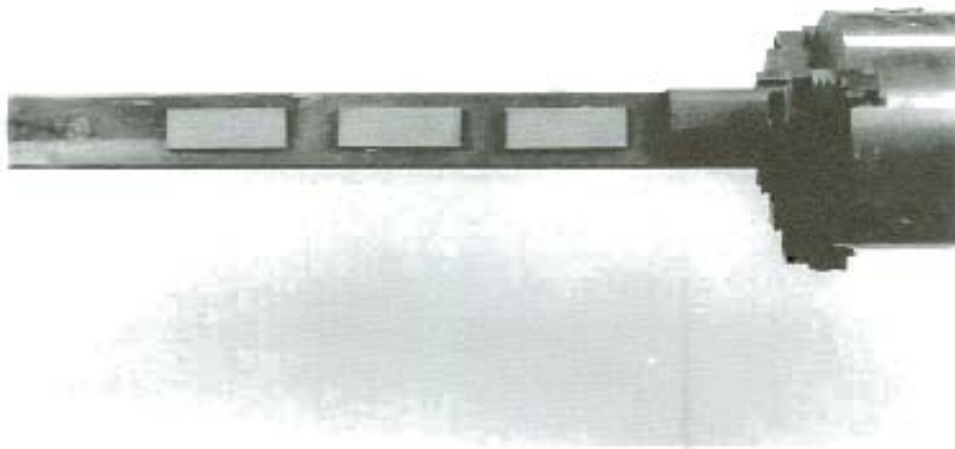
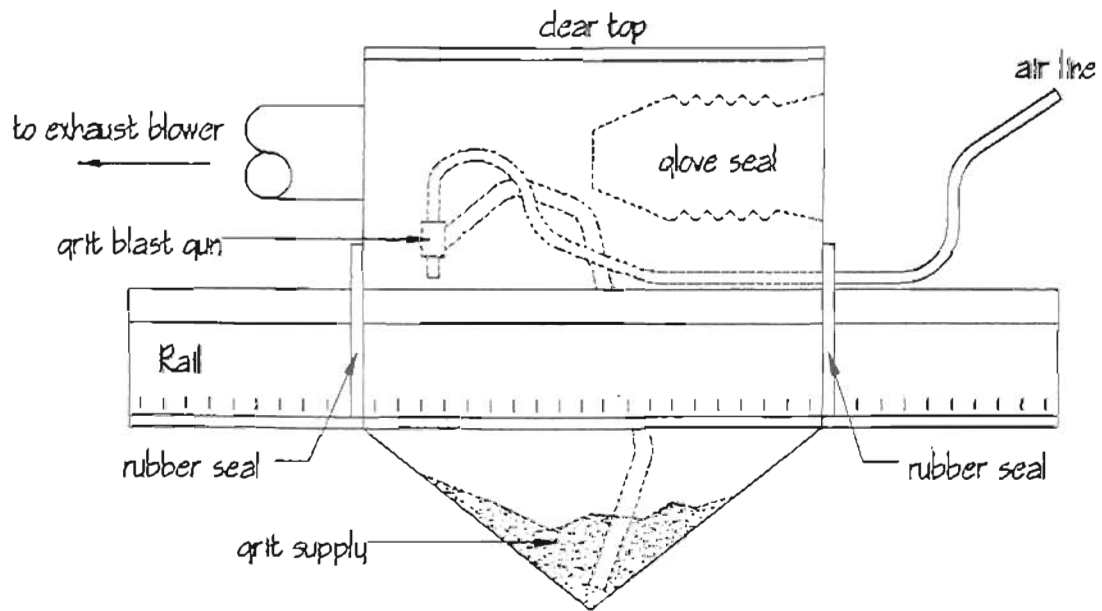
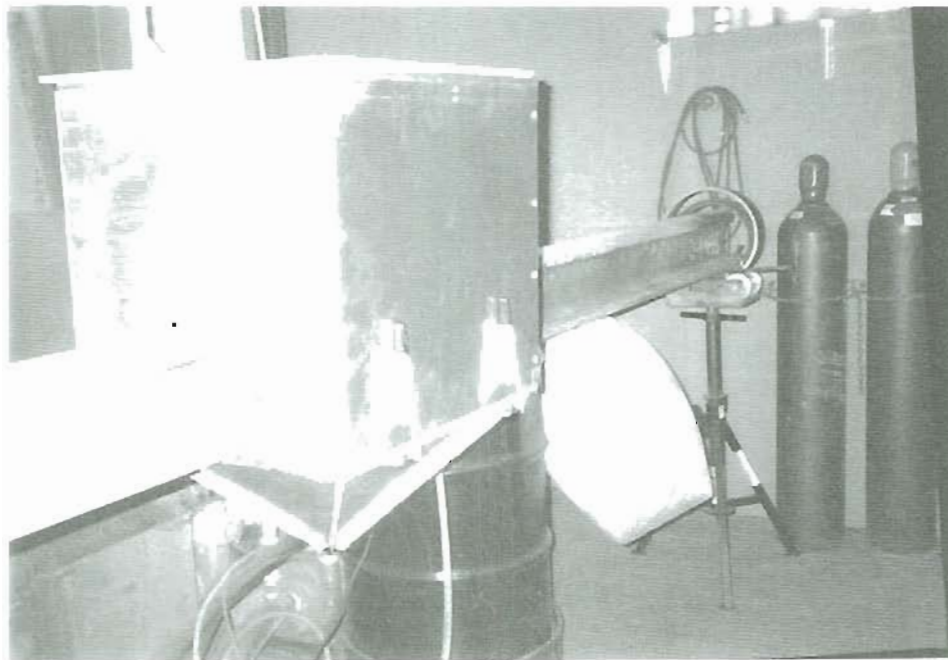


Figure 2.7 Photograph showing flat steel coupons attached to graphite bar, ready for spraying. 1-3 steel coupons could be sprayed at a time.



(a)



(b)

Figure 2.8. Portable grit blasting booth as attached to large rail section. a) Schematic drawing.¹³⁶ b) Photograph showing FAST, full size rail being prepared.

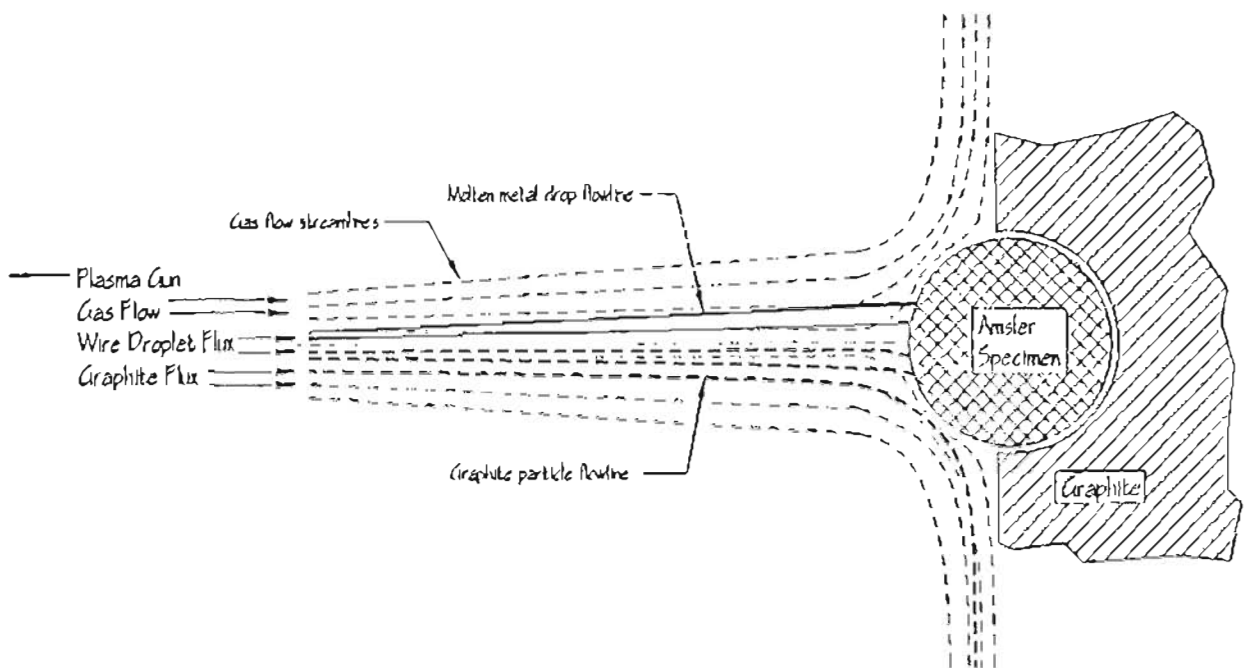


Figure 2.9. Schematic drawing of graphite shield #1 showing shape and positioning during plasma spraying of Amsler rollers.¹³⁶ The half-moon prevented backside cooling, thus cooling jets impinged from the same direction as the particle and plasma.

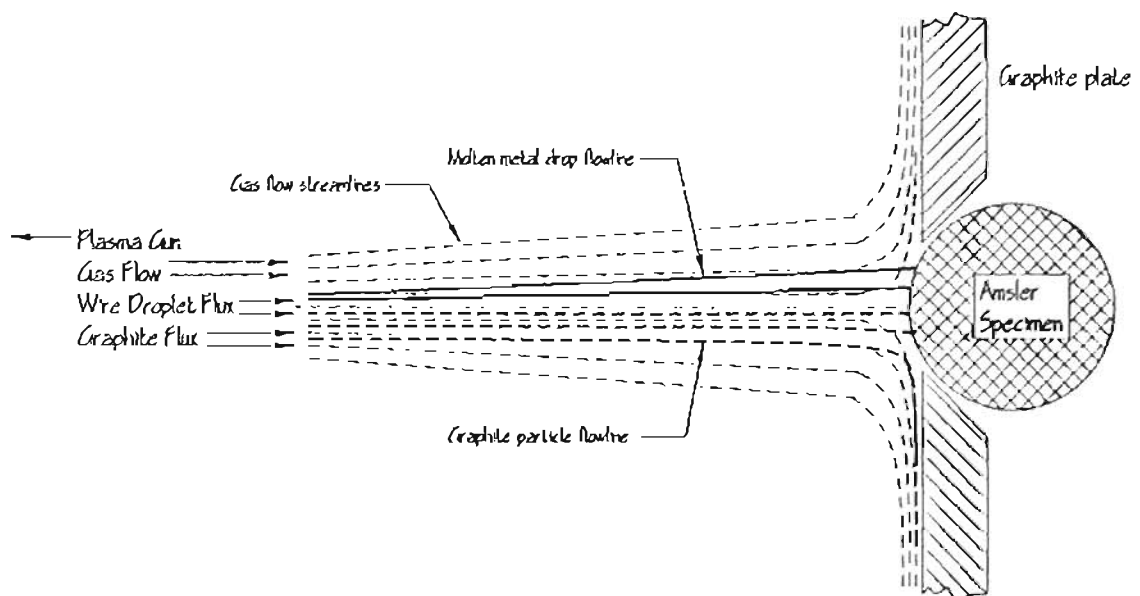
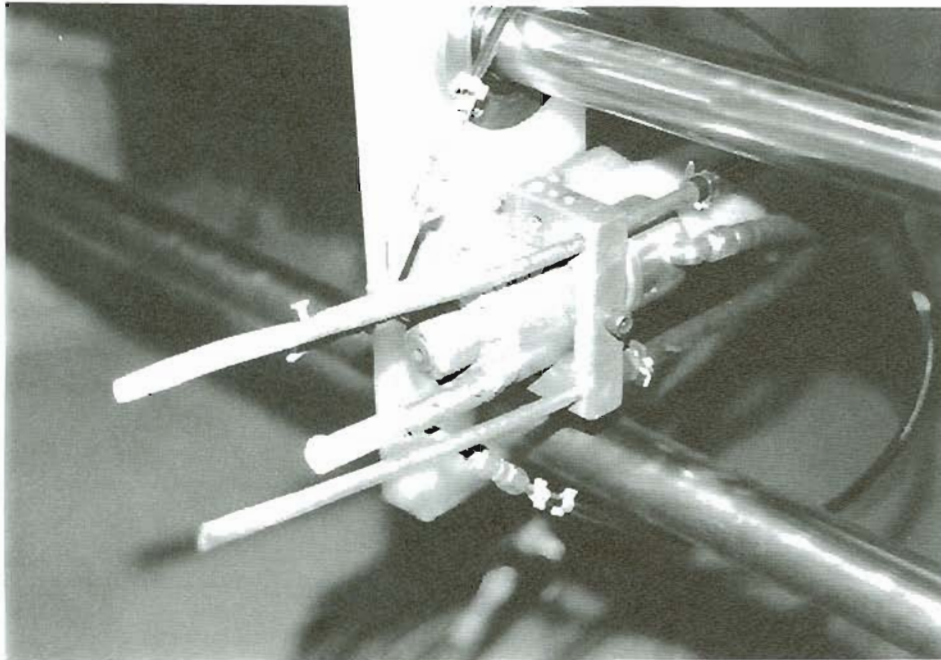


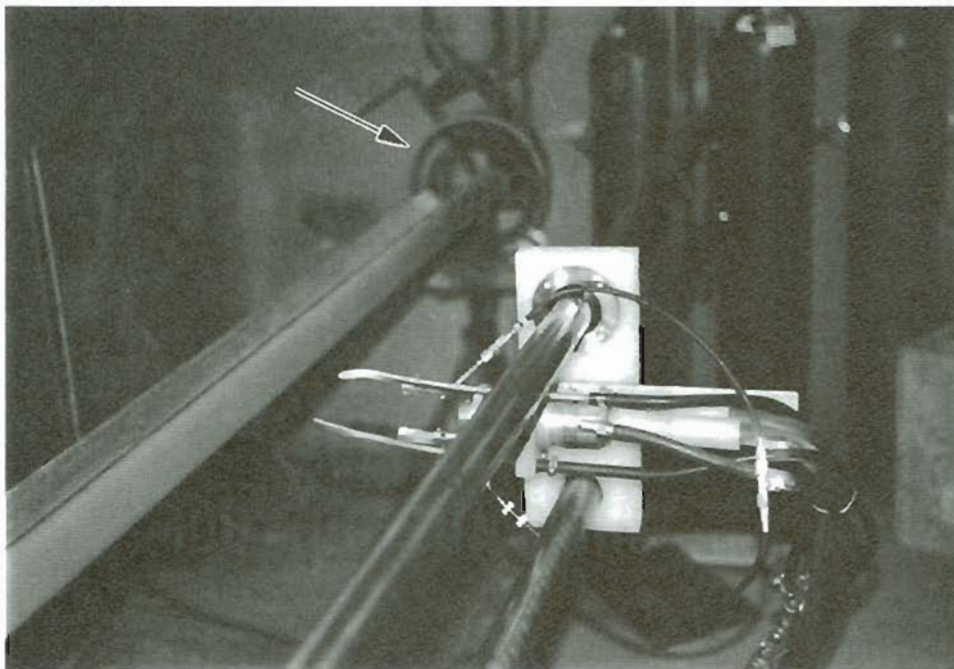
Figure 2.10. Schematic drawing of graphite shield #2 showing shape and positioning during plasma spraying of Amsler rollers.¹³⁶ Note: arrows indicate where backside cooling jets would impinge.



Figure 2.11. Photograph illustrating Track Lab Coupon and fixturing used to apply plasma sprayed coating of 1080 steel and nylon.

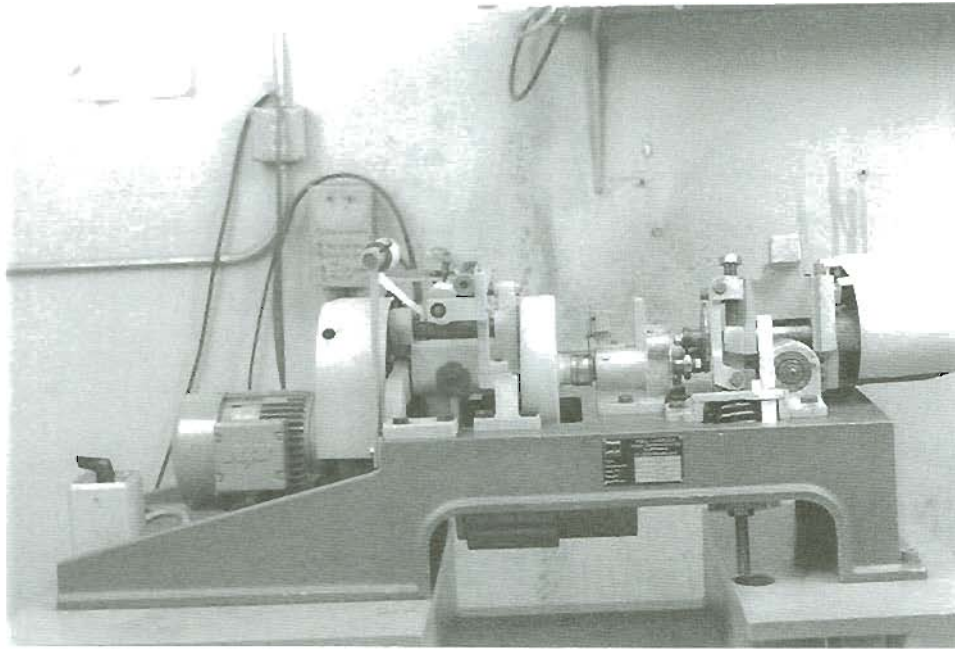


(a)

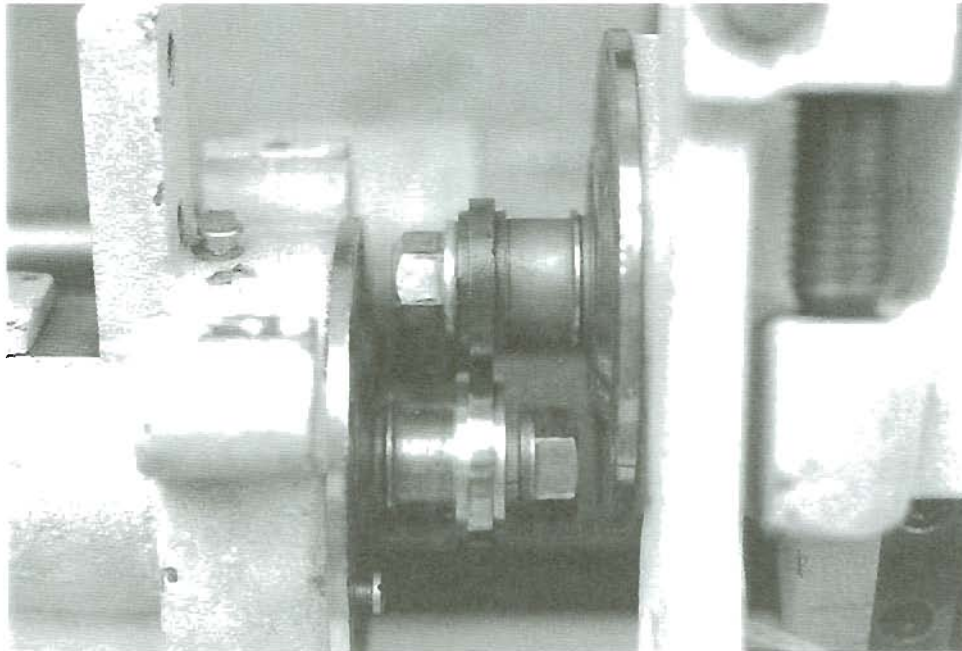


(b)

Figure 2.12. Photographs showing plasma gun and fixturing used to spray large rail sections. a) Closeup of gun showing powder feed tubes. b) Gun and rail following deposition of coating. Arrow denotes point of rotation used during coating deposition.



(a)



(b)

Figure 2.13. Photographs showing Amsler wear testing machine. a) Overview of machine. b) Two rollers mated and ready for testing; top roller is spray coated rail steel, bottom roller is as-machined wheel steel.

Chapter Three

Results

3.1 Introduction

All of the coatings investigated in this study were evaluated by means of microstructural characterization and performance under rolling / sliding conditions. Image analysis and metallography provided information as to the coatings microstructure and more importantly the volume fraction of retained solid lubricant. Image analysis was only performed on the nickel-coated graphite and copper containing 1080 steel coatings. Polymer coatings were analyzed using the SEM and FTIR, as they were too thin to be resolved optically. Rolling / sliding wear tests were performed on all of the coating systems, with variations on contact pressure and slip ratio.

The results are listed for each coating system. Performance results are listed as the friction coefficient and durability. The baseline friction coefficient for a 1080 steel coating without any added solid lubricants is 0.46. Friction values for the other coatings systems are compared to this value. Durability of the coating is defined as the number of test cycles the coating can endure before interfacial debonding or when the friction coefficient approaches the base line value of 0.46. The graphite / steel coating system is presented followed by the copper / steel coatings and finally the polymer / steel coating system, which was used for both small and large scale wear performance evaluation.

3.2 Graphite

3.2.1 Introduction

Graphite is a well known solid lubricant. If graphite particles could be contained within a wear resistant steel matrix there was reason to believe friction and wear could be reduced. The goal was to entrap a sufficient quantity of graphite to create a durable lubricating film without compromising the structural integrity of the 1080 steel coating.

Several types of graphite material were used in an effort to produce a graphite and 1080 steel composite coating. These included graphite powder, graphite-flake powder, nickel-coated graphite powder, and cast iron powder. Various geometries were used as substrates during the early work. Flat steel coupons were spray coated to provide fast metallographic analysis during the early stages of coating development. Amsler rollers and round blanks were used for the majority of the testing once basic parameters had been established. The coating microstructures and their corresponding wear performance is presented for each set of test experiments.

3.2.2 Graphite Powder

Flat Coupons

Flat bars were sprayed initially to determine coarse graphite deposition parameters. The two types of graphite used included a fine ($< 50 \mu\text{m}$) powder and graphite powder ($< 500 \mu\text{m}$) made from lathe turnings in-house. A wide range of gas parameters and injection distances were used. The spray parameters and retained graphite volume fractions of 1080 steel /graphite coatings on flat coupons are shown in Table 3.1. Figures 3.1 through 3.3 illustrate the large retention of graphite obtained over a wide range of gas

parameters. Figure 3.1 is a coating sprayed at the low range of gas parameters: 200 slpm N₂ and no secondary gas at a working distance of 225 mm. Figure 3.3 was sprayed at the high end of the gas parameters: 270 slpm N₂ / 70 slpm H₂ / 225 mm. The coupons clearly retained graphite at a wide range of gas parameters when the powder was injected at 25 mm from the anode.

The graphite powder injection distance had the greatest effect on the retention of graphite. It was illustrated that when graphite was injected at 25 mm from the anode it was retained in volumes of 20-30%. When the powder injection distance was increased to 65 mm the amount of retained graphite fell to 10-15 %. When the powder injection distance increased to 115 mm the graphite retention fell to < 5%. Figure 3.4a and b illustrates the coating microstructure of a sample sprayed with a powder injection distance of 65 mm and 115 mm, respectively. At 165 mm there was virtually no retained graphite. Figure 3.5 illustrates a 1080 steel coating without any retained graphite, where powder injection distance equaled 165 mm.

Amsler Rollers

Using the results of the flat coupon microstructures, a set of parameters were established to spray Amsler rollers for performance evaluation. With few exceptions the gas parameters remained at 230 slpm N₂ / 30 slpm H₂. The working distance increased from 225 mm in tests G1 through G8 to 235 mm in all further tests because the 1080 steel wire injection angle changed from 90° (normal to the plume) to 45°. Microstructure and performance results of Amsler wear tests include work with graphite powder, graphite-flake powder, and the aerodynamic shield, which was created to improve graphite retention.

Early Work

Graphite tests G1 through G8 account for the initial attempts at producing a self-lubricating graphite coating. Samples G4 through G6 utilized the graphite-flake powder, while all other samples in this series (G1 through G23) used the graphite powder made from lathe turnings. Table 3.2a lists the gas parameters and powder feeder conditions used to coat Amsler rollers with 1080 steel plus graphite. The wear test parameters, which include contact pressure and creepage, and performance results are shown in Table 3.2b. Comments within the table note any specifics of the individual tests. It is noted that these coatings were sprayed with only one powder injection tube.

The results of these early tests indicate none of the coatings showed a reduced friction from the baseline $\mu = 0.46$ for a 1080 steel coating without any solid lubricants. The wear durability appeared to be equivalent to the 1080 steel coatings. This comparison was made by observation of both coating's degradation appearance. Microstructural observation confirmed the lack of any retained graphite particles. The graphite /1080 steel coatings tended to debond early in the test (< 2000 revolutions). Wear was especially poor for coatings tested at $P_o = 1220 \text{ N/mm}^2$ and 35% creep. Figure 3.5 illustrated the microstructure of a graphite / 1080 steel coating where no graphite was retained. This figure also serves as a microstructural reference of a 1080 steel coating without solid lubricant additives.

Aerodynamic Shield

An aerodynamic shield was created to alter the flow of graphite particles in the plasma plume. Retention of graphite requires that molten steel particles capture solid, unmeltable graphite particles. The two shield geometries were an attempt to

increase the interaction of steel and graphite particles during spraying.

Table 3.3a lists the spray parameters used in conjunction with the aerodynamic shields. Samples G9 through G11 were sprayed with Shield #1, which is illustrated in Figure 2.10. Samples G12 through G14 and samples G17 through G19 were sprayed with the second design iteration shield (Shield #2), which is illustrated in Figure 2.11. Samples G15 and G16 were sprayed without a shield. The performance results and test parameters are given in Table 3.3b. Creep is calculated from the actual diameters of the test rollers. The coating thickness would vary between samples, thus creep would also vary. Two creep modes were used. Low creep was targeted at 5%, but varied between 4% and 6%. High creep was aimed at 35%, but ended up within 34% and 37%.

Of the samples sprayed only two, G12 and G16, had any appreciable graphite retention. Sample G12 was tested at $P_o = 900$ N/mm² and 5% creep. The friction coefficient (μ) equaled 0.3 and the durability was in excess of 10,000 revolutions. This performance was contingent on low creep (5%) and a low contact pressure (900 N/mm²). When sample G12 was tested at 35% creep it failed within 200 revolutions. The microstructure for sample G12 is shown in Figure 3.6a. Sample G16 had a similar microstructure and performed equivalently to G12. The friction coefficient was again equal to 0.3, under conditions of creep = 5% and $P_o = 900$ N/mm². The durability exceeded 10,000 revolutions. The microstructure of G16 is illustrated in Figure 3.6b. It is of interest to note that each coating was sprayed with the same parameters except for the presence of the aerodynamic shield for sample G12.

Dual Wire

Two wire feeds were used in samples G20 through G23 to increase the flux density of molten steel particles in the plume and the chances of graphite particle capture and retention. Tables 3.4a

and b summarize the results of spray parameters and wear behavior. G22 and G23 were sprayed using Shield #2. The Amsler test results indicate that friction reduction was not achieved, which is corroborated by metallography showing few, if any retained graphite particles in the coating. The microstructure of these coatings were similar to other non-graphite containing samples.

Synopsis

The samples G12 and G16 were the only samples to show any retained graphite and friction reduction. The results from testing G16 suggest the aerodynamic shield was not necessary to increase the chances of graphite retention. Solid particle graphite appeared to retain itself in the 1080 steel coating by random occurrence as opposed to being a direct function of spray parameters.

Table 3.1. Spray parameters and results for early microstructural evaluation of graphite powder / 1080 steel coatings. Plasma gas flow rate was a major variable, however working distance remained at 225 mm.

Sample	Plasma Gas N ₂ / H ₂ (slpm)	Power (kW)	Powder Feeder Gas (slpm)	Injection Distance (mm)	Graphite Volume (%)
M1	200 / 0	109	43	165	-
M2	230 / 30	130	43	165	-
M3	270 / 70	140	43	165	-
M4	250 / 110	140	43	165	-
M5	230 / 30	130	43	115	< 5
M6	230 / 30	130	43	65	10-15
M7	230 / 30	130	57	65	10-15
M8	230 / 30	130	57	25	20-30
M9	200 / 0	109	57	25	20-30
M10	270 / 70	140	57	25	25-35
M11	250 / 100	140	57	25	25-35
M12	230 / 30	130	85	25	20-30

Powder Injection @ 45°; Powder Feed Rate = 15 RPM; I= 350 Amps

Table 3.1a. Spray parameters for graphite powder / 1080 steel coatings G1 through G8. Gas parameters were a major variable, with working distance remaining at 225 mm. Graphite material was powder from lathe turnings except as noted, where commercial graphite flake was used.

Sample	Gas Parameters N ₂ / H ₂ (slpm)	Power (kW)	Coating Thickness (mm)	Powder Feed (RPM)	Powder Gas (slpm)
G1	250 / 100	140	0.97	15	57
G2	250 / 85	140	1.1	15	57
G3	230 / 30	130	1.5	10	42
G4 *	200 / 0	109	0.97	15	42
G5 *	250 / 70	140	0.95	15	42
G6 *	230 / 30	130	0.98	15	42
G7	230 / 30	130	0.88	15	28
G8	230 / 30	130	0.98	10	42

Powder Injection Distance= 25 mm @ 45°; Working Distance= 225 mm.
I= 350 Amps; * Commercial graphite flake powder

Table 3.2b. Amsler performance test conditions and results for graphite / 1080 steel coatings G1 through G8.

Sample	P_o (N/mm ²)	Creep ¹ (%)	Test Length (revs.)	Friction Coefficient (μ)	Comments
G1	1220	5.15	150	-	D
G2	900	5.21	840	0.46	D
G3	1220	33.2	430	0.46	D
G4	900	6.24	1000	0.46	T
G5	900	6.24	1000	0.46	T
G6	900	6.25	1650	0.42	D
G7 #1	900	35.43	600	0.49	T
G7 #2	1220	5.21	1150	0.46	D
G8 #1	900	35.8	< 200	-	T
G8 #2	1220	4.9	1500	0.46	T

¹ Creep calculated from roller diameters
Comments: D= Debond; T= Test terminated

Table 3.3a. Spray parameters for graphite powder / 1080 steel coatings G9 through G19. Gas parameters were 230 slpm N₂ / 30 slpm H₂, with a working distance of 235 mm. Graphite powder from lathe turnings was used for all samples.

Sample	Coating Thickness (mm)	Powder Feeder (RPM)	Powder Gas (slpm)	Comments
G9	0.87	15	36	S1
G10	0.90	15	36	S1
G11	0.89	18.5	42	S1
G12	0.95	18.5	42	S2
G13	0.98	15	42	S2
G14	1.06	15	42	S2
G15	1.09	15	42	NS, I
G16	0.96	18.5	42	NS, I
G17	1.13	18.5	42	S2, N
G18	1.05	18.5	57	S2
G19	0.98	18.5	70	S2

Powder injection distance= 25mm @ 45 degrees; Maximum feed rate= 18.5 RPM.
Power= 130 kW @ 370 V and 350 A
Comments: S1= Shield #1; S2= Shield #2; NS= No shield; N= 90 degree powder injection angle; I= Powder injection distance=15 mm.

Table 3.3b. Amsler performance Test conditions and results for graphite powder / 1080 steel coatings G9 through G19.

Sample	P_o (N/mm ²)	Creep ¹ (%)	Test Length (revs.)	Friction Coefficient (μ)	Comments
G9	900	6.16	1500	0.46	T
G10	900	5.96	2500	0.46	T
G11	700	36.6	2080	0.46	D
G12 #1	900	6.24	11,000	0.30	T
G12 #2	900	35.9	< 200	-	T
G13 #1	1220	36.1	1800	0.46	T
G13 #2	900	36.1	850	0.46	T
G13 #3	900	6.43	2550	0.46	D
G14	900	4.23	2740	0.46	T
G15	900	4.76	2000	0.46	T
G16 #1	900	3.9	2000	0.30	-
G16 #1*	1220	3.9	13,950	0.30	T
G16 #2	900	33.2	< 200	-	T
G17 #1	900	34.4	480	0.46	T
G17 #2	1220	3.9	2100	0.46	T
G18	1220	5.5	760	0.46	T
G19	1220	4.6	1500	0.46	T

¹ Creep calculated from roller diameters; * Test continued at higher contact pressure
Comments: D= debond; T= test terminated

Table 3.4a. Spray parameters for graphite powder / 1080 steel coatings G20 through G23. Gas parameters were 230 slpm N₂ / 30 slpm H₂, with a working distance of 235 mm. Graphite powder from lathe turnings was used for all samples. Two 1080 steel wires were used.

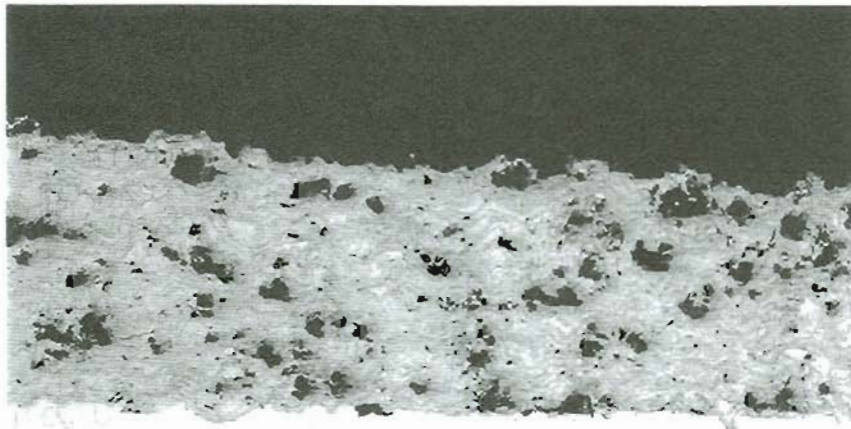
Sample	Coating Thickness (mm)	Powder Feeder (RPM)	Powder Gas (slpm)	Comments
G20	1.07	15	42	NS
G21	0.87	15	42	NS
G22	1.05	18.5	42	S2
G23	0.98	17.8	57	S2,I

Powder Injection= 25mm @ 45 degrees; Maximum powder feed rate= 18.5 RPM;
 1080 Wire injection=15 and 28 mm; Power= 130 kW @ 370 V and 350 A
 Comments: S2=Shield #2; NS=No shield; I= Powder injection distance= 85 mm.

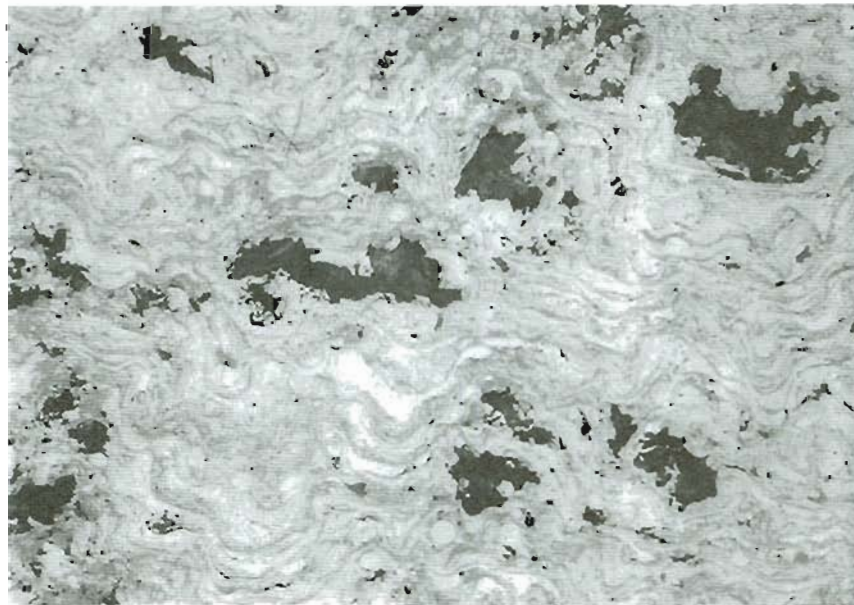
Table 3.4b. Amsler wear test conditions and results for graphite powder /1080 steel coatings G20 through G23.

Sample	P_o (N/mm ²)	Creep ¹ (%)	Test Length (revs.)	Friction Coefficient (μ)	Comments
G20	1220	4.61	1000	0.46	T
G21#1	1220	6.64	2100	0.46	T
G21#2	900	6.61	2080	0.46	D
G22	900	6.24	1500	0.46	T
G23 #1	1220	4.56	3800	0.46	D
G23 #2	900	4.56	500	0.46	T

¹ Creep calculated from roller diameters.
Comments: D=debond; T= test terminated.



<----> 200 μm (50x)



<----> 50 μm (200x)

Figure 3.1. Photomicrograph of graphite / steel coating M9 showing presence of graphite particles. Gas parameters 200 slpm N_2 / no secondary gas, 225 mm working distance. Graphite injection = 25 mm @ 45°. Graphite volume = 20-30%.



<----> 200 μm (50x)



<----> 50 μm (200x)

Figure 3.2. Photomicrograph of graphite / steel coating M8 showing presence of graphite particles. Gas parameters 230 slpm N_2 / 30 slpm H_2 , 225 mm working distance. Graphite injection = 25 mm @ 45°. Graphite volume = 20-30%.

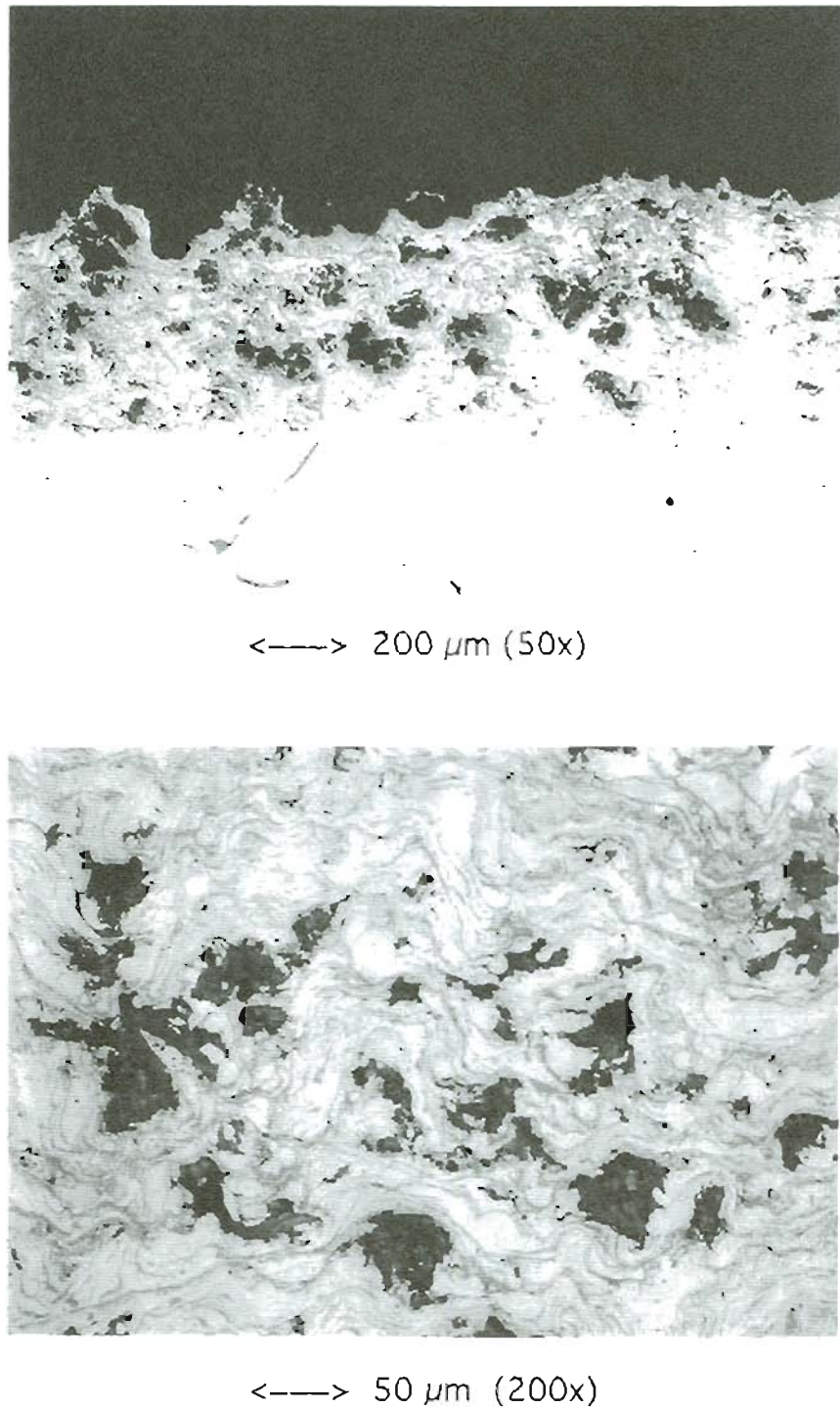


Figure 3.3. Photomicrograph of graphite / steel coating M10 showing presence of graphite particles. Gas parameters 270 slpm N_2 / 70 slpm H_2 , 225 mm working distance. Graphite injection = 25 mm @ 45°. Graphite volume = 25-35%.



(a) 200x

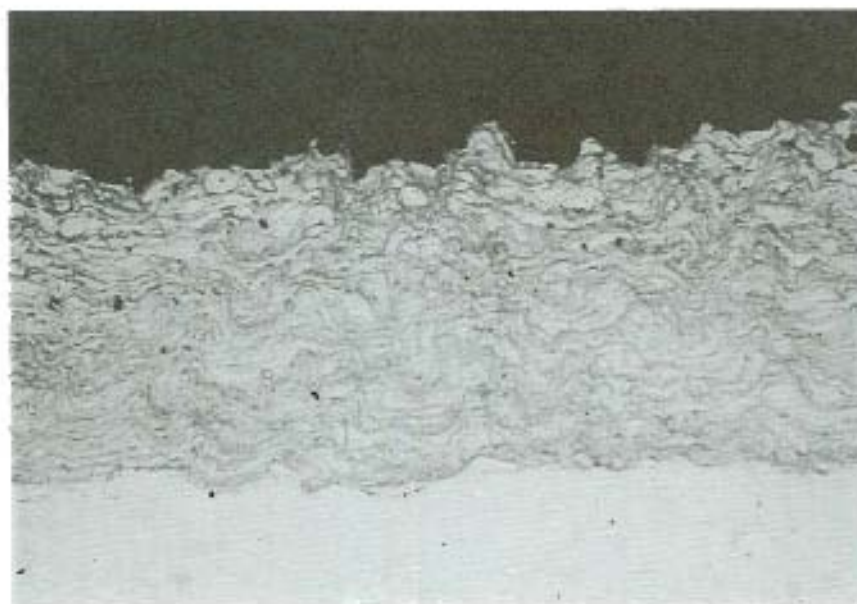


(b) 200x

Figure 3.4. Photomicrograph of graphite / steel coatings showing reduction of graphite particles as injection distance (l) increases. Gas parameters: 230 slpm N_2 / 30 slpm H_2 , 225 mm working distance. a) M7, $l=65$ mm, 10-15% graphite. b) M5, $l=115$ mm, < 5% graphite



<----> 200 μm (50x)



<----> 50 μm (200x)

Figure 3.5. Photomicrograph of graphite / steel coating M2 showing lack of graphite particles. Gas parameters: 230 slpm N_2 / 30 slpm H_2 , 225 mm working distance. Graphite injection = 165 mm @ 45° .



(a) 200x



(b) 200x

Figure 3.6. Photomicrograph of graphite / steel coatings applied to Amsler roller. Gas Parameters: 230 slpm N₂ / 30 slpm H₂, 235 mm working distance. Powder injection distance= 25 mm @ 45°. a) G12, sprayed with shield #2. b) G16, sprayed without shield.

3.2.3 Nickel-Coated Graphite

Nickel-coated graphite was sprayed with 1080 steel in an attempt to produce durable, self-lubricating coatings. The nickel-coated graphite powder was utilized when attempts with graphite powder failed. A thin nickel shell surrounding a graphite particle helps the graphite to simulate a meltable material. This should increase the chances of retention in the 1080 steel coating.

The deposition of nickel-graphite / steel coatings was explained in the experimental section. All of the nickel-graphite / steel coatings were formed using the same plasma spray technique. Nickel-graphite / steel coating performance was evaluated by the friction coefficient and durability. Metallography and image analysis were used to evaluate the amount of nickel-graphite retained in the steel coating. Wear performance was compared to the amount of retained nickel-graphite. Three coating thicknesses were evaluated, 1 mm, 0.5 mm, and 0.25 mm.

Initial Studies

The first samples focused on the mere retention of graphite. Tables 3.5a and b summarize the spray parameters and performance results of samples G25 through G27. These coatings were deposited directly onto Amsler rollers. Coating deposition on flat coupons was not performed because graphite retention on flat geometry had already been proven. Also, there was no available test to evaluate the flat coupon's wear performance. Performance was poor, with durability being less than 2000 revolutions for most samples. Most of the samples debonded prior to test termination. Some friction reduction was evident, with μ varying between 0.16 and 0.38. Figure 3.7a illustrates the coating microstructure of G27 showing the total dispersion of nickel-graphite particles. Nickel-graphite was deposited at and near the interface, which may have reduced the durability. Figure 3.7b is a close-up of the interface showing the

presence of nickel-graphite particles. Figures 3.8a and b are higher magnification photomicrographs of samples G25 and G27, which illustrate the microstructure and the range of retained nickel-graphite volume fractions.

1 mm Coatings

To avoid any detrimental effect nickel-graphite may have on the substrate / coating adhesion, a layer of 1080 steel (only) was sprayed onto the substrate. This was done for all further nickel-graphite / steel coatings. The coatings in this set were 1 mm in thickness with nickel-graphite dispersed throughout the coating matrix. Tables 3.6a and b illustrate the spray parameters and performance results of samples G28 through G33. The coatings vary in volume fraction from 6 to 24 % nickel-graphite. Figures 3.9a and b are low magnification (50x) photomicrographs of samples G28 and G33. The photos illustrate the low and high values for nickel-graphite volume fraction in this series. Note the lack of graphite near the interface. The particles which do reside at the interface are imbedded alumina grit. This was minimized in later samples by reducing the dwell time on the sample during grit blasting. Figures 3.10a through f illustrate the range of coating microstructures for samples G28 through G33.

The durability was less than 6000 revolutions for all samples except G32 and G33, with debonding occurring almost every test. The friction coefficient was a consistent 0.14 through most of the test, but rose steadily to 0.16-0.18 beyond 5000 revolutions. This pattern of friction coefficient behavior was consistent for all of the nickel-graphite containing steel coatings tested at 5% creep. Sample G32 was examined after debonding. The coating separated between lamella, rather than at the interface. Figure 3.11a and b illustrate this interlamellar failure. Figure 3.11b closely shows the network of cracks which formed in the coating during testing. Wear tests at 35% creep failed within 200 revolutions. When tested at

35% creep ($P_o = 900 \text{ N/mm}^2$) the coating was worn away very rapidly (< 200 revolutions). Samples G32 and G33 were chosen for testing at 35% creep because of their large nickel-graphite volume fraction offered a better chance of forming a protective film.

Tables 3.7a and b illustrate the spray parameters and performance results of samples G34 through G37. These coatings also had a thickness of 1 mm, but contained nickel-graphite in only the top 30-50% of the coating microstructure. The low wear rate of the previous series suggested nickel-graphite dispersed throughout the matrix was neither necessary nor desirable. This series of coatings displayed increased wear performance over samples G28 through G33. Test durability exceeded 10,000 revolutions and friction remained at $\mu = 0.14$. The incident of debonding was reduced, with only two samples out of eight failing by debonding. Four other tests, though, were terminated due to severe edge effects.

Edge effects occur when large pieces of coating break off of the sample near or at the edge of the wear track. It is believed these samples would have debonded had the test continued. Edge effects were more severe in the samples with a higher nickel-graphite volume fraction. The nickel-graphite steel coatings were again degraded severely when tested at 35% creep. Neither G35 or G36 lasted beyond 200 revolutions. Figures 3.12a and b illustrate the microstructure and interface of samples G34 and G37. These represent the high and low values of nickel-graphite for this series. Figures 3.13a through d show higher magnification photographs of the microstructure for specimens G34 through G37.

0.5 mm Coatings

The high incidence of debonding displayed by the 1 mm thick coatings prompted the reduction of thickness to 0.5 mm. Tables 3.8a and b summarize spray parameters and coating performance. The durability of these coatings was excellent, with this series

performing the best over all the graphite and nickel-graphite coatings (including the 0.25 mm coatings mentioned later). It is noted that the creep increased to 8% due to the fixed, as-machined diameters of the Amsler rollers prior to spraying.

Sample G38 survived nearly 17,000 revolutions. Debonding only occurred when the test parameters were altered. For example G38 was tested at $P_o = 1315 \text{ N/mm}^2$, which increased the applied load from 1750 N to 2000 N. Sample G40 was tested at 400 RPM on the Amsler, as opposed to the standard 200 RPM. A new phenomenon was observed, which involved small coating particles to be removed from the wear track during testing. The dominating wear mode in the 1 mm coatings were edge effects. Edge effects were minor though in the 0.5 mm coatings. Wear track particles were the cause of friction increase and ultimately coating failure.

The nickel-graphite was contained in only the top 200 μm of the coating. Figures 3.14a and b illustrate samples G38 and G41, which again represent the range of nickel-graphite content. Figures 3.15a through d represent the microstructures of samples G38 through G41.

0.25 mm Coatings

The thickness of the nickel-graphite / steel coating was reduced to 0.25 mm in attempt to further improve durability. Tables 3.9a and b illustrate the spray parameters and performance results of samples G50 through G54. The durability of this series was comparable to that of the 0.5 mm coatings, with test durations exceeding 10,000 revolutions. Their ability to maintain friction reduction was also comparable. Only sample G50 had a relatively large change in friction, $\mu = 0.14$ to $\mu = 0.28$, for a test of 6310 revolutions. Tests were terminated at 10,000 revolutions and declared successful. Removed wear track particles were the main source of coating degradation, with almost no evidence of edge effects. The graphite was effectively in only the top 100 μm .

Figures 3.16a through d illustrate the microstructure of samples G50 through G53. Sample G54 had a very thin layer ($< 30 \mu\text{m}$) of pure nickel-graphite deposited over a 0.25 mm steel matrix. The wear performance was comparable to G50 through G53.

Low Volume Nickel-Graphite

Coatings with low nickel-graphite volume fraction were sprayed utilizing a low feed wheel in the powder feeder. The coatings ranged from 1 - 5 % nickel graphite by volume. Table 3.10 and b summarize the spray parameters and wear performance of samples G42 through G45. Only G45 had sufficient nickel-graphite (5%) to control friction. The other samples had friction values comparable to steel coatings without added solid lubricants. The samples debonded in four of the six tests. The coatings had varying thicknesses around 0.5 mm, but G42 was only 0.25 mm thick. The limited performance of these samples suggested that a minimum of 5% graphite was needed to form a lubricating film between rollers. Figures 3.17a and b illustrate the coating microstructure of G45 (1%) and G44 (5%). Figures 3.18a through d show the microstructure of all four samples, G42 through G45, at a higher magnification.

Repeatability Tests

The most durable 0.5 mm nickel-graphite / steel coatings (G38, G39, and G40) were reproduced to confirm the performance results. Tables 3.11a and b summarize the spray parameters and performance results of the repeatability tests. The microstructures were similar to previously shown samples. The durability and friction reduction was excellent, behaving similarly to the original coatings. This series further evaluated the effect of test parameters on coating performance. The coating G46 was tested at 400 RPM and failed within 2000 revolutions. Test G46 #3 and

G48 #2 were tested against roughened bottom rollers. Both samples had diminished life with little friction reducing capability. The incidence of debonding was evident but generally occurred only after a significant amount of revolutions (> 6000).

Synopsis

The optimized nickel-graphite containing 1080 steel coatings exhibited excellent durability and friction reduction under certain conditions. Wear test environment though, not retained nickel-graphite volume fraction, determined the overall performance. The nickel-graphite containing coatings degraded rapidly (< 200 revolutions) when tested at 35% creep. If the bottom roller (wheel steel) was roughened through knurling, shot blasting, or even by a rough finishing cut during machining, the coating failed to reduce friction appreciably. When the Amsler machine was ran at 400 rpm rather than 200 rpm, the coating again degraded rapidly. The friction coefficient rose to 0.4 or 0.5 during these tests.

Table 3.5a. Spray parameters for nickel-graphite powder / 1080 steel coatings G25 through G27. Gas parameters were 230 slpm N₂ / 30 slpm H₂ with a working distance of 235 mm.

Sample	Powder Feeder (RPM)	Coating Thickness (mm)	Graphite Volume (%)
G25	10	1.5	10
G26	10	0.95	10
G27	15	1.0	24

Powder injection distance= 25 mm @ 45°; Powder gas = 36 slpm
Power= 130 kW @ 370 V and 350 A

Table 3.5b. Amsler performance test conditions and results for nickel-graphite powder / 1080 steel coatings G25 through G27.

Sample	P_o (N/mm ²)	Creep ¹ (%)	Test Length (revs.)	Friction Coefficient (μ)	Comments
G25 #1	900	36.1	< 200	0.5	T
G25 #2	1220	4.7	800	0.47	D,E
G26 #1	900	5.4	1200	0.38	T
G26 #2	1220	37.2	< 200	0.5	T
G27 #1	900	4.9	3500	0.20	D,E
G27 #2	1220	5.1	2100	0.16	D,E
1. Creep was calculated from as-sprayed roller diameters Comments: D= debonded; E= severe edge effects; T= test terminated					

Table 3.6a. Spray parameters for 1 mm nickel-graphite powder / 1080 steel coatings G28 through G33. Gas parameters were 230 slpm N₂ / 30 slpm H₂ with a working distance of 235 mm.

Sample	Powder Feed (RPM)	Coating Thickness (mm)	Graphite Volume (%)
G28	5	0.95	6
G29	7.5	0.87	8
G30	10.0	0.91	10
G31	12.5	0.96	12
G32	15.7	1.0	22
G33*	18.6	0.98	34

Powder injection distance= 25 mm @ 45 °; Powder gas= 36 slpm
 Power= 130 kW @ 370 V and 350 A
 * Maximum powder feed rate

Table 3.6b. Amsler performance test conditions and results for 1 mm nickel-graphite powder / 1080 steel coatings G28 through G33.

Sample	P_o (N/mm ²)	Creep ¹ (%)	Test Length (revs.)	Friction Coefficient (μ)	Comments
G28 #1	1220	5.14	3900	0.14	D
G28 #2	900	5.04	4750	0.14	D
G29 #1	1220	6.67	5540	0.14	D
G29 #2	1315	6.24	1230	0.14	D,E
G30 #1	1220	6.24	2320	0.14	D
G30 #2	1315	6.25	1730	0.14	D,E
G31 #1	1220	5.43	600	0.14	D,E
G31 #2	1220	5.21	3300	0.14	D,E
G32 #1	900	35.8	< 200	0.50	T
G32 #2	1220	4.9	8500	0.14	D
G33 #1*	900	5.3	8000	0.14	
G33 #2*	1220	5.3	4450	0.14	D
G33 #3	900	34.8	< 200	0.50	T

1. Creep was calculated from as-sprayed roller diameters.
Comments: D= debonded E= severe edge effects T= test terminated
* Test continued at higher contact pressure

Table 3.7a. Spray parameters for 1 mm nickel-graphite powder / 1080 steel coatings G34 through G37. Gas parameters were 230 slpm N₂ / 30 slpm H₂ with a working distance of 235 mm.

Sample	Powder Feed (RPM)	Coating Thickness (mm)	Graphite Volume (%)
G34	5.0	0.91	6
G35	7.5	0.79	8
G36	10.0	0.92	10
G37	12.5	0.95	12

Powder injection distance= 25 mm @ 45°; Powder gas= 36 slpm
Power= 130 kW @ 370 V and 350 A

Table 3.7b. Amsler performance test conditions and results for 1 mm nickel-graphite powder / 1080 steel coatings G34 through G37.

Sample	P_o (N/mm ²)	Creep ¹ (%)	Test Length (revs.)	Friction Coefficient (μ)	Comments
G34 #1	1220	5.3	800	0.14	D
G34 #2	1220	5.46	12,340	0.14	W
G35 #1	1220	6.24	9590	0.14	E,T
G35 #2	1315	5.73	< 200	0.5	D
G36 #1	1220	5.58	2830	0.14	E
G36 #2	900	35.1	< 200	0.5	T
G37 #1	1220	5.73	5000	0.14	E,T
G37 #2	1315	5.12	3340	0.14	E,T

1. Creep was calculated using the diameters of as-sprayed rollers.
Comments: D= debonded; E= severe edge effects; T= test terminated; W= wear track particle removal.

Table 3.8a. Spray parameters for 0.5 mm nickel-graphite powder / 1080 steel coatings G38 through G41. Gas parameters were 230 slpm N₂ / 30 slpm H₂ with a working distance of 235 mm.

Sample	Powder Feed (RPM)	Coating Thickness (mm)	Graphite Volume (%)
G38	5.0	0.42	6
G39	7.5	0.47	8
G40	10.0	0.45	10
G41	12.5	0.52	12

Powder injection distance= 25mm @ 45°; Powder gas= 36 slpm
Power= 130 kW @ 370 V and 350 A

Table 3.8b. Amsler performance test conditions and results for 0.5 mm nickel-graphite powder / 1080 steel coatings G38 through G41.

Sample	P_o (N/mm ²)	Creep ¹ (%)	Test Length (revs.)	Friction Coefficient (μ)	Comments
G38 #1	1220	8.02	16,940	0.14	W
G38 #2	1315	8.21	280	0.40	W,D
G39 #1*	1220	7.57	930	0.50	W,D
G39 #2	1220	8.02	11,680	0.14	W
G40 #1	1220	7.23	6790	0.14	W
G40 #2	900	36.7	< 200	0.50	T
G41 #1	1220	7.42	4210	0.14	W
G41 #2	1220	7.42	8740	0.14	W

1. Creep was calculated using the diameters of as-sprayed rollers.
Comments: D= debonded; E= severe edge effects; T= test terminated; W= wear track particle removal.
* Sample tested at 400 RPM on Amsler.

Table 3.9a. Spray parameters for 0.25 mm nickel-graphite powder / 1080 steel coatings G50 through G54. Gas parameters were 230 slpm N₂ / 30 slpm H₂ with a working distance of 235 mm.

Sample	Powder Feed (RPM)	Coating Thickness (mm)	Graphite Volume (%)
G50	5.0	0.25	6
G51	7.5	0.25	8
G52	10.0	0.23	10
G53	10.0	0.27	12
G54	10.0	0.25	-

Powder injection distance= 25 mm @ 45°; Powder gas= 36 slpm
Power= 130 kW @ 370 V and 350 A

Table 3.9b. Amsler performance test conditions and results for 0.25 mm nickel-graphite powder / 1080 steel coatings G50 through G54.

Sample	P_o (N/mm ²)	Creep ¹ (%)	Test Length (revs.)	Friction Coefficient (μ)	Comments
G50 #1	1220	8.18	6,310	0.14 - .28	W,T
G50 #2	1220	7.96	8,400	0.14 - .25	D,W
G51 #1	1220	7.88	10,000	0.14 - .16	W,T
G51 #2	1220	35.4	< 200	0.50	T
G52 #1	1220	6.87	10,000	0.14-0.17	W,T
G52 #2*	1220	7.32	270	0.50	T
G53	1220	8.02	10,000	0.14-0.18	W,T
G54	1220	7.96	6,000	0.15	T

1. Creep was calculated using the diameters of as-sprayed rollers
 Comments: D= debonded; T= test terminated; W= wear track particle removal
 * Roughened bottom roller (120 grit sand paper)

Table 3.10a. Spray parameters for 0.5 mm (low volume) nickel-graphite powder / 1080 steel coatings G42 through G45. Gas parameters were 230 slpm N₂ / 30 slpm H₂ with a working distance of 235 mm.

Sample	Powder Feed (RPM) *	Coating Thickness (mm)	Graphite Volume (%)
G45	1.5	0.48	1
G42	2.5	0.49	3
G43	5.0	0.52	5
G44	7.5	0.5	5

Powder injection distance= 25 mm @ 45°; Powder gas= 36 slpm
 Power= 130 kW @ 370 V and 350 A
 * Low Feed Powder Wheel

Table 3.10b. Amsler performance test conditions and results for 0.5 mm (low feed) nickel-graphite powder / 1080 steel coatings G42 through G45.

Sample	P_o (N/mm ²)	Creep ¹ (%)	Test Length (revs.)	Friction Coefficient (μ)	Comments
G42 #1	1220	6.45	770	0.38	D
G42 #2	1220	6.39	1000	0.46	T
G43 #1	1220	5.78	130	-	D
G43 #2	1220	5.63	530	0.35	D
G44	1220	6.78	6740	0.14	D,W
G45	1220	5.98	300	0.46	T
¹ . Creep is calculated using the diameters of as-sprayed rollers Comments: D= debonded; T= test terminated; W= wear track particle removal					

Table 3.11a. Spray parameters for 0.5 mm nickel-graphite powder / 1080 steel coatings G50 through G54. Gas parameters were 230 slpm N₂ / 30 slpm H₂ with a working distance of 235 mm. These samples are repeat tests of the best performing 0.5 mm coatings

Sample	Powder Feed (RPM)	Coating Thickness (mm)	Graphite Volume (%)
G46	5.0	0.44	6
G47	7.5	0.45	8
G48	10.0	0.49	10
Powder injection distance= 25 mm @ 45°; Powder gas= 36 slpm Power= 130 kW @ 370 V and 350 A			

Table 3.11b. Amsler performance test conditions and results for repeat tests of 0.5 mm nickel-graphite powder / 1080 steel coatings G46 through G48.

Sample	P _o (N/mm ²)	Creep ¹ (%)	Test Length (revs.)	Friction Coefficient (μ)	Comments
G46 #1	1220	7.50	6150	0.14	D,W
G46 #2	1220	6.95	7170	0.14	D,W
G46 #3	1220	6.57	1200 ³	0.3	D
G46 #4	1220	8.11	17,110	0.14-0.16	T,W
G46 #5	1315	7.56	11,860	0.14-0.17	D,W
G46 #6	1220	7.46	670 ²	0.41	T
G46 #7	900	7.34	1100 ²	0.44	T
G47 #1	1220	5.63	9310	0.14	D,W
G47 #2	1315	6.78	5680	0.14	D
G48 #1	1220	7.77	12,000	0.14	T,W
G48 #2	1220	7.43	3820 ⁴	0.38	T
¹ Creep is calculated using the diameters of as-sprayed rollers ² Sample tested at 400 RPM on Amsler ³ Roughened bottom roller via alumina grit blast ⁴ Roughened bottom roller via 120 grit sand paper. Comments: D= debonded; T= test terminated; W= wear track particle removal					



(a) 50x



(b) 200x

Figure 3.7. Photomicrographs of nickel-graphite / steel coatings showing dispersion of graphite particles. (G25). Gas parameters: 230 slpm N_2 / 30 slpm H_2 , 235 mm working distance. a) Low mag view of coating. b) Close-up of interface showing graphite particles.

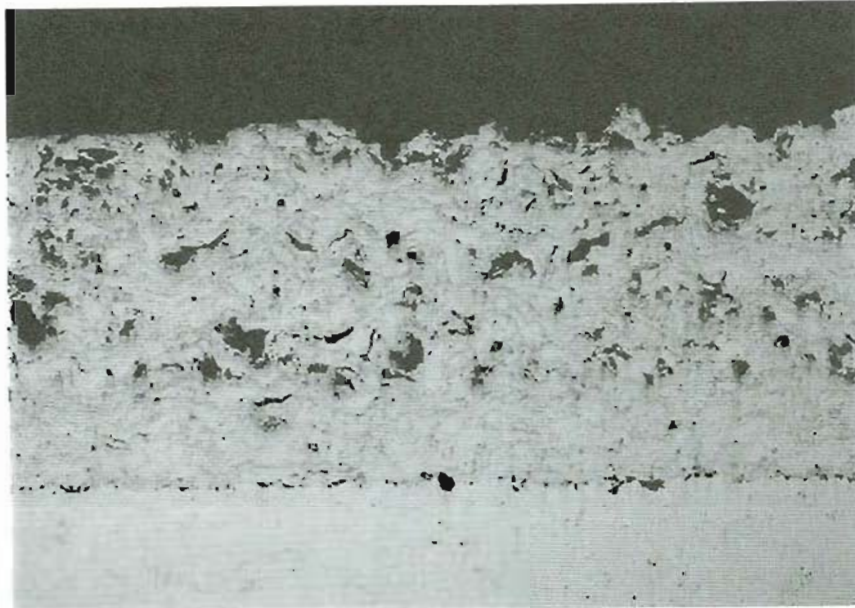


(a) 200x

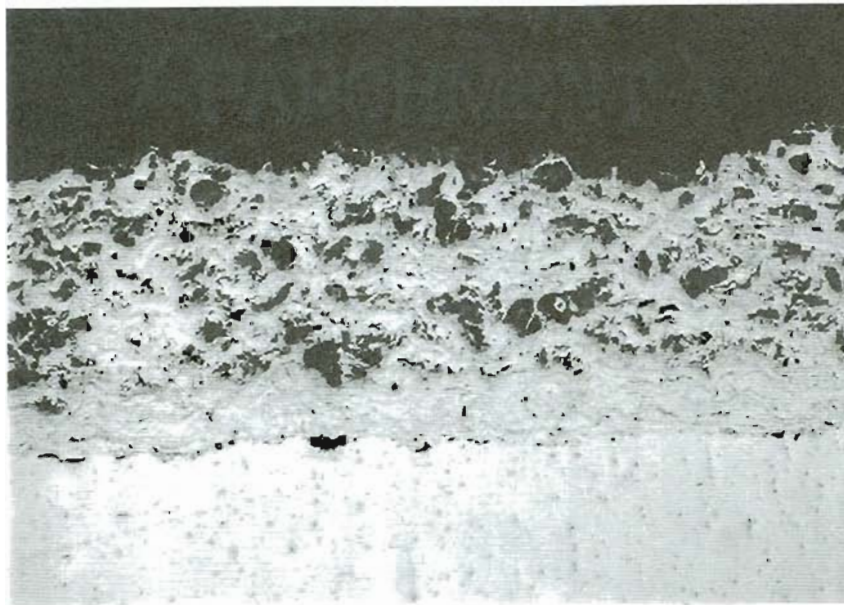


(b) 200x

Figure 3.8. Photomicrographs of 1 mm nickel-graphite / steel coatings showing microstructure. Gas parameters: 230 slpm N_2 / 30 slpm H_2 , 235 mm working distance. a) Sample G25, graphite volume= 10%. b) Sample G27, graphite volume= 24%.



(a) 50x



(b) 50x

Figure 3.9. Photomicrographs of 1 mm nickel-graphite / steel coatings showing microstructure. Note: graphite is dispersed away from the interface. Gas parameters: 230 slpm N_2 / 30 slpm H_2 , 235 mm working distance. a) Sample G28, graphite volume= 6%. b) Sample G33, graphite volume= 34%.



(a) 200x



(b) 200x

Figure 3.10. Photomicrographs of 1 mm nickel-graphite / steel coatings showing microstructure. Gas parameters: 230 slpm N_2 / 30 slpm H_2 , 235 mm working distance. a) Sample G28, graphite volume= 6%. b) Sample G29, graphite volume= 8%.

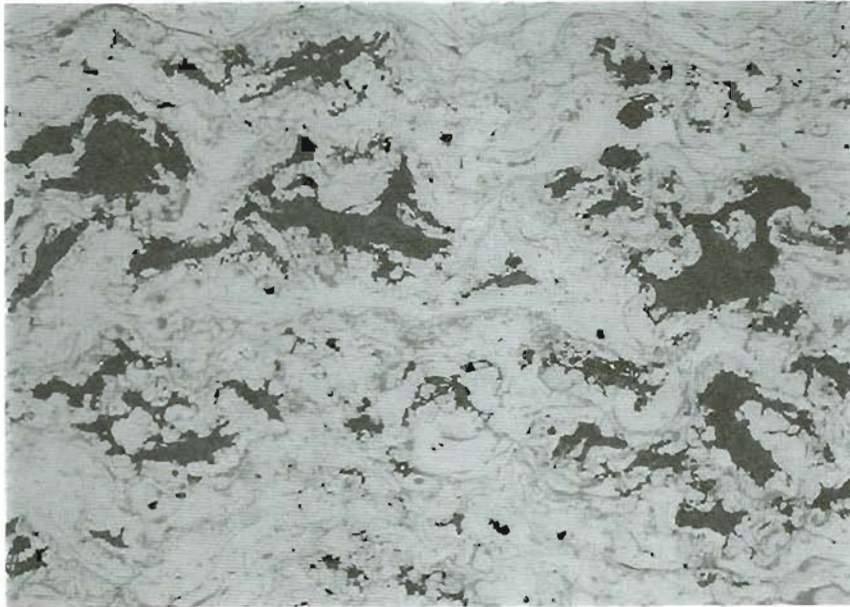


(c) 200x



(d) 200x

Figure 3.10. Continuation, of 1 mm nickel graphite/steel coatings. c) G30, graphite volume = 10%. d) G31, graphite volume = 12%.

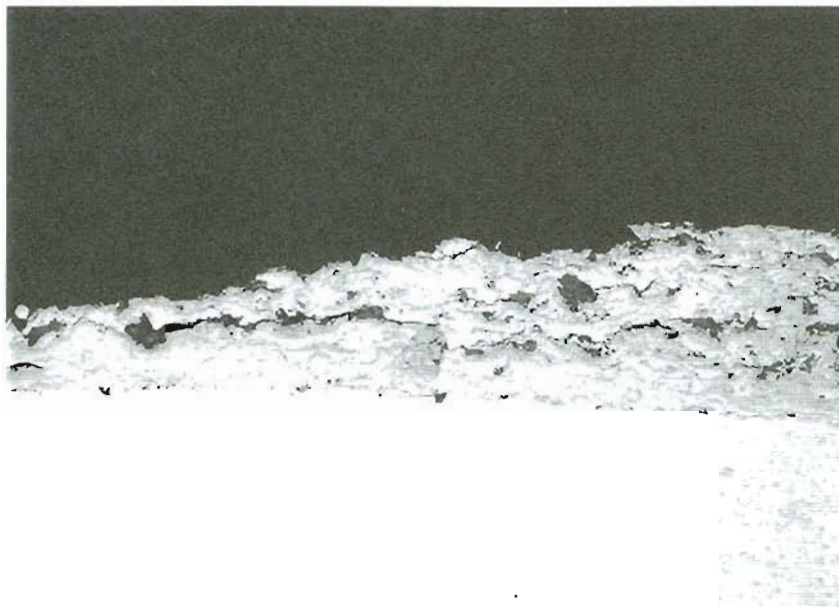


(e) 200x

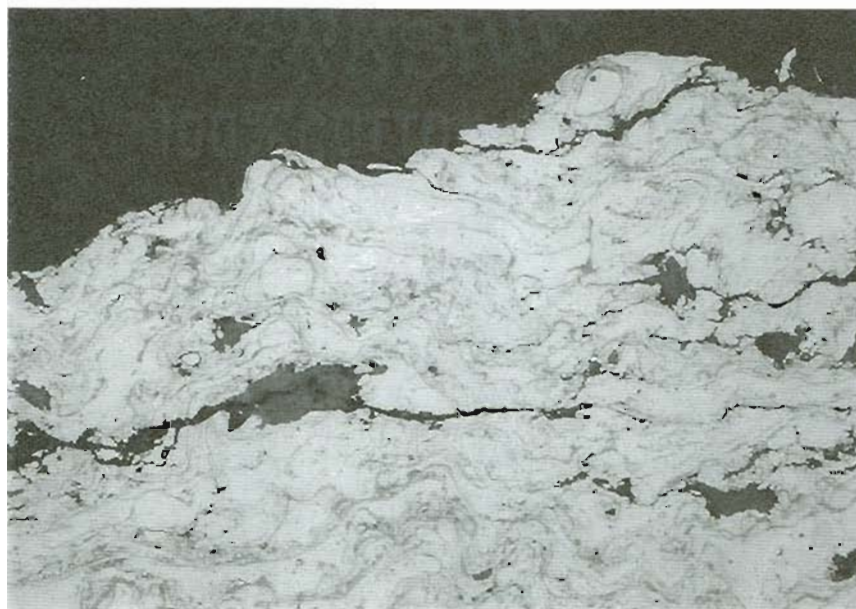


(f) 200x

Figure 3.10. Continuation, of 1 mm nickel graphite/steel coatings. e) G32, graphite volume = 22%. f) G33, graphite volume = 34%.



50x

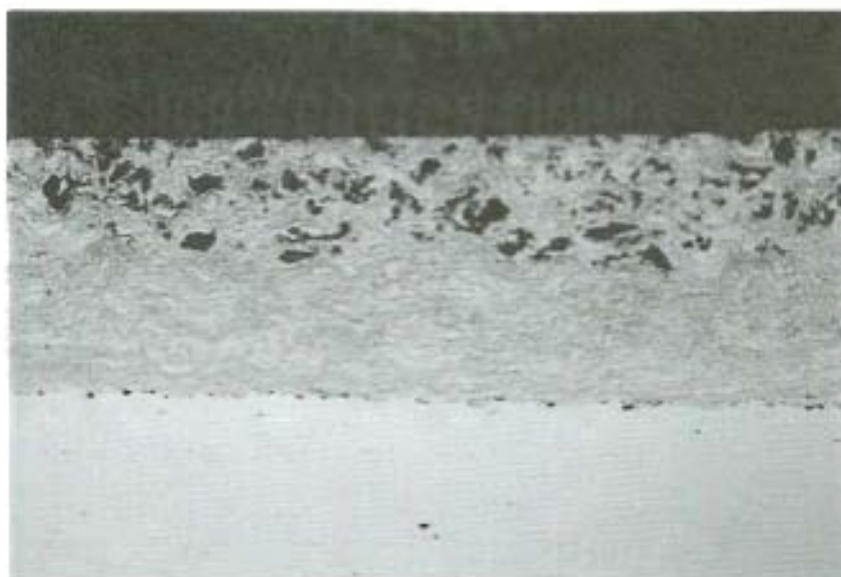


200x

Figure 3.11. Photomicrographs of Sample G32 showing cracks which run within coating microstructure. Cracks propagate between graphite particles. Sample was tested at $P_0=1220 \text{ N/mm}^2$ and 5% creep. Sample debonded after 8500 revolutions.



(a) 50x



(b) 50x

Figure 3.12. Photomicrographs of 1 mm nickel-graphite / steel coatings showing range of microstructure. Note: graphite is only dispersed in top $400\mu\text{m}$. Gas parameters: 230 slpm N_2 / 30 slpm H_2 , 235 mm working distance. a) Sample G34, graphite volume= 6%. b) Sample G37, graphite volume= 12%.



(a) 200x



(b) 200x

Figure 3.13. Photomicrographs of 1 mm nickel-graphite / steel coatings showing microstructure. Gas parameters: 230 slpm N_2 / 30 slpm H_2 , 235 mm working distance. a) Sample G34, graphite volume= 6%. b) Sample G35, graphite volume= 8%.



(c) 200x



(d) 200x

Figure 3.13. Continuation, of 1 mm nickel graphite/steel coatings. c) G36, graphite volume = 10%. d) G37, graphite volume = 12%.

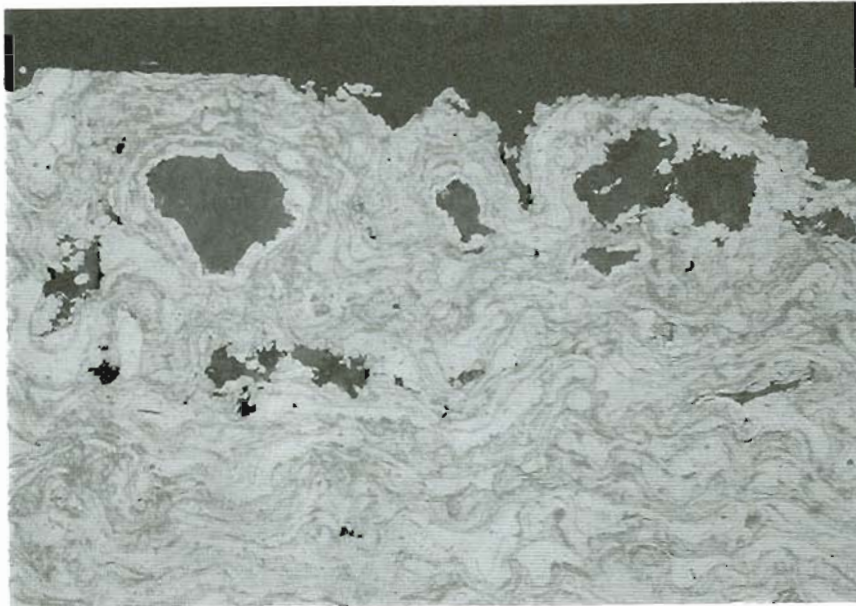


(a) 100x



(b) 100x

Figure 3.14. Photomicrographs of 0.5 mm nickel-graphite / steel coatings showing range of microstructure. Note: graphite is only dispersed in top $200\mu\text{m}$. Gas parameters: 230 slpm N_2 / 30 slpm H_2 , 235 mm working distance. a) Sample G38, graphite volume= 6%. b) Sample G41, graphite volume= 12%.

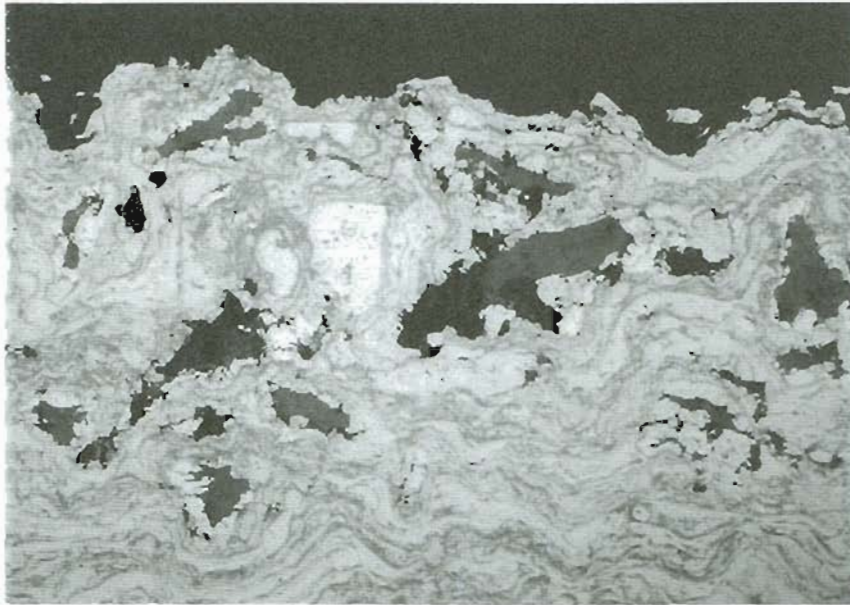


(a) 200x

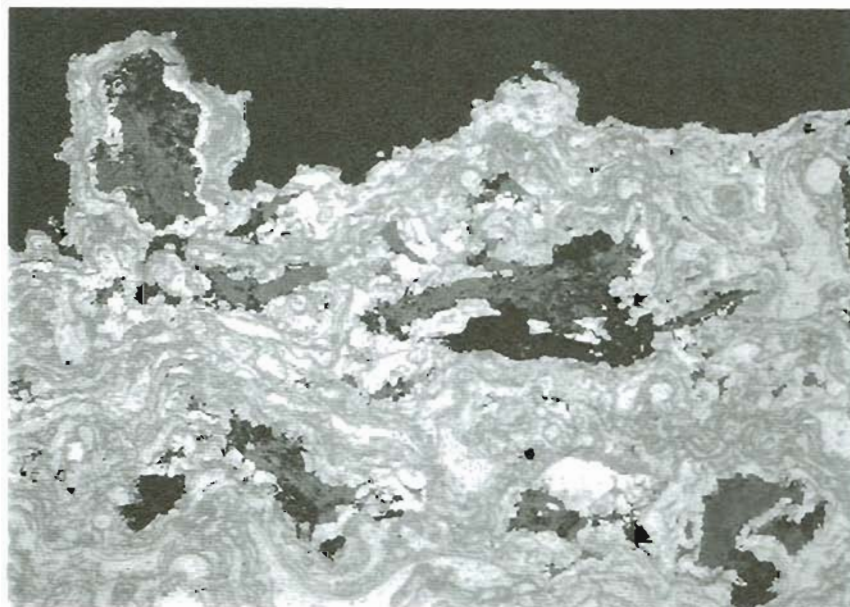


(b) 200x

Figure 3.15. Photomicrographs of 0.5 mm nickel-graphite / steel coatings showing microstructure. Gas parameters: 230 slpm N_2 / 30 slpm H_2 , 235 mm working distance. a) Sample G38, graphite volume= 6%. b) Sample G39, graphite volume= 8%.

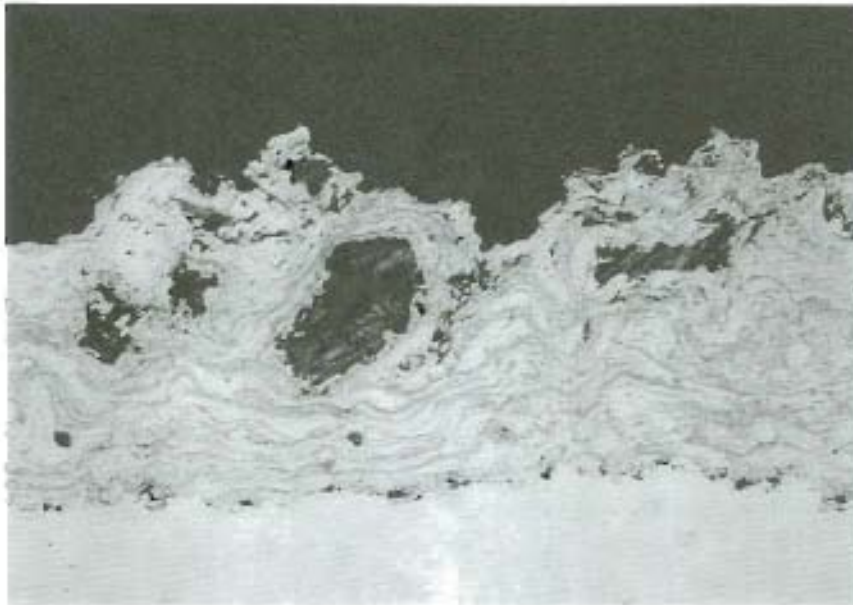


(c) 200x

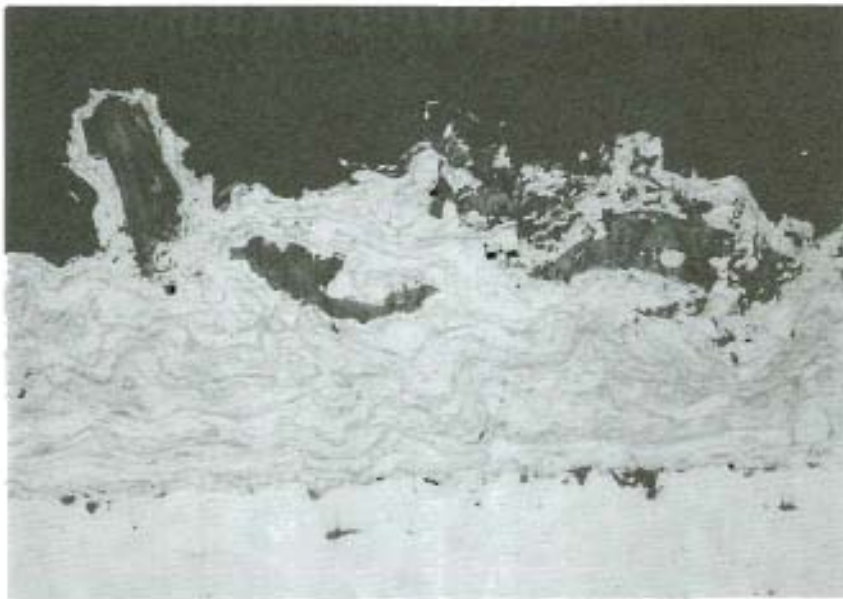


(d) 200x

Figure 3.15. Continuation, of 0.5 mm nickel graphite/steel coatings. c) G40, graphite volume = 10%. d) G41, graphite volume = 12%.

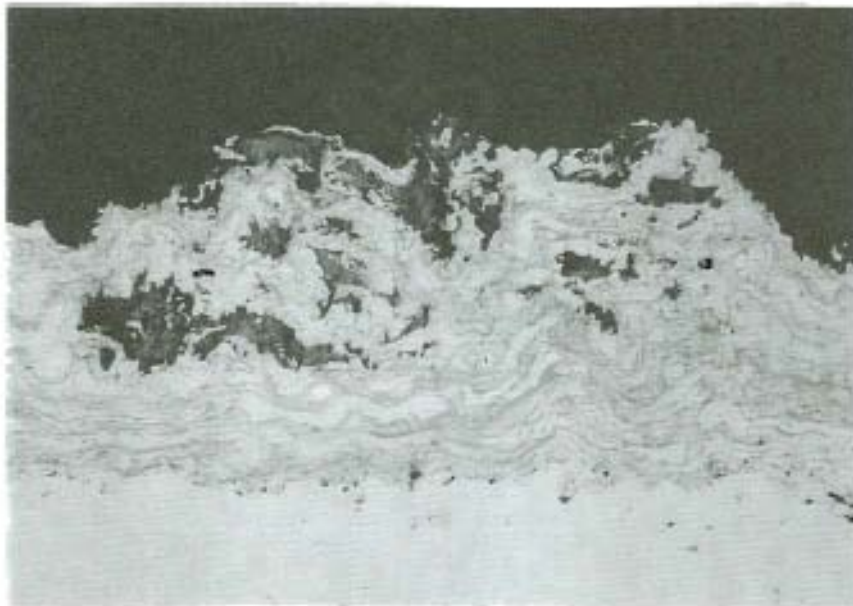


(a) 200x



(b) 200x

Figure 3.16. Photomicrographs of 0.25 mm nickel-graphite / steel coatings showing microstructure. Note: graphite is only dispersed in top 200 μm . Gas parameters: 230 slpm N_2 / 30 slpm H_2 , 235 mm working distance. a) Sample G50, graphite volume= 6%. b) Sample G51, graphite volume= 8%.



(c) 200x



(d) 200x

Figure 3.16. Continuation, of 0.25 mm nickel graphite/steel coatings. c) G52, graphite volume = 10%. d) G53, graphite volume = 12%.



(a) 100x



(b) 100x

Figure 3.17. Photomicrographs of nickel-graphite / steel coatings showing range of microstructure. Coatings were produced with low powder feed wheel. Gas parameters: 230 slpm N_2 / 30 slpm H_2 , 235 mm working distance. a) Sample G45, graphite volume= 1%. b) Sample G44, graphite volume= 5%.



(a) 200x



(b) 200x

Figure 3.18. Photomicrographs of low volume nickel-graphite / steel coatings showing microstructure. Gas parameters: 230 slpm N_2 / 30 slpm H_2 , 235 mm working distance. a) Sample G45, graphite volume= 1%. b) Sample G42, graphite volume= 3%.



(c) 200x



(d) 200x

Figure 3.18. Continuation, of 0.25 mm nickel graphite/steel coatings. c) G43, graphite volume = 5%. d) G44, graphite volume = 5%.

3.2.4 Cast Iron Powder

Gray cast iron powders can have graphite volume fractions of 10-20%. The powder used for samples G55 through G58 had roughly 15% free graphite. When cast iron powder was deposited with 1080 steel the subsequent microstructures were absent of graphite. Metallography revealed a microstructure similar to that of a 1080 steel coating without any solid lubricant particles. Amsler wear tests confirmed the lack of graphite as $\mu=0.46$ for all four tests. Subsequently, the wear tests were terminated within 2500 revolutions. Table 3.12 is a summary of the spray parameters and performance results for samples G55 through G58.

Table 3.12. Spray parameters and performance results for cast iron powder / 1080 steel coatings (samples G55 through G58). Gas Parameters: 230 slpm N₂ / 30 slpm H₂, 235 mm working distance. Amsler wear test parameters: P_o= 900 N/mm², 5% creep.

Sample	Powder Feed (RPM)	Powder Injection (mm)	Coating Thickness (mm)	Durability (revs.)	Comments
G55	2	25	1.16	2500	T
G56	5.5	25	0.98	2000	T
G57	10	85	1.07	2000	T
G58 *	15.7	85	1.16	1850	D
Powder Injection @ 45°; Powder Gas= 42 slpm; μ = 0.46 (steady state)					
Comments: D= debond; T= test terminated.					
* Sample G58 was sprayed using two 1080 steel wires.					

3.3 Copper

In the previous section graphite, a well known solid lubricant, was combined with steel to form a composite coating. A less conventional material to act as a solid lubricant comes in the form of a soft metal. Soft metals have been used in the metal working industry as a means of controlling friction during forming and drawing. It was postulated that a thin soft metal film may provide similar lubrication and friction control in a rolling / sliding contact situation. Several soft metals exist which have low shear strength and high ductility. Copper, because of its availability, was chosen as suitable material to be dispersed within a 1080 steel coating to control friction.

Copper was evaluated in wire feedstock and powder form. The results of copper / 1080 steel coatings are divided into two sections: coatings created using copper wire and those using copper powder. Coating microstructures were evaluated on flat coupons initially. Later work involved Amsler wear testing of the coatings to determine durability and degree of friction reduction. Tables summarize the metallographic and wear results. Photomicrographs illustrate coating microstructure or features of interest.

3.3.1 Copper Wire Feedstock

Initial work with copper consisted of coatings created by co-spraying 1080 steel wire with copper wire. These coatings were sprayed onto a flat substrate. The microstructure of the coupons demonstrated the limitations of the system and lead to the determination of the best spray parameters. Amsler rollers were coated and tested. The parameters were refined in an attempt to improve the wear durability. Ultimately, the gas parameters remained constant and the only variables became wire feed rate and wire injection distance.

The flat coupons were sprayed in three sets. Each set had a fixed wire injection distance with varying wire feed rate. The gas parameters remained at 230 slpm N₂ / 30 slpm H₂ with a working distance of 235 mm. Tables 3.13 through 3.15 summarize the spray parameters and metallographic results. Copper volume fractions were estimated in most samples. Copper volume fractions were not determinable for samples created with a copper wire feed rate less than 3.1 kg/hr, instead a range of copper volume is given. At copper feed rates below 2.9 to 3.1 kg/hr, depending on injection distance, the molten particles were not directed down the center of the plume. As a result the coupons had a very heterogeneous microstructure over the area sprayed. One area would have 80-90% copper while the other end had less than 10%. Figure 3.19 illustrates the concentration gradient which resulted from low wire feed rates. When wire feed rate exceeded 3.1 kg/hr the microstructure remained homogenous.

Virtually no contrast existed between spray coated 1080 steel and copper. It was found that the steel matrix could be stained with a 2% nital etch and the copper would remain unchanged. Figure 3.20 illustrates the contrast of an etched and unetched copper / steel coating. These photos also illustrate characteristic, low magnification microstructures. All photomicrographs were etched to better reveal the copper structure and distribution.

The microstructures of the coatings summarized in Tables 3.13 to 3.15 are shown in Figures 3.21 through 3.23. The figures illustrate the characteristic microstructures over the range of copper wire feed rates, at a given wire injection distance. Micrographs of samples whose wire feed rate was less than 3.1 kg/hr were taken mid-sample. This allowed the average copper content to be recorded, instead of the non-characteristic extremes.

The microstructures have very similar morphologies, with the volume fraction being the only major difference. The copper deposition was very efficient, in that low wire feed rates yielded large copper volume fractions. A critical feed rate, which

corresponds to the 3.1 kg/hr, marked a large increase in copper volume fraction. This increase was less significant as copper wire was injected farther from the anode (downstream). For example, Figure 3.21d was sprayed at an injection distance of 25 mm and wire feed rate of 4.3 kg/hr. Figure 3.23d was also sprayed at a wire feed rate of 4.3 kg/hr, but the wire injection distance was 85 mm. The morphology was slightly altered, but more importantly the volume fraction of copper was about 10% greater in Figure 3.21d. The effect of injection distance on copper volume fraction was important when coating Amsler rollers.

The most desirable feed rate from a deposition point of view was that which enabled the copper wire to melt off in the center of the plume. This feed rate was dubbed 'ideal', and would vary depending on the injection distance due to thermal gradients. Unfortunately the 'ideal' feed created a coating with 60-70% copper by volume. Changing feed rates and injection distance became the only means of altering copper volume fraction. The coupon results demonstrated the system constraints of spraying copper wire, but since no wear data were generated, no real conclusions of performance could be drawn.

Amsler Rollers

The flat coupon results aided in the selection of spray parameters for coating deposition onto Amsler rollers. The gas parameters were again 230 slpm N₂ / 30 slpm H₂ with a working distance of 235 mm. The effect of injection distance, injection angle, and wire feed rate were all investigated in an attempt to maximize coating performance. Several sets of Amsler rollers were sprayed and tested but the performance results remained fairly consistent. The copper volume fractions were estimated.

Table 3.16a and b summarize the spray parameters and performance results for copper /steel coatings AC1 through AC10. The wire injection distance was 25 mm with insertion at 45

degrees. The 'ideal' wire feed rate was 3.6 kg/hr for this injection distance and angle. Thus, it was used for several of the tests. These rollers were tested at different contact pressures ranging from 700 N/mm² to 1220 N/mm² with slip ratios of 5 or 35%. The slip ratio varied depending on the exact coating thickness, but generally remained within $\pm 1\%$.

The performance of these coatings was poor under these contact conditions. Durability never exceeded 2000 revolutions. This set of tests attempted to test a wide range of copper volume fractions against a wide range of contact conditions. No trend was observed that would correlate contact conditions or copper volume to performance. All of these coatings were run to failure with every sample debonding. Figure 3.24 illustrates the range of microstructures observed in samples AC1 through AC10. The copper volume fraction shows a large increase when the 'ideal' feed rate is reached. The difference in copper volume between a feed rate of 2.4 kg/hr and 3.6 kg/hr is nearly 50%. This no-middle-ground phenomenon was inherent to the plasma system when co-spraying copper wire and steel wire.

All of the coatings displayed material transfer to the bottom roller during testing. Visual observation suggested the amount of material which transferred was proportional to the copper volume fraction. The contact pressure effected the morphology of the transferred material. When contact pressure was low ($P_o = 700$ to 900 N/mm²), the material was in the form of globules. When contact pressure was high ($P_o = 1220$ N/mm²) the transferred copper would form a thin film. Figure 3.25 illustrates the appearance of the two transferred copper morphologies. The transferred film morphology had some influence on friction coefficient. Some samples which were tested at high contact pressure or high creep did show some friction reduction. This small improvement over the baseline $\mu = 0.46$ is overshadowed though, by the poor durability.

The poor performance of samples AC1 through AC10 prompted the exploration of different parameters. It was observed in the

1080 steel that wire injection at 90° was less efficient. Injecting copper wire at 90° may reduce the amount retained in the coating but still allow the 'ideal' wire feed rate to be used. When injection angle was changed to 90° the wire feed rate required for the wire to melt off at plume center was reduced to 2.4 kg/hr. This value remained fairly constant over the range of wire injection distances. Injection distance was varied in an attempt to further reduce the retained copper volume fraction.

Table 3.17a and b summarize the spray parameters and performance results for samples AC11 through AC14. The injection distances were 10, 40, 60, and 100 mm. The wear tests were very short, with a high degree of globule material transfer. Friction reduction was not observed. Figure 3.26 illustrates the microstructures of samples AC11 through AC14. The copper morphology changed as injection distance increased, with average particle size being an order of magnitude larger when injection distance increased from 10 to 100 mm. These larger particles produced a rougher coating surface, which degraded rapidly during wear testing.

The overall performance of the copper wire coatings was disenchanting. All wire injection possibilities were attempted, but all yielded the same result. It was concluded that copper powder as opposed to wire would have a greater chance of producing a durable, self-lubricating coating.

3.3.2 Copper Powder

Given the poor results of copper wire feedstocks, a copper powder as a feedstock was used. Coatings with 1080 steel and copper powder produced more predictable microstructures with regards to the amount of copper consistently retained in the coatings. Quantification of microstructural elements was possible and performed on these samples. Microstructural and metallographic

evaluation was the same as performed on the copper wire / steel coatings.

Amsler Tests

The performance of copper / 1080 steel coatings was well understood by the time copper powder was used. The work with copper powder is an attempt to increase the coating's performance through better control of copper volume fraction and copper particle size. Flat coupons were not sprayed with copper powder, instead round witness samples were sprayed together with Amsler rollers to provide an exact metallographic record.

Tables 3.18a and b summarize the spray parameters and performance results of samples AC16 through AC21. These coatings consisted of two sets of three. In samples AC16 through AC18 large bore (6.4 mm i.d.) powder feed tubes were used. These are the only samples where large bore feed tubes were used (this covers all coating systems: graphite, polymers, etc.). In AC19 through AC21 the standard (1.9 mm i.d.) powder feeder tubes were used. The different tubes made only a small difference in the delivery of copper. The powder feed gas flow rate was adjusted to deliver powder to the center of the plume for each given orifice size. Figure 3.27 illustrates the copper / steel coating microstructures over a range of copper volume fractions. The copper volume varied between 10% and 43%.

The durability of samples AC16 through AC21 was poor. The longest test lasted 1440 revolutions. All of the samples debonded and produced material transfer to the bottom roller. Friction reduction was minimal, with a value of $\mu = 0.38$ being the lowest. A friction coefficient of 0.38 was the lowest value achieved for any of the copper / 1080 steel coatings, made with wire or powder. Several of the coatings were tested at both low and high contact pressures and/or 35% and 5% creep. The more severe test conditions appeared to only reduce durability even further. Debonding was a

frequent occurrence for the copper coatings. Figure 3.28 illustrates an interfacially cracked coating still intact to the Amsler roller. Figure 3.29 illustrates a roller with debonded coating partially removed.

Low Feed Wheel

The copper volume fraction was 10% at the lowest powder feed rate in samples C16 through C21. Evaluation of coating performance at copper <10% was desirable. It was hypothesized a very low volume of copper could offer some lubrication without compromising the steel coating integrity. A low feed powder wheel was employed to produce copper and steel coatings AC30 through AC35. Two 1080 steel wires were co-sprayed with the copper powder for samples AC31, AC32, and AC35, as opposed to one wire in all other tests. This was done to further dilute the copper powder.

Table 3.19a and b summarize the spray parameters and performance results for samples AC30 through AC35. These coatings were again tested at a wide range of contact pressures and slip ratios. The results were similar to the other copper / steel coatings, with low durability and minimal friction reduction. The longest test was only 1140 revolutions. Low copper volume coatings showed only minimal material transfer, with samples AC31 and AC32 showing none at all. Figure 3.30 illustrates the range of microstructures tested. These coatings varied in copper volume from 6% to 25%.

3.3.3 Synopsis

All of the copper containing steel coatings illustrated poor durability and minimal friction reduction. Test length rarely exceeded 1000 revolutions. Friction reduction was minimal, with $\mu=0.38$ being the lowest value achieved. All of the samples debonded, regardless of material transfer, copper volume fraction, or loading.

The copper source material, wire or powder feedstocks, made little difference in overall performance. Most of the copper / steel coatings exhibited some material transfer to the bottom roller. The amount of material transferred was a function of copper volume fraction, with the morphology being a function of contact pressure.

Table 3.13. Spray parameters and copper volume fraction results for copper wire / 1080 steel coatings applied to flat coupons. Copper wire injection distance = 25 mm. Samples C1 through C7. Gas parameters were 230 slpm N₂ / 30 slpm H₂ with a working distance of 235 mm.

Sample	Wire Feed Rate (kg/hr)	Copper Volume (%)
C1	4.3	70-80
C2	3.9	65-75
C3*	3.6	60-70
C4	2.9	15-90
C5	2.4	10-80
C6	1.9	10-80
C7	1.4	5-75

Copper wire injection angle= 45°
Power= 130 kW @ 370 V and 350 A
* Optimum wire feed rate.

Table 3.14. Spray parameters and copper volume fraction results for copper wire / 1080 steel coatings applied to flat coupons. Copper wire injection distance= 45 mm. Samples C8 through C17. Gas parameters were 230 slpm N₂ / 30 slpm H₂ with a working distance of 235 mm.

Sample	Wire Feed Rate (kg/hr)	Copper Volume (%)
C8	3.3	60-70
C9	3.9	50-60
C10	4.3	50-60
C11	4.8	45-55
C12	3.6	50-60
C13	2.9	25-90
C14	2.4	20-90
C15	1.9	20-90
C16	1.4	10-80
C17*	3.1	70-80
Copper wire injection angle= 45° Power= 130 kW @ 370 V and 350 A * Optimum wire feed rate.		

Table 3.15. Spray parameters and copper volume fraction results for copper wire / 1080 steel coatings applied to flat coupons. Copper wire injection distance= 85 mm. Samples C18 through C23. Gas parameters were 230 slpm N₂ / 30 slpm H₂ with a working distance of 235 mm.

Sample	Wire Feed Rate (kg/hr)	Copper Volume (%)
C18	1.9	15-75
C19	2.4	20-90
C20*	2.9	70-80
C21	3.3	65-75
C22	3.9	60-70
C23	4.3	45-55

Copper wire injection angle= 45°
Power= 130 kW @ 370 V and 350 A
* Optimum wire feed rate.

Table 3.16a. Spray parameters for copper wire / 1080 steel coatings AC1 through AC10. Gas Parameters equaled 230 slpm N₂ / 30 slpm H₂, with a working distance of 235 mm.

Sample	Wire Feed (kg/hr)	Coating Thickness (mm)	Copper Volume (%)
AC1	1.9	1.1	20
AC2	2.4	0.97	20
AC3	3.6	0.94	70
AC4	4.3	1.1	80
AC5	3.6	2.1	70
AC6	3.6	0.94	70
AC7	2.9	0.75	50
AC8	3.6	1.0	70
AC9	3.9	0.75	70
AC10	2.9	0.73	50
Wire injection distance= 25 mm @ 45° Power= 130 kW @ 370 V and 350 A			

Table 3.16b. Amsler performance test conditions and results for copper wire / 1080 steel coatings AC1 through AC10.

Sample	Contact Pressure (N/mm ²)	Creep ¹ (%)	Test Length (revs.)	Friction Coefficient (μ)
AC1	900	4.43	1,950	0.47
AC2	900	5.18	1,650	0.46
AC3 #1	900	5.35	520	0.46
AC3 #2	700	35.3	340	0.46
AC4 #1	900	4.43	230	-
AC4 #2	700	34.4	280	-
AC5 #1	700	1.63	650	0.43
AC5 #2	900	31.7	160	-
AC6 #1	1220	5.35	120	-
AC6 #2	900	35.3	310	0.42
AC7 #1	1220	6.44	760	0.38
AC7 #2	700	36.4	670	0.38
AC8	700	35.0	1,230	0.38
AC9	700	36.3	650	0.43
AC10	700	36.5	260	-
1. Creep calculated from as-sprayed roller diameters. Friction coefficient not measurable for tests under 300 revs.				

Table 3.17a. Spray parameters for copper wire / 1080 steel coatings AC11 through AC14. Gas Parameters equaled 230 slpm N₂ / 30 slpm H₂, with a working distance of 235 mm.

Sample	Wire Injection (mm)	Coating Thickness (mm)	Copper Volume (%)
AC11	100	1.1	35
AC12	60	0.45	70
AC13	40	0.61	40
AC14	10	0.70	25

Wire injection angle= 90 degrees; Wire feed rate=2.4 kg/hr.
Power= 130 kW @ 370 V and 350 A

Table 3.17b. Amsler performance test conditions and results for copper wire / 1080 steel coatings AC11 through AC14.

Sample	Contact Pressure (N/mm ²)	Creep ¹ (%)	Test Length (revs.)	Friction Coefficient (μ)
AC11	900	4.43	210	-
AC12 #1	900	8.20	290	-
AC12 #2	700	38.1	360	0.50
AC13 #1	900	7.26	340	0.48
AC13 #2	700	37.2	230	-
AC14 #1	900	6.73	280	-
AC14 #2	700	36.7	650	0.43

1. Creep calculated from as-sprayed roller diameters.
Friction coefficient not measurable for tests under 300 revs.

Table 3.18a. Spray parameters for copper powder / 1080 steel coatings AC16 through AC21. Gas Parameters equaled 230 slpm N₂ / 30 slpm H₂, with a working distance of 235 mm.

Sample	Powder Feed (RPM)	Feed Tube Diameter (mm)	Powder Gas (slpm)	Coating Thickness (mm)	Copper Volume (%)
AC16	0.5	6.4	43	0.72	10
AC17	1.0	6.4	43	0.88	18
AC18	1.5	6.4	43	0.95	22
AC21	2.0	1.9	26	0.87	24
AC20	2.5	1.9	26	0.93	32
AC19	3.0	1.9	26	0.89	43

Powder injection distance= 15 mm @ 45 degrees.
Power= 130 kW @ 370 V and 350 A

Table 3.18b. Amsler performance test conditions and results for copper powder / 1080 steel coatings AC16 through AC21.

Sample	Contact Pressure (N/mm ²)	Creep ¹ (%)	Test Length (revs.)	Friction Coefficient (μ)
AC16	900	36.6	590	0.37
AC17 #1	900	35.7	750	0.38
AC17 #2	1220	35.7	620	0.37
AC18	900	35.3	1440	0.37
AC21 #1	900	35.7	1360	0.39
AC21 #2	1220	35.7	330	0.48
AC20 #1	900	35.3	820	0.41
AC20 #2	1220	5.40	470	0.41
AC19 #1	900	35.6	200	-
AC19 #2	1220	5.63	870	0.43

1. Creep calculated from as-sprayed roller diameters.
Friction coefficient not measurable for tests under 300 revs.
All samples debonded prior to test termination

Table 3.19a. Spray parameters for copper powder / 1080 steel coatings AC30 through AC35. Low feed powder wheel was employed. 1 or 2 steel wires were co-sprayed with copper. Gas Parameters equaled 230 slpm N₂ / 30 slpm H₂, with a working distance of 235 mm.

Sample	Feed Rate (RPM)*	1080 Steel Wires	Coating Thickness (mm)	Copper Volume (%)
AC30	1	1	0.67	10
AC31	1	2	0.91	6
AC32	2	2	0.97	7
AC33	2	1	0.96	14
AC34	3	1	0.75	25
AC35	3	2	1.12	15

* Low feed wheel (60% feed of normal wheel)
 Powder injection distance= 15 mm @ 45 degrees.
 Power= 130 kW @ 370 V and 350 A

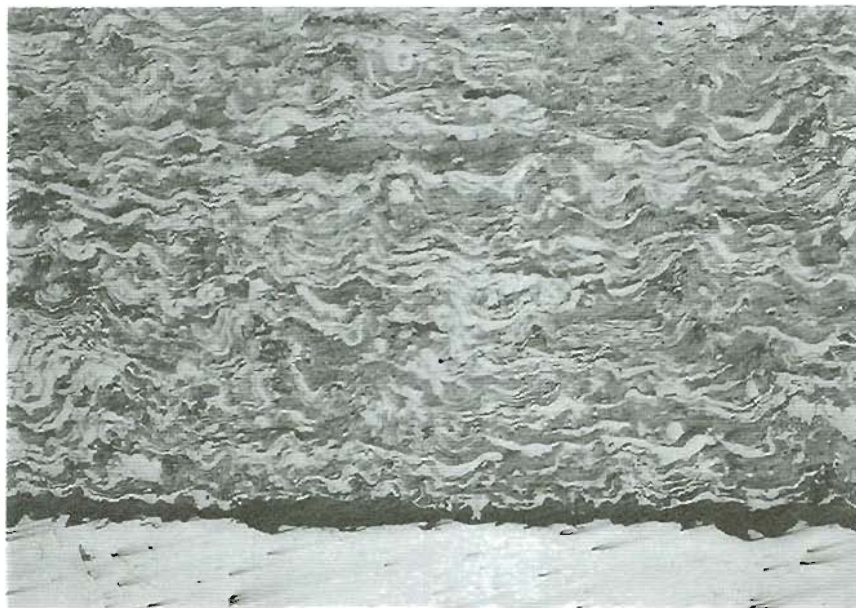
Table 3.19b. Amsler performance test conditions and results for low feed wheel deposited copper powder / 1080 steel coatings AC30 through AC35.

Sample	Contact Pressure (N/mm ²)	Creep ¹ (%)	Test Length (revs.)	Friction Coefficient (μ)
AC30 #1	900	36.8	340	0.41
AC30 #2	900	6.91	670	0.43
AC31 #1	1220	35.5	340	0.42
AC31 #2	900	35.5	430	0.41
AC32 #1	700	35.2	1340	0.48
AC32 #2	900	35.2	1140	0.47
AC33 #1	1220	5.24	780	0.42
AC33 #2	900	35.2	640	0.44
AC34	1220	6.44	980	0.45
AC35 #1	900	34.3	320	0.47
AC35 #2	1220	5.63	560	0.44

1. Creep calculated from as-sprayed roller diameters.
All samples debonded prior to test termination

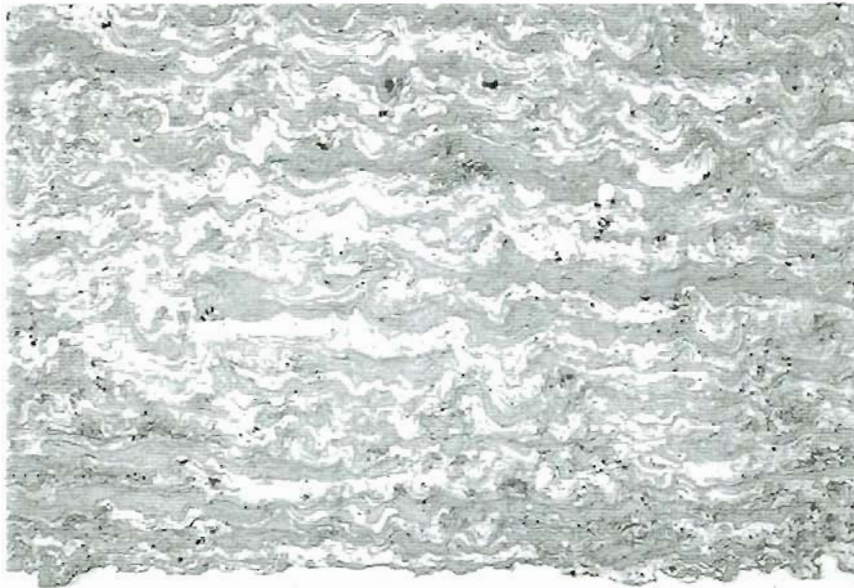


(a)

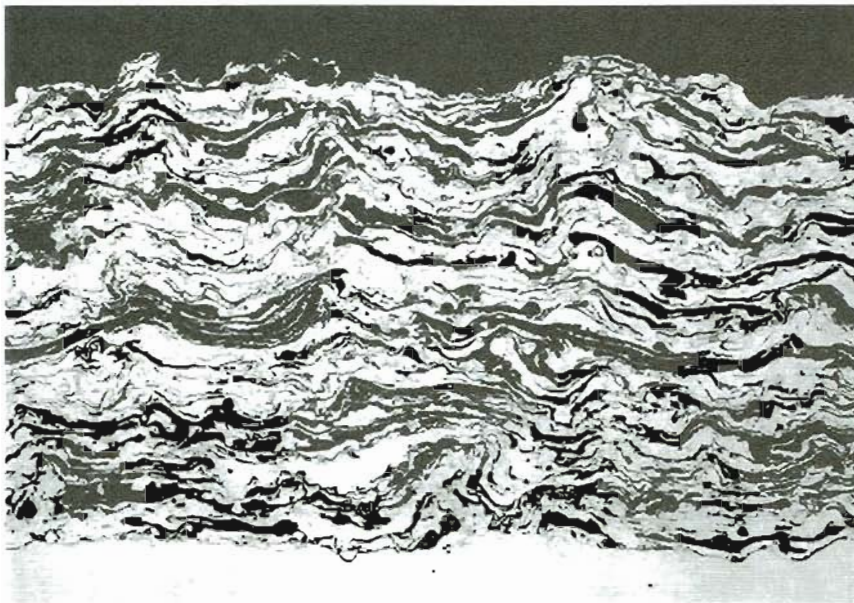


(b)

Figure 3.19. Photomicrographs of copper wire / 1080 steel coating (Sample C5) illustrating heterogeneous microstructure. a) Copper depleted region (Vol.=10%). b) Copper saturated region (Vol.=80%). Copper appears dark. As-polished. 50x.



(a)



(b)

Figure 3.20. Photomicrographs of copper wire / 1080 steel coatings illustrating contrast enhancement achieved by over-etching the steel matrix. a) as-polished sample (C16). b) 2% Nital etched sample (C17). 50x.



(a)



(b)

Figure 3.21. Photomicrographs of characteristic copper wire / 1080 steel coatings illustrating microstructure and copper volume fraction at varying wire feed rates. Wire injection distance= 25 mm @ 45°. a) 1.9 kg/hr (Sample C6). b) 2.9 kg/hr (Sample C4). 2% Nital. 200x.



(c)



(d)

Figure 3.21. Continuation, illustrating: c) 3.6 kg/hr (Sample C3).
d) 4.3 kg/hr (Sample C1). Flat coupon substrate.
2% Nital etch. 200x.



(a)



(b)

Figure 3.22. Photomicrographs of characteristic copper wire / 1080 steel coatings illustrating microstructure and copper volume fraction at varying wire feed rates. Wire injection distance= 45 mm @ 45°. a) 1.9 kg/hr (C15). b) 2.9 kg/hr (C13). 2% Nital. 200x.

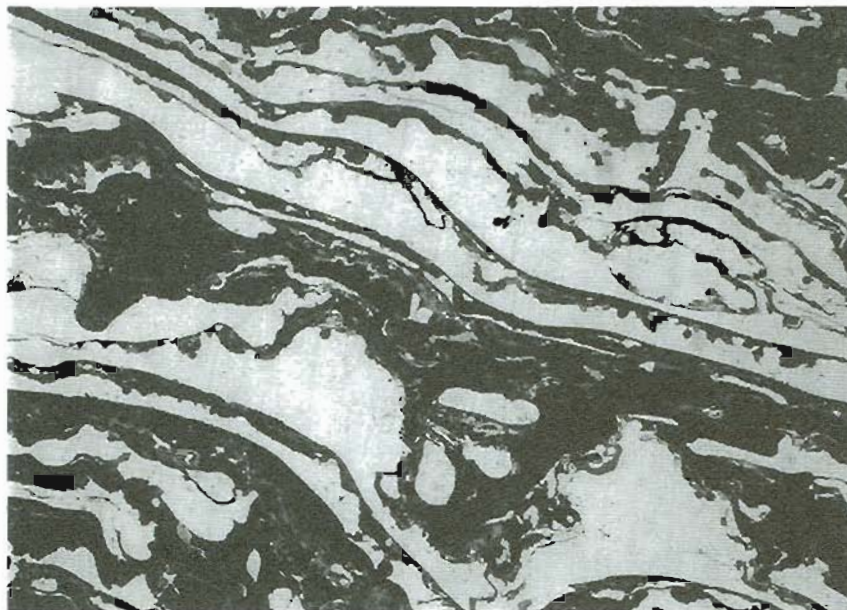


(c)



(d)

Figure 3.22. Continuation, illustrating: c) 3.1 kg/hr (Sample C17).
d) 4.3 kg/hr (Sample C10). Flat coupon substrate.
2% Nital etch. 200x.



(a)

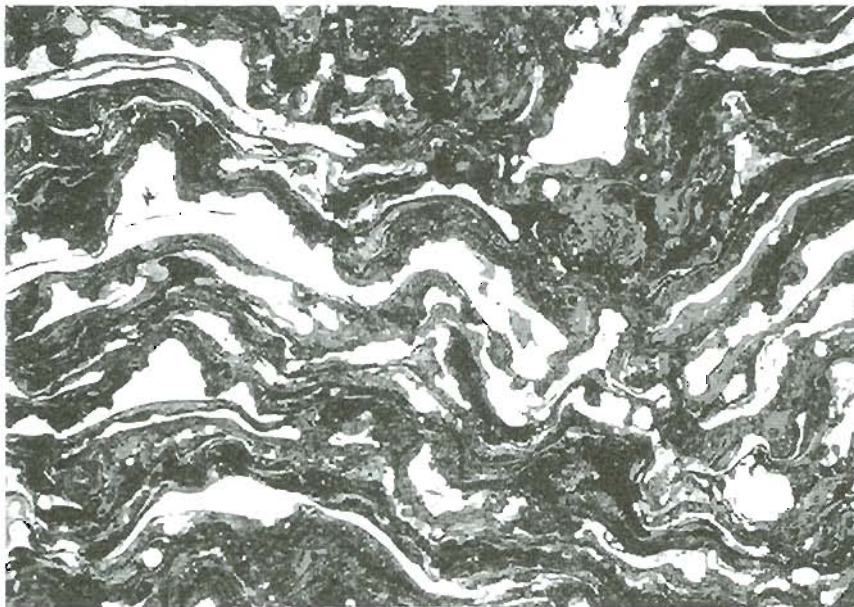


(b)

Figure 3.23. Photomicrographs of characteristic copper wire / 1080 steel coatings illustrating microstructure and copper volume fraction at varying wire feed rates. Wire injection distance = 85 mm @ 45°. a) 1.9 kg/hr (C18). b) 2.9 kg/hr (C20). 2% Nital. 200x.

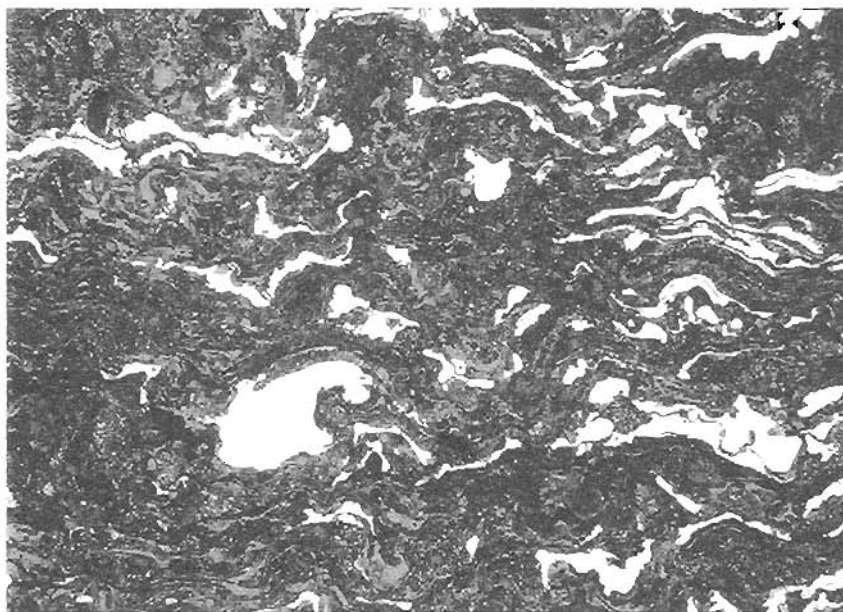


(c)

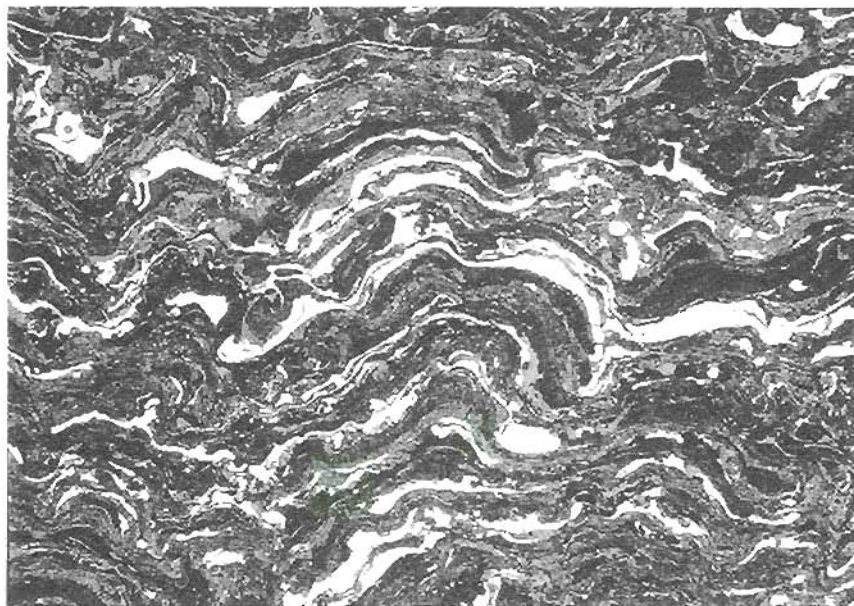


(d)

Figure 3.23. Continuation, illustrating: c) 3.3 kg/hr (Sample C21).
d) 4.3 kg/hr (Sample C23). Flat coupon substrate.
2% Nital etch. 200x.



(a)

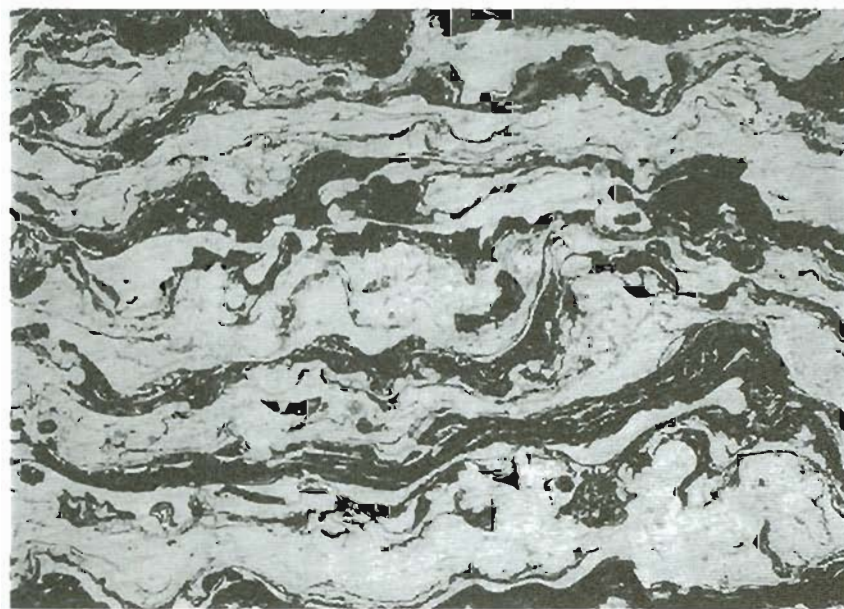


(b)

Figure 3.24. Photomicrographs of characteristic copper wire / 1080 steel coatings deposited onto Amsler rollers at varying wire feed rates. Wire injection distance = 25 mm @ 45°. a) 1.9 kg/hr (Sample AC1). b) 2.4 kg/hr (Sample AC2). 2% Nital etch. 200x.

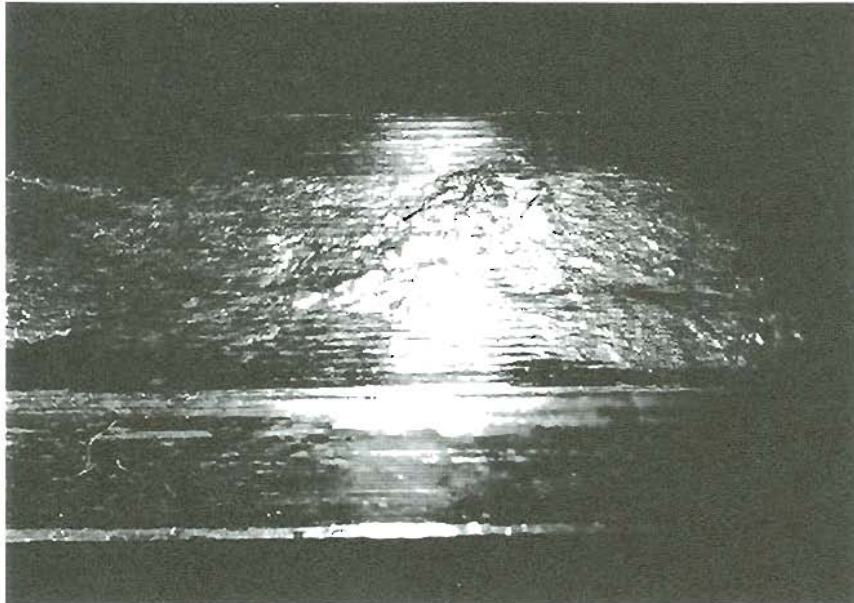


(c)

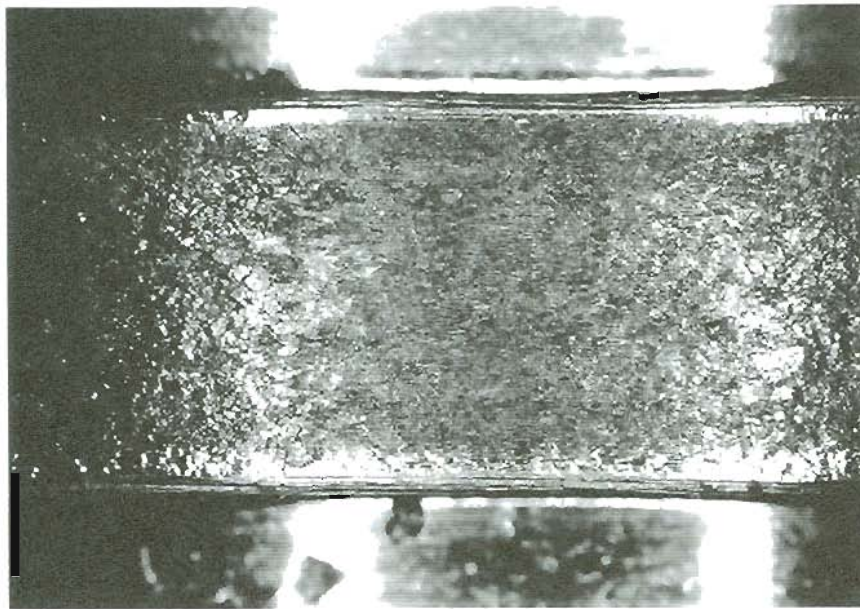


(d)

Figure 3.24. Continuation, illustrating: c) 3.6 kg/hr (Sample AC3). d) 4.6 kg/hr (Sample AC4). Flat coupon substrate. 2% Nital etch. 200x.

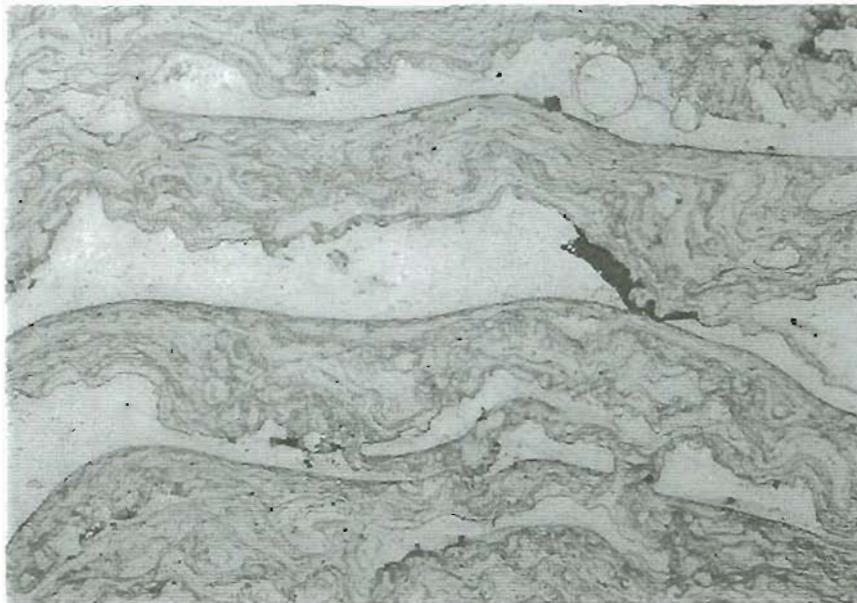


(a)

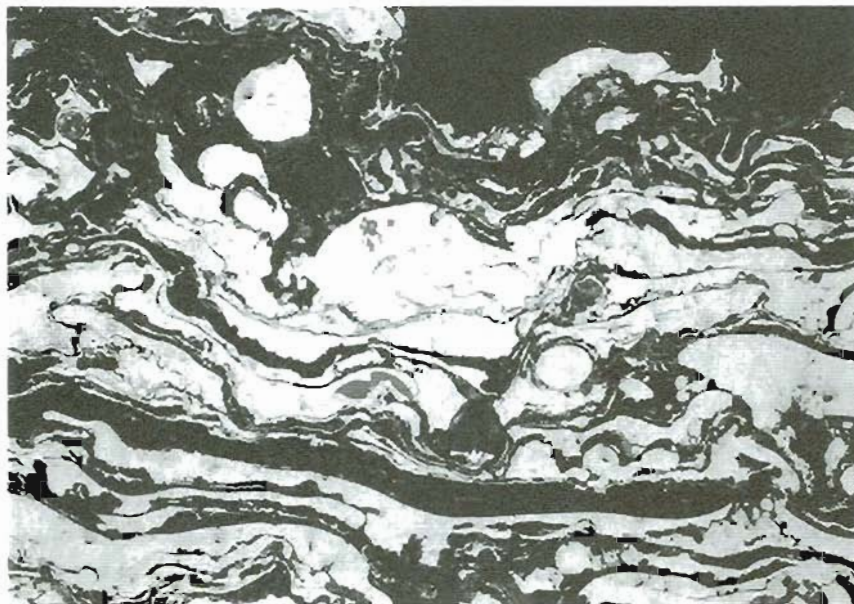


(b)

Figure 3.25. Photographs of copper material transferred to bottom roller during wear testing. a) Sample AC3 tested at low contact pressure, $P_o=700 \text{ N/mm}^2$. Creep= 35%. b) Sample AC6 tested at high contact pressure $P_o= 1220 \text{ N/mm}^2$. Creep=35%. 10x.



(a)

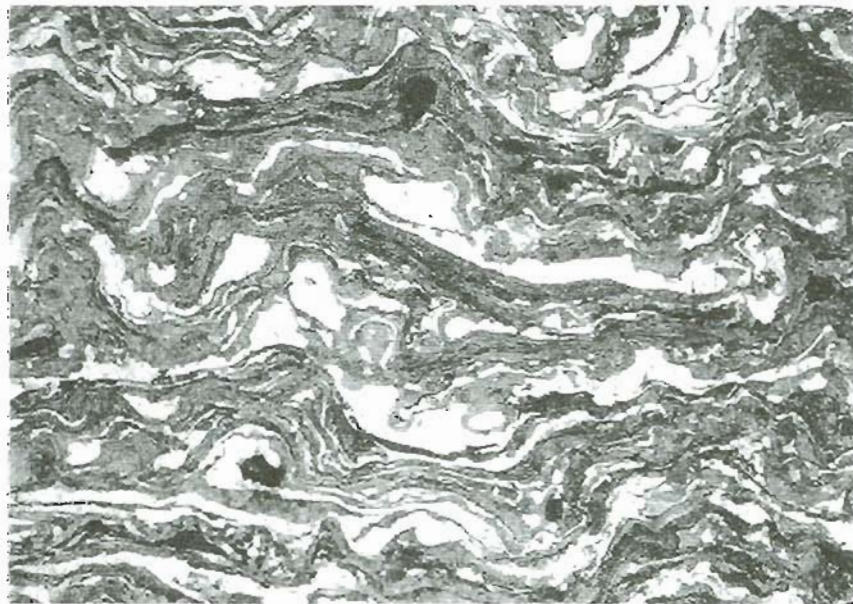


(b)

Figure 3.26. Photomicrographs illustrating copper wire / 1080 steel coating microstructure at varying wire injection distances. Injection angle= 90 degrees. Wire feed rate= 2.4 kg/hr. a) 100 mm (sample AC11). b) 60 mm (sample AC12). 2% Nital etch. 200x.

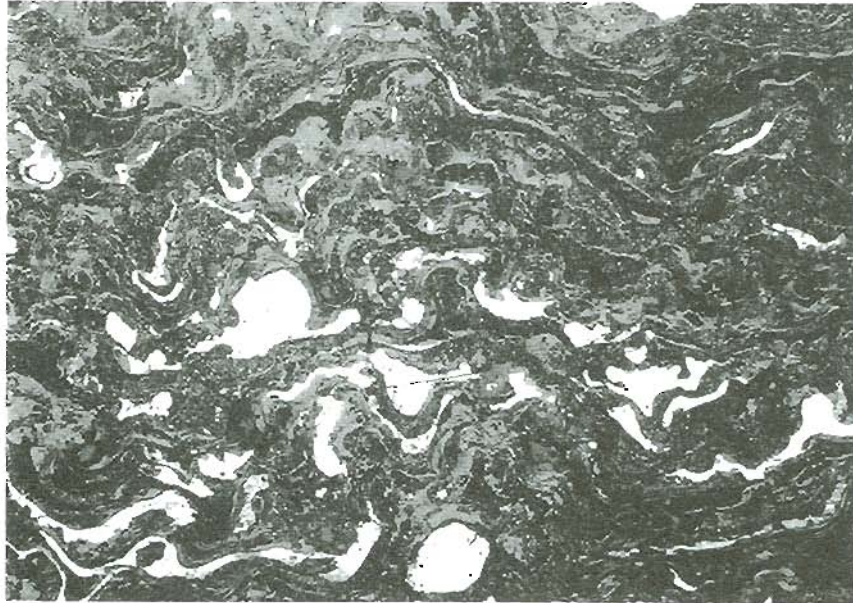


(c)

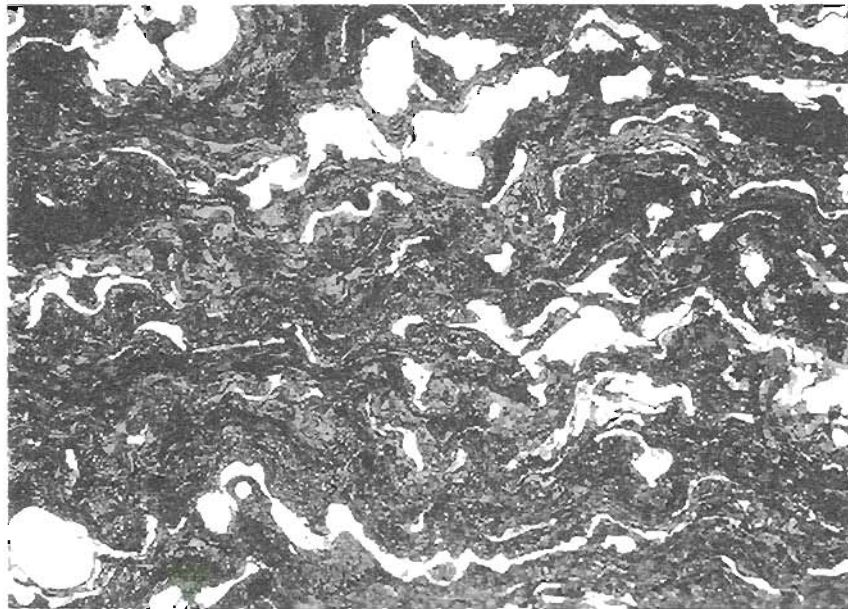


(d)

Figure 3.26. Continuation, illustrating: c) 40 mm (Sample AC13).
d) 10 mm (Sample AC14). 2% Nital etch. 200x.

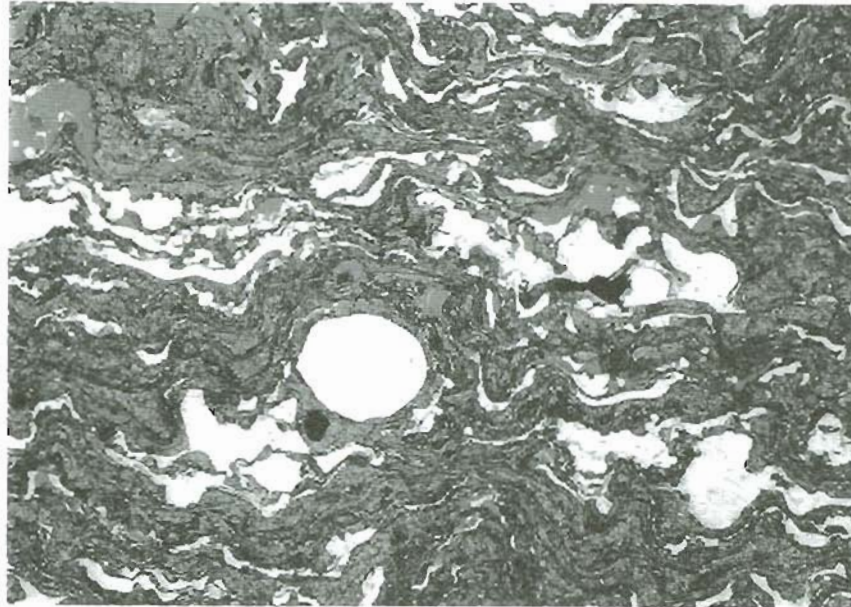


(a)

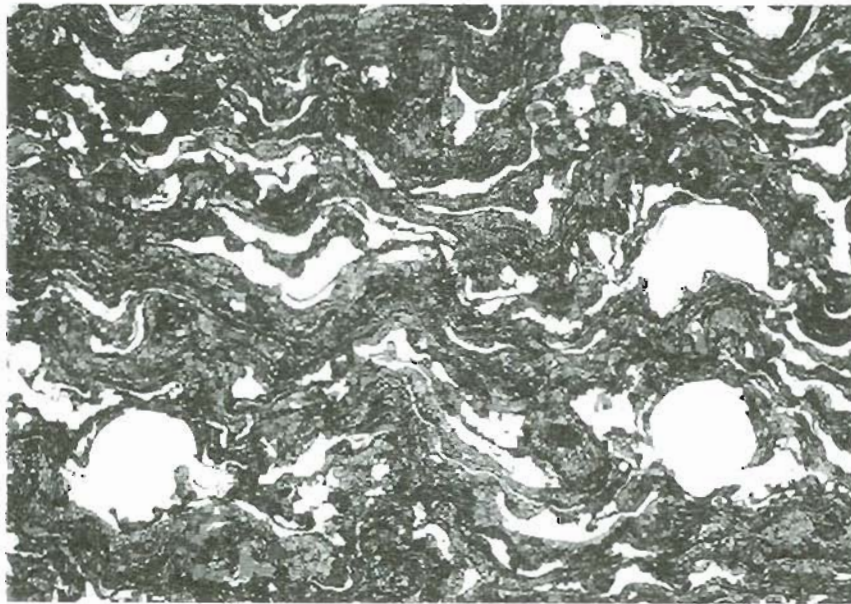


(b)

Figure 3.27. Photomicrographs illustrating copper powder / 1080 steel coating microstructures (of six samples) over a range of retained copper volume %. Copper injected at 15 mm @ 45° at varying feed rates. a) 10% (Sample AC16) b) 18% (Sample AC17). 2% Nital etch. 200x.

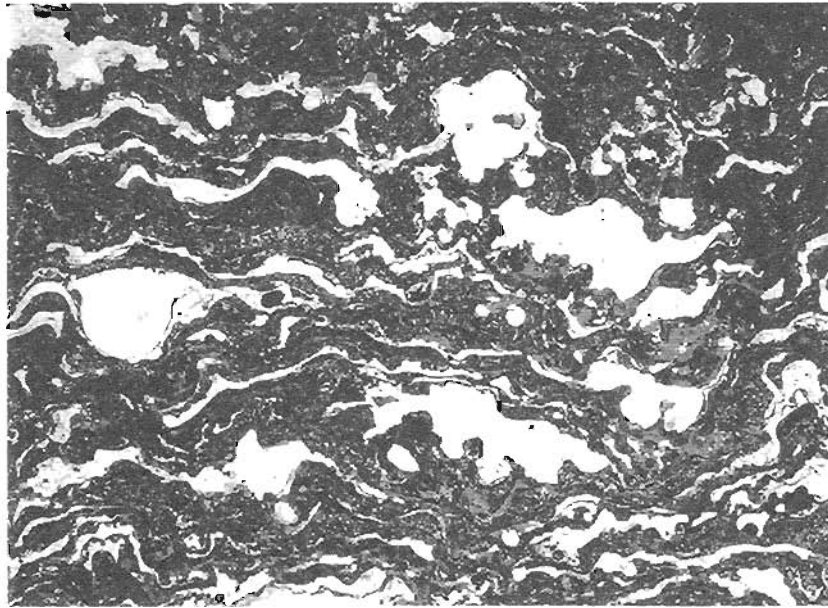


(c)

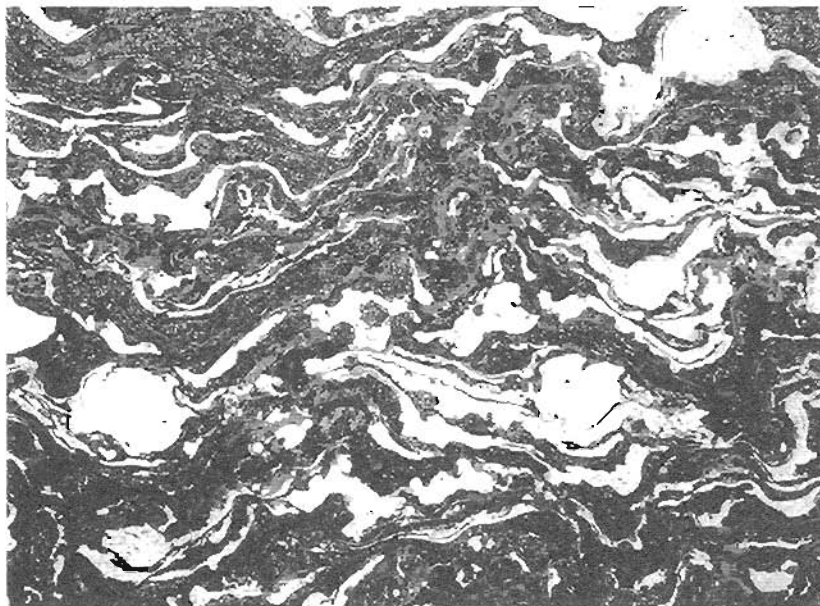


(d)

Figure 3.27. Continuation, illustrating: c) 22% (Sample AC18).
d) 24% (Sample AC21). 2% Nital etch. 200x.

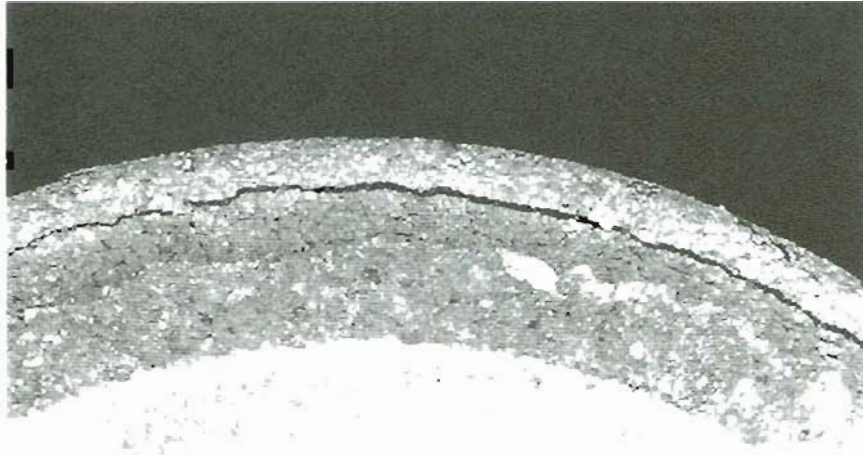


(e)



(f)

Figure 3.27. Continuation, illustrating: e) 32% (Sample AC20).
f) 43% (Sample AC19). 2% Nital etch. 200x.



(a)



(b)

Figure 3.28. Photographs illustrating debonded copper / 1080 steel coating still intact on the Amsler roller.
a) Side view, 6x. b) Corner view, 5x.

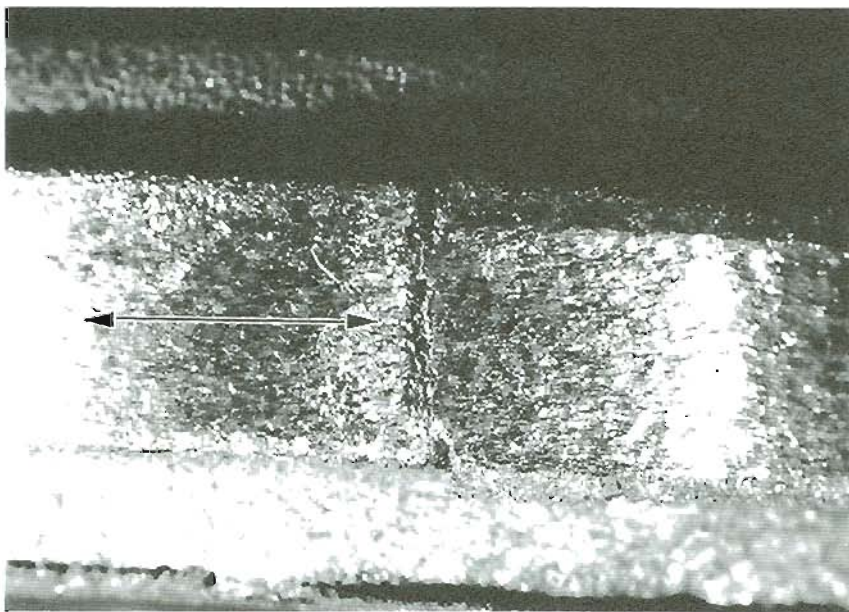
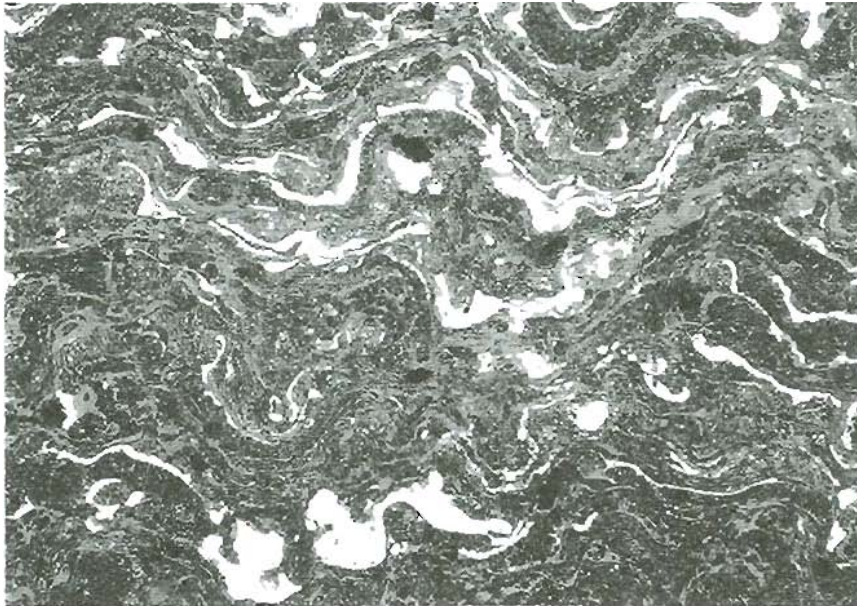
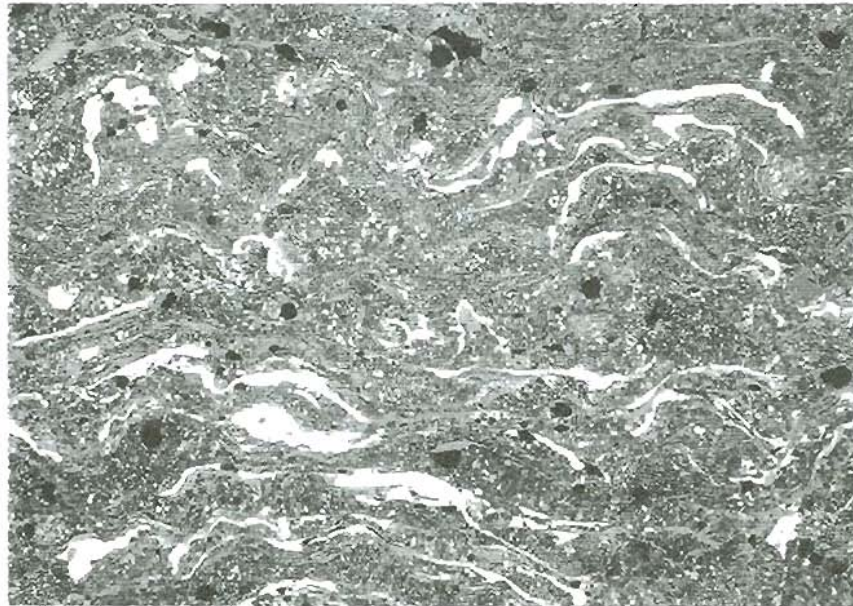


Figure 3.29. Photograph illustrating wear track following debonding of copper / 1080 steel coating. Arrow denotes area where coating debonded. 10x.

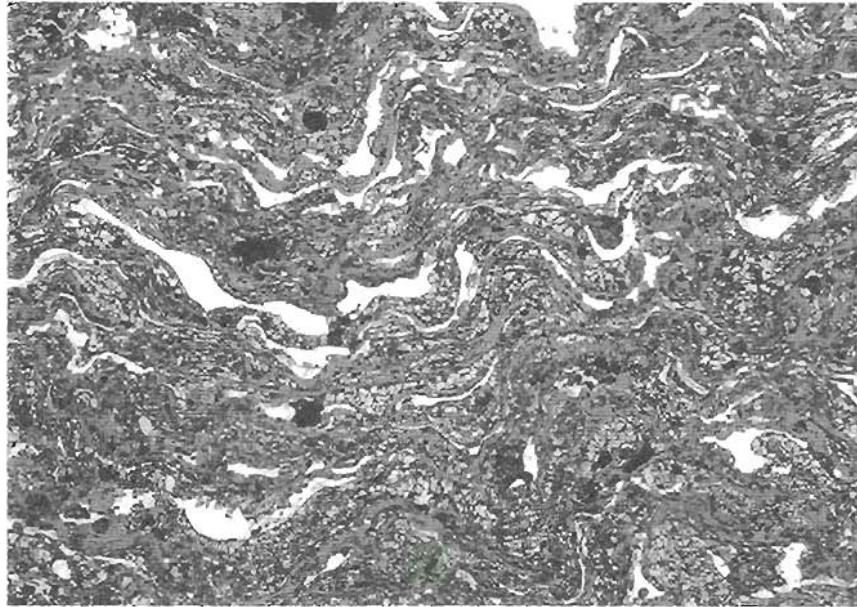


(a)

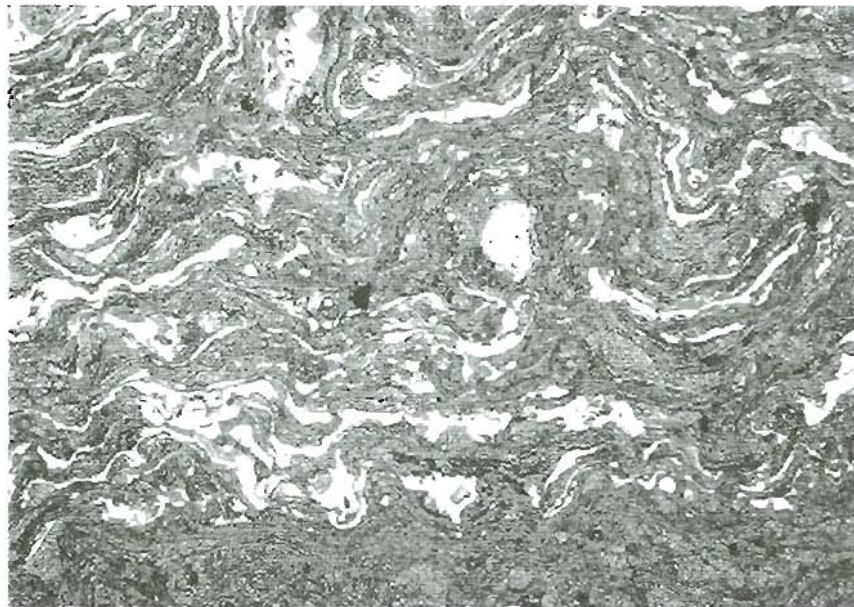


(b)

Figure 3.30. Photomicrographs illustrating copper powder / 1080 steel coating microstructures (low feed wheel) over a range of retained copper volume %. Copper injected at 15 mm @ 45° at varying feed rates. a) 10% (Sample AC30) b) 6% (Sample AC31). 2% Nital etch. 200x.

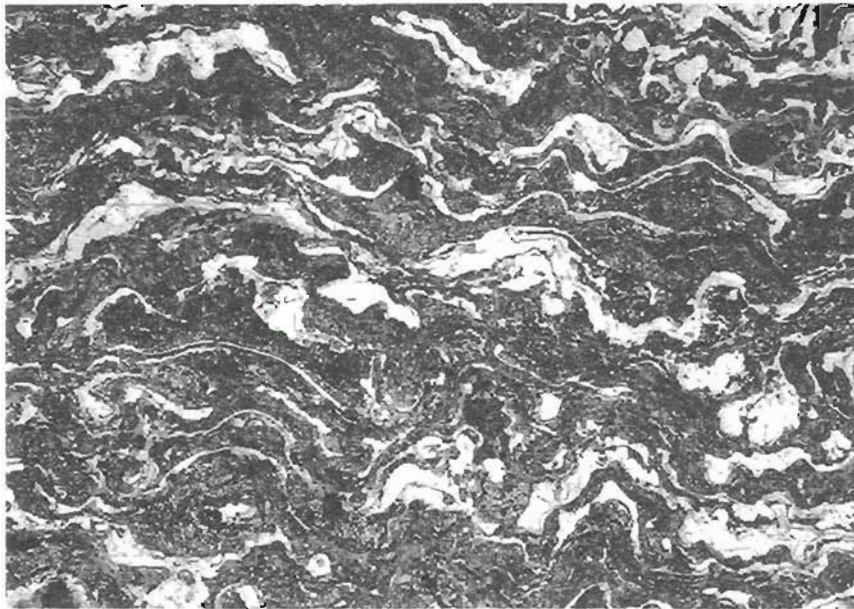


(c)

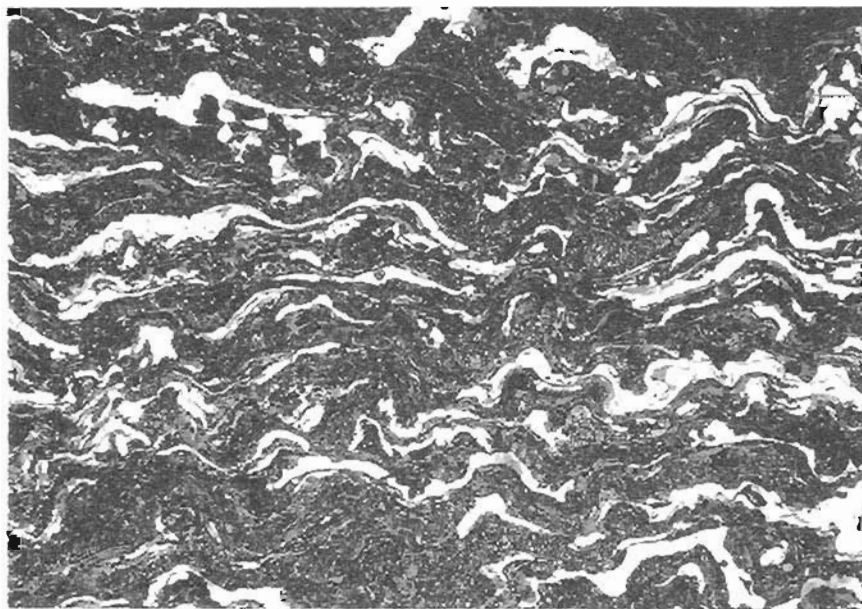


(d)

Figure 3.30. Continuation, illustrating: c) 7% (Sample AC32).
d) 14% (Sample AC33). 2% Nital etch. 200x.



(e)



(f)

Figure 3.30. Continuation, illustrating: e) 25% (Sample AC34).
f) 15% (Sample AC35). 2% Nital etch. 200x.

3.4 Polymers

Polymers are often used in applications where low friction and wear are required. Polymer in bulk form or as a thin film can produce low friction when tested against a hardened steel counterface. This type of wear environment could exist between wheel and rail. It was postulated that a thin polymer film applied to the rail would reduce friction when the “hardened steel” wheel rolled across it. The polymer film would thereby reduce or eliminate steel on steel contact.

The polymer was sprayed on top of the steel coating's surface as opposed to being included within it. This gave the polymer coating strength and rigidity, without compromising the integrity of the steel coating. Several types of polymers were investigated. Some of the polymers were mixed with solid lubricants or combined with other polymer materials. The deposition process, nonetheless, remained constant

The coating performance was evaluated on the Amsler, which measured coating durability and the average friction coefficient. Most wear tests were performed at $P_0 = 1220 \text{ N/mm}^2$ and 35% creep unless otherwise specified. The tests were run to failure, which occurred by debonding of the steel coating, or more commonly, polymer coating degradation. An increased friction coefficient, generally between $\mu = 0.25-0.30$, signaled the polymer film had worn through. The polymer films were analyzed using several techniques to describe and investigate the degradation behavior.

3.4.1 Initial Work

Initial research evaluated a wide variety of polymer materials in an effort to pinpoint those most suited to rolling/sliding wear. These polymer materials included Kynar, Torlon, Nylon 11, and ultra high molecular weight polyethylene (UHMW). The spray parameters

for applying these polymer materials onto steel coatings were based on parameters developed in previous work.¹⁷⁸

The steel coating was applied at the standard gas parameters 230 slpm N₂ / 30 slpm H₂ with a working distance of 235 mm. All of the polymers were applied at the gas parameters 200 slpm N₂ / 50 slpm H₂ and a working distance of 255 mm. These parameters remained constant throughout the polymer / steel coating investigation. In a small number of tests 308 L-Si stainless steel was substituted for 1080 steel. The gas parameters for depositing stainless steel were 230 slpm N₂ / 75 slpm H₂ with a working distance of 235 mm. The polymer gas parameters remained the same. The steel coating thicknesses were very consistent, often within 75 μm of 0.25 mm, 0.5 mm, etc. The creep values are presented as 5% or 35%, but some minor variation occurred within those values. The variation is on the order of 1% and consequently was ignored.

Table 3.20 summarizes the wear performance and spray parameters of Kynar and Torlon. Initial friction values for these polymers were around 0.10 and appeared independent of testing conditions. Three steel coating thicknesses (0.7, 0.5, 0.25 mm.) were tested with Kynar. Torlon was only tested on a 0.5 mm steel coating. The polymer was applied to a thickness of 50 to 75 μm . The ideal polymer film thickness was unknown in this initial work. The thin steel coatings (0.25 mm) had the best performance and resistance to debonding. The final friction value (μ) was given as the friction coefficient slowly increased from $\mu = 0.10$ during the test. The durability of Kynar was excellent when the steel coating was 0.25 mm. With the debonding of thicker steel coatings the full life of Kynar was not realized. Torlon had mediocre performance and after only a few tests was eliminated.

The effect of applied load on friction coefficient was investigated. The load was increased from 500 N to 2200 N, barring debonding. Table 3.21 summarizes the change in friction coefficient as a function of load for Nylon, UHMW, Kynar, and Torlon polymer

materials. Friction coefficient appeared independent of load for the Nylon and Kynar (plus steel) coatings. The friction coefficient increased slightly with load for the UHMW and Torlon coating systems. The steel coating thicknesses were 0.7 mm for the Nylon and Kynar and 0.5 mm for the UHMW and Torlon, and had no effect on friction unless the steel coating failed.

3.4.2 Nylon

Nylon coatings were the focus of the bulk of the polymer coating investigation. Nylon 11 material was available in bulk and initial tests indicated it had potential. Both dry and lubricated tests were performed. Initial work with nylon used 0.7 mm steel coatings. The increased resistance to debonding that 0.25 mm steel coatings offered had not been realized when this early work was performed. Later work utilized the more durable 0.5 and 0.25 mm steel coatings. The thickness of nylon ranged from 30-75 μm .

Neat Nylon / 1080 Steel Coatings

The effect of load on the friction coefficient is summarized in Table 3.21. The friction increased from a value of $\mu = 0.06$ at 500 N to $\mu = 0.1$ at 2200 N. The increments between load increases were only 100 to 200 revolutions. This experiment only showed there were no gross changes in friction as a function of load. Nothing could be said as to the friction behavior during an extended wear test.

Table 3.22 is a summary of the performance tests of 0.7 mm steel coatings with nylon. The loading conditions varied in the first several tests, with contact pressures of 860 and 1050 N/mm^2 . The vast majority of the tests were performed at a contact pressure of 1220 N/mm^2 . Creep was 5% or 35%, with 35% being the dominant slip ratio used for further polymer / steel coating tests. Barring debonding, the average durability was 8,100 revolutions at $P_0 = 1220$

N/mm² and 35% creep. The final friction coefficient averaged 0.27. When creep was reduced to 5% the durability increased almost fourfold. The final friction value was the same, as was the degree of wear, but the degradation process was much slower. The final friction level (generally between 0.25 and 0.30) signaled that nearly all of the polymer had been worn away. If the tests were continued, steel on steel coating wear occurred, and friction rose rapidly.

Table 3.23 and 3.24 summarize the performance results for the 0.5 and 0.25 mm coatings. The average test durations were 8870 revolutions and 9250 revolutions for the 0.5 mm and 0.25 mm coatings, respectively. These samples were tested at 35% creep and $P_o=1220$ N/mm². When creep was reduced to 5% for the 0.25 mm coatings the durability again saw a four fold increase. The average durability for two tests was 44,705. The final friction coefficient was $\mu=0.29-0.31$. At the test end the steel coating was beginning to debond in thin sections. This surprisingly did not cause total coating failure. This type of 'limited' debonding was not observed in the 0.5 to 1 mm coatings, where any debonding caused total coating failure.

Neat Nylon / 308 L-Si Stainless Steel Coatings

Stainless steel was used in an attempt to reduce the incidence of debonding. The rolling/sliding wear and friction behavior of stainless steel coatings was investigated in previous work.¹⁸⁰ It was determined that stainless steel coatings had inferior durability to 1080 steel coatings when tested against wheel steel. With an overlay polymer however, the stainless steel wear properties would be irrelevant. The tenacious chromium oxides were thought to reduce debonding. This being the case, the durability of the polymer / steel system could be improved.

Table 3.25 summarizes the tests with 0.25 mm nylon / stainless steel coatings. The coatings had excellent durability, with the average test length equaling 13,060 when run to failure. The

Comments column in Table 3.25 indicates whether the test was terminated or partial debonding occurred. In samples SS1 and SS2 the test was prematurely terminated when the coating visually appeared to be worn away. In the later tests the coating was run until debonding occurred, despite coating appearance.

The friction coefficient remained around 0.20, even at test end when the coating began to partially debond. When creep was reduced to 5% the durability tripled to 43,000 revolutions. This value was comparable to the 0.25 mm nylon / 1080 steel coatings. However, the friction value remained around $\mu = 0.13$, until the stainless steel coating began to debond. Overall the nylon / stainless steel coatings had superior performance over the nylon / 1080 steel coatings.

Solid Lubricant + Nylon / 1080 Steel Coatings

To further enhance the durability of nylon / 1080 steel coatings, solid lubricants were blended with the neat nylon powder. Two common solid lubricant powders were used, graphite and MoS_2 . Table 3.26 summarizes the results of 0.25 mm and 0.5 mm steel coatings with nylon/graphite or nylon/ MoS_2 polymer coatings. The durability was increased, with average test length rising by 10%. The coating degradation process was unchanged and the friction coefficient was still around $\mu = 0.27$ at test termination. MoS_2 increased the performance of nylon to a greater degree than graphite. Overall, the performance increase mimicked that achieved by the nylon / stainless steel coatings, but without the improved friction reduction.

3.4.3 PTFE

PTFE (Teflon™) is widely known for its low friction coefficient and resistance to wear. PTFE was applied to the 1080 steel coating anticipating it would behave similarly to bulk PTFE. PTFE was evaluated as a neat powder and in blended form. Nylon was

added in increasing amounts to form a blended polymer. The spray deposition parameters of PTFE were similar to the other polymers. Table 3.27 summarizes the results of PTFE / 1080 steel coatings. The durability of these coatings was poor; with a 0.5 mm steel thickness, half of the samples debonded.

100% PTFE coatings had the lowest friction value for any of the polymer / steel systems. The final friction value was only $\mu=0.12$ at nearly 5000 revolutions. This is overshadowed though by the low durability, which was about half of the best performing nylon / steel coatings. The initial friction value was on the order of $\mu=0.05$. Neat PTFE powder exhibited little wetting when sprayed and as a result could not form a continuous coating. Instead, individual particles adhered to the surface. The coating which did form was not easily measurable. Figure 3.31 illustrates the as-sprayed morphology of neat PTFE. At the onset of a wear test most (> 60%) of the unadhered PTFE particles were lost from the system.

In an effort to retain the PTFE it was blended with nylon. Nylon was easily melted, having good wetting, and could act as a carrier for the PTFE. The polymer coating adhesion improved as the nylon weight fraction was increased. At 75% nylon, the polymer appeared to deposit and adhere in the same manner as neat nylon. Wear tests however, illustrate this 75-25 blend did not perform as well as nylon / steel coatings or as well as 100% PTFE / steel coatings. The blends in-between had similar mediocre performance, with the trend indicating that either powder in neat form was superior to a mixture. The initial and final friction coefficients also rose as the weight fraction of nylon increased. PTFE in neat form did not appear to be suited to plasma spray deposition.

3.4.4 UHMW

UHMW is a wear resistant polymer with far reaching industrial applications. UHMW was deposited in the same manner as nylon, and was intended to increase the overall performance of the polymer /

steel coating system. UHMW was deposited onto 1080 steel in neat form and blended with solid lubricant powders. Graphite and MoS₂ were used, and the weight fractions were the same as in the blended nylon powders: 2.5 : 1. The UHMW / steel coatings were tested at 35% creep and $P_o = 1220 \text{ N/mm}^2$. Table 3.28 summarizes the performance results of both neat and solid lubricated UHMW / steel coatings. The durability was excellent, barring debonding. The effect of added solid lubricants was an increase of durability by 10-20%. The average durability for UHMW (both blended and neat) was 10,670 for the 0.5 mm steel coatings and 9330 for the 0.25 mm steel coatings. These averages exclude the samples which debonded. The final friction coefficient average was smaller for the UHMW / steel coatings ($\mu=0.21$) than for the nylon / steel coatings ($\mu=0.28$). The overall behavior though, was inferior to the best performing nylon / steel coatings.

UHMW appeared to require a higher heat input to fully wet the polymer coating, when compared to nylon. The standard gas parameters for depositing polymers (200 slpm N₂ / 50 slpm H₂) were always used at 340 V and 350 A, which yielded a power input of 119 kW. Lower power inputs were attempted in an effort to discover the minimum input requirements. Table 3.29 summarizes the results of UHMW deposition at varying power inputs. A sample was sprayed at the standard power input of 119 kW for comparison. Its performance was similar to other UHMW / steel coatings. As power was reduced the wetting of the UHMW decreased. Figure 3.32 is an SEM photo of a fully melted and wetted, continuous UHMW film deposited at 119 kW. Figure 3.33 is an SEM photo illustrating UHMW particles which were deposited at 90 kW and did not wet. The coatings performance and friction reduction decreased with power input. When power input fell below 105 kW the UHMW coating had no beneficial influence on friction or wear of the steel coating. The best performance appeared to require the standard 119 kW input during deposition. On the positive side however, is UHMW's increased resistance to thermal degradation.

3.4.5 Surface Modification

Polymers were generally coated on to as-sprayed steel coatings for performance evaluation. However, the question remained whether nylon would perform well when applied to surfaces roughened by other means. The unique surface texture of a plasma sprayed coating enabled the polymers to achieve good durability. If this surface could be reproduced, then the time consuming step of steel coating deposition could be eliminated.

When nylon was deposited on an as-machined Amsler roller, the durability was very low (<1000 revs @ $P_o = 900 \text{ N/mm}^2$ and 5% creep).¹⁷⁸ Various surface modification techniques were attempted to improve the performance. These included: grit blasting, grinding, groove cutting, and combinations thereof.¹⁷⁹ The groove cutting was performed on a lathe, where depth and thread pitch could be varied. The grinding operation utilized a precision lathe mounted, fine wheel grinder to give a uniform surface texture. Table 3.30a summarizes the surface preparation techniques used. Table 3.30b summarizes the subsequent performance results. Initial and final friction values are listed, as they had a wider variation than the nylon / steel coating values.

The Amsler test and nylon application parameters were equivalent to those used on the previous polymer / steel coatings. The nylon film durability was significantly reduced in the absence of a 1080 steel coating substrate. The best performer was Sample SM6 with 6400 revolutions. This sample combined grit blasting and machined grooves. This value was still half of that achieved in the nylon / stainless steel coatings and the nylon / 1080 steel coatings with solid lubricants. In light of the poor performance, this method of surface modification was abandoned.

3.4.6 Lubricated tests

Amsler performance tests of polymer / steel coatings had been done under dry, unlubricated conditions to this point. Uncoated rail steel is often lubricated by applied grease or natural rainfall in the field. Thus, it was of interest to evaluate the performance of polymer / steel coatings under lubricated conditions. The best performing coating series, nylon / 308 L-Si stainless steel (0.25 mm coating), was assessed under both grease and water lubricated conditions. For both grease lubricated tests, the initial applied lubricant was 0.40 cm³. An additional 0.2 cm³ was applied at each 500 revolution increment. The water lubricant was a continuous drip. Durability and friction reduction were recorded at the contact conditions of: $P_0=1220 \text{ N/mm}^2$ and 35% creep.

Table 3.31 summarizes the performance results of the lubricated tests. The durability was decreased by 50-75%, with the best performance only lasting 4570 revolutions (Sample WL1). All of the coatings debonded. The water lubricated tests accelerated the coating degradation, but had little influence on the friction coefficient behavior. The initial friction was $\mu=0.10$, the same as the dry tests, and the friction increased steadily, although at an accelerated rate. The water lubricant did maintain a friction value of $\mu=0.22$ though, after the entire polymer coating had been worn off and steel coating / wheel steel contact had commenced. The grease lubricant enabled the friction coefficient to remain at $\mu=0.10$ during the entire test.

The grease also reduced the life of the polymer coating. It appeared that once the polymer was worn off, the steel coating would debond. Only a small fraction of the applied lubricant remained in the contact zone, this was enough though, to maintain low friction, even when metal on metal contact occurred. Overall, the lubricants appeared to degrade the coating more than preserve it.

3.4.7 Polymer Reapplication

Most performance tests of nylon /steel coatings were run until the polymer coating had nearly worn off. Some polymer did remain, but in general, was not enough for continued friction and wear reduction. As a result, the steel coating remained relatively unworn after wear testing. The question arose whether the polymer coating, if re-applied, would exhibit the same endurance as a polymer applied over an as-sprayed steel coating. In addition, what type of surface preparation of the steel coating would be necessary prior to re-application.

Both 1080 steel and 308 L-Si stainless steel coatings were investigated. The original nylon coating was run to failure, with care taken to avoid metal on metal contact. Two surfacing techniques were used prior to polymer reapplication. The first, was a surface cleaning only with acetone. The second was a limited surface texturing via grit blasted steel shot, followed by cleaning with acetone. The nylon coating was reapplied at the standard gas parameters. The nylon coating thickness was 35-50 μm . The samples were tested at $P_o = 1220 \text{ N/mm}^2$ and 35% creep. The original nylon / steel coatings 1080 or 308 L-Si were sprayed at the standard parameters. To minimize the chance of debonding steel coatings were limited to 0.25 mm.

Table 3.32 summarizes the performance results of the re-applied nylon coatings. Samples RS1 through RS3 were cleaned only prior to nylon re-application. The other samples RS4 through RS9 were surface textured. Neither of these techniques or combinations improved the coating durability or friction reduction appreciably. The re-applied nylon coating was shed in the first few hundred revolutions. The remainder of the test was accelerated degradation leading to an increased friction coefficient ($\mu = 0.3$) or debonding. The results suggest that a new steel coating must be applied, if the polymer is to adhere and behave as a lubricant.

3.4.8 Interrupted tests

The polymer coatings were too thin to be resolved optically in either the as-sprayed or as-tested condition. SEM imaging provided limited information when polymer coatings were analyzed only before, or after, testing. The degradation process of the polymer was very similar, regardless of the polymer material (nylon, UHMW, etc.). Observation of polymer coatings at different degrees of wear yielded greater understanding of the degradation mechanisms.

Interrupted tests were performed on a nylon / 1080 steel coating. The tests involved six identical Amsler rollers with a 0.25 mm steel coating and the standard 35-50 μm nylon coating. The rollers were wear tested to varying degrees of failure, from the initial break-in to the point where the nylon film was worn off. Wear test parameters were $P_o = 1220 \text{ N/mm}^2$ and 35% creep. Each specimen was sectioned to observe the degree of coating degradation using optical and SEM analysis.

The progression of polymer film degradation was charted with a series of photographs and observations taken during a wear test. Seven stages were defined which describe the wear progression. Table 3.33 summarizes the location of each stage in terms of revolutions and friction coefficient for these specific samples. These numbers represent approximate values at which these stages occurred. The measured friction coefficient and visual appearance determine when each stage has begun and ended, and this varies slightly for different samples. Figures 3.34 through 3.40 are photographs illustrating the progression of film degradation (Stages 1 through 7) during an Amsler test of a typical polymer /steel coating. The sample was photographed intermittently from test beginning to failure of the nylon film.

The post test analysis was performed primarily using secondary electron imaging in the SEM. The polymer wear track surface of each sample was analyzed to determine the morphology and structure of the polymer film at each stage. Figures 3.41

through 3.46 document the polymer surface wear of stages one through six. These SEM photographs illustrate the loss of nylon coating and provide a good visual description of the nylon degradation. In brief, the polymer coating loses material to the point where a continuous film is non-existent, or is unable to control friction. At test end only patches of polymer remained, residing in the valleys of the steel coating. The interrupted tests gave a better understanding of the degradation of the polymer film, providing observations that define each stage and ultimately, the failure of the polymer.

3.4.9 Polymer Film Analysis

The interrupted tests provided details of the polymer's behavior, but gave no analysis as to changes in its molecular structure. Both plasma spraying and wear testing had potential to alter the bonding characteristics of a polymer, specifically nylon in this study. Fourier transform infrared spectroscopy was employed to study the nylon films. Nylon films were observed in the melted, as-sprayed, and as-tested forms. Analysis of the as-tested samples focused on the film remaining on a worn nylon / steel coated roller and the film which transferred to the bottom wheel steel roller.

The spectra from the FTIR analysis yielded specific information about the various bonding linkages of the nylon structure. Figure 3.47 is a characteristic FTIR spectrum, utilizing attenuated total reflectance (ATR), of an as-sprayed nylon sample. The wave number (cm^{-1}) defines the important peaks and gives definite structural information, whereas the relative intensity (y-axis) is dependent on sample thickness and other external factors, and can vary between like samples. The important peaks focus on the behavior of the amide linkage. A peak at 3309 cm^{-1} represents the stretching between nitrogen and hydrogen, and is known as the Amide I peak. The stretching between carbon and hydrogen in the methylene groups is illustrated by peaks at 2925 cm^{-1} and

2856 cm^{-1} . The carbonyl peak, which represents stretching between the oxygen and carbon in the amide linkage, is located at 1734 cm^{-1} . The Amide II peak, at 1569 cm^{-1} , represents vibration within the entire amide linkage. Shifts in these peaks within identical samples represent structural changes. To fully represent the polymer film both ATR and specular reflectance were performed. ATR detects surface region characteristics (1-2 μm) relative to the bulk. Specular reflectance (SR) characterizes the actual surface, which can vary greatly from the subsurface.

All of the nylon spectra: worn, melted, etc., looked similar with no gross differences. Only when nylon was pyrolyzed by intense overheating did the spectrum become unrecognizable. Subtle variations did, however, indicate some change had taken place. Figure 3.48 is the resultant (SR) when the as-melted spectrum was subtracted from the as-sprayed spectrum. A negative peak around 1660 cm^{-1} indicates an increased intensity in the carbonyl peak of the as-sprayed nylon. This represents an increase in the number of C-O bonds. The negative peak results when the as-sprayed peak is subtracted from zero, as no peak exists in the as-melted sample at the shifted location.

The SR spectrum of a worn nylon film subtracted from an as-sprayed film is illustrated in Figure 3.49. The film was taken from the bottom roller and represents transferred material during a wear test. A shift in the Amide I and Amide II linkage is represented by a negative peak. This shift of the amide linkage intensities indicates the transferred film has a less ordered structure. This is compared to the as-melted, as-sprayed, and even the top roller nylon film. The film which remains on the top roller at the end of a test has the same degree of order as the as-sprayed nylon films. The as-melted nylon though, has the highest degree of order. These relative order relationships come from the shifting in an intensity peak away from the published ideal bulk nylon properties.¹⁰⁶ Further analysis would be required to elaborate on the exact changes in structure nylon

experienced. These results suggest that the spray process is not a factor in the wear durability of nylon steel coatings.

Focussed Ion Beam Machining

During both wear testing and FTIR analysis the question arose of the thickness of the transferred polymer coating. The thickness was immeasurable with standard calipers. In order to measure the film, a small cross section had to be cut using a focused ion beam (FIB). The FIB uses accelerated gallium ions to micro-machine sections out of material. A cross section of the bottom roller was cut with a diamond saw and the FIB machined away the residual disturbed metal and polymer. Figure 3.50 illustrates a cross section view of the transferred nylon film and bottom roller substrate. The film is on the order of 1 μm in thickness. The thickness of the film suggests that a large majority of the polymer is lost from the system during wear testing. This film was formed after wear testing approximately 8000 revolutions.

3.4.10 Synopsis

The performance of the polymer / steel coating system was superior to either the graphite or copper systems. As a result more analysis was put into the mechanisms of polymer wear in an effort to fully understand its limitations. The nylon / 308 L-Si stainless steel coating system was the top performer. Nylon / 1080 steel coatings were a close second. The steel coating thickness played a larger role than the actual material itself. The greatest debonding resistance and subsequent durability occurred when the steel coating was 0.25 mm thick. The coatings excellent performance was slightly renewable through polymer reapplication, and lubricants only accelerated degradation. Nonetheless, the polymer coating performed much better than was ever anticipated.

Table 3.20. Amsler performance test results of Kynar and Torlon polymers / 1080 steel coatings.¹⁷⁹ Gas parameters (1080 steel) were 230 N₂ / 30 H₂ with a working distance of 235 mm. Nylon gas parameters were 200 slpm N₂ / 50 slpm H₂ with a working distance of 255 mm.

Sample	Contact Pressure (N/mm ²)	Creep (%)	Durability (revs.)	Steel Coating Thickness (mm)	Final Friction (μ)
Kynar 1	860	5	18,000	0.7	0.18
Kynar 1*	1050	5	1,100	0.7	0.23
Kynar 2	1220	5	4,100 ^D	0.7	0.20
Kynar 3	1220	35	450 ^D	0.7	0.10
Kynar 4	1220	35	7,400 ^D	0.5	0.16
Kynar 5	1220	35	7,100 ^D	0.5	0.20
Kynar 6	1220	35	16,000	0.25	0.31
Kynar 7	1220	35	15,000	0.25	0.31
Torlon 1	1220	35	3,600	0.5	0.39
Torlon 2	1220	35	3,700	0.5	0.38

* Test continued at higher contact pressure; D= Steel coating debonded.
Nylon coating thickness 50-75 μ m. Initial μ = 0.08 - 0.10.
Power= 130 kW @ 370 V and 350 A for steel coatings.
Power= 119 kW @ 340 V and 350 A for polymer coatings.

Table 3.21. Friction coefficient as a function of applied load for polymer / 1080 steel coatings.¹⁷⁹ Gas parameters (1080 steel) were 230 N₂ / 30 H₂ with a working distance of 235 mm. Nylon gas parameters were 200 slpm N₂ / 50 slpm H₂ with a working distance of 255 mm. Creep= 5%.

Load (N)	Nylon (μ)	UHMW (μ)	Kynar (μ)	Torlon (μ)
500	0.060	0.005	0.124	0.021
600	0.080	0.013	0.138	0.035
700	0.093	0.021	0.148	0.037
800	0.094	0.019	0.130	0.039
900	0.095	0.021	0.161	0.047
1000	0.096	0.026	0.156	0.058
1100	0.097	0.031	1.160	0.053
1200	0.097	0.033	0.151	0.057
1300	0.100	0.032	0.144	0.061
1400	0.080	0.037	0.145	0.061
1500	0.078	0.038	0.145	0.063
1600	0.093	0.046	0.143	0.066
1700	0.094	0.049	0.140	0.065
1800	0.094	0.049	0.138	0.067
1900	0.095	0.058	0.125	0.069
2000	0.096	0.050	debond	0.071
2100	0.096	0.055	-	0.070
2200	0.100	0.053	-	0.074

Steel coating thickness= 0.7 mm for Nylon and Kynar.
Steel coating thickness= 0.5 mm for UHMW and Torlon.
Polymer thickness= 50-75 μ m.

Table 3.22. Amsler performance test results of nylon / 1080 steel coatings N1 through N15.¹⁷⁹ Gas parameters (1080 steel) were 230 N₂ / 30 H₂ with a working distance of 235 mm. Nylon gas parameters were 200 slpm N₂ / 50 slpm H₂ with a working distance of 255 mm. Coating thickness= 0.7 mm.

Sample	Contact Pressure (N/mm ²)	Creep (%)	Durability (revs.)	Final Friction (μ)
N1	860	5	18,000	0.19
N1*	1050	5	12,300	0.24
N2	1050	5	29,500	0.27
N3	1220	5	13,600	0.14
N4	1220	5	9,000	0.10
N5	1050	35	17,300	0.28
N6	1220	35	8,400	0.26
N7	1220	35	3,700 ^D	0.13
N8	1220	35	2,000 ^D	0.13
N9	1220	35	4,700 ^D	0.12
N10	1220	35	2,700 ^D	0.12
N11	1220	35	7,600	0.26
N12	1220	35	9,000	0.28
N13	1220	35	8,000	0.26
N14	1220	35	7,800	0.25
N15	1220	35	7,600	0.27

* Test continued at higher load; D= Steel coating debonded.
Nylon coating thickness 50-75 μ m. Initial μ = 0.10.
Power= 130 kW @ 370 V and 350 A for steel coatings.
Power= 119 kW @ 340 V and 350 A for polymer coatings.

Table 3.23. Amsler performance test results of nylon / 1080 steel coatings N16 through N21. Gas parameters (1080 steel) were 230 N₂ / 30 H₂ with a working distance of 235 mm. Nylon gas parameters were 200 slpm N₂ / 50 slpm H₂ with a working distance of 255 mm. Wear test parameters: P_o= 1220 N/mm², Creep= 35%. Coating thickness= 0.5 mm.

Sample	Durability (revs.)	Final Friction (μ)
N16	8,300	0.27
N17	7,700	0.27
N18	9,500	0.31
N19	7,430 ^D	0.30
N20	9,750	0.31
N21	10,560	0.34

D= Steel coating debonded. Initial μ = 0.10.
Nylon coating thickness 50-75 μ m.
E= 130 kW @ 370 V, 350 A for steel coatings.
E= 119 kW @ 340 V, 350 A for polymer coatings.

Table 3.24. Amsler performance test results of nylon / 1080 steel coatings N22 through N29. Gas parameters (1080 steel) were 230 N₂ / 30 H₂ with a working distance of 235 mm. Nylon gas parameters were 200 slpm N₂ / 50 slpm H₂ with a working distance of 255 mm. Wear test parameters: P₀= 1220 N/mm², Creep= 35%. Steel coating thickness= 0.25 mm.

Sample	Durability (revs.)	Final Friction (μ)
N22	9,000	0.28
N23	5,800 ^D	0.26
N24	8,920	0.30
N25	11,460	0.35
N26	10,450	0.33
N27	9,870	0.31
N28	10,100	0.31
N29	9,250	0.30

D= Steel coating debonded. Initial μ = 0.10.
Nylon coating thickness 50-75 μ m.
E= 130 kW @ 370 V, 350 A for steel coatings.
E= 119 kW @ 340 V, 350 A for polymer coatings.

Table 3.25. Amsler performance test results of nylon / 308 L-Si stainless steel coatings SS1 through SS7. Gas parameters (308 L-Si) were 230 N₂ / 75 H₂ with a working distance of 235 mm. Nylon gas parameters were 200 slpm N₂ / 50 slpm H₂ with a working distance of 255 mm. P_o = 1220 N/mm², Steel coating thickness= 0.25 mm.

Sample	Creep (%)	Durability (revs.)	Final Friction (μ)	Comments
SS1	35	9,300	0.22	T
SS2	35	9,060	0.20	T
SS3	35	13,310	0.20	D
SS4	35	12,810	0.20	D
SS5	35	13,050	0.20	D
SS6	5	43,050	0.13	D
SS7	5	42,370	0.14	D

Comments: D= debond; T= test terminated.
Power= 133 kW @ 380 V, 350 A for steel coatings.
Power= 119 kW @ 340 V, 350 A for polymer coatings.
Initial μ = 0.10. Polymer thickness= 25-50 μ m.

Table 3.26. Amsler performance test results of nylon + solid lubricants / 1080 steel coatings NS1 through NS8. Gas parameters (1080 steel) were 230 N₂ / 30 H₂ with a working distance of 235 mm. Nylon gas parameters were 200 slpm N₂ / 50 slpm H₂ with a working distance of 255 mm. Wear test parameters: P_o= 1220 N/mm², Creep= 35%.

Sample	Steel Coating Thickness (mm)	Solid Lubricant	Test Duration (revs.)	Final Friction (μ)
NS1	0.5	MoS ₂	13,300	0.26
NS2	0.5	MoS ₂	11,600	0.27
NS3	0.5	Graphite	11,000	0.27
NS4	0.5	Graphite	10,000	0.28
NS5	0.25	MoS ₂	11,000	0.28
NS6	0.25	MoS ₂	11,200	0.27
NS7	0.25	Graphite	9800	0.28
NS8	0.25	Graphite	8600	0.30

Polymer thickness = 25-50 μ m; Initial μ = 0.08
Power= 130 kW @ 370 V, 350 A for steel coatings.
Power= 119 kW @ 340 V, 350 A for polymer coatings.

Table 3.27. Amsler performance test results of PTFE / 1080 steel coatings PT1 through PT8. Gas parameters (1080 steel) were 230 N₂ / 30 H₂ with a working distance of 235 mm. Nylon gas parameters were 200 slpm N₂ / 50 slpm H₂ with a working distance of 255 mm. Wear test parameters: P₀= 1220 N/mm², Creep= 35%. Coating thickness= 0.5 mm.

Sample	PTFE (%) ¹	Durability (revs.)	Polymer Thickness (μm)	Initial Friction (μ)	Final Friction (μ)
PT1	100	4950 ^D	< 15	0.05	0.12
PT2	100	6460 ^D	< 15	0.05	0.12
PT3	75	4540 ^D	< 15	0.08	0.19
PT4	75	5800	< 15	0.07	0.22
PT5	50	5670	< 15	0.09	0.20
PT6	50	4250	< 15	0.10	0.21
PT7	25	3770 ^D	20-30	0.10	0.21
PT8	25	4870	30-30	0.11	0.27

1. Balance of polymer was Nylon 11. D= Steel coating debonded.
E= 130 kW @ 370 V, 350 A for steel coatings.
E= 119 kW @ 340 V, 350 A for polymer coatings.

Table 3.28. Amsler performance test results of UHMW / 1080 steel coatings PE1 through PE6. UHMW was sprayed neat, and mixed with graphite or MoS₂. Gas parameters (1080 steel) were 230 N₂ / 30 H₂ with a working distance of 235 mm. Nylon gas parameters were 200 slpm N₂ / 50 slpm H₂ with a working distance of 255 mm. Wear test parameters: P₀= 1220 N/mm², Creep= 35%.

Sample	1080 Steel Coating Thickness (mm)	Solid Lubricant	Durability (revs.)	Final Friction (μ)
PE1 #1	0.50	-	11,220	0.19
PE1 #2	0.50	-	3030 ^D	0.13
PE1 #3	0.50	-	9750	0.23
PE1 #4	0.50	-	11,940	0.28
PE2 #1	0.50	MoS ₂	6830 ^D	0.18
PE2 #2	0.50	MoS ₂	9750	0.20
PE3 #1	0.50	Gráphite	8340 ^D	0.18
PE3 #2	0.50	Graphite	7960 ^D	0.19
PE4 #1	0.25	-	7200	0.24
PE4 #2	0.25	-	7780	0.25
PE4 #3	0.25	-	8840	0.24
PE4 #4	0.25	-	8720	0.26
PE5 #1	0.24	MoS ₂	8,620	0.20
PE5 #2	0.25	MoS ₂	11,200	0.27
PE6 #1	0.25	Graphite	11,540	0.20
PE6 #2	0.25	Graphite	10,760	0.22

Initial μ =0.06-0.08 for all samples; D= debond; Polymer thickness= 30-50 μ m.
E= 130 kW @ 370 V, 350 A for steel coatings.
E= 119 kW @ 340 V, 350 A for polymer coatings

Table 3.29. Amsler performance test results of UHMW / 1080 steel coatings PE7 through PE10. Input power was varied to observe effect on UHMW wetting. Gas parameters (1080 steel) were 230 N₂ / 30 H₂ with a working distance of 235 mm. Nylon gas parameters were 200 slpm N₂ / 50 slpm H₂ with a working distance of 255 mm. Wear test parameters: P₀= 1220 N/mm², Creep= 35%. 1080 steel coating thickness was 0.5 mm.

Sample	Power Input (kW)	Voltage Input (V)	Durability (revs.)	Final Friction (μ)
PE7	119	340	9650	0.20
PE8	105	350	7430	0.22
PE9	90	360	1000	0.46
PE10	74	370	1000	0.47

PE7 and PE8 polymer thickness = 35-50 μ m. I=350 A.
PE9 and PE10 polymer thickness < 15 μ m.

Table 3.30a. Surface modification parameters of as-machined Amsler rollers sprayed with nylon only.¹⁷⁹ Nylon spray parameters were 200 slpm N₂ / 50 slpm H₂ with a working distance of 255 mm. Power= 133 kW at 380 V and 350 A.

Sample	Surface Preparation	Grit Size (mesh)	Groove Pitch (grooves/mm)	Groove Depth (μm)
SM1	Grit	36	-	-
SM2	Grit	36	-	-
SM3	Groove	-	2	38
SM4	Ground	-	-	-
SM5	Ground	-	-	-
SM6	Grit, Groove	36	2	38
SM7	Grit, Groove	20	2	76
SM8	Grit, Groove	20	0.5	76
SM9	Grit, Groove	36	2	76
SM10	Grit, Groove	36	0.5	76

Grit= Grit blasting; Groove= Grooves cut into Amsler running surface.
Ground= Amsler running surface ground with fine grinding wheel.

Table 3.30b. Wear performance results for surface modified Amsler rollers with nylon coating only.¹⁷⁹
 (Samples SM1 - SM10). $P_0=1220 \text{ N/mm}^2$, Creep=35%.

Sample	Durability (revs.)	Initial Friction (μ)	Final Friction (μ)
SM1	5,200	0.09	0.35
SM2	5,500	0.09	0.40
SM3	2,200	0.07	0.57
SM4	640	0.08	0.57
SM5	820	0.08	0.57
SM6	6,400	0.08	0.23
SM7	2,800	0.12	0.28
SM8	3,500	0.08	0.34
SM9	2,500	0.10	0.34
SM10	3,700	0.07	0.24

Table 3.31. Amsler performance results for nylon / 308 L-Si stainless steel coatings tested under lubricated conditions. Coatings were applied with the standard gas parameters. $P_o=1220 \text{ N/mm}^2$. Creep=35%. Steel coating thickness= 0.25 mm.

Sample	Lubricant Type ¹	Durability (revs.)	Final Friction (μ)	Comments
WL1	H ₂ O	4570	0.22	D, X
WL2	H ₂ O	3420	0.21	D, X
WL3	H ₂ O	3670	0.22	D, X
GL1	Grease	4160	0.10	D
GL2	Grease	2790	0.10	D

¹ H₂O= plain tap water; Grease= Texaco 904. Initial $\mu=0.10$.
D= Debond of steel coating; X= entire polymer coating wore off prior to debonding.

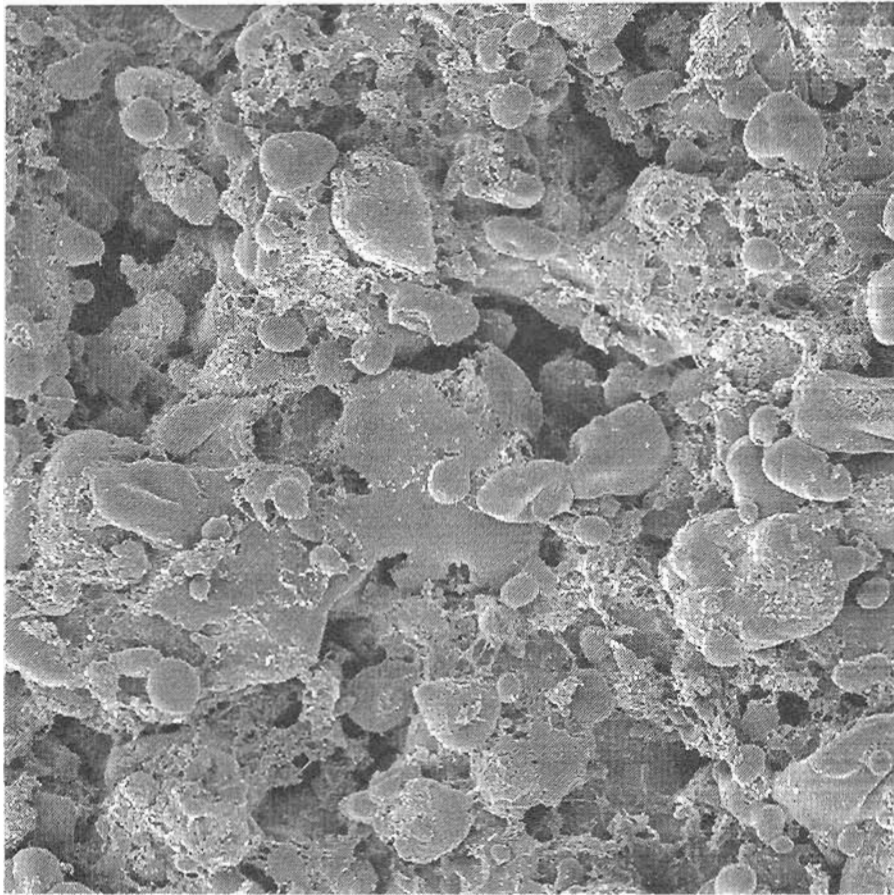
Table 3.32. Amsler performance test results of resprayed nylon /1080 steel coatings RS1 through RS9. Samples were tested to nylon coating failure prior to respraying. $P_0 = 1220 \text{ N/mm}^2$. Creep = 35%.

Sample	Steel Coating	Surface Treatment	Durability (revs.)	Final Friction (μ)	Gas Flow N_2 / H_2 (slpm)
RS1	1080	C	2450	0.39	230/30
RS2	1080	C	2840	0.31	230/30
RS3	1080	C	3100	0.30	230/30
RS4	1080	T	3360	0.30	230/30
RS5	1080	T	370 ^D	0.11	230/30
RS6	1080	T	1140	0.24	230/30
RS7	308 L-Si	T	4290	0.30	230/75
RS8	308 L-Si	T	4160	0.30	230/75
RS9	308 L-Si	T	4520	0.32	230/75

Steel Coating Thickness = 0.25mm; Initial $\mu = 0.10$. D = debond of steel coating.
 C = Clean only with acetone prior to spraying.
 T = Texture surface by grit blasting with steel shot, clean with acetone.

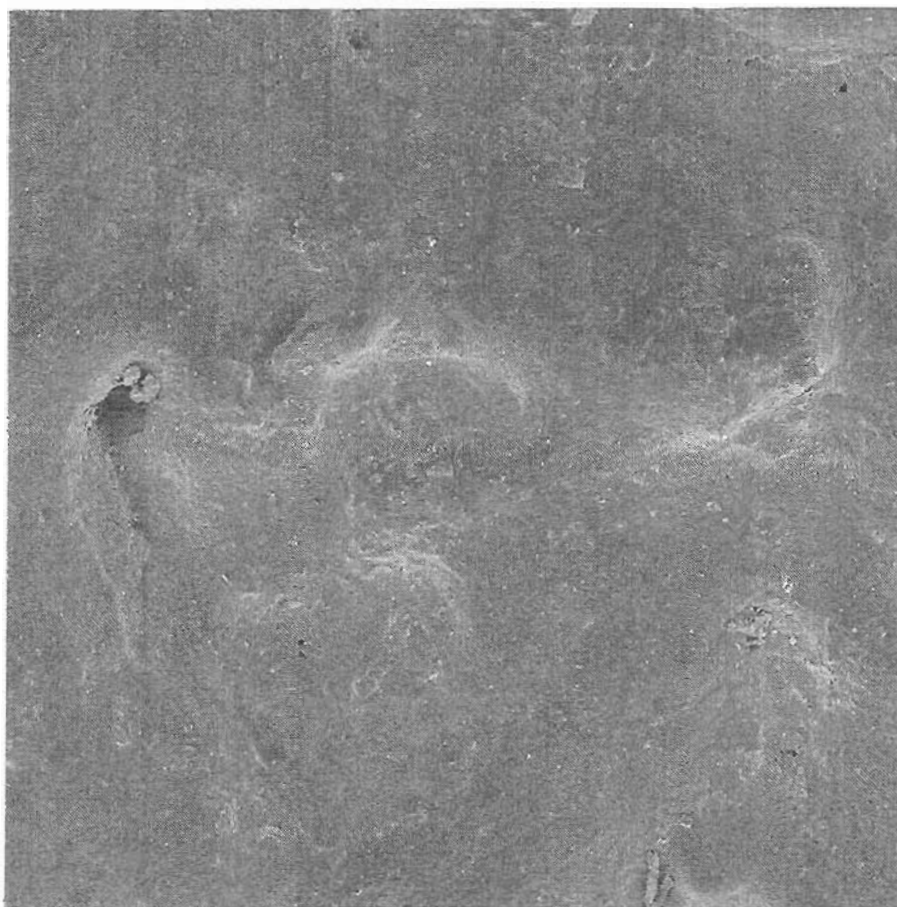
Table 3.33. Results of interrupted tests. All samples were sprayed at the standard gas parameters. $P_0=1220$ N/mm², Creep= 35%. The test revolutions represent the point at which each stage occurred. Coating thickness= 0.25 mm.

Degradation Stage	Sample	Revolutions	Final Friction (μ)
1	IN2f	30	-
2	IN2e	1100	0.10
3	IN2d	4000	0.11
4	IN2c	4050	0.16
5	IN2b	6100	0.27
6	IN2a	8920	0.24
7	IN2	11,230	0.34



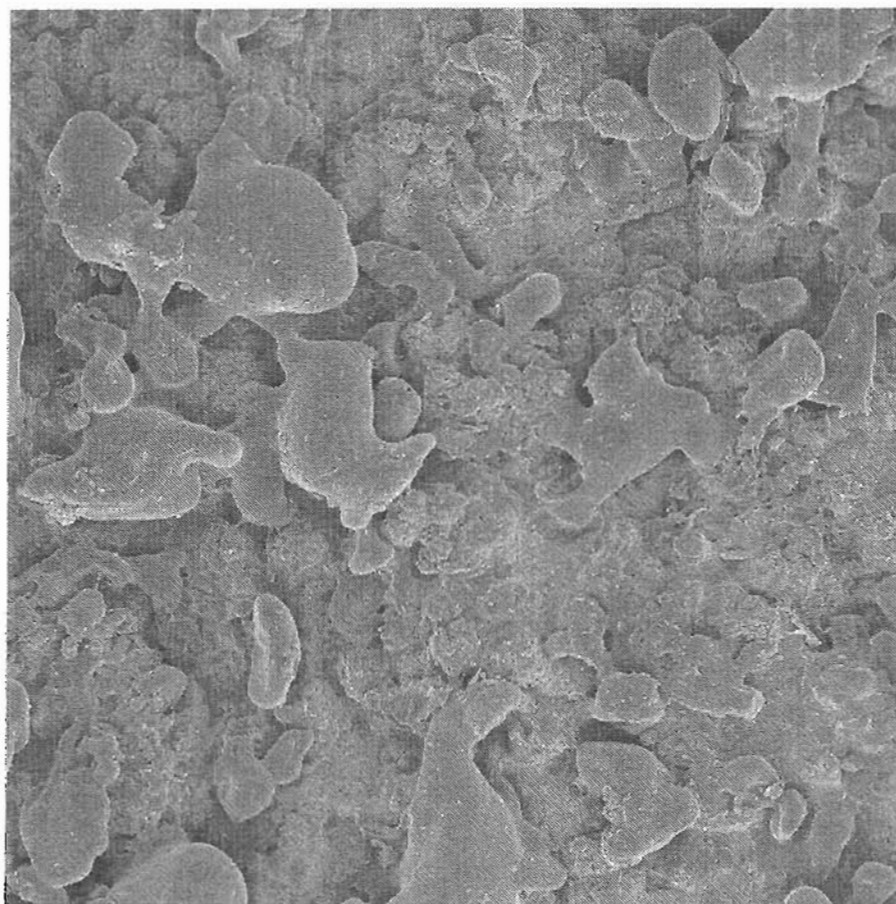
<----> 5 μm

Figure 3.31. SEM photograph illustrating non-wetting PTFE particles after plasma spray deposition. Gas parameters 200 slpm N_2 / 50 slpm H_2 , with a working distance of 255 mm. SE imaging. 200x.



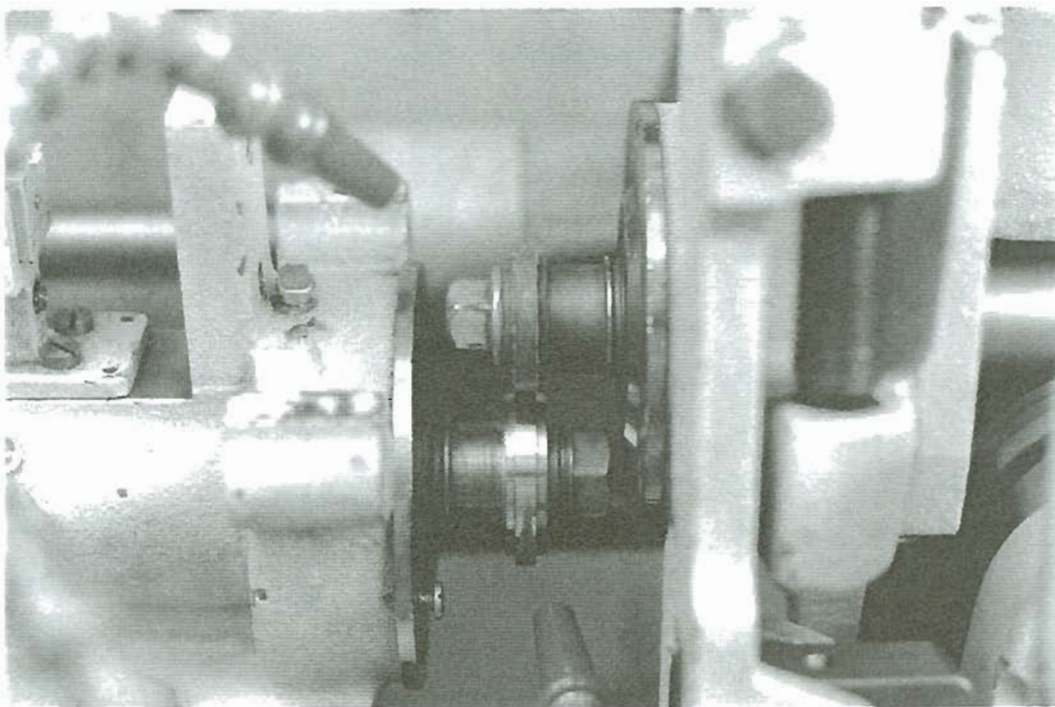
<---> 5 μ m

Figure 3.32. SEM photograph illustrating fully adhered and wetted UHMW coating after plasma spray deposition. Gas parameters 200 slpm N_2 / 50 slpm H_2 , with a working distance of 255 mm. SE imaging. 200x.



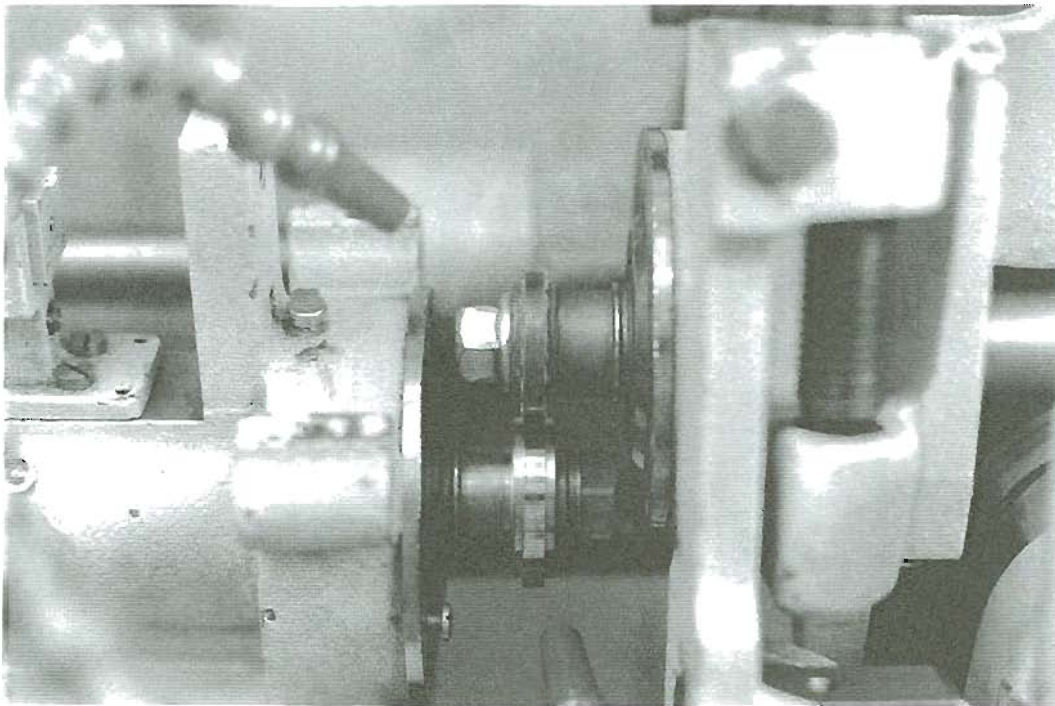
<----> 5 μ m

Figure 3.33. SEM photograph illustrating non-wetting UHMW particles after plasma spray deposition. Gas parameters 200 slpm N_2 / 50 slpm H_2 , with a working distance of 255 mm. SE imaging. 200x.



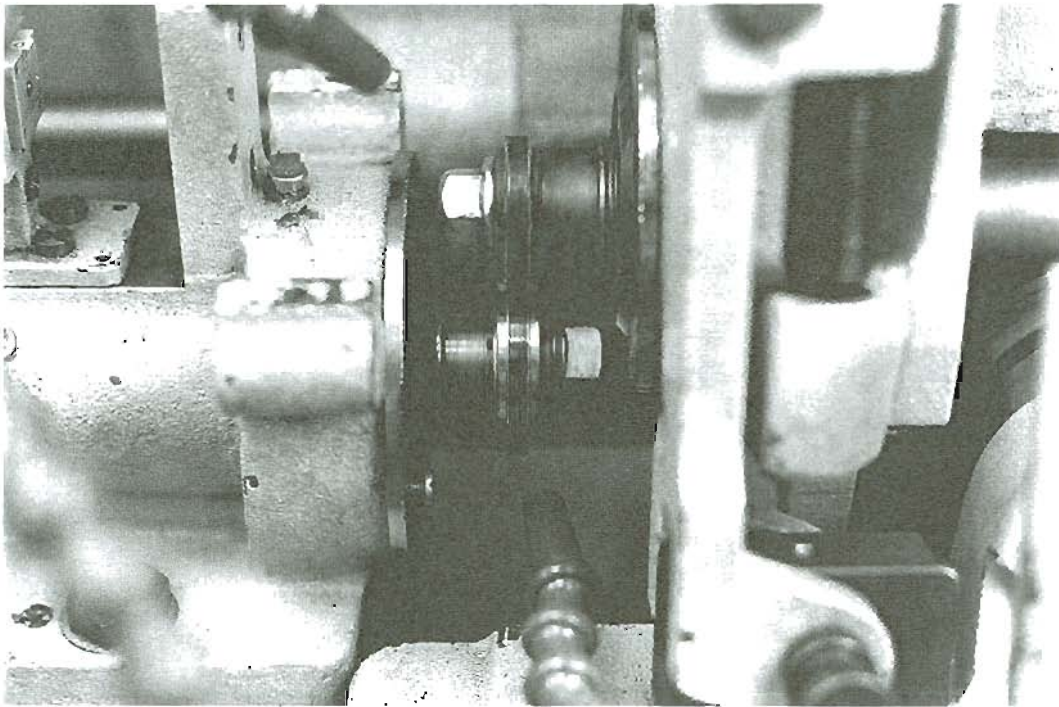
<-----> 1 cm

Figure 3.34. Photograph of nylon / steel coating wear process. Stage I shows excess nylon being shed. Revolutions= 50. $P_o = 1220 \text{ N/mm}^2$. Creep=35%.



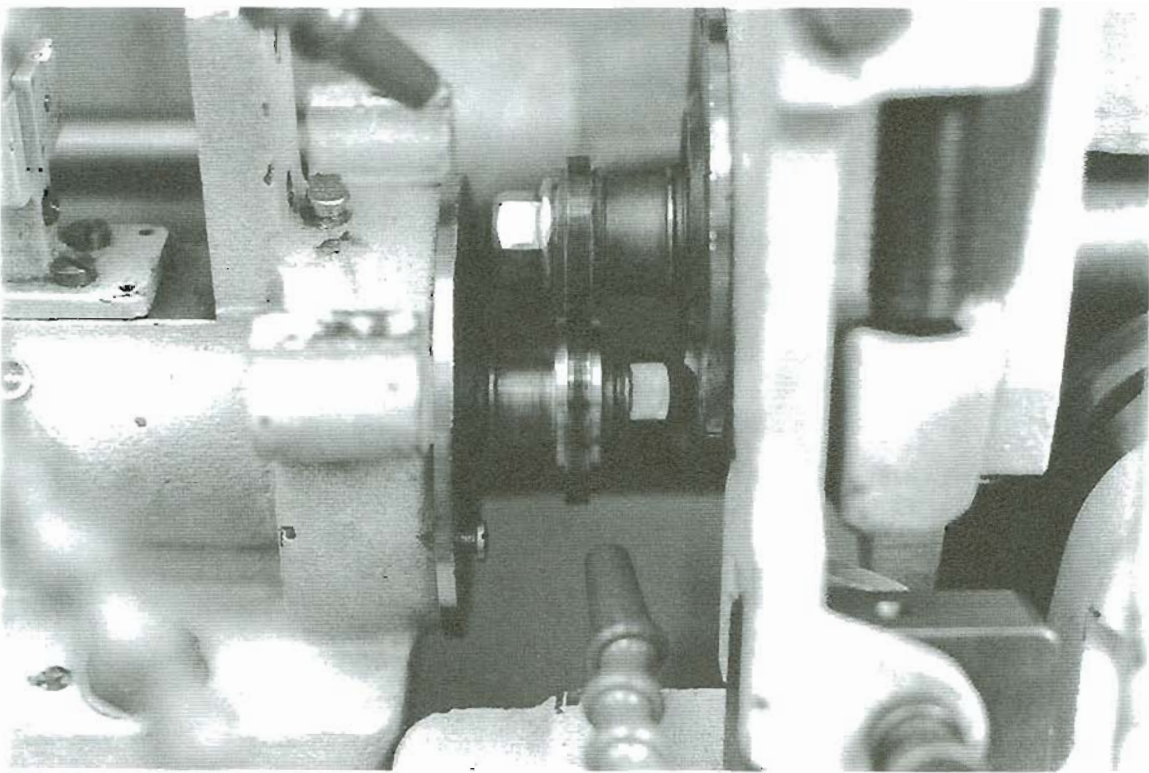
<-----> 1 cm

Figure 3.35. Photograph of nylon / steel coating wear process. Stage II is steady state wear of thin polymer film. Revolutions= 1200. $\mu= 0.10$. $P_o= 1220 \text{ N/mm}^2$. Creep=35%.



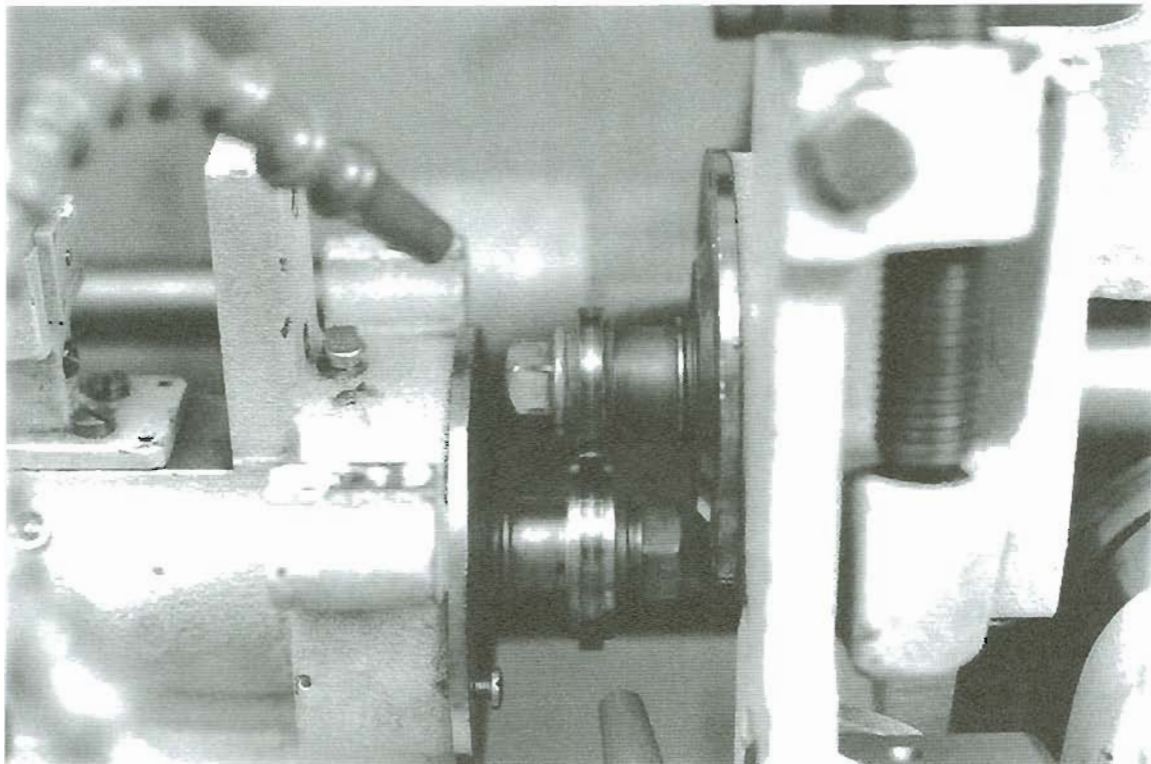
<-----> 1 cm

Figure 3.36. Photograph of nylon / steel coating wear process. Stage III occurs when nylon particles are transferred to the bottom roller. Revolutions= 4200. $\mu = 0.11$. $P_0 = 1220 \text{ N/mm}^2$. Creep=35%.



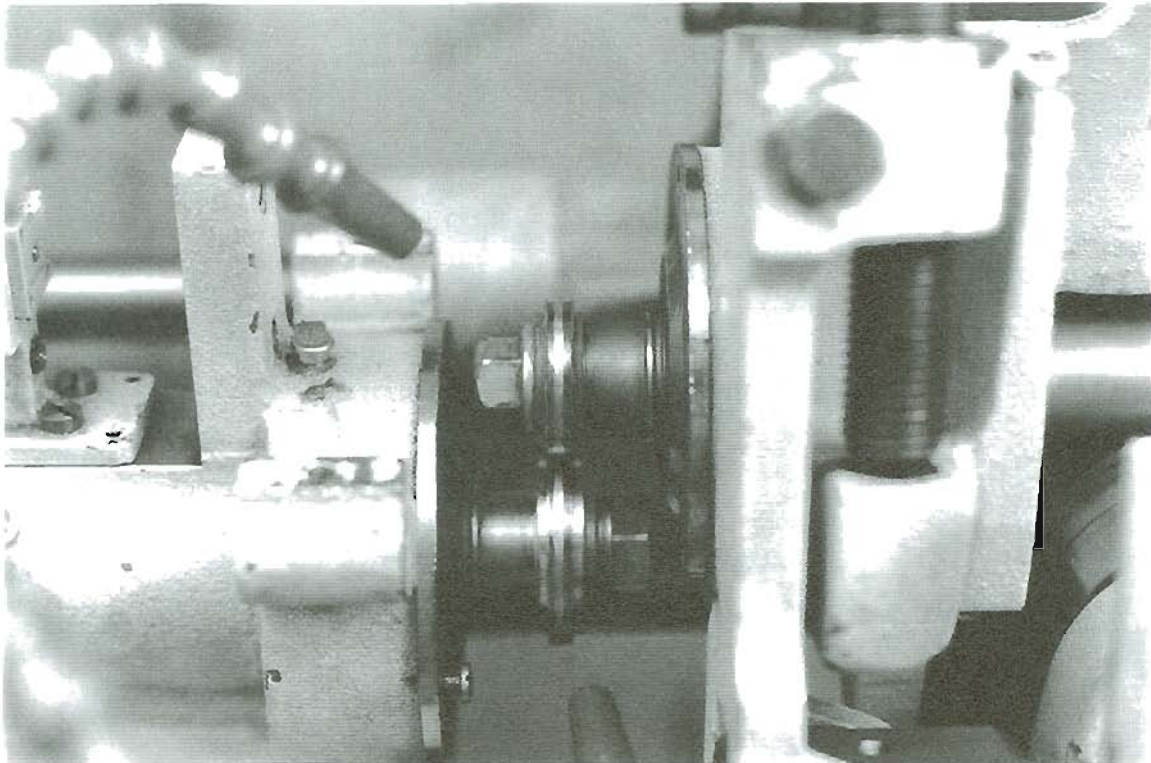
<-----> 1 cm

Figure 3.37. Photograph of nylon / steel coating wear process. Stage IV illustrates the growth of a nylon film on the bottom roller. Revolutions= 4300. $\mu= 0.16$. $P_o= 1220 \text{ N/mm}^2$. Creep=35%.



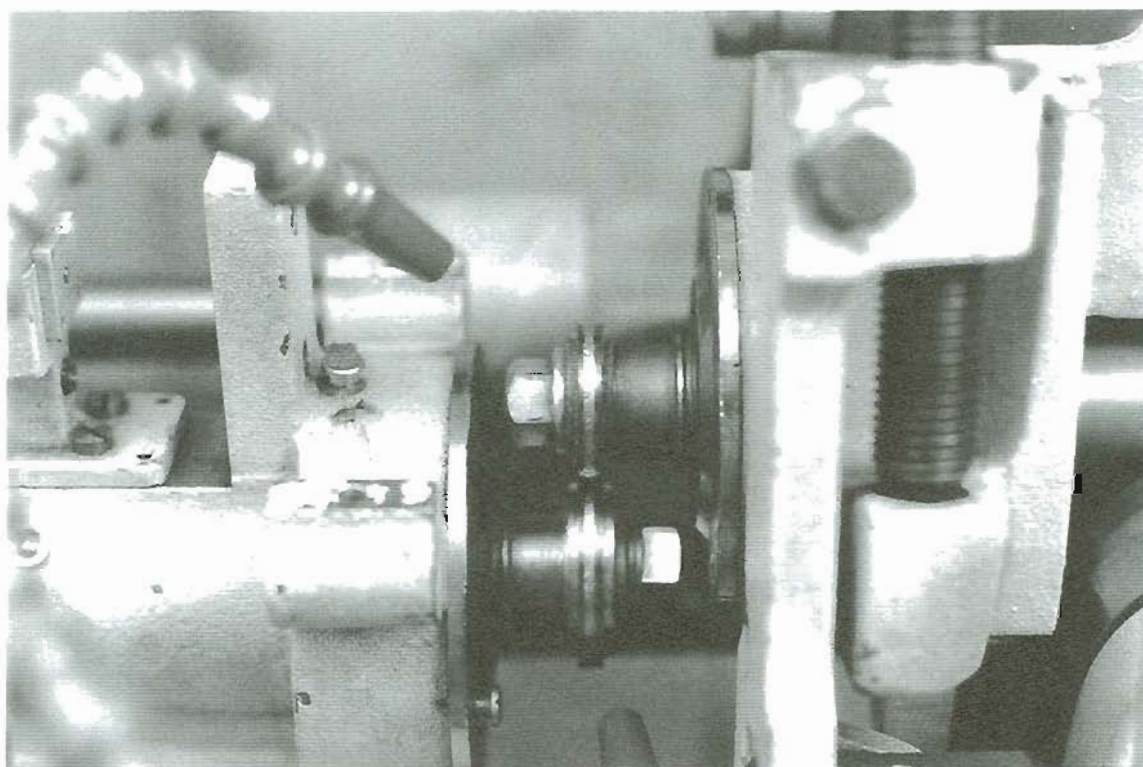
<-----> 1 cm

Figure 3.38. Photograph of nylon / steel coating wear process. Stage V, the polymer film wears through in the form of a ring, which illustrates the exposed steel area. Revolutions= 6300. $\mu = 0.27$. $P_0 = 1220 \text{ N/mm}^2$. Creep=35%.



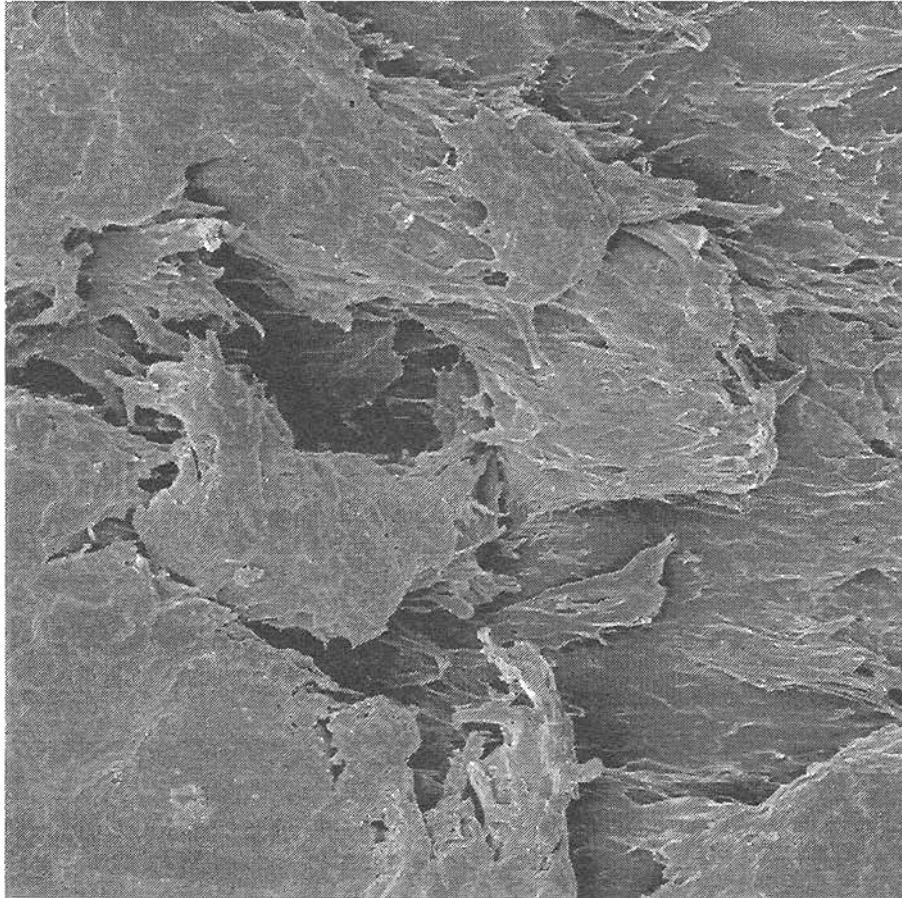
<-----> 1 cm

Figure 3.39. Photograph of nylon / steel coating wear process. Stage VI, the wear ring expands to fully expose steel coating. Steel coating on steel contact begins. Revolutions= 9050. $\mu= 0.24$. $P_o= 1220 \text{ N/mm}^2$. Creep=35%.



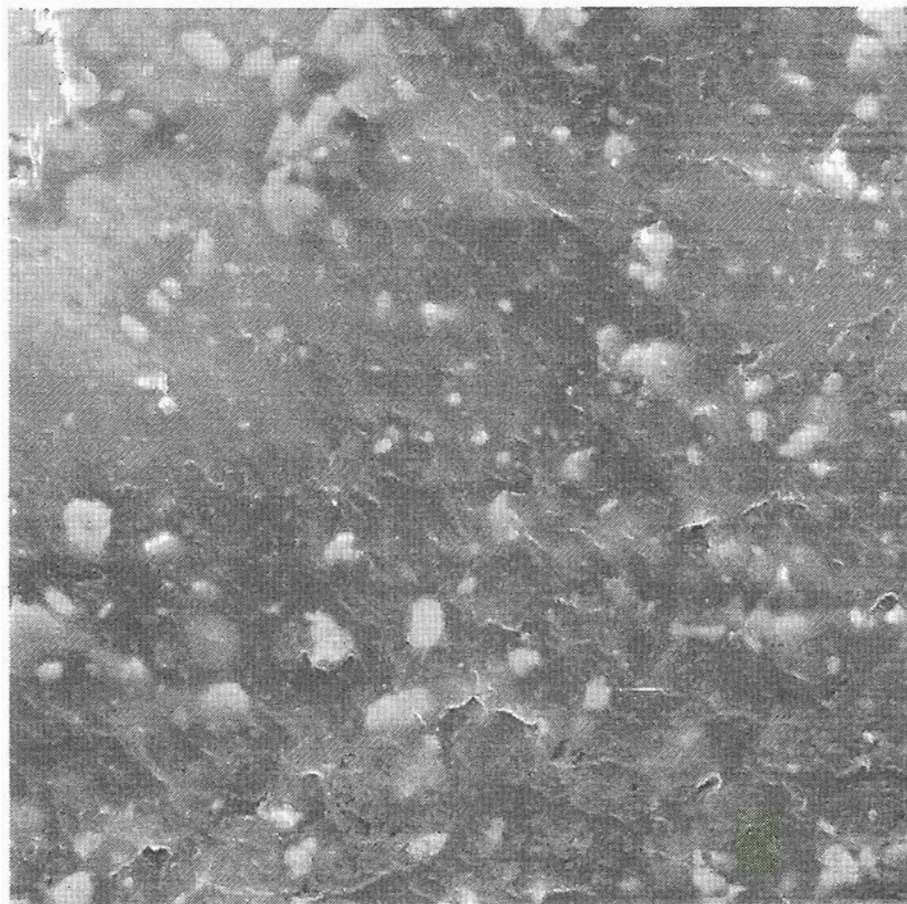
<-----> 1 cm

Figure 3.40. Photograph of nylon / steel coating wear process. Stage VII, full steel coating on steel contact occurs and proceeds to Type III wear. Revolutions= 11,560. $\mu= 0.35$. $P_0= 1220 \text{ N/mm}^2$. Creep=35%.



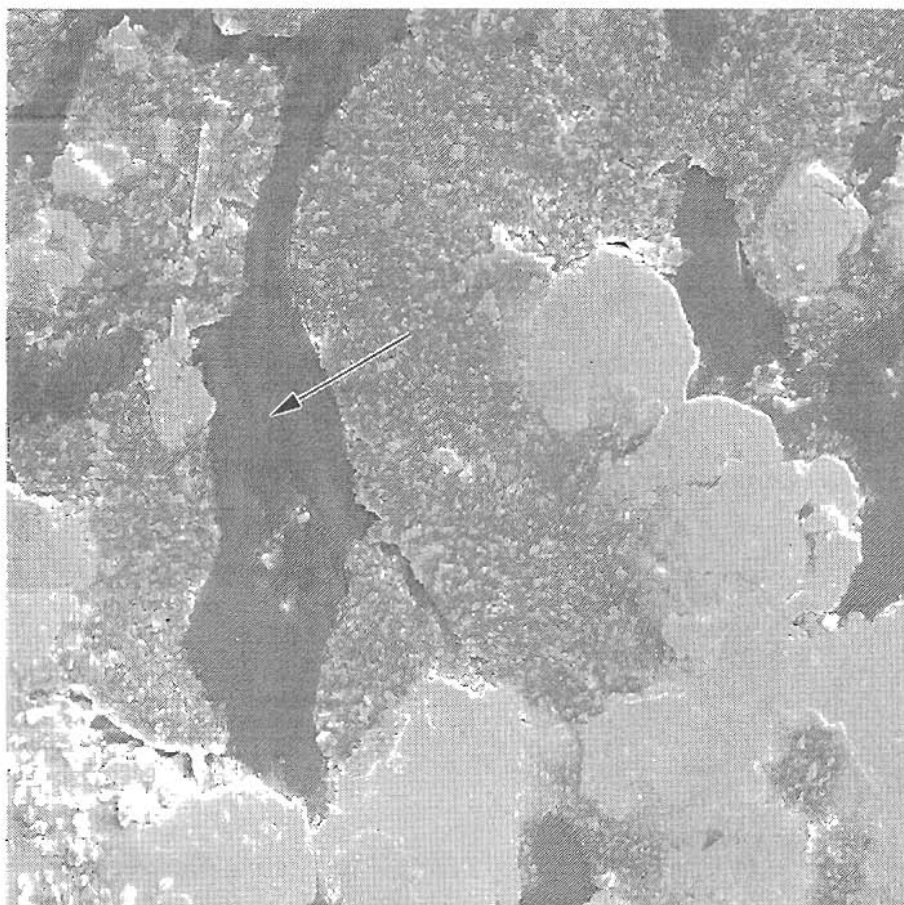
<----> 2 μm

Figure 3.41. SEM photograph illustrating Stage I of nylon / steel coating wear process. Excess polymer is shredded from its as-sprayed continuous film state. SE imaging. 500x.



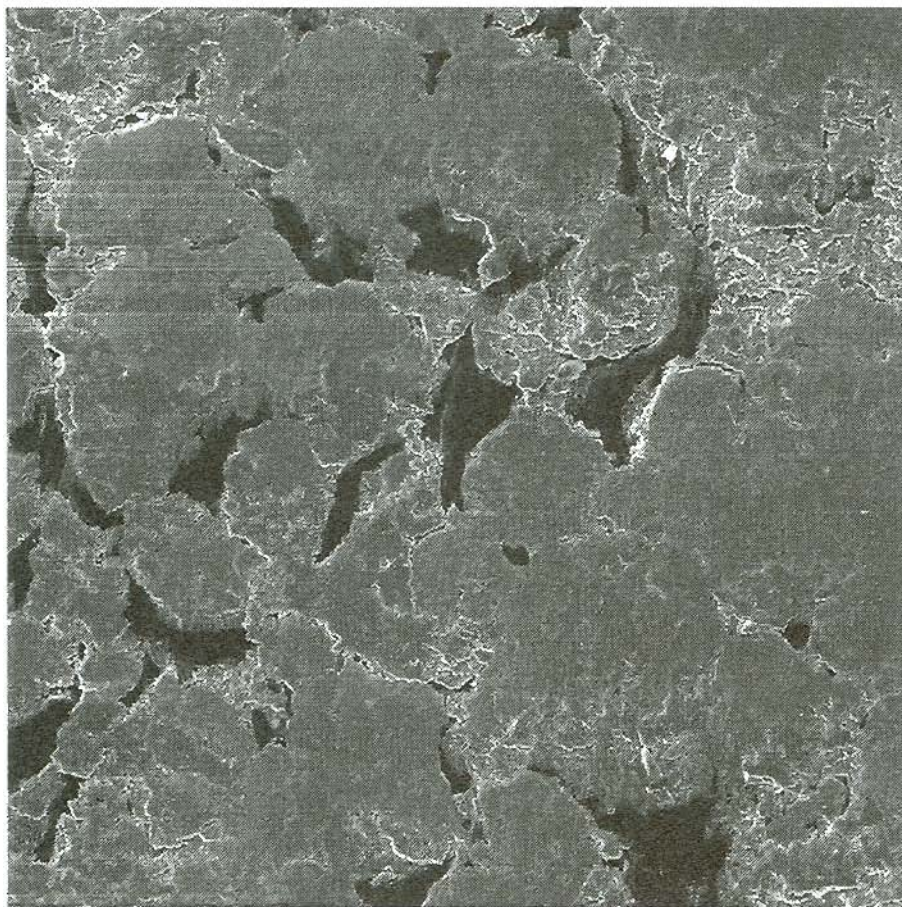
←—→ 1 μm

Figure 3.42. SEM photograph illustrating Stage II of nylon / steel coating wear process. Smooth, continuous polymer film is formed. SE imaging. 1000x.



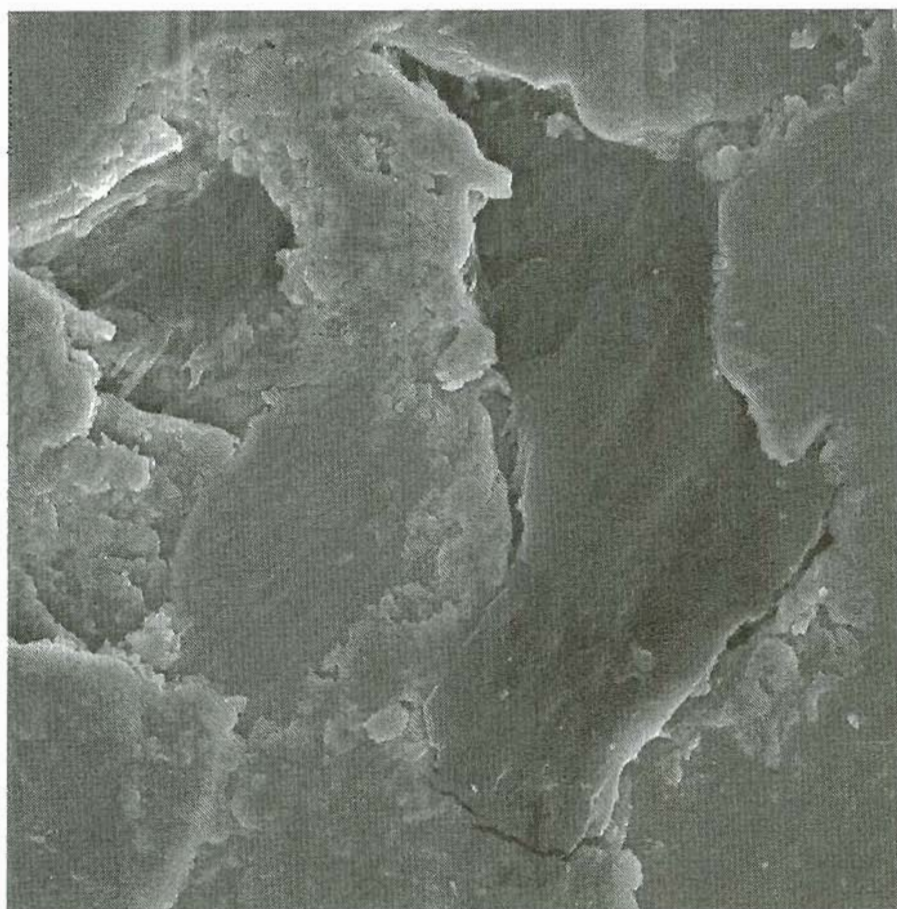
<---> 5 μ m

Figure 3.43. SEM photograph illustrating Stage III of nylon / steel coating wear process. Wear of polymer film continues. Arrow denotes area where polymer has anchored into steel coating valley. Darker color is a result of thicker nylon material. SE imaging. 200x.



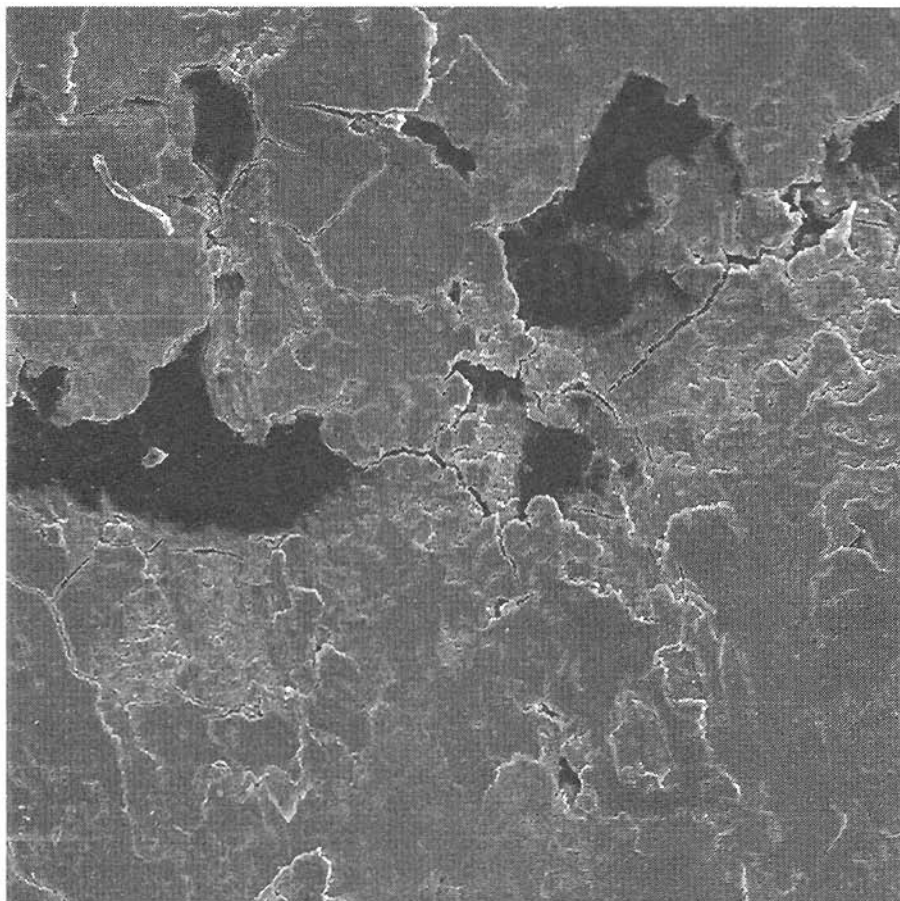
<---> 10 μm

Figure 3.44a. SEM photograph illustrating Stage IV of nylon / steel coating wear process. Most of nylon film has worn off, leaving a very thin, transparent film and excess nylon concentrated in steel coating valleys. SE imaging. 100x.



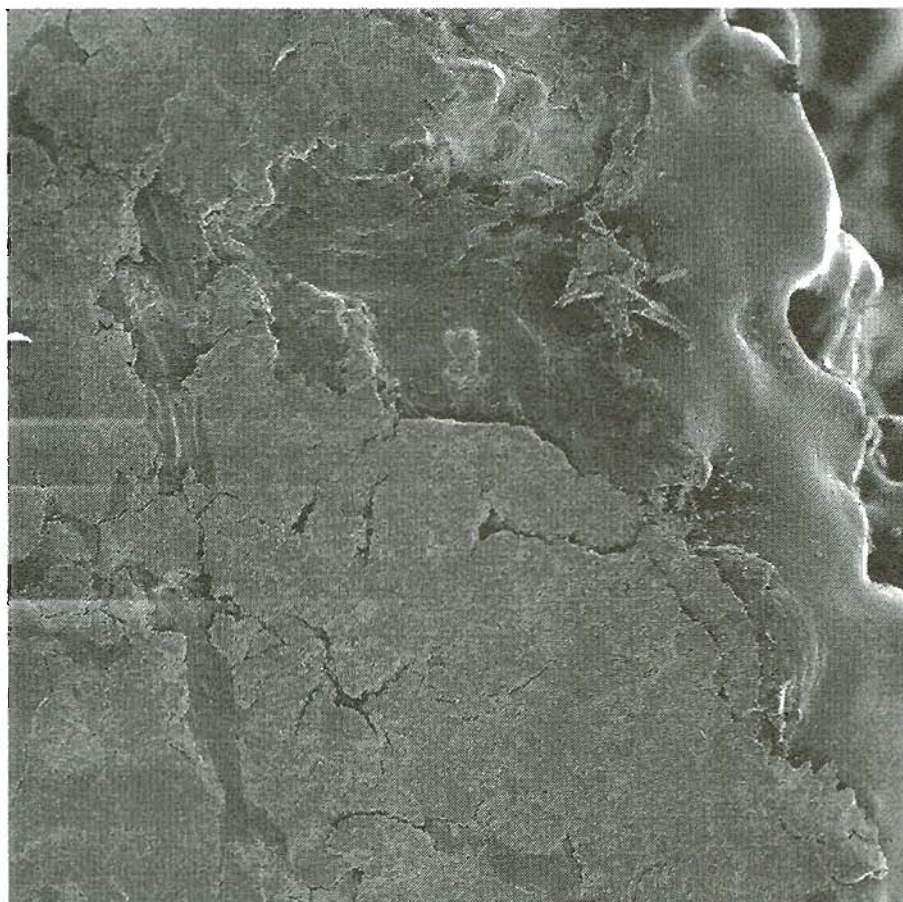
<----> 1 μm

Figure 3.44b. SEM photograph illustrating Stage IV of nylon / steel coating wear process. Closeup of nylon material anchored in steel coating valley. SE imaging. 1000x.



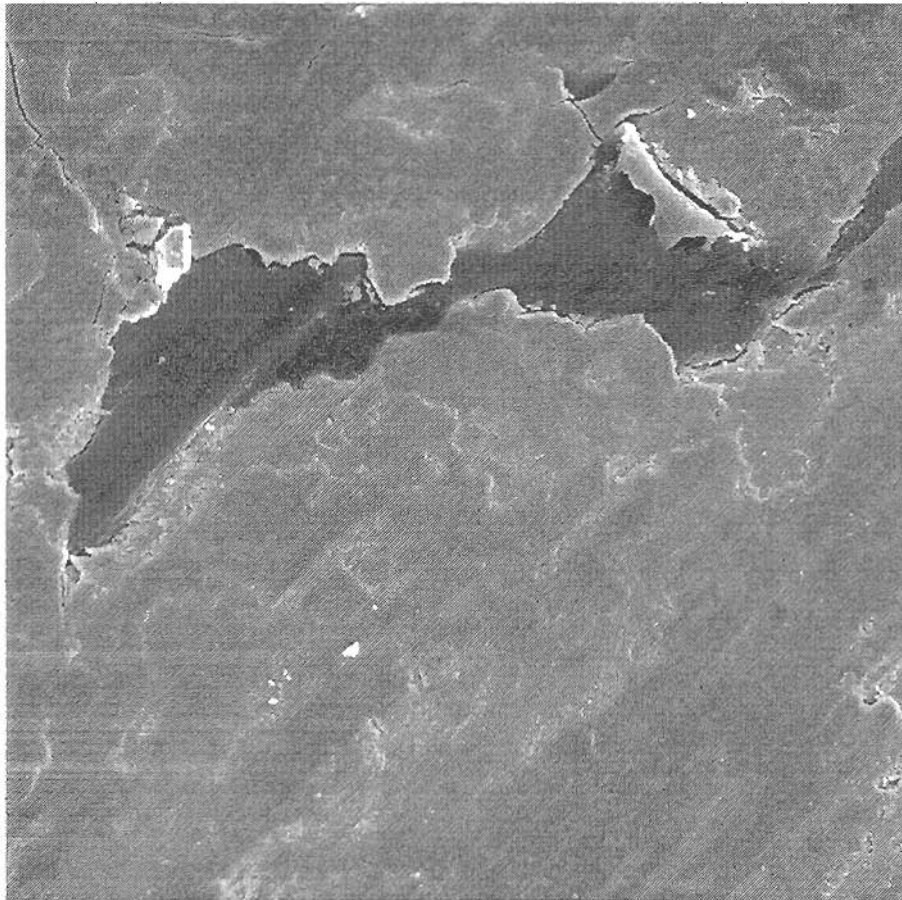
←—→ 5 μ m

Figure 3.45a. SEM photograph illustrating Stage V of nylon / steel coating wear process. Nylon is concentrated in steel coating valleys. Cracks are beginning to form on steel coating surface. SE imaging. 200x.



<---> 10 μ m

Figure 3.45b. SEM photograph illustrating Stage V of nylon / steel coating wear process. View of Amsler roller edge showing as-sprayed nylon and worn nylon in steel coating valleys. Cracks in steel coating surface are also apparent. SE imaging. 100x.



<----> 2 μm

Figure 3.46. SEM photograph illustrating Stage VI of nylon / steel coating wear process. Only sparse nylon material exists which is anchored in steel coating valleys. Steel coating wear surface is still smooth. SE imaging. 500x.

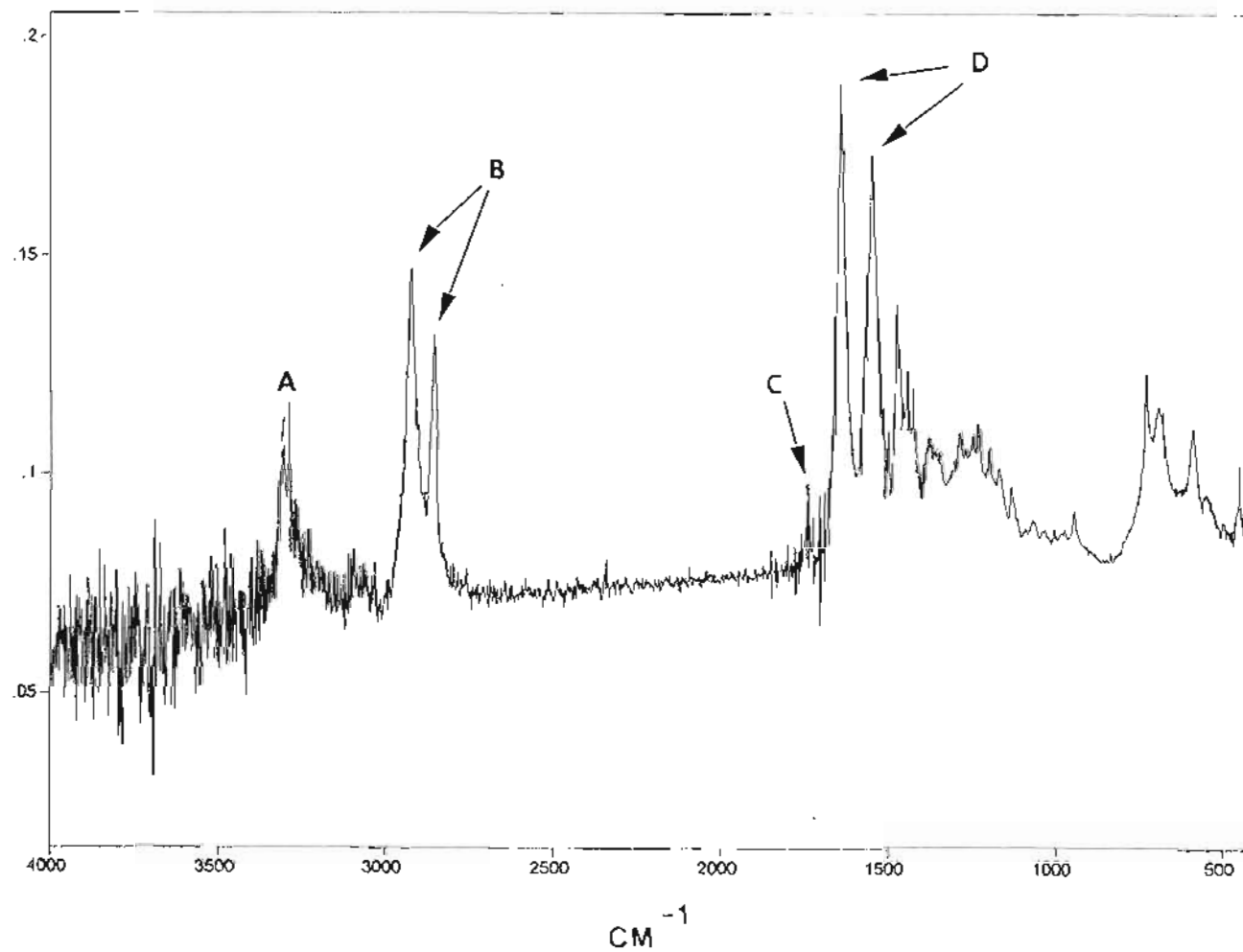


Figure 3.47. FTIR spectrum of as-sprayed nylon film, using ATR. The spectrum represents the characteristic peaks of the amide linkage. a) Amide I stretch (3309 cm^{-1}). b) C-H stretch of methylene groups (2925 cm^{-1} and 2856 cm^{-1}). c) Carbonyl (C=O) stretch (1734 cm^{-1}). d) Amide II stretch (1639 cm^{-1} and 1643 cm^{-1}).

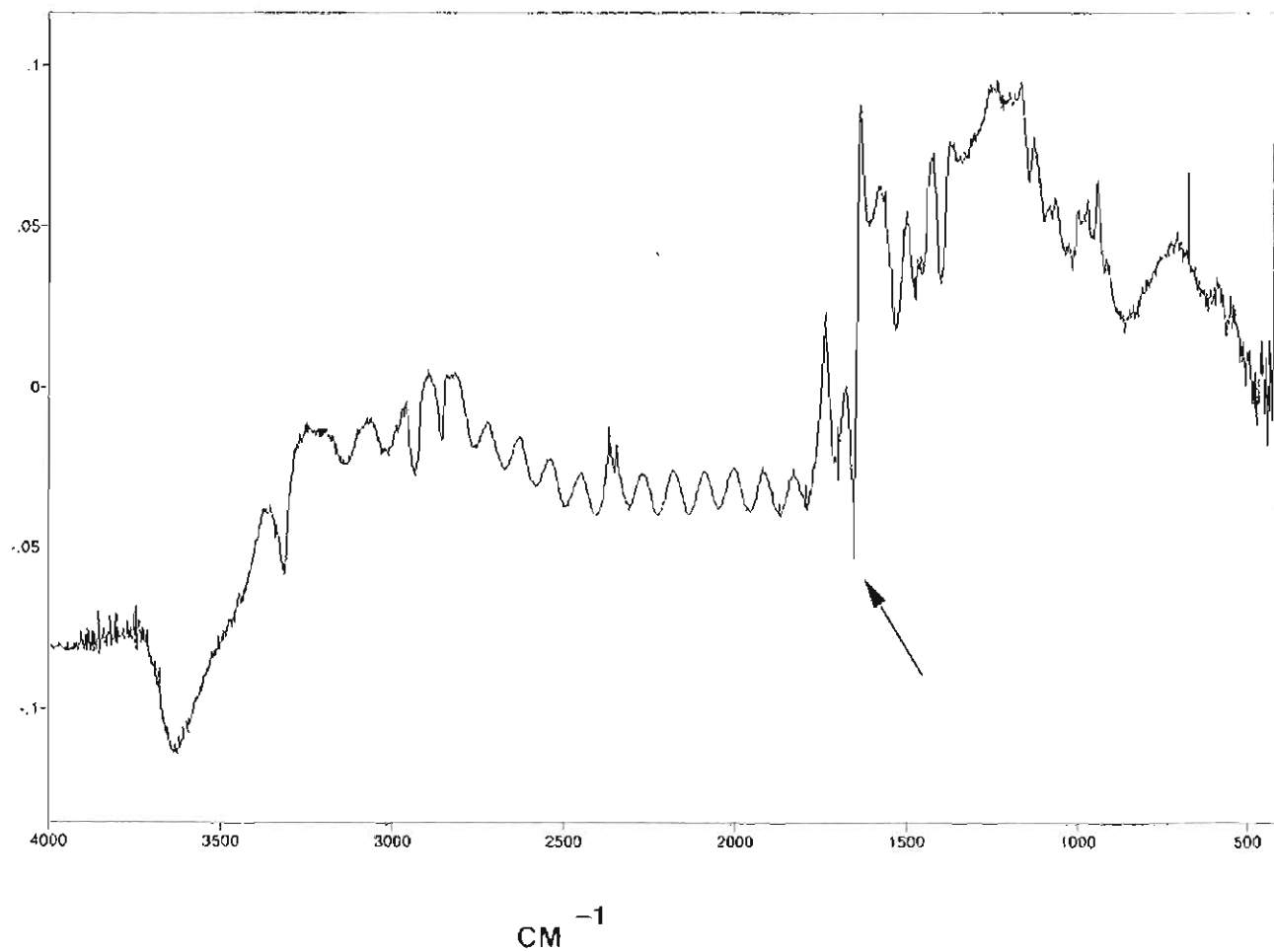


Figure 3.48. Resultant subtractive (as-sprayed - as melted) FTIR spectrum of two analyzed nylon films, using SR. The spectrum represents the shift in the carbonyl (C=O) peak at the film surface when nylon is plasma sprayed as opposed to being melted. The arrow identifies the negative peak.

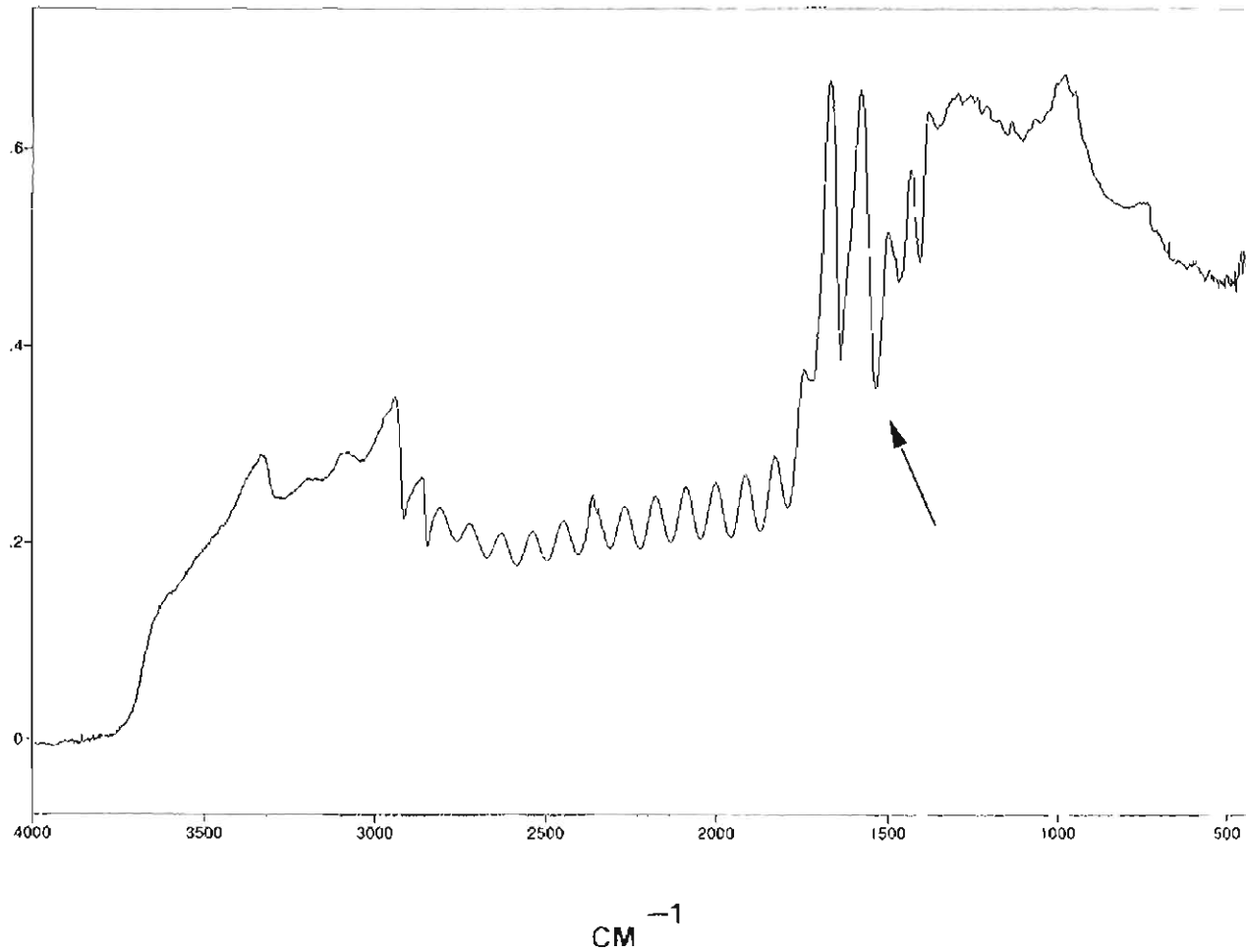
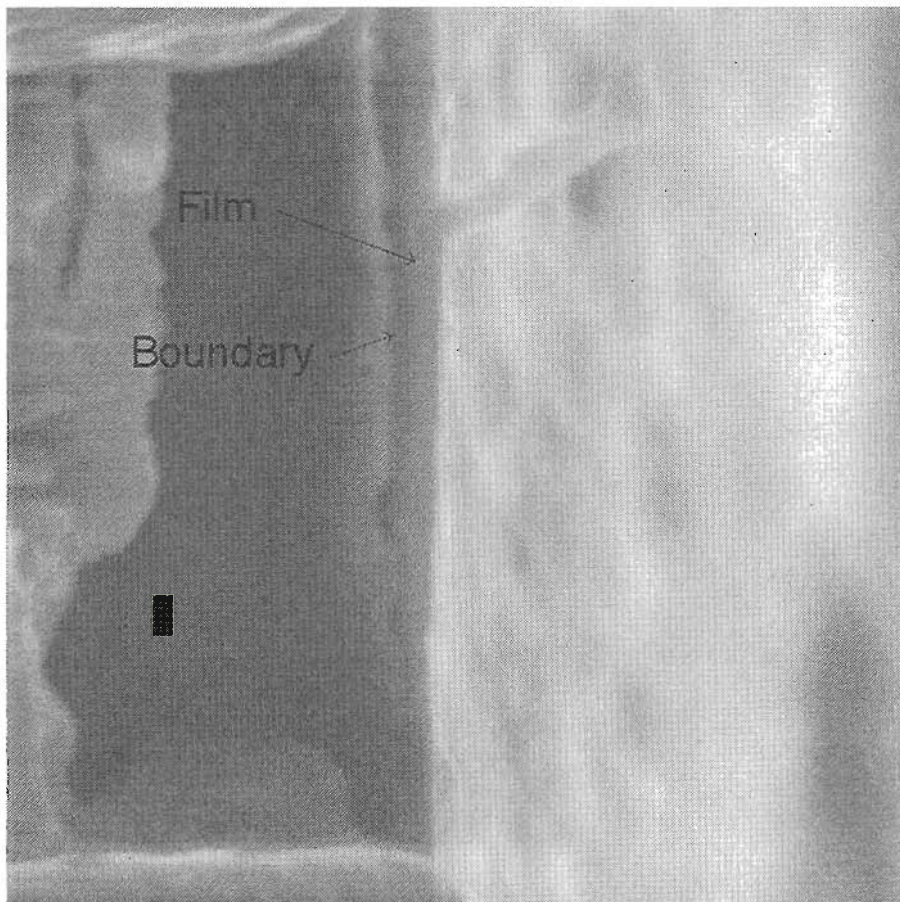


Figure 3.49. Resultant subtractive (as-sprayed - as worn) FTIR spectrum of two analyzed nylon films, using SR. The spectrum represents the shift in the Amide II peak at the film surface when nylon is transferred to the bottom roller during wear testing. The arrow identifies the negative peak.



<----> 2 μm

Figure 3.50. SEM photo illustrating cross section of transferred nylon film. Cross section was cut with FIB. The film is on the order of 1 μm thick.

3.5 Steel Coating Deposition on Full Scale Rail Sections

Exhaustive studies have been made with coatings applied to Amsler rollers. The round geometry and closed-system nature of the Amsler tests prompted new coating evaluation techniques. The deposition of steel coatings and polymer / steel coatings on rail head would allow for performance evaluation which closer approximated the field.

3.5.1 Parameter Optimization

The rail heads that were sprayed with the standard gas flow rate (230 slpm N_2 / 30 slpm H_2) and working distance (235 mm) illustrated the need for modified spray parameters. Initial coatings deposited onto rail head had evidence of large oxide volume fractions. The oxide content and coating morphology were clearly different than similar (parameter) coatings sprayed on to Amsler rollers. Table 3.34 is the matrix of gas parameter and working distance changes used to re-optimize the 1080 steel coating on rail head. This table also lists the results with respect to change in porosity and oxide volume fraction.

Figures 3.51 and 3.52 illustrate how porosity increases when nitrogen is varied from 230 slpm. Figures 3.53 through 3.57 illustrate the effect of varying hydrogen. When hydrogen is increased to 50 and 75 slpm the oxide volume fraction is reduced. At 100 and 125 slpm H_2 though, small particles disappear and porosity increases. If H_2 is eliminated, oxide volume fraction increases. The effect of working distance is illustrated in Figure 3.58 and 3.59. Deviation from 235 mm appears to increase porosity. For comparison, Figure 3.60 illustrates the microstructure for the standard parameters, 230 slpm N_2 / 30 slpm H_2 with a working distance of 235 mm, when deposited on rail head.

3.5.2 Large Scale Testing

Several full scale track specimens were spray coated and tested at the AAR facility for accelerated testing (FAST) in Pueblo, Colorado. Three types of samples were spray coated. Track lab samples (TL) consisted of 4340 steel coupons in the shape of the rail head. Rolling load machine (RLM) samples consisted of 5 foot sections of rail. Finally, the track test (TT) sample was a 12 foot rail section. Table 3.35 summarizes the performance results of the various samples. Performance was measured in million gross tons (mgt), which evaluates durability with respect to the number of trains and cars that pass over the coating. Early samples were 1080 steel coating only, while later samples consisted of a nylon / 1080 steel coating or nylon / 308 L-Si stainless steel coating. Figure 2.11 illustrated the track lab coupon geometry in the fixture used for spray coating. Figure 2.12 illustrated the twelve foot (TT) sample in the as-sprayed condition.

Table 3.34. Summary of 1080 steel coating deposition on rail head to optimize spray parameters. Shaded areas illustrate the change in variables from the standard 230 slpm N₂ / 30 slpm H₂ / 235 mm working distance. Results are presented as an increase or decrease in oxide and porosity volume fraction.

Nitrogen (slpm)	Hydrogen (slpm)	Working Distance (mm)	Power (kW)	Results
200	30	235	116	Increased P
275	30	235	126	Increased P
230	0	235	116	Increased P and O
230	50	235	126	Reduced O
230	75	235	133	Reduced P and O
230	100	235	140	Increased P
230	125	235	140	Increased P
230	30	200	130	Increased P
230	30	250	130	Increased P

Abbreviations: O= oxide volume fraction; P= porosity volume fraction

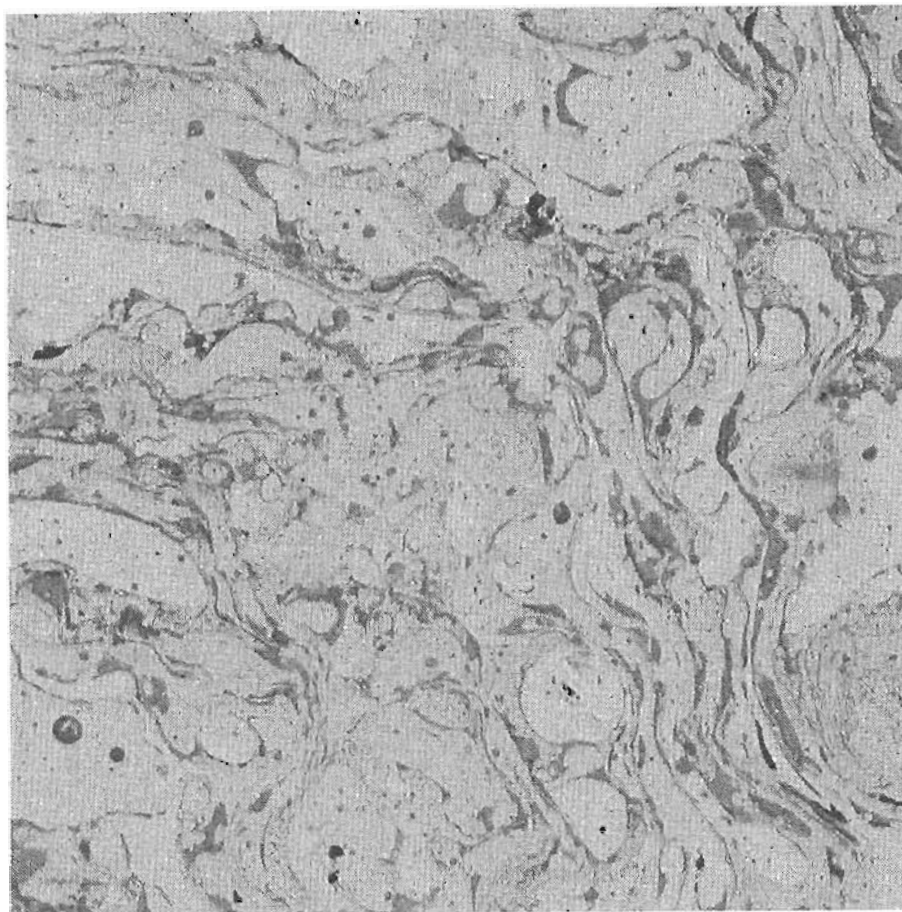
Table 3.35a. Spray parameters for steel, polymer/steel coatings deposited onto full scale test samples for evaluation at FAST. Polymer gas parameters: 200 slpm N₂ / 50 slpm H₂ / 255 mm.

Sample	Gas Parameters N ₂ /H ₂ (slpm)	Coating Material	Steel Coating Thickness (mm)	Rail Type or Material
TL1	230 / 30	1080 steel	> 1.25	4340
TL2	230 / 30	1080 steel	> 1.25	4340
TL3	230 / 75	1080 steel	0.5 - 1	4340
TL4	230 / 75	308 L-Si/nylon	0.5	4340
RLM1	230 / 30	1080 steel	> 1.25	Standard
RLM2	230 / 75	1080 / nylon	1.0	new HH
RLM3	230 / 75	1080 / nylon	0.5	new HH
RLM4	230 / 75	1080 / nylon	1.0	worn HH
RLM5	230 / 75	1080 / nylon	0.5	new HH
TT1	230 / 75	1080 / nylon	0.25-0.5	worn HH

Material type: 4340= SAE 4340 steel coupon; HH= head hardened standard carbon rail; Standard= standard carbon rail (300 BHN)

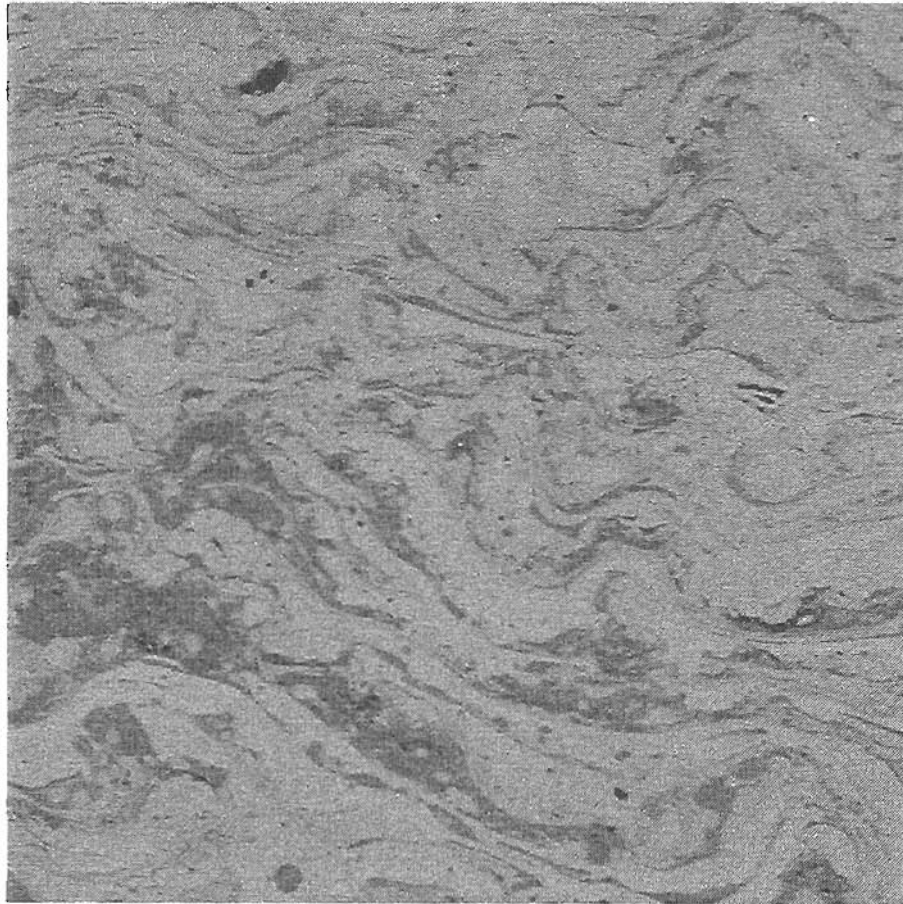
Table 3.35b. Performance results of large scale test samples at FAST. Test length is measured in million gross tons (mgt).

Sample	Test Length (mgt)	Comments
TL1	0.12	Track Lab 45t car
TL2	0.32	Track Lab 45t car
TL3	5.33	Track Lab 45t car
TL4	4.8	Track Lab 45t car
RLM1	2.2	Old RLM, L= 45t, pure rolling
RLM2	0.2	New RLM, L= 35t, high creep
RLM3	0.24	New RLM, L= 35t, high creep
RLM4	1.72	New RLM, L= 35t, pure rolling
RLM5	2.3	New RLM, L= 35t, pure rolling
TT1	1.3	FAST, 75 125t cars + 4 loco.



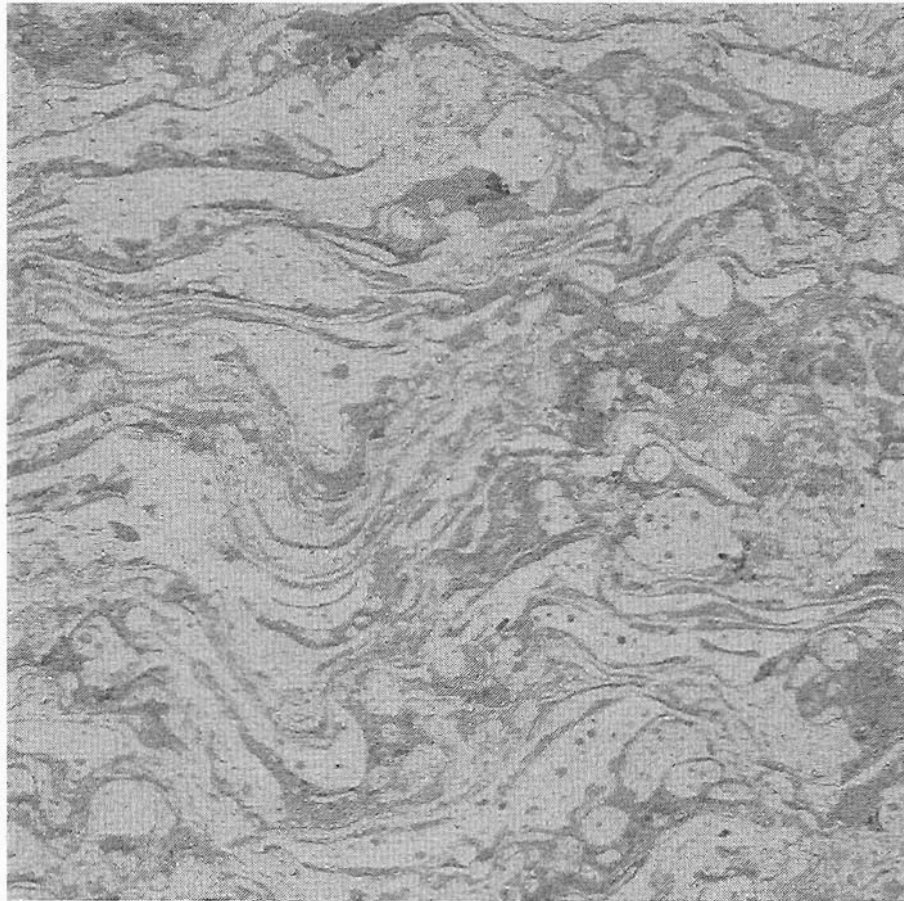
<----> 2 μm

Figure 3.51. SEM photograph illustrating 1080 steel coating microstructure as-deposited on rail head. Gas parameters: 200 slpm N_2 / 30 H_2 with a 235 mm working distance. SE imaging. 500x.



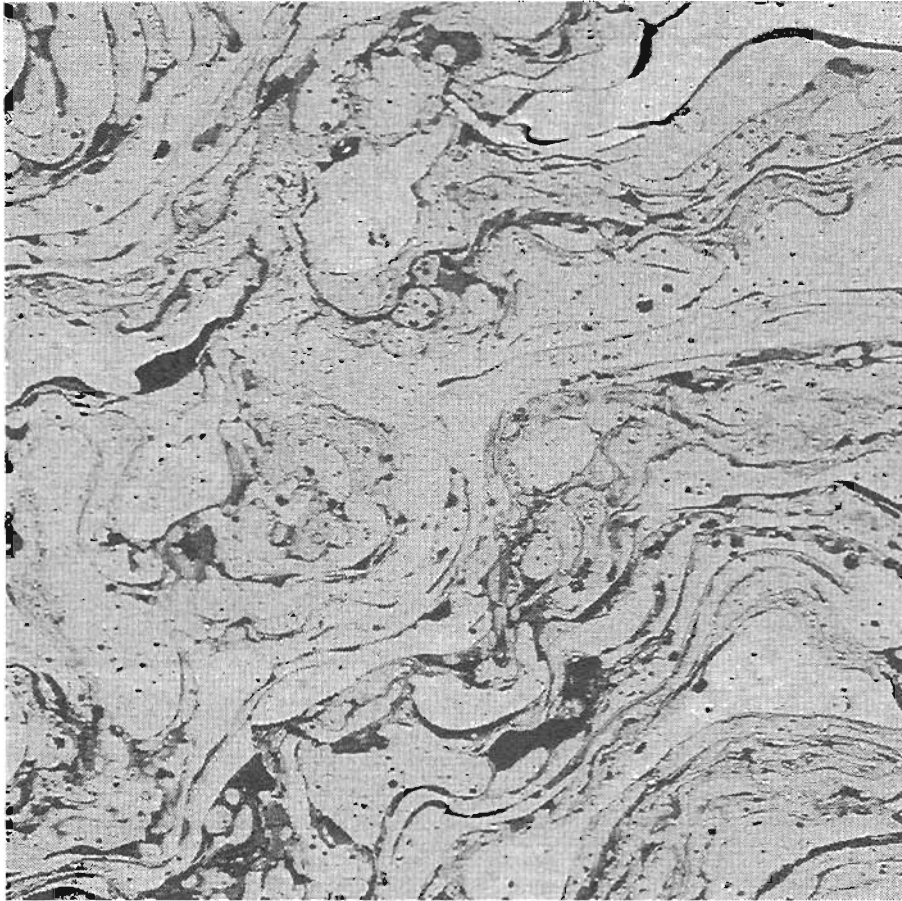
←—→ 2 μm

Figure 3.52. SEM photograph illustrating 1080 steel coating microstructure as-deposited on rail head. Gas parameters: 275 slpm N_2 / 30 H_2 with a 235 mm working distance. SE imaging. 500x.



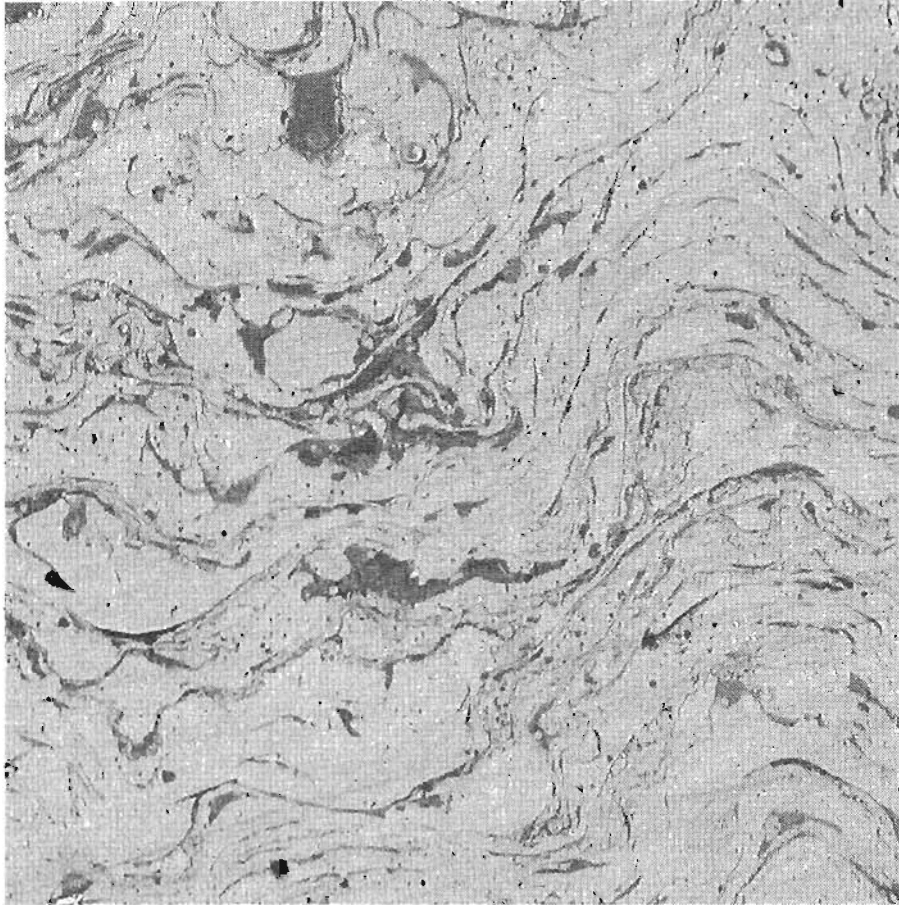
<—> 2 μm

Figure 3.53. SEM photograph illustrating 1080 steel coating microstructure as-deposited on rail head. Gas parameters: 230 slpm N_2 / 0 H_2 with a 235 mm working distance. SE imaging. 500x.



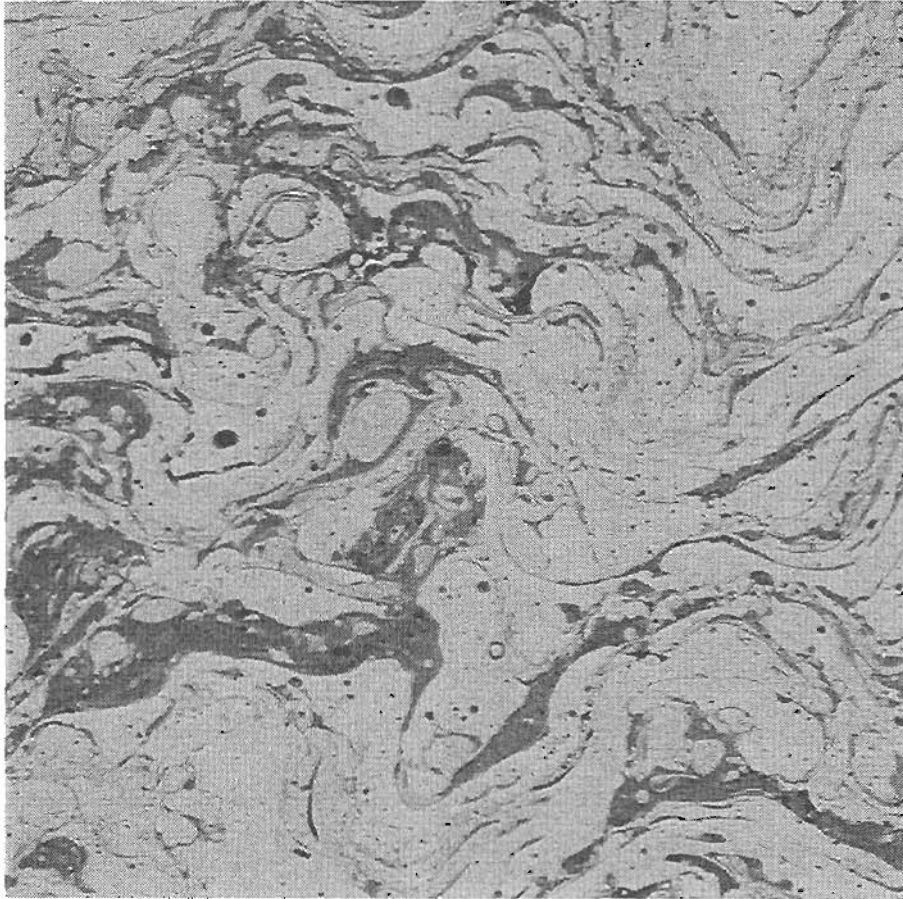
<—> 2 μm

Figure 3.54. SEM photograph illustrating 1080 steel coating microstructure as-deposited on rail head. Gas parameters: 230 slpm N_2 / 50 H_2 with a 235 mm working distance. SE imaging. 500x.



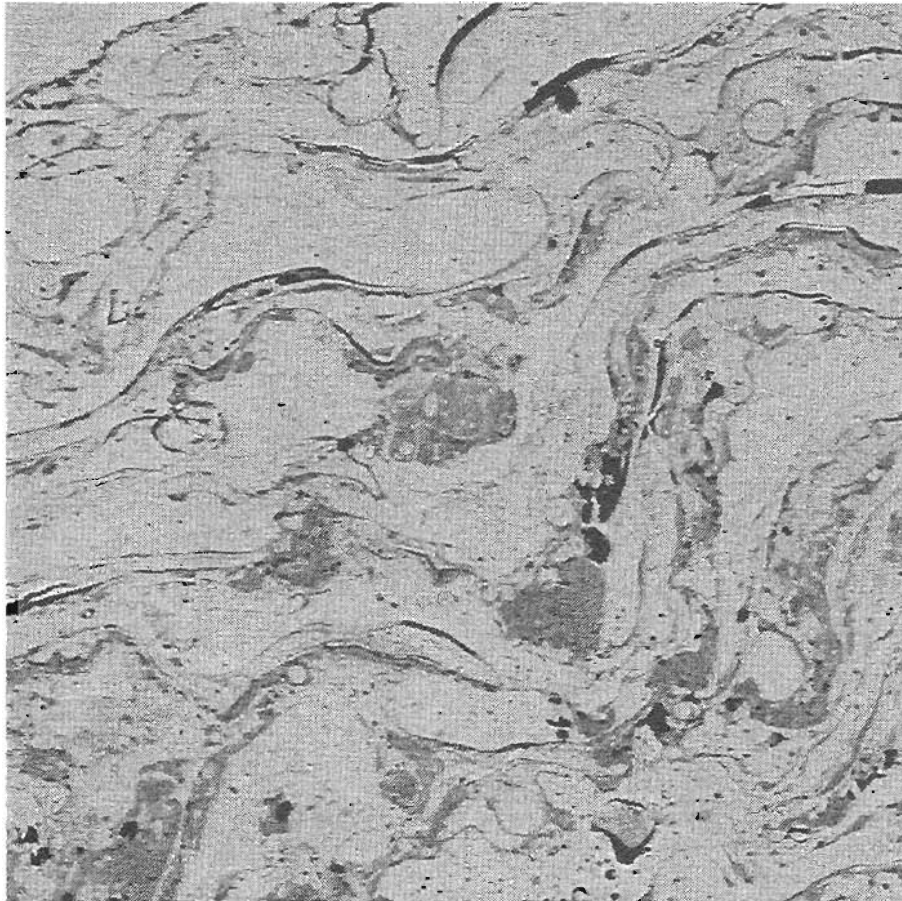
←→ 2 μm

Figure 3.55. SEM photograph illustrating 1080 steel coating microstructure as-deposited on rail head. Gas parameters: 230 slpm N_2 / 75 H_2 with a 235 mm working distance. SE imaging. 500x.



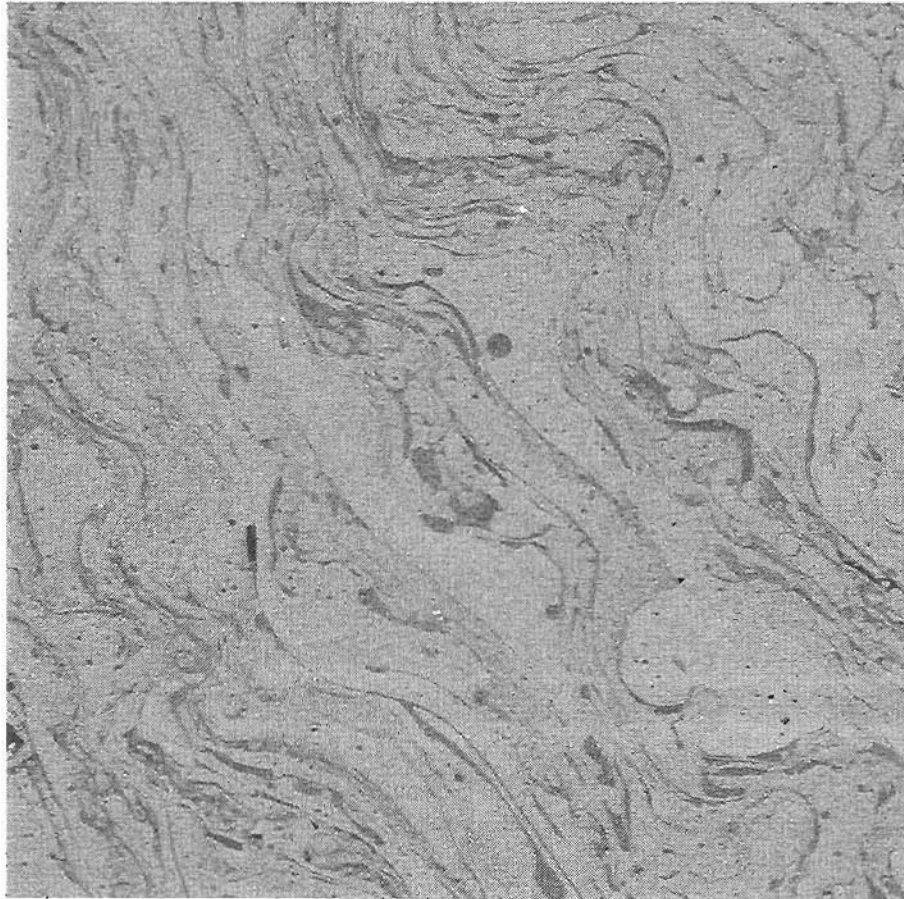
←—→ 2 μm

Figure 3.56. SEM photograph illustrating 1080 steel coating microstructure as-deposited on rail head. Gas parameters: 230 slpm N₂ / 100 H₂ with a 235 mm working distance. SE imaging. 500x.



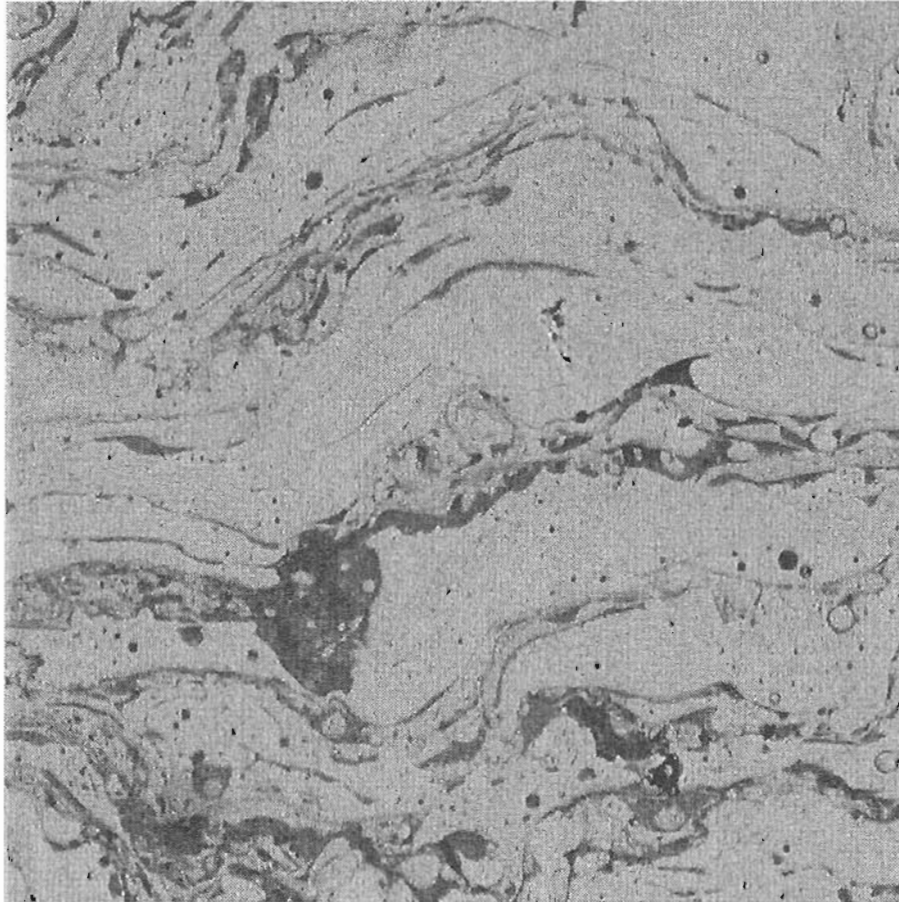
<—> 2 μm

Figure 3.57. SEM photograph illustrating 1080 steel coating microstructure as-deposited on rail head. Gas parameters: 230 slpm N_2 / 125 H_2 with a 235 mm working distance. SE imaging. 500x.



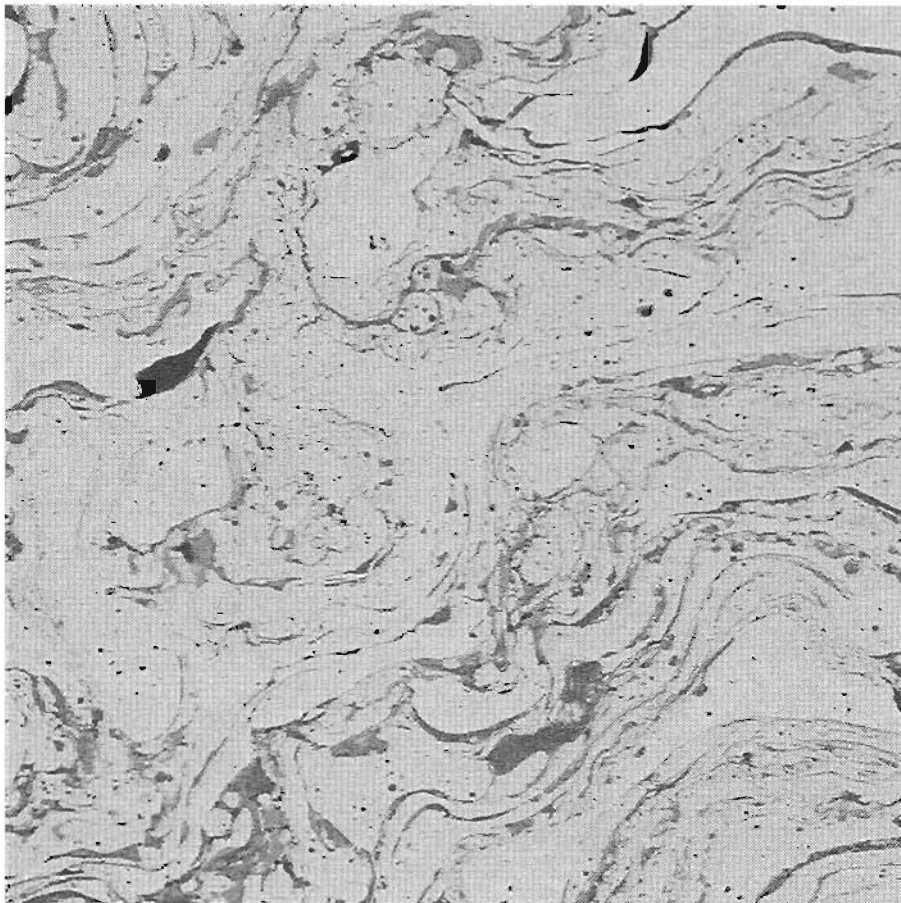
<----> 2 μm

Figure 3.58. SEM photograph illustrating 1080 steel coating microstructure as-deposited on rail head. Gas parameters: 230 slpm N_2 / 30 H_2 with a 200 mm working distance. SE imaging. 500x.



←—→ 2 μm

Figure 3.59. SEM photograph illustrating 1080 steel coating microstructure as-deposited on rail head. Gas parameters: 230 slpm N_2 / 30 H_2 with a 250 mm working distance. SE imaging. 500x.



←—→ 2 μm

Figure 3.60. SEM photograph illustrating 1080 steel coating microstructure as-deposited on rail head. This photo illustrates the microstructure at the standard gas parameters: 230 slpm N_2 / 30 H_2 with a 235 mm working distance. SE imaging. 500x.

Chapter Four Discussion

4.1 Introduction

In the results section the experimental data was presented. Certain results had a significant impact on the direction of the research, others were dead ends. In this section the results from the three coating systems: graphite, copper, and polymers, will be discussed individually. The relationship of spray parameters, wear testing, and microstructural characterization will be discussed. The individual test results will then be drawn together to explain the coating system as a whole. This will focus on goals achieved, failures, and how the results reflected the coating's development. A synopsis will be presented for each coating section summarizing the details of discussion.

4.2 Graphite

4.2.1 Introduction

Early work with graphite focused on graphite and graphite flake powder. This built the foundation of the understanding of graphite as a lubricant and sprayable material. Cast iron powder was also investigated. The work with nickel-coated graphite powder came as a last attempt to create a graphite / steel coating. Its success spawned the most research interest and subsequent effort in understanding its wear performance and failure mechanisms. The discussion attempts to explain the reasons behind the results. This analysis takes the form of investigating the

plasma spray process and the wear behavior. Each coating system is analyzed and conclusions are drawn.

The performance test parameters, creep and contact pressure, were based on past work by Clayton and Danks.¹⁸² These parameters were an attempt to produce wear in the laboratory that was observed in the field. In a sense these conditions attempted to mimic what a material would experience on an actual track. By using contact pressures of 700 N/mm² to 1315 N/mm² and creep values of 5% and 35%, the results can be used to predict field performance and be compared to work done previously on rail steel wear behavior.

4.2.2 Graphite Powder

Early work with graphite was performed with both graphite and graphite flake powder on flat coupons, round blanks, and Amsler rollers. The wide parameter envelopes of failure suggested the material was inherently difficult, if not impossible, to retain with the given spray processes.

Flat Coupons

Initial experiments were performed to narrow down the spray parameters and to observe if graphite could even be retained in the coating. Flat bars provided an inexpensive substrate for fast metallographic turnaround. The graphite powder created from lathe turnings provided an inexpensive source of material, the particle size of which could be controlled. Commercially available graphite powder had been found to be either too fine or too coarse and impure.

Table 3.1 listed the parameters and results for the flat coupon testing. The coatings were only evaluated optically after being sectioned and polished. Graphite volume fraction was estimated. Performance testing was not done, as wear performance evaluation required the coatings be reproduced on an Amsler specimen.

This initial experiment of twelve steel coupons indicated gas parameters had little influence on the retained quantity of graphite. This was shown in Figures 3.1 through 3.3. These figures represent graphite retention from 200 slpm N₂, with no secondary gas through 270 slpm N₂ / 100 slpm H₂, a relatively wide gas envelope. The reducing atmosphere of the 270 slpm N₂ / 70 slpm H₂ parameter may have retained the most graphite. It was thought the higher volume of hydrogen would slow the oxidation of graphite. The amount of graphite saved from oxidation was shown however to be marginal, if any.

The most influential parameter was found to be graphite injection location into the plume. Injection distance was measured from the anode nozzle. Several distances were attempted in early tests because the ideal injection point was unknown. It was hypothesized graphite injected downstream would increase the density of graphite particles capable of being retained. In reality the opposite turned out to be true. When graphite was injected at large distances, 115 to 165 mm, little or no graphite was retained, with the retained amount decreasing with distance from the plume. The overall trend indicated that the most graphite was retained when the powder was injected nearest the plume, 25 to 65 mm and at 45 degrees. This is due to the fact that the density of molten steel particles decreases downstream, reducing graphite capture. Figure 4.1 illustrates the dispersion of molten particles as distance from the plume increases.

Graphite by nature is more difficult to spray than metal powders. When plasma spraying one relies on the particles impacting the substrate in the molten state so that they adhere and solidify. Graphite does not melt, but sublimates to form carbon dioxide or carbon monoxide depending on the plume conditions. Assuming it does not sublime and does impact the surface, it must be in the near vicinity of a molten particle to adhere. Figure 4.2 and 4.3 illustrate how 'graphite particle capture' is more probable when injection distance is small. The higher density of molten particles

has a higher probability of capturing free graphite particles. The injection distances were thus configured to inject graphite particles directly ahead of the molten steel droplets as they were ablatively stripped from the wire.

Thus, two mechanisms are proposed in the retention of graphite. The first is capture of the graphite as it enters the plume by a molten steel particle, the probability of which is increased by injecting graphite near the wire. The second is capture of graphite by a molten particle, aided by the aerodynamic shield, when it is in the vicinity of the Amsler roller surface.

The angle of injection was found to be ideal at 45 degrees. Powder injected at 45 degrees would join the plasma stream and flow to the substrate, at 90 degrees some powder would escape the stream. At powder injection distances beyond 65 mm the angle had no effect. Injection at 90 degrees was avoided because powder had a higher propensity to escape from the system. This observation carried over to the subsequent nickel-graphite and cast iron powders, thus 45° injection became the standard. The powder feed rate (measured in RPM) was always operated near maximum feed. Early tests suggested retention of excessive graphite would not be a factor.

Amsler Rollers

Graphite was retained on flat surfaces but proved to be more evasive with a curved surface. A large quantity of time was spent changing parameters just to retain graphite in a circular steel coating. The parameter changes initially focused on injection distance and location, but later required adjustment of the plasma flow as it impinged on to the substrate.

The difficulty of spraying graphite was recognized in the flat coupon tests. The flat coupons revealed graphite could be retained, but gave no insight to how graphite would effect coating performance, mainly friction control. It was decided to model the

desirable microstructure after that of a gray cast iron, that being a dispersion of graphite in a pearlite and ferrite matrix. Gray cast iron contains a volume fraction between 20-30% graphite. Amsler wear tests of gray cast iron rollers show it to be extremely durable (>10,000 revolutions) at $P_o = 900 \text{ N/mm}^2$ and 5% creep. The friction coefficient remained around 0.10 throughout the test and the wear rate was very low ($10 \mu\text{g/m/mm}$). This is an equivalent value to wheel / rail boundary lubrication with grease.

The sample appeared to form a continuous lubricating graphite film. If this film was disturbed however, the wear rate would increase rapidly with complete material degradation in a matter of a few hundred revolutions. Testing conditions of 35% creep and $P_o = 900 \text{ N/mm}^2$ were severe enough to destroy the lubricating graphite film. The sample would degrade to Type III wear in < 500 revolutions and friction (μ) would be > 0.5. If creep remained at 35%, but contact pressure was reduced to $P_o = 700 \text{ N/mm}^2$, the film degraded at an observable rate. Within 3000 revolutions the friction would climb from 0.10 to 0.3. Beyond that, degradation increased to Type III wear and forced test termination.

The performance of gray cast iron illustrates that graphite film degradation is a direct result of loading and creep conditions. With further analysis it would be possible to find the contact conditions where the film became unstable. From observation though, the creep plays a bigger role than the loading conditions in film degradation. This phenomenon is explained further in the nickel-graphite / steel coatings discussion.

Samples G1 through G8, shown in Tables 3.2a and b illustrated early lack of success in retaining graphite. Samples G1 through G8's performance was inferior to a 1080 steel coating, with interfacial debonding occurring frequently. The question arises whether the injection of powder changes plume conditions away from optimum. The microstructure of a 1080 steel coating with no graphite appears similar to a 1080 steel coating sprayed without the codeposition of graphite. This suggests that the addition of graphite and carrier gas

into the plume has no measurable effect on the steel coating microstructure.

The gas parameters were varied in the first attempts (G1 through G5) to duplicate the successful microstructures of the flat coupons. None of these samples had any retained graphite. Further samples were sprayed at the optimized steel coating parameters of 230 slpm N₂ / 30 slpm H₂ and a working distance of 235 mm. By holding the gas parameters constant one less variable was introduced into an already complex system.

The 0.46 friction coefficient of samples G1 through G8 was reflective of a steel coating without solid lubricant particles. The value for the coefficient of friction was a significant indicator of graphite retention.

These early tests utilized graphite powder made in-house from lathe turnings. Given its failure, a fine (< 25 μm) graphite flake powder was utilized instead. Spray attempts G4 through G6 proved the powder to be too fine. During spraying a large cloud of powder was observed near the entrance of the plume. High velocity and turbulent flow within the plume made penetration of such a fine, low density powder difficult. Also, given the small particle size it may not have been able to form a lubricating film had it been retained. There is no way to know how graphite particle size would have affected the formation of a lubricating film, as a range of retained particle sizes was never achieved. Later tests returned to the in-house produced graphite powder.

Aerodynamic Shield

The circular geometry of the Amsler rolling/sliding test samples combined with rotational motion greatly enhanced the difficulty of retaining graphite. This problem's solution was approached from the idea that lamellar flow around the rotating Amsler roller carried the low density graphite particles away from

the surface. This phenomenon is illustrated in Figure 4.4. Breaking up the lamellar flow might lead to greater graphite retention.

The rotational motion was believed to play a small role compared with the circular geometry. A simple metallographic test was devised to confirm this idea. Normal rotation speed is 200 RPM when spraying Amsler rollers. A metallographic blank was sprayed at a rotation speed of 0, 36, and 110 RPM. No graphite was present in any of the samples, thus confirming that rotation speed played little, if any role in the lack of retention of graphite. This left roller geometry and aerodynamic flows as the explanation.

A shield could break up the lamellar flow created by the plasma jet, thereby disrupting the plasma / particle flow. The fixture could force particles that would otherwise flow around the Amsler roller to stagnate. If plume gases, and subsequently particles stagnated immediately in front of the Amsler sample, graphite may remain in the vicinity and be captured by an incoming molten steel particle. In theory this shield would increase the density of graphite capable of being captured. Two shields were created in an attempt to realize graphite retention.

The first iteration failed to aid the retention of graphite. Adequate cooling was difficult because of the half moon shield geometry, which was illustrated in Figure 2.9. The positions of the cooling jets may have exacerbated the loss of graphite from the system by impinging on the area graphite was to be captured. The shield may not have been able to create the correct plume stagnation. This shield did not have a satisfactory cooling system nor did it allow any of the plasma jet to flow around the Amsler roller. The entire plume energy was absorbed by the shield, causing accelerated overheating of both the shield and Amsler rollers.

The second shield iteration, illustrated in Figure 2.10, used back side cooling built into the shield. This shield as closely approximated a flat surface as possible given the system constraints. The plume appeared to stagnate upon impact of the shield. The target height, being the area between the shield slits,

was less than half an inch. The circumference of the roller was 6x larger than the half inch slit, thus only a fraction of the total flux was reaching the roller surface.

The plasma plume increases in diameter as a function of distance from the anode. The density of molten steel and graphite particles decreases also, as illustrated in Figure 4.1. This phenomenon is indicative of the plasma system and can not be altered easily. Thus, the density of particles penetrating the slits in the shield and impacting the Amsler roller is as low as 10% of the original flux injected into the plume.

Table 3.3a and b summarize the performance of the coatings made with the aerodynamic shields. Only one sample had evidence of retained graphite. The other samples behaved as a 1080 steel coating without added solid lubricant material. Sample G12 retained graphite sufficient enough to reduce friction. The amount was less than 5%, with a friction coefficient of $\mu = 0.30$ being attained. This performance was inferior to plain gray cast iron. Sample G12 was tested at mild loading conditions to avoid destroying it. Observation of the surface during wear testing suggested a surface film. The wear track topography did not display the same break-in that is observed with non-graphite containing coatings. With 1080 steel coatings the rough as-coated surface would grow smooth during the first 100 revolutions. Sample G12's surface retained the as-sprayed appearance. This suggested the coating was not degrading at the same rate a 1080 steel coating does. Not until 8000 revolutions did the coatings topography resemble that of a 1080 steel coating.

Samples G13 and G14 were attempts to repeat G12. The exact procedure was followed, with no retained graphite being the result. The samples were wear tested and observed metallographically. It became obvious how the samples would perform when the microstructure was observed. Samples G15 and G16 were attempts which mimicked G12 except for the shield. Sample G16 achieved equivalent graphite retention of G12, but without utilizing the shield during coating deposition. The volume fraction was again less

than 5%. The performance of both G12 and G16 were equivalent, with $\mu=0.3$, and durability exceeding 10,000 revolutions. These results strongly suggest that retention of graphite was a random occurrence, with the nature of the system being too complex to predict or understand completely. The other samples in G9 through G19 contained no appreciable graphite. Further attempts were made in an effort to repeat the two somewhat successful samples, but were not successful.

The performance of both G12 and G16 was indicative by a graphite film which formed on the surface. The film only required a small amount of graphite to form, but was fragile and was destroyed when contact conditions became too severe. The lubricating film was first observed when testing gray cast iron Amsler rollers. The nickel-graphite / steel coatings offered a better means of observation of this graphite film.

Dual 1080 Wires

The failure of the shield to provide predictable results prompted the experimentation of two wire deposition. The shields attempted to increase the graphite / molten steel particle interaction. Spraying two wires was an attempt to increase the density of molten steel particles in the plume and thereby increase the chances of capturing solid graphite particles. Table 3.4b summarizes the results. Again, no appreciable graphite was retained, as shown by metallography, yielding no friction reduction.

The two wires increased the density of molten particles within the plume. It was postulated the higher particle density would increase the probability of solid graphite particles being intercepted and incorporated into the coating. This seemed plausible as with the inception of two wire spraying came little increase in the plume size. The diameter of the particle flux was nearly equivalent to the flux of a single wire when it reached the target. The diameter increased by roughly 15%, as determined by eye. This

would equate to an increased particle density of 1.5 times over spraying with a single steel wire, assuming 100% melt off efficiency.

During the deposition of any coating the goal was to have a high density of ideal particles in the plume center. Gas parameters were adjusted in early steel coating work to create the maximum number of small ideal particles for a given working distance. Analysis of single splats allowed for determination of ideal particles.³ This assured that the area the plume was traversing over was being impacted by the optimum particle density.

A schematic of two wires reacting in the plasma plume is shown in Figure 4.5. Adding a second wire to the turbulent plasma plume created a new variable. Although the particle flux did not increase appreciably, there was definite interaction between the wires. The wire nearest the anode created a bow wave shock in the plume gases as molten metal was stripped off by ablative melting.¹⁶⁴ The molten flux down stream was redirected by bow shock and resulting flow turbulence. When the wires were within 6 to 12 mm of each other their interaction redirected the downstream wire's particle flux. Figure 4.6 illustrates the redirection of molten particles when the downstream wire was brought too close to the upstream wire. The redirected flux would diverge 40-70 mm from the downstream (235 mm) target. The target or Amsler roller was only being impacted by particles from the first wire. The second wires contribution was < 25%, with mostly large, non-idealized particles reaching the target. The redirection became more significant the closer the two wires came to each other. When the second wire was 13 mm or more down stream the interaction became minimal. The particle spread was still roughly 30% larger than for a single steel wire. The study of interacting wires clearly is not a trivial matter. Further explanation and analysis are given in the copper wire / 1080 steel discussion section.

G20 through G23 were coated at idealized two wire conditions, yet still did not retain any appreciable graphite. The shield had no

effect on retaining graphite. The deposition efficiency when creating these coatings indicated only 60% traverse time was necessary. This does not help in understanding the lack of graphite retention but is a positive note to the success of two wire spraying, which is uncharted territory. The wear tests of these samples yielded equivalent performance to the single wire steel coatings which did not contain graphite (G1 through G19). The microstructure confirmed the lack of retained graphite, but otherwise appeared as the other non graphite containing steel coatings. The oxide volume fraction and porosity appeared to be unaffected.

Synopsis

Dozens of Amsler samples and flat steel coupons were sprayed with 1080 steel and graphite powder, but only two contained any appreciable graphite. This lack of success suggested a material modification was necessary as opposed to further parameter modification. The series of rollers gave understanding to the difficulty of spraying materials which do not melt. This could be applied to a thermal spray system with inadequate temperature to melt its particles, (I.E. HVOF spraying refractories). These tests allowed study of twin wire spraying, which was used in the copper wire / 1080 steel coating production. The low reliability of this system forced the search for alternate graphite sources. These included cast iron powder and a nickel-coated graphite powder.

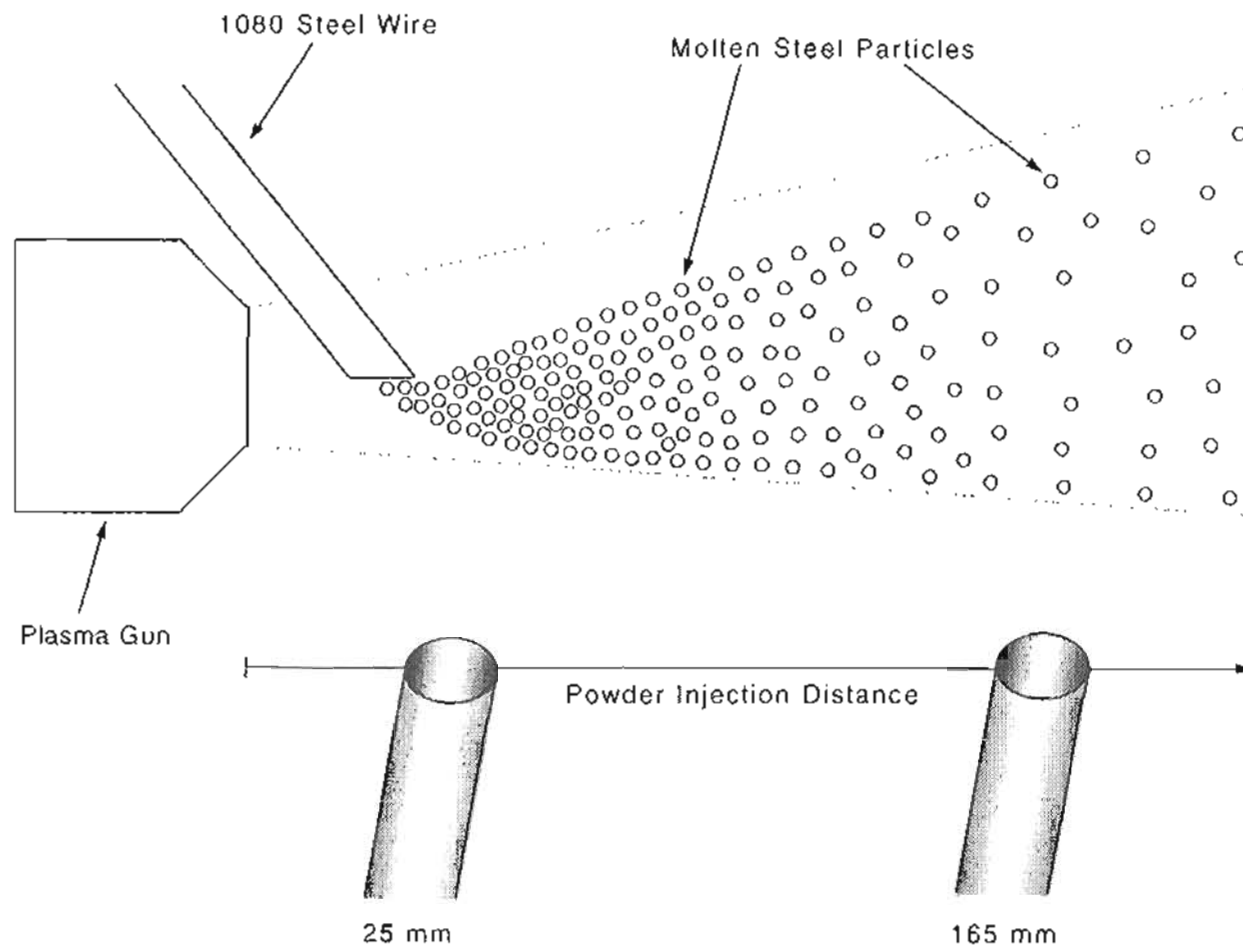


Figure 4.1. Schematic drawing of the plasma plume showing the dispersion of molten steel particles as distance from the plume increases. The density of steel particles is much greater at 25 mm than at 165 mm.¹⁷⁷

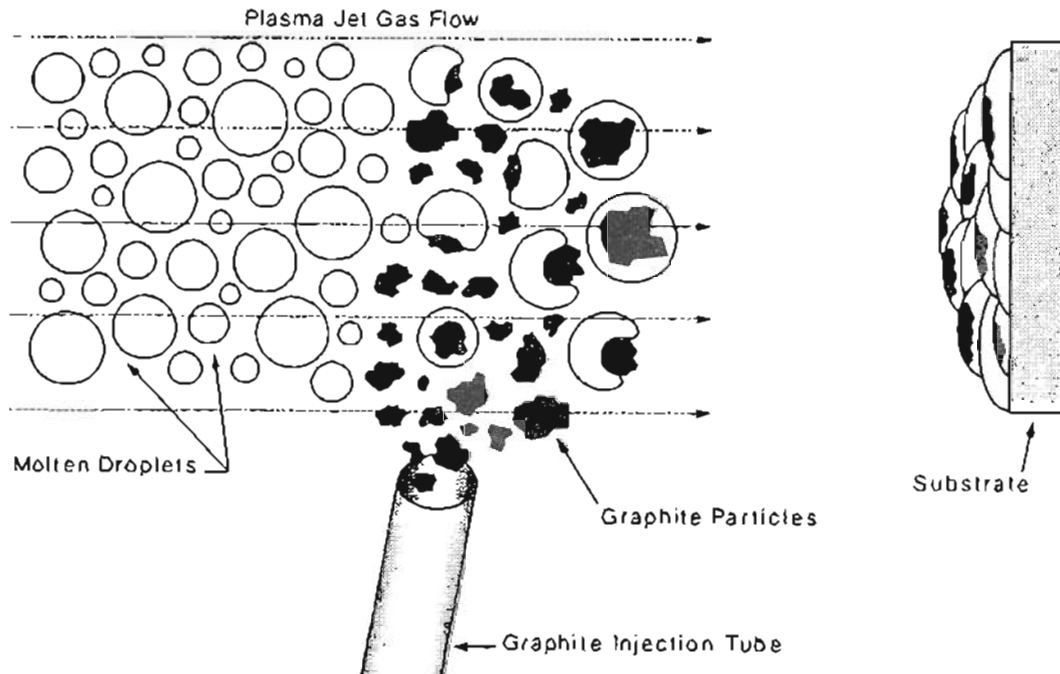


Figure 4.2. Schematic drawing of the plasma plume showing capture of solid graphite by molten steel particles at a powder injection distance of 25 mm.¹⁷⁷ Note the high density of molten steel droplets.

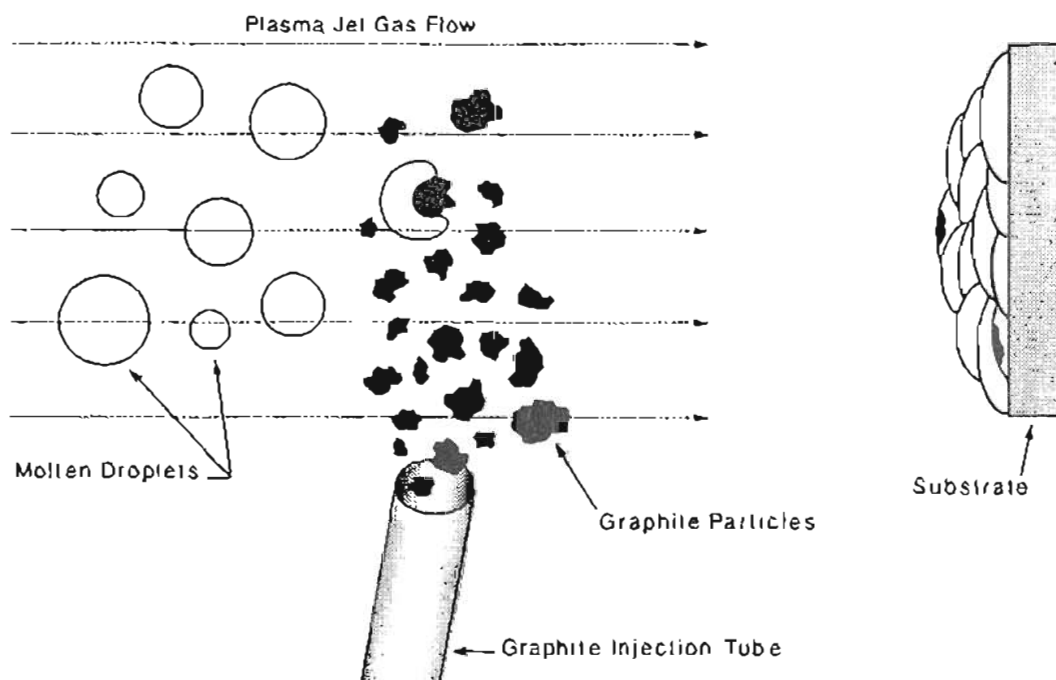


Figure 4.3. Schematic drawing of the plasma plume showing capture of solid graphite by molten steel particles at a powder injection distance of 165 mm.¹⁷⁷ Note the low density of molten steel droplets.

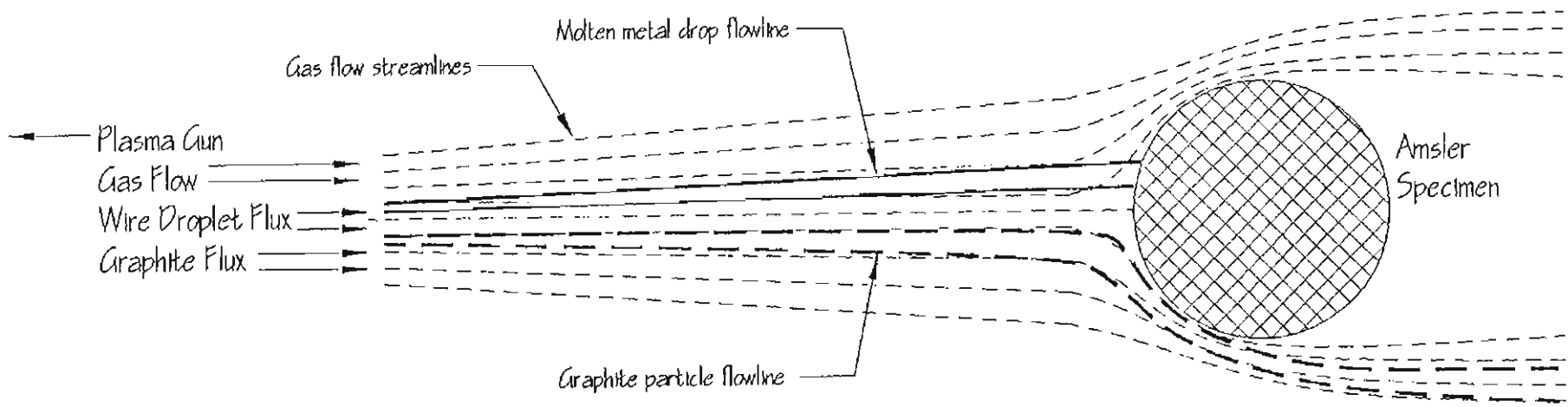


Figure 4.4. Schematic drawing of the plasma plume showing the flow of molten steel particles and solid graphite particles when deposited onto an Amsler roller.¹³⁶ The molten steel particles impact the roller surface, while the solid graphite is carried around the circular Amsler roller by lamellar flow.

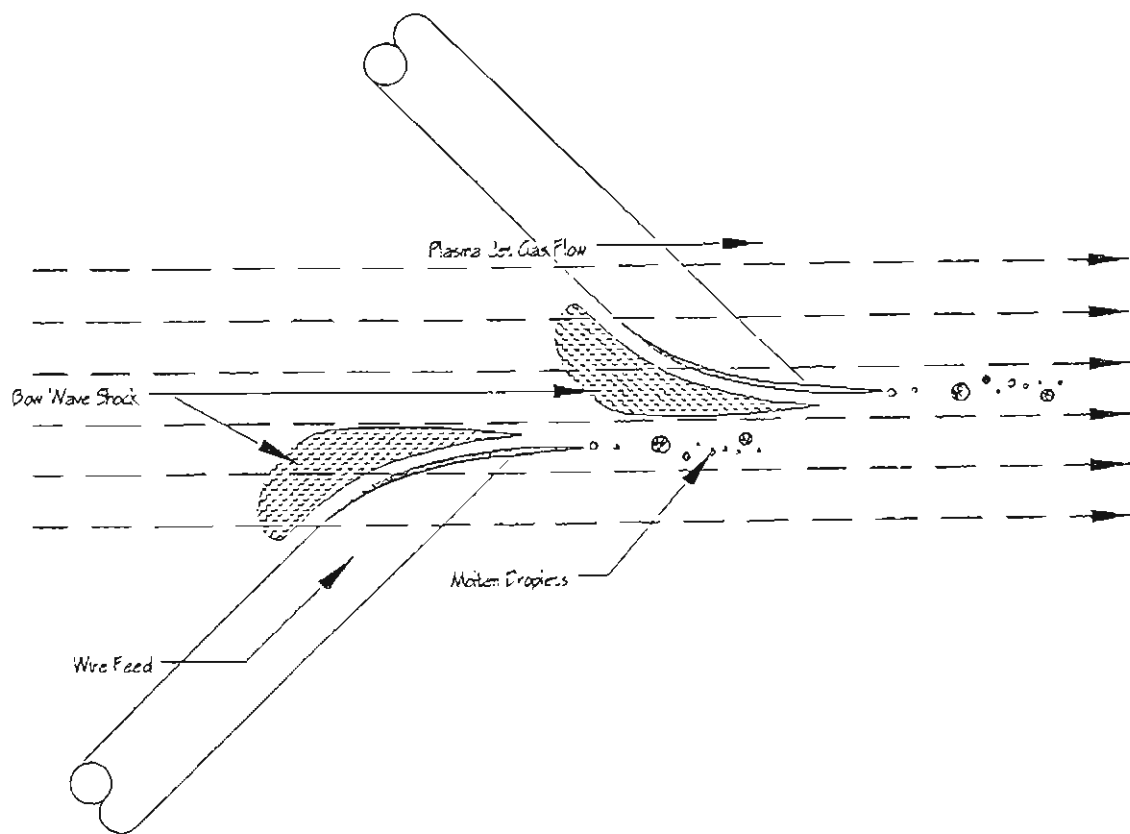


Figure 4.5. Schematic drawing of the plasma plume showing the bow wave shocks with two, diametrically opposed, offset wire feeds into a supersonic flow.¹³⁶ The offset distance is large enough to avoid molten particle interaction.

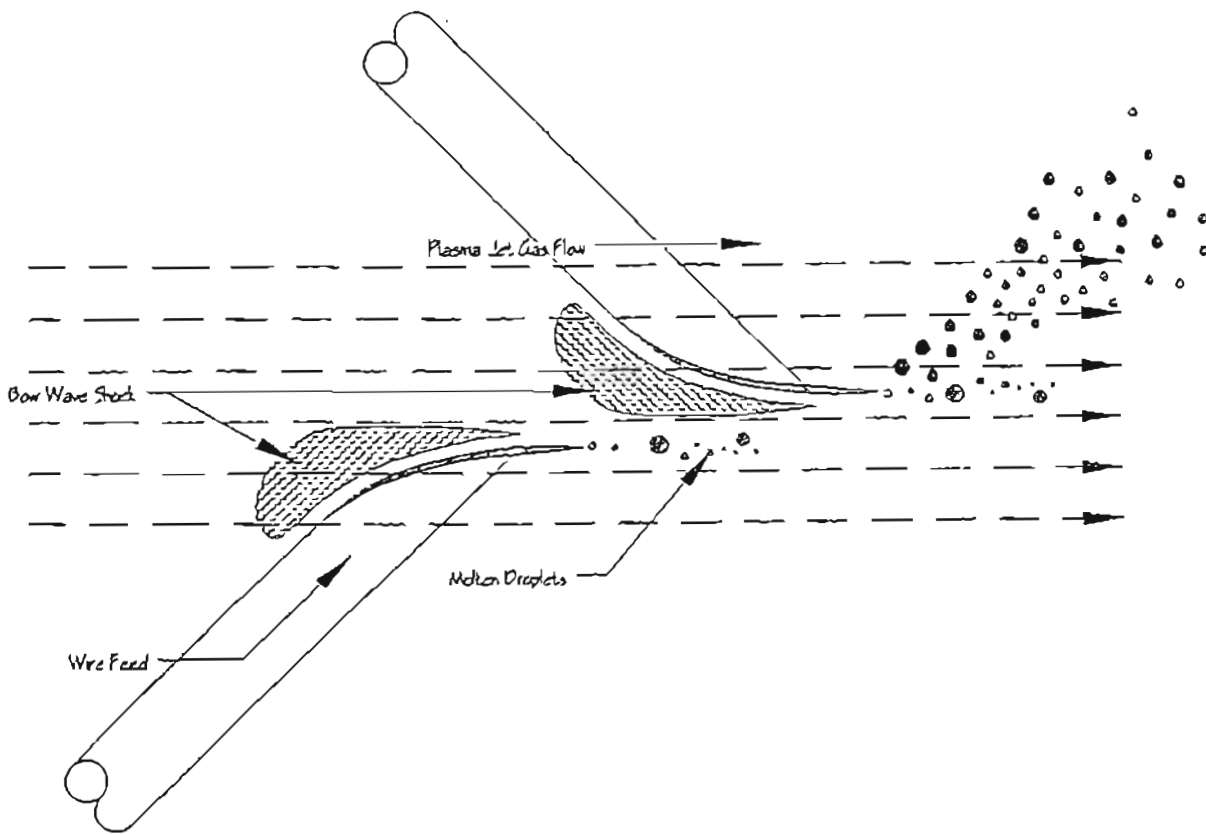


Figure 4.6. Schematic drawing of the plasma plume showing the bow wave shocks with two, diametrically opposed, offset wire feeds into a supersonic flow.¹³⁶ The offset distance is too small causing molten particle interaction. Particles from the downstream wire are redirected away from plume center by the bow shock of the upstream wire.

4.2.3 Nickel-Coated Graphite

Introduction

The retention of graphite in the 1080 coating was made possible by the use of a metal encapsulated graphite powder. The nickel-coated graphite (also referred to as nickel-graphite) provided consistent results and significant improvement over the solid graphite powder in terms of sprayability. This was shown by metallography and performance results. The spray process became predictable as opposed to the chance meeting of solid graphite and molten steel. The quantity of retained graphite could be adjusted by simply varying the powder feeder parameters. The reason why the nickel coated graphite worked, how it worked, and its limitations is discussed in detail.

Metal encapsulation of the graphite particles allowed the once solid, unmeltable particle to become softened and plastically deformable. The nickel shell comprised only a small fraction of the total particle volume but was enough to simulate a fully molten particle. This particle would adhere to the substrate in the same manner as the 1080 steel particles. The morphology of both nickel-coated graphite and graphite particles were similar, both being random shapes that ranged from spherical to cylindrical. Figure 2.1 illustrates the nickel-coated graphite's morphology. Since only one type of each powder was used (graphite or nickel-graphite) no conclusions can be drawn as to the effect of shape in coating deposition.

Nickel-graphite powder allowed the quantity of retained graphite to be controlled through by its generally predictable deposition. Graphite was now retainable in small or large quantities. The efficiency of graphite deposition was excellent. To retain only small volume fractions (< 5%) it was necessary to use a low feed wheel in the powder feeder. With the high and low feed

wheels, the deposition of graphite from 1% to over 30% was possible.

Microstructural Characterization.

A specific metallographic preparation technique was developed for the nickel-graphite containing coatings, as prior plain graphite coatings were unsuccessful in retaining graphite. Particle pullout during polishing was evident in the early samples. This was caused by hydrodynamic forces (in polishing) acting upon the brittle graphite particles. It was necessary to overcome this problem because a pulled out particle could be mistaken as a porosity and make quantification less accurate. The actual polishing technique is outlined in the experimental section. This was modeled after the technique used for polishing graphitic and spherical cast iron.¹⁷⁶

The optical microscope and image analyzer provided the quickest information about the coating. Since a witness sample was spray coated along side the Amsler rollers a metallographic record was available for all coatings. Analysis of the coatings through image analysis allowed for the quantity of retained graphite to be correlated with its wear performance.

The image analyzer was used exclusively with the nickel-graphite coatings as the plain graphite coatings did not contain any appreciable graphite. The thicker coatings (1 mm) were easier to quantify than the thin 0.5 mm coatings. The area which contained graphite was physically larger and could be easily defined with image analysis equipment. The 0.25 mm coatings were too thin to be accurately quantified by image analysis. As a result their nickel-graphite volume fraction was estimated by comparison to the known quantities of the 0.5 mm and 1 mm coatings

Samples G28 through G33 contained nickel-graphite dispersed throughout their matrix, the other samples G34 through G54 only contained nickel-graphite in the top 30% of the coating. The photomicrographs in Figure 3.10 illustrate this dispersion. Figures

3.13 through 3.15 illustrate how nickel-graphite dispersion was contained in only the top 30% of the coating. The area which was measured for nickel-graphite could thus only include the top 30%, if an accurate measurement was to be taken. This forced the operator to adjust the image to contain a field within the top 30% off the sample. If half the field was in a nickel-graphite / steel area and the other half in the 1080 steel underlayer the results would be skewed. Thus, the field was not purely random but positioned for each measurement.

It can be argued though, that the initial transverse cross sectioning of the sample was random. Increasing the random sampling was accomplished by reducing the measurement field size (half the TV screen area as opposed to the entire screen) and increasing the number of fields measured. Thirty fields were used for the 1 mm coatings, but sixty were used for the 0.5 mm coatings. The reported values of graphite volume fraction are averages. In some cases the standard deviation was 75% of the average value. The range was very broad, which indicates graphite's dispersion is not wholly homogeneous. The image analysis results at best describe a trend and give a range of retained second phase lubricant particles.

Wear Behavior of Nickel-Graphite

It was observed the graphite particles would form a protective film over the entire coating. The film was not resolvable optically. The best visual clue as to the film's existence was the surface texture of the sprayed roller. During the entire wear test the coating surface did not degrade as observed with 1080 steel coatings. The nickel-graphite / steel coating's surface instead remained smooth and virtually unchanged. The thickness of this film was not easily measured. The film did not appear to transfer to the bottom roller.

Energy dispersive spectroscopy (EDS) confirmed the presence of a graphite film on the coated top roller. This confirmation was made by measuring carbon characteristic x-rays being emitted from the surface. The amount of carbon was not determined, only that it existed. The peak intensity varied depending on if the spot was placed near a graphite particle. The bottom roller showed no evidence of residual carbon. If carbon was present, the amount was below detection level. The reason why the film did not transfer is unknown. One idea though is that the graphite had oriented itself on the coated roller's surface. Contact with the smooth wheel roller gave it no opportunity to transfer appreciably (i.e. no significant asperities to latch onto).

The graphite film was very fickle regarding testing conditions. If the film was disturbed by either a rough surface or increased surface speed it degraded rapidly and did not control friction. The increase in surface speed may have increased the vibration between the two roller surfaces. The graphite must form an oriented film parallel to the wear surface to act as a lubricant. It is speculated the graphite particles were unable to align themselves when testing conditions were not ideal. A rough bottom roller would contain relatively large peaks and valleys, which could abrade away any oriented film which formed on the top roller. If the coating had a very large volume of graphite it is possible the valleys would become filled with graphite debris, thereby simulating a smooth surface. The amount of graphite in the coated rollers was not adequate to fill these valleys. When the surface speed was increased it is believed the graphite film was worn away by opposing asperities before it could build up a lubricating film. At normal 200 RPM operation a 35 mm Amsler roller has a surface speed of 0.37 m/s. This value is doubled to 0.74 m/s when the Amsler roller is revolved at 400 RPM. A rotation speed in-between may give more information as to the effect of surface speed on graphite lubricity. The rotation speed however is constrained by the Amsler machine which has only two rotation modes.

The lubricity of the graphite reduced the wear rate to less than 20 $\mu\text{g}/\text{m}/\text{mm}$ when measured. This rate was almost too small to measure. To determine wear rate the weight loss of the coated roller is plotted against the number of revolutions. Using a linear regression, the average slope is calculated. From this slope the wear rate is determined. Wear rate is defined in units of $\mu\text{g}/\text{m}/\text{mm}$, which equates to μg of material lost per meter rolled per mm of contact width. The value can be normalized as all Amsler samples had a 5 mm contact width. Nearly all tests (including the copper and polymer systems) were run uninterrupted. Thus, the data regarding wear rate are incomplete, but were calculated to determine a trend. Calculating a characteristic wear rate is useful to compare work with uncoated rail steels and 1080 steel coatings. Some uncoated rail steels have wear rates in the thousands ($\mu\text{g}/\text{m}/\text{mm}$). 1080 steel coatings had wear rates ranging from 200 to 800 $\mu\text{g}/\text{m}/\text{mm}$.³ With typical wear rates less than 20 $\mu\text{g}/\text{m}/\text{mm}$ for the nickel-graphite and polymer systems the success of adequate lubrication is realized.

Wear Mechanisms

The actual wear rate of graphite coatings was very small. Virtually all of the weight loss came from edge effects or wear track particle removal. The thin coatings (0.25-0.5 mm) tended to resist edge effects but were vulnerable to wear track particle removal. The opposite was true for the thicker (1 mm.) coatings. Both failure mechanisms were present though on all samples.

Edge effects were first defined and are explained in detail by McMurchie.³ Edge effects involve loss of coating in an area other than the wear track. During an Amsler wear test the bottom roller (5 mm wide) wears into the coated top roller (> 5 mm wide); the result allows unsupported coating to be put under load. An unsupported coating is that which resides beyond the 5 mm wide substrate. When an Amsler roller is sprayed, coating is built up beyond the 5 mm width. This material which resides beyond the 5

mm has no substrate for support. Thus, it can crack off when put under load during a wear test. This is very probable because the two rollers may not align perfectly.

Figure 4.7 illustrates the mating conditions of two Amsler rollers. This figure illustrates the overspray of the steel coating and how the corner of the Amsler roller can act as a stress concentration point. When particles crack off of the edge during a wear test it is possible to take pieces of the wear track coating with them. This greatly weakens the integrity of the remaining coating. When numerous edge particles have been removed the coating is vulnerable to debonding. Figure 4.8a illustrates a large removed particle from the wear track during testing of Sample G36 #1. The test was terminated after only 2830 revolutions due to severe edge effects. Figure 4.8b is the same sample (G36) showing a crack at the edge of the coating, which if tested further would have been removed.

The top hat profile of an Amsler roller and the nature of the Amsler wear test is believed to be the cause for the edge effect phenomenon. Edge effects leading to debonding occur in 1 mm thick coatings primarily. In thinner coatings the amount of unsupported coating material is less, thus having less effect on the wear track integrity when removed.

Wear track particle removal (WTPR) was observed primarily in the thin coatings (< 0.5 mm.). It is speculated and somewhat observed that as the coating wears, subsurface cracks propagate from one graphite particle to other graphite particles. This forms a network of cracks which upon reaching critical size cause the particle to be pulled out by the contact forces between the two rollers. This mode of degradation is similar to the delamination wear mechanism defined by Suh.³³ In Suh's model subsurface voids are created, which coalesce and form a wear sheet which is removed by contact forces.

It is speculated that in the nickel-graphite / steel coatings cracks propagate between graphite particles. The cracks are formed

at the subsurface and propagate into a network. When the network reaches critical size a large wear "sheet" is removed. The removed particles are large because graphite particles form a coarse dispersion in the matrix. By comparison a metal would be relatively homogenous with wear particles forming in much smaller areas. The wear particles caught in the contact zone caused a marginal increase in friction. The friction coefficient (μ) never exceeded 0.2 until a significant quantity of wear particles had been removed from the coating surface.

The mechanism of wear track particle removal was investigated using the SEM. Secondary electron (SE) imaging revealed the topography of the pulled out particle. Back scattered electron (BSE) imaging revealed compositional variations within the coating. Figures 4.9 and 4.10 are SEM photographs illustrating the difference in appearance of a removed particle using SE and BSE imaging. These images were taken from different samples and show the range of size and shape of the removed particles. The removed particle size generally ranges from 50 to 600 μm . In both BSE and SE imaging dark areas identify graphite particles. The contrast though, is much greater in BSE imaging mode because the subsurface average atomic number (Z) is identified, as opposed to only the surface topography. EDS was performed to confirm the dark areas were in fact graphite (carbon) concentrations. These images help support the hypothesis that nickel-graphite particles form a network of cracks resulting in the removal of the coating material.

The coatings with larger volume fractions of graphite had a higher incidence of wear track particle removal. The progression of decay though was similar for all graphite coatings. Figure 4.11 is a macrograph of sample G48 (10% graphite) after testing 10K revolutions. Removed particle craters encompass over 15% of the coating's surface. These craters coupled with wear debris caused the friction coefficient to rise to only 0.17. The coatings generally did not show signs of severe wear until wear track removed particles covered 30% or more of the coatings' surface. Figure 4.12a

and b illustrate how graphite volume fraction effected the rate of wear track particles being removed. Figure 4.11a illustrates sample G46 #5 (6% graphite) after testing for 5,000 revolutions. Figure 4.11b illustrates sample G41 #2 (12% graphite) also after 5,000 revolutions. The surface degradation was much greater for sample G41, with a conservative estimate being 2-3 times as great. This sample had a shorter wear life and experienced an increase in friction earlier in the test. These figures suggest that a large volume fraction of nickel-graphite is not beneficial. If sufficient graphite is present to form and maintain a lubricating film, then any extra only accelerates coating degradation. It is noted however, that the scatter between wear tests make it difficult to quantify the effect of graphite volume % on durability.

Generally, when a coating reaches the state illustrated in Figure 4.11b it will debond or the friction coefficient will rise at an accelerated rate causing rapid wear. Coatings with graphite volume fractions between 5 and 10% tended to have the best performance. Beyond 10% the coating degradation was noticeably accelerated. With increased wear came increased wear debris. Some of this debris became trapped in the contact zone. It appeared the quantity of wear debris was a function of nickel-graphite volume fraction. It is not known however, if this increase in debris had a significant effect on the coating's degradation.

The Amsler test is a good example of the limitations of a closed system. In an open system, such as wheel rolling over rail, fresh wheel material would constantly be contacting the coating. A large accumulation of wear debris would not occur. The question then becomes could a graphite film be formed on the new surface, and would this film be able to act as a protective lubricant.

Initial Work

The early 1080 steel and nickel-graphite coatings (G25 - G27) were considered successful despite the poor wear performance.

Graphite was retained in quantities of 10% to 24%, and the friction coefficient was reduced to 0.16 in one test. Graphite was trapped at the interface during spraying, which weakens the coating / substrate bond. These particles are illustrated in Figure 3.7b. The demise of these thick coatings (>1 mm), was primarily from edge effects which lead to debonding.

Edge effects coupled with an unoptimized spray procedure, explain why the performance was poor. These coatings were created when the surface preparation procedures were still being perfected. These coatings having such a large volume of graphite overall (dispersed throughout the entire 1 mm. coating) were weakened against debonding. If the maximum shear stress resided at the interface or within the coating, as postulated, then the network of graphite particles would be subjected to large shear forces. The brittle nature of graphite would preclude any fracture resistance, thus cracks would propagate readily throughout the matrix. This phenomenon would be similar to the formation of and removal of wear track particles. These coatings were a good beginning to prove the nickel graphite / steel system had friction reduction potential.

1 mm Coatings

G28 through G33 coatings were produced initially assuming that the wear rate of the coating would require a reservoir of fresh lubricant. They were nominally 0.8 - 1.0 mm in thickness, and contained graphite throughout their structure, except near the interface. The wear rate of these graphite coatings was two orders of magnitude below the 1080 steel coatings. These thick coatings had relatively poor performance due to edge effects. The friction coefficient remained at 0.14 for all tests until excessive wear debris became trapped in the contact zone.

G32 and G33 had very large volume fractions of graphite as indicated in Table 3.6a. Edge effects appeared to worsen with increasing graphite volume fraction. Despite this, the coatings

illustrated good durability. This suggests that edge effects do not hinder coating performance unless they cause debonding.

The edge effects observed in thick graphite coatings were much worse than those of a 1080 steel coating. Failure generally occurred as a result of edge effects causing debonding. When possible, the test would be terminated to preserve the coating (for subsequent analysis) when severe edge effects were observed. The wear rate of nickel-graphite / steel coatings was inherently low, with most of the coating remaining unaffected during the wear test. Thus, graphite which was dispersed within the coating had no effect on friction reduction. This graphite did however, weaken the structural integrity of the steel matrix. These 'extra' graphite particles increased the number of crack initiation sites. This prompted further experiments to include graphite only near the surface.

1 mm Coatings Part II

Samples G34 through G37 were also 0.8-1.0 mm thick, but the retained graphite was only contained in the top 0.3 mm of the coating. The performance was better than the comparable G28 through G31. Referring to Tables 3.7a and b, the most durable coatings were G34 and G35. These coatings had the lowest volume fractions of graphite. This further supports the hypothesis that only a small fraction of graphite is needed to form a lubricating film, with an increasing amount acting to degrade coating integrity.

Edge effects were present but were less severe than in samples G28 through G31. The test lives were conservative as wear testing was sometimes terminated due to a high volume of edge effects. When tested at higher contact pressure ($P_o = 1315 \text{ N/mm}^2$ instead of $P_o = 1220 \text{ N/mm}^2$) one sample (G35) could not form a protective film and illustrated a steel coating friction value of 0.46. It was observed that coatings which did not have a low initial friction (0.14-0.16) would not exhibit a low wear rate nor would

their friction value drop as the test progressed. These coatings would have a nominal friction value of 0.35 to 0.46.

The reason why a lubricating graphite film can not form later in a test is unclear. One reason may be that the bottom roller, once roughened by the abrasive as-sprayed coating surface, can not reclaim the smooth surface necessary to form a protective film. Sample G37 was also tested at $P_o = 1315 \text{ N/mm}^2$, but showed friction reduction with a decreased durability. This sample had a higher graphite volume fraction (12% as opposed to 8%) which may have enhanced its ability to form a lubricating film. The higher loads, though, accelerated the edge effects, explaining the shorter test life. The behavior of sample G35 is very important in predicting how these coatings may react in the field where a smooth counterface can not be relied upon nor expected. If the coatings are to be practical they will need to be less sensitive to their wear environment.

0.5 mm Coatings

Samples G38 through G41 were nominally 0.4-0.6 mm thick and contained graphite in the top 0.2 mm of the coating. These coatings had excellent durability compared with the previous two sets. Edge effects were not a significant factor. Table 3.8a and b illustrated the results. Samples G38 and G39 had excellent durability, being the top performers of ALL graphite coatings. These samples had graphite volume fractions less than 10%. The same good endurance / low graphite volume trend was shown in the previous set with samples G34 and G35. The top performing G39 failed to reduce friction when the wear test speed was increased from 200 rpm to 400 rpm. The increased surface speed from 0.37 m/s to 0.74 m/s was enough to prevent an adequate lubricating film from being formed.

The failure mechanism for the 0.5 mm coatings was chiefly wear track particle removal, and followed the pattern explained

earlier. Sample G38's test was ended early due to loss of wear track particles. Sample G40 had a measured wear rate of only 5 $\mu\text{g}/\text{m}/\text{mm}$ prior to debonding. This low wear rate was typical for the thin coatings. When the coating did debond the entire coating was not removed, with 25-30% remaining intact. The debonding occurred at both the interface and within the coating structure. This suggests multiple mechanisms of failure.

The failure of debonding between layers is again a result of cracks propagating between graphite particles. This behavior was illustrated clearly in Figures 3.11a and b. The crack propagation mechanism probably played a role in all graphite coating debondings. The interfacial debonding is less understood and could have been the product of inadequate surface preparation or large subsurface shear forces. The interface is inherently a weak point because only mechanical bonding exists. Within the coating structure the molten particles form some metallurgical bonding. The brittle nature of graphite though overshadows any benefit, yielding interlamellar cracking and failure. The decreased incidence of edge effects and debonding in the 0.5 mm coatings suggested thinner coatings may further reduce debonding or possibly eliminate it.

0.25 mm Coatings

Samples G50 through G53 were nominally 0.2 - 0.3 mm thick coatings. Tables 3.9b illustrated the performance. These coatings were similar to the 0.5 mm coatings as to their degradation and failure modes. These coatings experienced wear track particle removal but had a lower incidence of debonding. The 0.25 mm coatings appear to be more resistant to debonding for the same reason the 0.5 mm were better than the 1 mm coatings- reduced edge effects and a possible shift of maximum shear stresses away from the interface. Unfortunately, the calculation of where the maximum shear stress occurs and the stress profile are non-trivial

problems. This is due to the composite nature of the coating and hence the elastic modulus (E), is unknown.

The friction coefficient in the 0.25 mm coatings would rise as the test progressed. This is why the friction coefficient is slightly larger for these samples in the result tables. In the 0.5 mm coatings μ remained fairly constant, with a significant increase only occurring near test end. Particles trapped in the contact zone appeared to have a greater effect on the increase in friction for the 0.25 mm coatings compared to the 0.5 mm coatings. The reduced quantity of available graphite may have been a factor. The volume fractions were similar in the graphite / steel zone as in the thicker coatings, but this zone was only 100 μm thick. The small area of graphite concentration increased the rate of wear track particle development.

It is believed that the wear track, once particles were removed, had no appreciable underlying graphite to help restore the lubricating film. The coating therefore needed a graphite reservoir, just not in the amounts seen in the 1 mm coatings. The reduced incident of debonding combined with the good performance made this coating very successful. The coating's degradation was only mildly effected by the lack of a graphite reservoir. In addition, the reduced incident of debonding helped understand the nature of how thickness effects performance on a generic level. It is noted the debonding problem also encompasses substrate geometry and surface preparation which have no relation to the nature of graphite coatings. Overall, the 0.25 mm coatings had good performance, with respect to durability and degradation behavior, outperforming the 1 mm coatings, and a close second to the 0.5 mm coatings.

Low Volume Coatings

A low feed wheel was required for coatings with < 6% graphite to be produced. The retention of sprayed nickel-graphite was very efficient. The volume fractions listed in Table 3.10a are

approximations. These coatings had about 1 to 6% nickel-graphite and illustrate that a critical amount of graphite was necessary to form a protective film. The required volume fraction appears to be 5%, but may be lower if very low contact pressures (900 N/mm²) are used.

The friction reduction for this set was poor with frequent debonding. These samples were made using recycled rollers. This being a roller which was previously coated, tested, and having the tested coating machined off. The surface, even after grit blasting was probably not the same as a new amsler roller. Recycling though, only explains the reasoning behind the increased debonding frequency and plays no role in the retention of graphite. The friction reduction was a simple function of retained graphite. All of the samples had sufficient durability to form a lubricating film, if that was possible. None of the samples debonded immediately upon loading and testing. These samples were much like the graphite samples G12 and G16, except a friction value of 0.3 was not considered successful. Tests which did not yield $\mu < 0.2$ were generally terminated within 3000 revolutions. These coatings were not expected to perform as well as the other (> 6% nickel-graphite) coatings. They did illustrate the threshold of nickel-graphite necessary to form a lubricating film-making them successful.

Repeatability

Coatings which had good durability were reproduced to verify repeatable results. The best performing coatings were G38-G40 which were 0.5 mm thick, with 5-10% nickel-graphite. These samples had consistent durability greater than 11,000 revolutions. The coatings had achieved the balance of sufficient graphite to form a durable lubricating film without compromising the coating integrity.

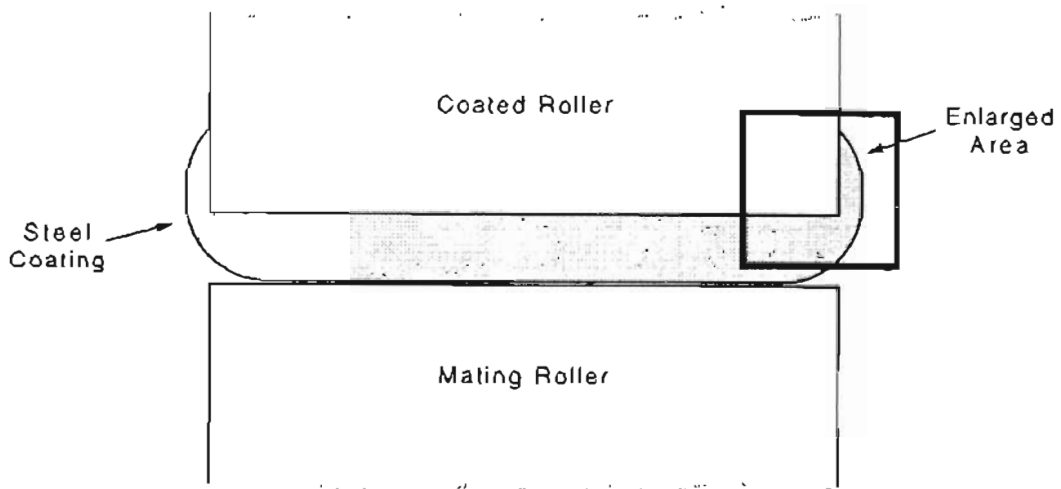
Table 3.11a and b summarize the results of these repeat tests. Repeat samples of G38 (G46) were tested seven times because G38

had the highest overall durability (16,940 revs.) of any graphite / steel coating. Within these tests the condition of the bottom roller was changed or the surface speed was increased. The test sensitivity of nickel-graphite / steel coatings was reaffirmed. These repeat tests also confirmed that the excellent performance was not an aberration but was consistent. Repeat samples of G39 and G40 (G47, G48) also confirmed the good durability of this series. The number of tests was reduced to three each because the wear behavior was well documented in tests G46 #1 through #7. If field testing of nickel-graphite / steel coatings was to be done, G46 (G38) would be the first recommendation.

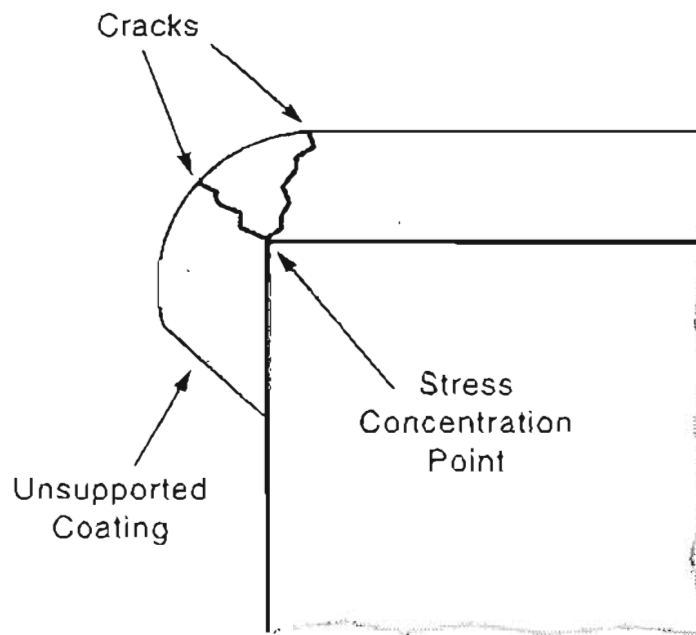
Synopsis

The nickel-coated graphite containing coatings were very successful in showing that a graphite / steel system could be produced which both reduced friction and provided good durability. The friction reduction was present provided graphite volume fraction was greater than 5%. This amount of graphite appeared to be sufficient to form a lubricating film. This was a rough value though, and was a function of loading conditions. When graphite reached approximately 10%, the loading conditions had less of an effect on graphite's ability to form a lubricating film. The condition of the mating surface, i.e. bottom roller was critical, though, for all nickel-graphite / steel coatings.

Even the best performing samples (G38 -G41) and those with large volume fractions of graphite (G32 and G33) could not perform well if the bottom roller was roughened, had an increased surface speed, or had a very high slip ratio (creep= 35%). The coatings excelled when slip was lower (creep= 5%) and a smooth, machined bottom roller was used. Edge effects were the predominant failure mode of the 1 mm coatings, while wear track particle removal dominated the failure of the 0.5 and 0.25 mm coatings. Overall this series far excelled the graphite powder / steel coatings.

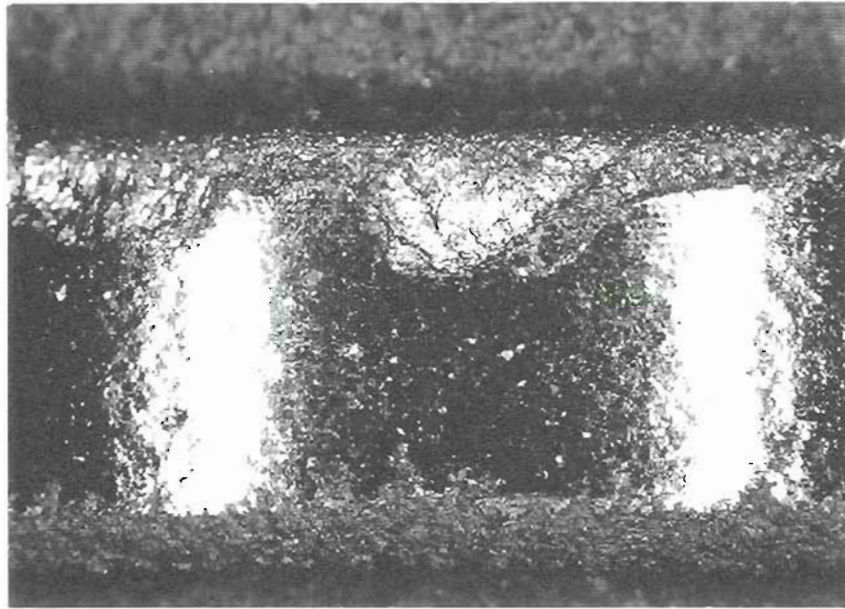


(a)

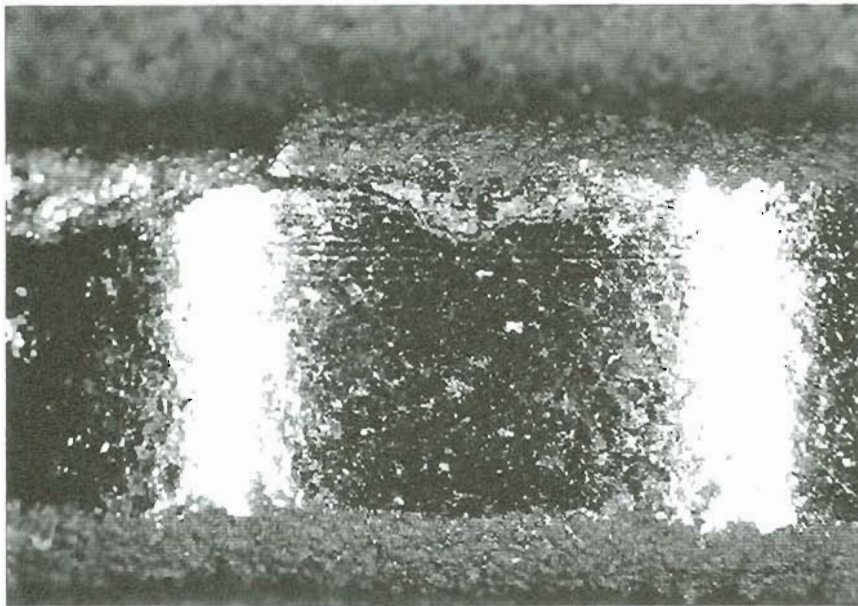


(b)

Figure 4.7. Schematic drawing of two mated Amsler rollers.¹⁷⁷
 a) overview showing coating overspray beyond 5 mm contact width. b) Enlarged area illustrating corner as a stress concentration point from which cracks can emanate.

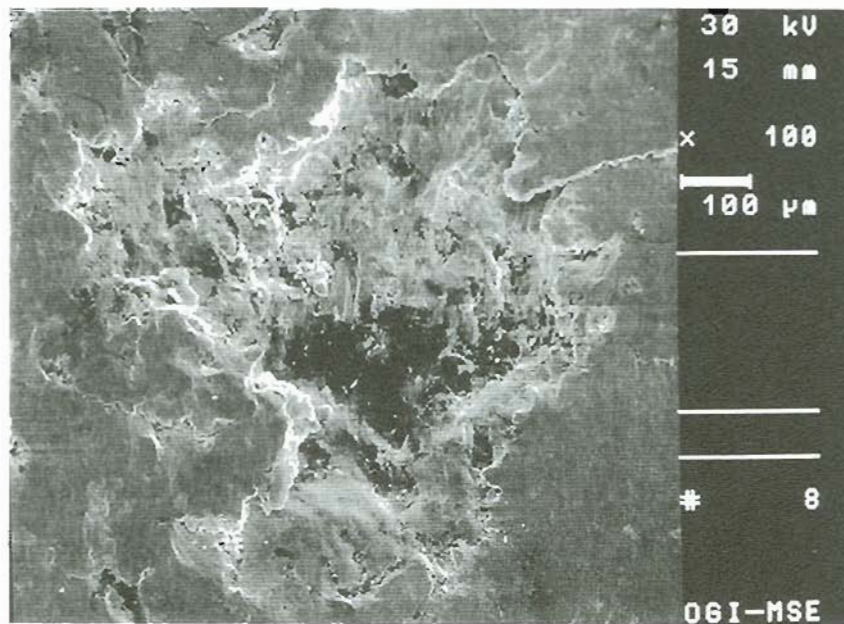


(a) 10x

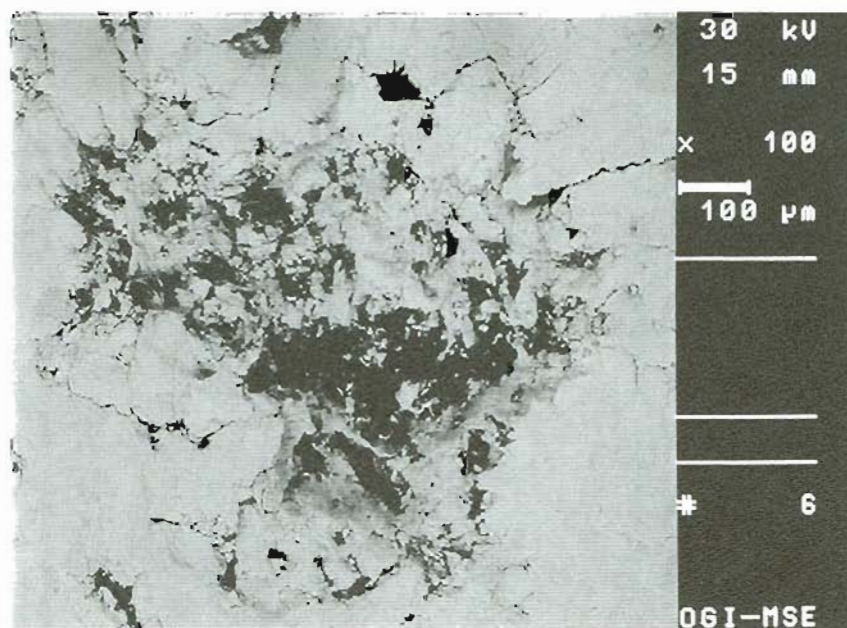


(b) 10x

Figure 4.8. Photographs of nickel-graphite / steel coatings showing edge effects. Sample G36 (10% Ni-graphite) Test= 2830 revs. at $P_o=1220$ N/mm² and 5% creep. a) Large removed particle which encroaches onto wear track. b) Crack in coating which would soon be removed had testing continued.

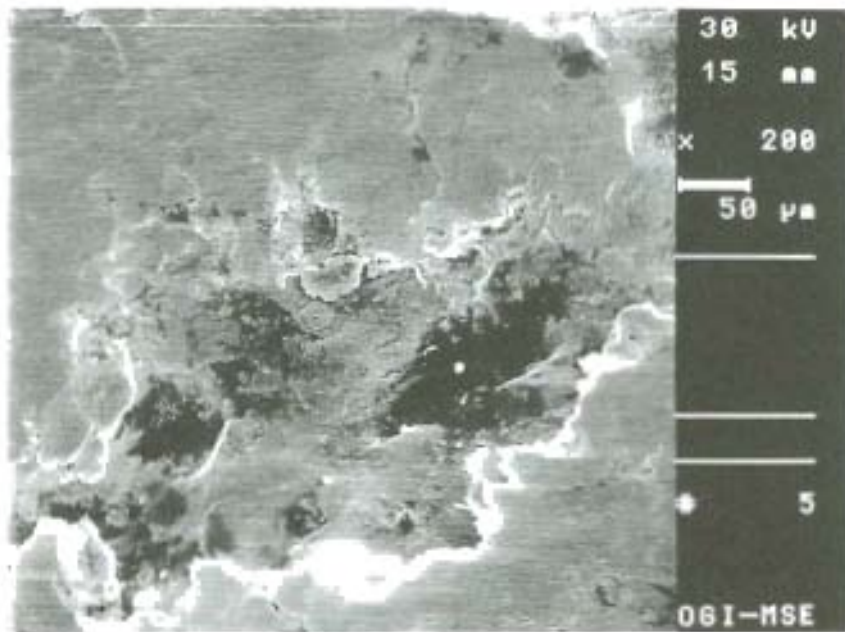


(a) 100x

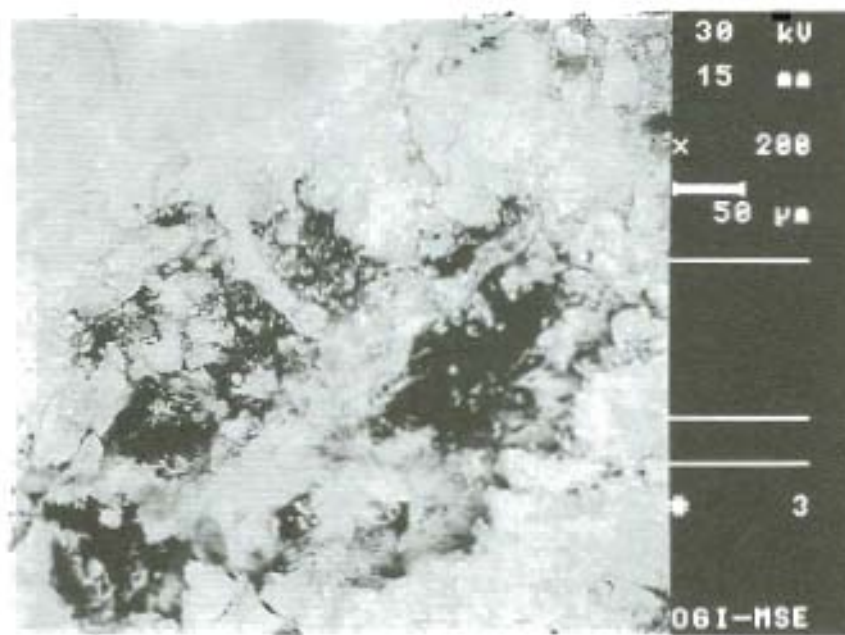


(b) 100x

Figure 4.9. SEM photographs illustrating removed wear track particle. Sample G46 (Ni-graphite= 6%). Test= 7170 revs. at $P_0=1220 \text{ N/mm}^2$ and 5% creep. a) SE imaging showing surface topography. b) BSE imaging showing concentration (dark areas) of graphite in the area of the removed particle.

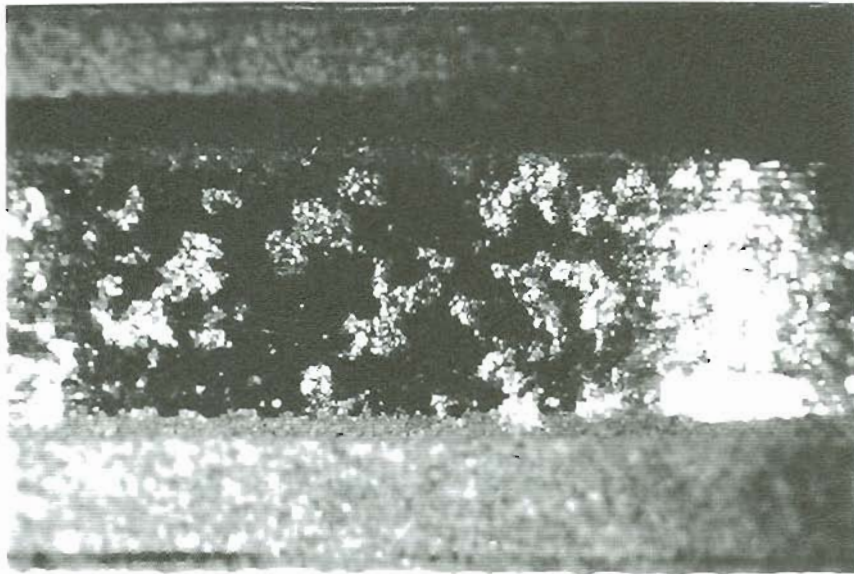


(a) 200x

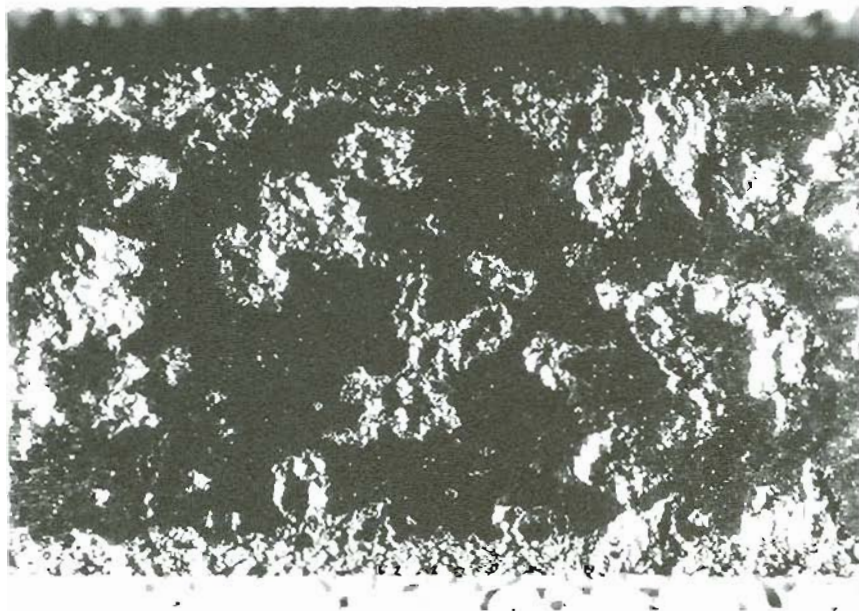


(b) 200x

Figure 4.10. SEM photographs illustrating removed wear track particle. Sample G48 (Ni-graphite= 10%) Test= 12000 revs. at $P_0=1220 \text{ N/mm}^2$ and 5% creep. a) SE imaging showing surface topography. b) BSE imaging showing concentration (dark areas) of graphite in the area of the removed particle.

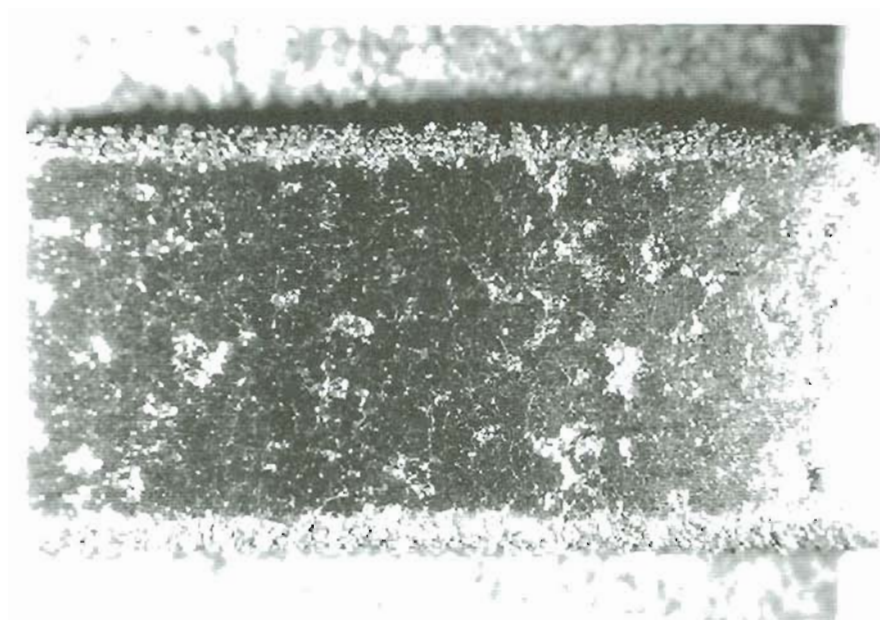


(a) 8x

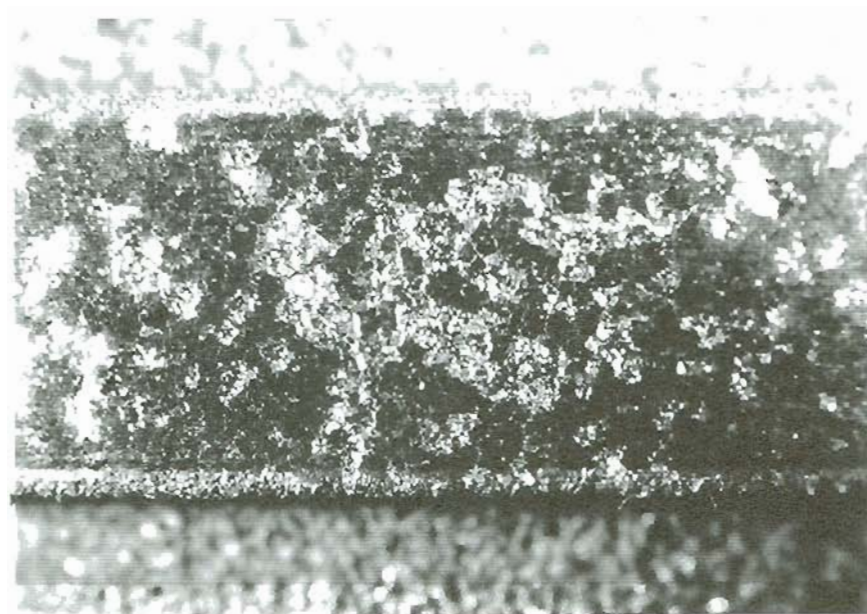


(b) 15x

Figure 4.11. Photographs illustrating removed wear track particles. Sample G48 (Ni-graphite = 10%), after 10k revs. at $P_0 = 1220 \text{ N/mm}^2$ and 5% creep. a) Overview of surface. b) Close-up showing density of removed particles (approximately 15%).



(a) 10x



(b) 10x

Figure 4.12. Photographs illustrating effect of graphite volume fraction on rate of wear track particle removal. a) Sample G46 (Ni-graphite= 6%). b) Sample G41 (Ni-graphite= 12%). Both samples tested 5000 revolutions at $P_0=1220 \text{ N/mm}^2$ and 5% creep.

4.2.4 Cast Iron Powder

The work with cast iron as a source of graphite was attempted in light of the failure of the graphite powder. With 20-30% free graphite contained in a gray cast iron, it was felt as a powder it might act as a carrier of the solid-unmeltable graphite. The discussion is presented as observations of the spray process and the subsequent performance results

The gray iron powder was produced in-house from lathe turnings. The lathe spindle speed and cutter feed speed were adjusted to yield the smallest chips in the shortest amount of time. Smaller chip size was possible, but was time prohibitive. The coarse chips were resistant to fracture during ball milling. It was thought that the graphite flakes would act as crack initiation sites within the cast iron chips allowing them to be easily reduced in size. Instead the soft pearlite matrix deformed leaving free graphite powder in the mix. A hydraulic press compressed the chips with 10 ksi. The compression only deformed the chips and packed them tightly together; the mean chip size did not change. No process was discovered which could efficiently reduce the size of the cast iron chips. The upper size limit of the powder feeder was 900 μm . The as-turned chips were on the order of 1-3 mm, making them too large to feed. This method of powder production was thus abandoned.

A suitable cast iron powder was located commercially. Though it was a convenient size to feed and plasma spray it oxidized in the plume. The powder appeared as a bright orange cascade in the plasma plume. This suggested that a large volume of material was being lost to reaction with air entrained in the plume. The lack of evidence in the coating of any retained powder proved very little powder was incorporated. The powder feeder was set to deliver as high of volume of powder as possible, but this only resulted in a brighter and larger cascade within the plume. When the powder was injected farther down stream there was still no retention. It was

thought if the powder spent less time in the plasma plume, less would be lost to oxidation. Subsequently, a larger quantity of cast iron powder could be retained in the coating. When the 1080 steel wire was sprayed a certain amount oxidized, this oxidation would limit the free oxygen to react with the cast iron powder. Two steel wires should further limit the free oxygen. Sample G58 was sprayed with two steel wires and maximum powder flow, yet there was no powder retention. It became obvious that cast iron powder could not be sprayed in atmospheric conditions if any significant powder was to be retained in the 1080 steel coating.

The wear tests results and metallographic results concluded the cast iron was not a viable alternative. No retained graphite existed and there was no evidence any cast iron powder had been incorporated. Early termination of wear tests saved time when the coating had no friction reduction potential. Wear rate was not measured because initially friction reduction was the only result of interest. The conclusions of this work prompted the use of nickel-coated graphite powder as the last alternative to achieve graphite retention.

4.3 Copper / 1080 Steel Coatings

Copper and 1080 steel were combined to form a composite coating. Copper was to act as a second phase lubricant, much like graphite, in a wear resistant steel matrix. Copper, a soft metal, was investigated as a solid lubricant because of its low shear strength and high ductility. Several copper / steel coatings were produced, with retained copper volume fraction being the primary variable. Coating microstructure and wear behavior is discussed. Copper (wire or powder feedstocks) and steel coatings had unique wear and friction characteristics. The limitations and nature of copper as a plasma sprayable material is presented, as well as ideas as to why the coatings behaved as they did.

4.3.1 Copper Wire

Copper wire when cosprayed with 1080 steel consistently produced coatings with a wide range of copper (20%-80%). The wire feedstock was evaluated in the form of flat coupons and circular Amsler wear specimens. The wire presented unique problems in the control of deposition, mainly too large of a copper volume % was contained in the steel coating. The copper became the primary constituent which compromised coating integrity. Rigorous parameter adjustment was necessary to reduce copper volume and produce a durable copper / steel.

Parameter Effects

Several spray parameters were investigated during the course of copper / steel coating evaluation. Wire feed rate was the first parameter analyzed. It was observed that only one 'ideal' feed rate was possible for a given material injection distance. 'Ideal' was defined as the feed rate which enabled copper wire to melt off as it reached the center of the plume. This feed rate was determined by adjustment of feed to yield a particle flux along the plasma jet axis.

If the wire feed rate was too slow than the wire melted off at the edge of the plume or was 'skimmed' off. The result was a highly localized, heterogeneous copper density on the substrate. This skimming effect was less significant on the moving Amsler roller. This is because the target substrate is only 5 mm wide, unlike the flat coupon of 75 mm. This difference in width exaggerated the effect. Also, the movement of the Amsler roller at 200 RPM allowed a broader dispersion of incoming particles, as the plume would not strike the same place with each pass. When the wire was injected too fast the wire would shoot through the plume resulting in unmelted wire, or at best copper deposition away from the center of the plume.

Injection distance was varied to determine the effect on copper particle size and shape. It was observed that as copper wire was injected farther from the plume, the size of the individual particles were larger and the number of small, fine particles were reduced. Small particles are desirable in creating a high density, high quality coating. Small particles reduce porosity and have a tighter adhesion. Thus, maximizing the number of small copper particles became paramount. This was accomplished by injecting copper wire nearest to the plume. The trade-off however, was that more copper particles were retained on the substrate.

The effect of injection angle was less significant than distance. When copper wire was injected at 90 degrees the efficiency of deposition was reduced. It appeared that more small particles were being lost from the system. Thus, the copper volume fraction being retained was less. Figure 3.22b and 3.26c had similar injection distances and feed rates, except the wire was injected at 45 and 90 degrees, respectively. The copper volume was 10-15% greater when wire injection was 45 degrees. As injection distance increased the quality of the coating degraded at a much higher rate than if the copper was injected at 45 degrees, i.e. small copper particles were replaced with large copper islands. Figure 3.23b was a copper / steel coating with an injection distance of 85 mm at 45

degrees. Figure 3.26a was a coating with copper injected at 100 mm, but at 90 degrees. The latter figure illustrates large copper islands, whereas Figure 3.23b shows interconnected lamella. Hence, copper injected at 90 degrees was both less efficient and tended to produce larger particles with fewer of the desirable small particles.

Single particles were observed both alone (copper only) and with the corresponding 1080 steel via deposition onto a glass slide. There was no discernible difference in morphology, but the density of copper was much greater than steel. The reason was the melt off behavior of the copper respective to that of the 1080 steel wire. As injected wire melts off, the particle flux expands in the plume as it travels downstream. This phenomenon was illustrated in Figure 4.1. Copper wire's flux density of particles was 33% the size of the flux density of the 1080 steel. This being the case, the number of particles per unit area was greater for copper than for steel. With both particle fluxes applied to the same, relatively small, target the dominant material became copper. The only way to control this is to reduce the copper input into the plume. The reason for this difference in particle flux is unknown. It is possible the oxidation of steel in the atmosphere aided the particle spreading, whereas copper being less reactive, would be affected less by the atmosphere.

The final parameters: gas flow rate and working distance were investigated thoroughly in the development of the 1080 steel coating. Review was necessary, as adding copper changed both coating and plume conditions. Gas parameters appeared to have little effect on copper morphology. In addition copper was (initially hoped) to make up only a small part of the coating. The problem of copper retention overshadowed any effect gas parameters would have on the final coating. To avoid adding any new variables to the system, the gas parameters (230 slpm N₂ / 30 slpm H₂) developed for 1080 steel coatings were retained. Working distance also appeared to have little effect on copper morphology, thus it remained at 235 mm.

Flat Coupons

Copper's effect in a steel coating structure, primarily wear behavior, has not been investigated previously. The assumption it would act as a solid lubricant stems from its use in the metal working industry. The nature of soft metals as lubricants was discussed in the introduction. It was assumed that the ideal copper particle morphology would be similar to that of 1080 steel, this being a lamellar structure. This is a fair assumption as copper was to be only a minor constituent in the coating.

Metallography provided the most information about copper's interaction with 1080 steel. The microstructure was examined as a function of parameters. The effect of inadequate wire feed rate was illustrated in Figure 3.19. In this example the wire feed speed is reduced to lessen the quantity of copper entering the plume. The result is a high density of copper in one location. This dense area is in the same plane as the injection site of the copper wire. Assume the plasma jet is circular. If the wire is injected at the 3 o'clock position then the majority of copper will ride on the outside of the plume. The resulting particles will reside in that 3 o'clock position on the sample. Ultimately, the result appeared as a concentrated and a depleted zone on the steel coupon. Figure 3.21c illustrates one of many microstructures sprayed at the 'ideal' or optimum wire feed rate. The sample contained over 50% copper. The copper was distributed in lamellar islands vs. a more ideal, fine dispersion (as seen in the nickel graphite /steel coatings). Nevertheless, the distribution of copper was uniform.

Recalling that co-spraying two 1080 steel wires to form graphite / steel coatings presented some problems, it would be assumed the same effect would apply to copper and steel wires. Fortunately, the tight density of the copper particle flux minimized the two wire interaction. The bow shock effect did alter the copper's path if it was within 8 to 12 mm of the steel wire. The

alteration though was minimal and the copper stream remained well within the broad particle flux of the steel.

Overall the flat coupons allowed for a quick and inexpensive evaluation of coating microstructure. One limitation though was the geometry difference between a flat coupon and a round amsler roller. This was of minimal consequence though as the copper volume fraction and morphology were the most important factors.

Amsler Rollers

Several Amsler rollers were sprayed using various near ideal copper conditions. The initial samples, summarized in Table 3.16, gave a strong understanding of how copper / steel coatings degraded. With all of the samples debonding in less than 2000 revolutions and showing minimal friction reduction, it became clear that the copper system might not be feasible. Copper in large quantities failed for the very reason it was used- low ductility. The high loading and shear stresses generated in rolling / sliding contact were to deform the copper into a thin film. Unfortunately, when copper deformed it brought the more rigid steel coating with it. The severity of the phenomenon was a function of copper volume fraction. The copper transferred to the bottom roller at the early stages of the wear test; the surrounding steel matrix was lost from the system or mixed in with the copper film.

The high concentration gradient of copper illustrated in the flat coupons was not as severe in the Amsler rollers. This was due to the fact the roller was rotated during spraying. This suggested that wire feed rate could be reduced without detrimental effects. Where the copper was injected into the plume would be the corresponding area of concentration on the flat samples. This was the result of 'skimming' as explained. With the Amsler rollers this effect was not observed, rather, random areas would possess a larger concentration of copper. This phenomenon had no observable difference in the degradation of the coating during wear testing.

The transfer of film was still evident, though less copper was available to form a film. The different copper concentrations become academic though as they had no influence on coating durability.

In an attempt to reduce retained copper without compromising the optimum wire feed rate, copper wire was injected farther down stream (as with the flat steel coupons). The plasma plume temperature falls as the distance from the anode increases. Thus, the wire could still be sheared off at plume center with a lower feed rate. In addition, injecting wire farther down stream allowed for more copper to be lost from the system.

Sample AC11 was created with copper wire injected at 100 mm. The microstructure was shown in Figure 3.26a. This coating had very poor performance, with the sample proceeding to Type III (severe) wear and debonding within 400 revolutions. The result of down stream injection was very large particles, and only a small decrease in copper retained. The other samples in this series did not perform any better. Sample AC12 was one of the few 0.5 mm copper coatings. It was believed debonding may be reduced by the reduction of coating thickness. Any benefit though, was lost in the lack of coating integrity from copper particles.

The 100 mm injection distance had very poor wear performance because the coarse particles had a detrimental effect on the coating integrity. With large particles a fine lamellar structure is hard to achieve. It is believed the adhesion between copper and steel splats is not as strong as for steel on steel. Large particles create voids and large areas of poor adhesion. Since copper has higher ductility, large islands of copper will deform and cause loss of coating integrity. When a large number of small copper splats exist, their ability to flow is reduced as they are reinforced by the surrounding steel matrix.

There was a large amount of material transfer during most copper wear tests. Copper was smeared on to the bottom roller. The morphology of the smeared material would change depending on the

contact pressure. A thin film was produced at $P_o = 1220 \text{ N/mm}^2$ (Figure 3.25b) and globules (Figure 3.25a) were the result of tests where $P_o = 700 \text{ N/mm}^2$. The contact pressure would convert the globules to a thin, continuous film over the bottom roller surface. As contact pressure increased, local globules would be transferred to the full width and circumference of the roller. It was believed the thinner films would provide greater friction reduction. This stems from the metal working industry's use of thin metal lubricating films.

To shear the copper, allowing it to become a lubricant film, higher contact pressures were employed, at both 5% and 35% slip. This thin film was very tenacious in its adherence to the bottom roller. When the thin film was formed the coatings appeared to remain intact longer. The formation of the film was a function of copper volume fraction, the contact pressure, and slip ratio. Consequently, a general statement about the films effect on durability is difficult to make. In addition, the films formation and behavior become only an observation, because material transfer of either form did very little to reduce friction.

Material build-up is a test related problem that would not occur in the real world. The amount of material transferred greatly compromised the coating integrity. The closed system of two Amsler rollers allowed the transferred copper supply to remain local and intact. An equilibrium was reached where the wear process occurred between two mostly copper surfaces. This was true regardless of the load (and for most tests because the copper volume fraction was so large). Adhesion between the two pseudo-copper surfaces further exacerbated the coating break down. In an open system, fresh wheel counterfaces would have exhausted the supply of copper, greatly accelerating the coating break down.

The majority of time was spent evaluating parameters and their effect on copper / steel coating microstructure. In the end though it was realized that all of these parameters in their ideal form could not overcome system constraints nor the inherent lack of

copper's lubricating ability under rolling/sliding contact. Thus, the discussion of copper coating parameters becomes academic as no amount of adjustment could produce a wear resistant, friction reducing coating with copper wire.

4.3.2 Copper Powder

Given the limitations of copper wire deposition, copper powder was employed. Use of powder feedstock gave far superior control over the volume fraction retained in the coating. The problem of copper wire deposition efficiency was no longer relevant. The copper powder / steel coatings were evaluated in the same manner as the coatings produced with copper wire. The performance results and material behavior were much the same and large copper volume fractions still plagued the system.

Amsler Rollers

As with the copper wire coatings, metallographic blanks were produced to evaluate the coating microstructure. The blanks were round as opposed to flat coupons. The geometry was similar to an Amsler roller. This allowed metallographic blanks and Amsler rollers to be sprayed concurrently. The flat coupons would have evolved to round blanks while using copper wire, had the copper wire / 1080 steel system shown potential.

Copper powder gave more freedom in the production of varying volume fraction coatings. Copper powder was injected in large or small quantities without affecting its distribution. It was now possible to create coatings with very low copper quantities. The first iteration tested the limits of the powder feeder. At the powder feeder's slowest setting, copper was still present in amounts of at least 10%. The injection distance was not altered in an attempt to decrease retained copper. The copper wire results influenced this, but it is understood the melting processes are different. Large particles would not have formed in the same

manner as wire. The size of wire produced particles was a function of ablative melting.¹⁶⁴ With powder feedstock however, the magnitude of retained copper particles were determined by the size of powder used. The volume fraction reduction was shown to be minimal when copper wire was injected at 100 mm. Thus, changing injection distance would only add another unwanted variable.

Normal Feed

The range of copper volume fractions was influenced by subtle changes of the powder feed rate. Sample AC16 and AC17 had 10% and 18% copper, respectively, yet the feed rate was only increased by 0.5 RPM. The volume fraction of copper increased to over 40% when the powder feed rate was 3.0 RPM. The lower limit of powder delivery by the powder feeder had been achieved. The nature of the plasma system did not allow tight variations in the copper and steel coatings. (I.E. large plume, small target equating to a large number of lost particles from the system.) Consequently, a series of samples with only 1 or 2 % retained copper increments would be difficult, if not impossible to achieve.

Samples AC16 through AC18 utilized larger bore powder feed tubes. The different powder feed tubes required varying powder gas flow rates to deliver the copper powder to the center of the plume. This didn't change the coating microstructure for a given powder feeder RPM, as the amount of copper feed into the plume was a function of RPM only. The copper flux remained tight in the plume when copper powder was deposited. The size of the flux was comparable to that produced by the copper wire. Deposition with powder illustrated again that very little copper was necessary (relative to steel wire) to achieve high volume copper / steel coatings.

Samples AC16 through AC21 were wear tested and showed some reduction of friction. All but one sample (AC18) debonded within 1000 revolutions, with the other sample AC18 lasting 1440

revolutions. Again, a transferred film was present which behaved similarly to the copper wire / steel coatings. It appeared the correct combination of contact pressure, creep, and copper volume fraction provided the limited friction reduction. These conditions transformed the copper material into a thin film on the bottom roller. The thin film is the source of the limited friction reduction, with the mechanism of formation and behavior being similar to that of the copper wire / steel coatings.

The friction coefficient was still around $\mu = 0.38$, which is well above the target value of $\mu = 0.10$. The copper's effect on coating performance is independent of the material source. The coating is only affected by volume and morphology. The wear performance of samples AC16 through AC21 further support the idea that copper is incapable of providing adequate lubricity or endurance under rolling/sliding contact.

Low Feed Wheel

The controlling of copper volume was the most challenging problem. A low feed wheel was employed which delivered roughly 60% of the volume of the original wheel. This equated to almost one half the volume of copper delivered at a given powder feeder RPM. It was believed that if copper was to be successful a coating with less than 10% copper must be created. This stems from two observations. The first, is the large volume of transferred material during Amsler wear tests, and the second being the lack of coating integrity when copper volume fractions were large (10-50%).

To further dilute the quantity of retained copper, the powder was sprayed with two 1080 steel wires to double the steel flux. This was sufficient to lower copper volume fractions to below 10%, but the performance data of Table 3.19b indicated that copper now had little effect on lubricity. The copper quantity was still sufficient to cause premature debonding though. These low volume coatings displayed little or no material transfer. This supports the

assumption that the limited friction reduction was a product of thin copper film formation via material transfer.

The low feed wheel did allow for a wider range of copper volume fractions to be achieved. The end result was when copper was present in the coating in sufficient volume to provide any lubrication, the coating had almost no durability. Sample AC31 had 6% copper and displayed minimal friction reduction ($\mu=0.41$). It can be argued though that the coating was not durable enough to make a valid friction measurement. Tests on steel coatings have shown the steady state friction value ($\mu=0.46$) was not achieved until roughly 1000 revolutions. Sample AC32 survived beyond 1000 revolutions and displayed a more realistic steady state friction coefficient of $\mu=0.48$. The other samples with larger copper volume fractions degenerated quickly in the same manner as explained earlier.

Even with very low volume fractions the coating's integrity was compromised. When the volume fraction of copper was 6% the coating's appearance was that of a steel coating without any lubricant material. Yet, the coating debonded in less than 1000 revolutions. At larger volume fractions the copper color was readily evident with the coating appearing like pure copper at volume fractions above 20%. Despite the appearance though, the low volume coating did not behave anything like a steel coating with respect to durability. This observation helped conclude that copper in any retainable amount was detrimental to the steel coatings performance, acting as a contaminant, rather than a second phase lubricant.

Twin Wire spraying

The low feed wheel did provide an opportunity to further study the interaction of two co-sprayed steel wires. Co-spraying two steel wires was employed to increase the coating deposition rate and dilute the copper. The specific use with copper was unsuccessful as the copper system failed to achieve its objectives.

The interaction of two wires in the plume is a phenomena warranting further research. The interaction of two steel wires was more significant than that between copper and steel wires. The interaction occurs only when wires are brought in close proximity of one another. (This was detailed in the Graphite Discussion section.) Figures 4.5 and 4.6 illustrated the phenomenon of wire interaction. The work with copper powder and two 1080 steel wires confirmed that the two wires must be offset by 13 mm or more. Beyond 13 mm the particle interaction was minimized.

4.3.3 Synopsis

The overall poor performance precluded the copper and steel coating research from preceding further. The behavior of copper wire yielded consistent high volume % copper coatings. This was a limitation of the plasma spray system and could not be overcome easily. The copper powder despite its ease of deposition did little to improve the coating performance. Although a wide range of copper volume fraction coatings were produced, none indicated any potential. These coatings appear to be inappropriate for severe rolling/sliding contact environments, but may be suitable for less severe applications.

4.4 Polymers

The steel coating systems to this point have dealt with dispersed lubricants within the steel coating matrix. By applying the polymer as a thin surface coating unique wear behavior was observed. The dynamic nature of the polymer film degradation though, required close examination of the polymer film structure as well as its performance and wear characteristics.

The polymer films were characterized by their durability and friction coefficient when tested under rolling/sliding contact. The polymers were generally tested dry, with only a handful of lubricated tests. The polymer film was applied to varying steel coating thicknesses. Reapplication of the polymer following a test was also performed. Observation of each polymer system during testing allowed conclusions to be drawn regarding the polymer's potential. Analysis also included visual and SEM observation of the degradation process from test onset to termination or failure. The most significant information came from the FTIR results, which described changes in the molecular structure as a result of polymer application and wear testing.

The discussion presents the initial work and describes each of the coating systems. The characteristics of the polymers themselves are then presented, which focuses heavily on nylon / steel coatings. The interrupted tests describe the coating wear process. This is all followed by a synopsis of polymer coatings in general.

4.4.1 Initial Work

In order to apply a thin polymer film to a steel coating, a set of parameters had to be established. Early work of polymers on uncoated rail steel yielded a set of gas parameters which appeared to be suitable.¹⁷⁸ The application of polymers to plasma sprayed 1080 steel followed these early parameters. It was realized that

deposition of the polymer presented unique problems which had not been observed in the other lubricant systems. For one, the polymers would degrade rapidly if overheated. Care had to be taken to adequately cool the surface during polymer application. The thickness of the polymer was on the order of 25 to 75 μm , which made measurement difficult with conventional slide calipers. An appropriate polymer thickness could only be evaluated by subsequent wear performance.

On the positive side, the problem of steel coating debonding had been reduced through the reduction of steel coating thickness to 0.5 mm and 0.25 mm. This reduced the premature test failures which gave inconclusive data as to the wear behavior of the polymer coating itself. Kynar and Torlon were initially tested because they were readily available and believed to have potential. Nylon received the most attention because early performance was very impressive and the polymer itself, nylon 11, was in great supply. PTFE and UHMW were tested for comparison in attempt to find polymer wear performance even greater than the nylon.

The performance of the Kynar, barring debonding, rivaled the nylon. Table 3.20 illustrated the results, with durability exceeding 16,000 revolutions. This performance was unmatched, however Kynar was a difficult polymer to apply, it would overheat easily, causing embrittlement.¹⁷⁹ The limited number of tests performed on Kynar / 1080 steel coatings make a conclusion difficult to draw. The low friction coefficient at the end of the Kynar tests illustrated that polymer film did remain. Kynar's uniform friction coefficient over a wide range of loading further illustrates it had good adhesion to the steel coating surface. Creating a consistently good performing Kynar / steel coating was evasive and optimization was not pursued.

Torlon did not have good adherence to the steel coating surface. During wear testing Torlon would shed excess material as did the other polymers, but it didn't appear to form a steady state film. The friction coefficient rose at a much greater rate than the

Kynar or nylon. The large friction coefficient at test termination suggested that most of the polymer was worn away. If testing had continued the coating most likely would have degraded to steel coating on steel wear within 2000 revolutions. Neat Torlon powder requires a three step heat cure to cross link the polymer chains. Had this been done the performance would have likely improved. These extra steps however, would not be practical for coating application in the field. The secondary heating of the rail following coating deposition would be cost and time prohibitive. Torlon's friction behavior as a function of loading suggests the coating was test sensitive. If the wear tests of Torlon had been done at lower contact pressures or creep, the performance may have improved. However, coatings which could not survive the extreme conditions of $P_o = 1220 \text{ N/mm}^2$ and Creep = 35% were not considered practical for wheel/rail applications.

4.4.2 Nylon

The evaluation of nylon as a lubricant film received the most attention in the polymer / steel coating study. Early observations indicated that the degradation mechanism of polymers in general, were similar. It was felt that to fully understand this degradation, one characteristic system (nylon / 1080 steel) would have to be studied in depth. The results of the nylon coatings gave better understanding to the other polymer systems, particularly UHMW.

Neat Nylon / 1080 Steel Coatings

Initial tests with nylon / 1080 steel (0.7 mm) coatings were subject to frequent debonding. Debonding reduced the average life of 0.7 mm coatings by 26%. The debonding was still being studied during these early tests on nylon. Despite the frequent debonding, nylon exhibited a consistent degradation behavior from test to test. The point at which the polymer failed would vary in the number of

revolutions tested, but was always preceded by a series of events, which was illustrated in the interrupted tests. Nylon's friction behavior was independent of applied load. This suggests that nylon was not sensitive to test parameters, at least for the range at which they were tested.

The success of the polymer in acting as a lubricant stems from its adherence to the steel coating. Figure 4.13 is a schematic illustration of a polymer coating adhering to the rough steel coating surface. Figure 4.14 illustrates a cross section of a nylon / 1080 steel coating as viewed in the SEM. This figure shows the rough steel coating surface. This pinning mechanism between polymer and the steel coating surface is observed in each successful polymer system. The pinning allows the polymer to be anchored and increases the surface area which is adhered to the steel coating. Large contact pressures at the beginning of the wear tests force the polymer into these coating valleys.

The adhesion of the polymer is a surface effect. The actual steel coating thickness has no role in polymer performance provided it exhibits the same surface roughness and doesn't debond. Debonding of 0.7-1 mm thick steel coatings plagued this work. Subsequently, thinner steel coatings were utilized. The 0.5 mm and 0.25 mm coatings displayed an increase in debonding resistance, with only one debonding in each series. The investigation of 1 mm coatings was discontinued.

Neat Nylon / 308 L-Si Stainless Steel Coatings

The ideal coating matrix for use with polymers is subject to ongoing investigation. Initial work focused on stainless steel, as it was hypothesized it may offer greater debonding resistance than 1080 steel. This reasoning stems from the oxides formed by stainless steel. Chromium oxides are tougher and more adherent than iron oxide. It was felt that the oxides produced during spraying in atmospheric conditions weakened the coating. Analysis had

shown cracks in the iron oxide layers following full scale wear testing.¹⁸⁰ This prompted the search for a more debond-resistant coating. The actual wear properties of stainless steel are of minimal consequence as it will act only as a reservoir for the polymer coating.

Stainless steel appeared to have a greater durability than 1080 steel, with respect to debonding. The 0.25 mm coatings with nylon lasted 15-20% longer. The number of tests though, may not be adequate to fully describe the debonding behavior. In addition, the samples were not sprayed at exactly the same time or at exactly the same conditions, though every effort was made for exact reproduction. The polymer film appeared to be more durable when applied to a stainless steel coating. It is possible the stainless steel's surface is better suited to polymer retention. It may contain a larger number of asperities and cavities where the polymer may anchor. The overall performance was improved, but further testing is necessary.

Solid Lubricants + Nylon / 1080 Steel Coatings

With the addition of solid lubricants there was some increase in the durability of nylon. The ability of solid lubricants to reduce friction and wear of nylon has been observed elsewhere.¹⁰² The increased durability may have been a statistical aberration, but more likely, an actual effect of the lubricants. Observation suggests the lubricants are beneficial, and further testing would confirm this. Table 3.26 summarized the nylon + solid lubricant / 1080 steel coating performance. The apparent increased durability of nylon and solid lubricants (compared to neat nylon coatings, Tables 3.23 and 3.24.) suggested the lubricants were able to form a film. This film would be similar to that formed by graphite / 1080 steel coatings. The MoS₂ or graphite may align itself on top of the polymer and reduce wear. This film, if present, did not reduce the initial friction value appreciably ($\mu = 0.08$ vs. $\mu = 0.10$) and had no effect on the

friction behavior over the course of the test. EDS did not detect any transferred film on the bottom roller, for either MoS₂ or graphite. The overall benefit of added solid lubricants is questionable, but at the least had no adverse effect on the polymer wear or adhesion to the steel coating.

4.4.3. PTFE (Teflon™)

PTFE was the obvious choice when a polymer was selected to reduce friction. The inherent low friction nature of PTFE in other applications suggested it may perform well. The literature contains descriptions of several experiments pertaining to the wear of PTFE.^{86,88,91} There are no references to rolling/sliding contact, and the applied loads are generally less than 20 N, as opposed to 2000 N used in this research. PTFE generally undergoes a high temperature cure after it is applied to a surface.¹⁰⁶ This allows the individual particles to sinter together. When plasma sprayed the PTFE was deposited as a collection of particles. A slow cure was not performed, and as a result the particles remained as individual spheres. Figure 3.31 illustrated the individual PTFE particles.

PTFE has a large melt viscosity index.¹⁰⁶ This means that even at melting, the viscosity remains large and the polymers ability to wet is limited. The rotation of the Amsler roller further hinders the PTFE from flattening as it creates an outward centrifugal force on the softened PTFE particles. Increasing the heat input to melt the PTFE on the surface only caused it to burn, and risked overheating the steel coating. The low adhesion and lack of melting yielded PTFE coatings which were less than 13 μm thick. Mixing the PTFE with nylon increased the adhesion of PTFE to the steel coating.

When PTFE coatings were wear tested the pure PTFE appeared to be lost from the system due to its lack of adhesion. Some of the PTFE was retained though, and found its way into the steel coating valleys. The high pressure and contact zone heat may have been enough to partially soften the PTFE, allowing it to flow into these

steel coating valleys. The low friction coefficient for both pure PTFE tests indicates PTFE was retained. A very thin film formed. This film degraded in a similar manner to the nylon film, except it was much more accelerated. The limited number of tests with PTFE did not provide for a thorough analysis of the PTFE film.

The PTFE mixed with nylon had decreasing performance as nylon volume fraction increased. The adhesion and film thickness were increased with nylon, with the coating appearing nearly identical to a pure nylon coating when PTFE= 25%. Since the polymer film was thicker there was a greater material loss at the test onset. It is believed PTFE failed to lubricate the nylon coating (PTFE= 25%) because the film was a composite of melted nylon and unmelted PTFE. The PTFE worsened the structural integrity of the nylon because a continuous coating was not present. The 25% PTFE, nylon coating consisted of a matrix of melted nylon with a dispersion of solid, unadhered PTFE particles.

When nylon was an additive to PTFE (PTFE= 50% or 75%) the nylon may have prevented the PTFE from penetrating the deep coating valleys. If this were the case, PTFE would have no surface to which it could anchor. The contact forces during the wear test would eject PTFE from the system. These behaviors help explain why neat nylon and neat PTFE coatings out performed any mixture in-between. PTFE as a material did not appear suitable for plasma spray deposition.

4.4.4 UHMW

UHMW had equivalent performance to the nylon. From a deposition point of view, UHMW was superior to nylon in that it had a greater resistance to thermal degradation. UHMW required a greater heat input to melt and form an adherent coating, making UHMW more difficult to overheat. This may be an advantage when the polymer is sprayed in the field where conditions may not be as tightly controlled. When heat input is inadequate the resulting coating

appears as Figure 3.33. This structure was the result when lower amperages were used to plasma spray the UHMW film. The poor wetting of the UHMW coating sprayed at low power input could be avoided by increasing dwell times. Thus, a lower power system could be employed but would increase the overall spray time. The friction and degradation behavior followed the exact pattern as the nylon, and other polymers. This consistent behavior is more a function of the environment in which the polymer is tested as opposed to being intrinsic to the polymer itself.

Solid lubricants were not as effective as with nylon. This could be due to two reasons, the first is the mixing of the polymer powder prior to spraying. If the dispersion was not adequate, then concentrations of graphite or MoS₂ could be lost in the same manner as graphite was lost when trying to create graphite /steel coatings. The second reason may be that the UHMW as a lubricating film may not realize any benefit by added solid lubricants. Fillers are generally added to polymers to increase strength and for retention of shape.¹⁸¹ Only one reference was uncovered about the benefit of adding solid lubricants to polymers under sliding wear.¹⁰² The wear behavior of UHMW saw minimal increase in durability, and no decrease in friction or change in the coating degradation pattern, when solid lubricants were added. It is possible solid lubricants in different proportions (Weight fraction= 28% Graphite or MoS₂ for both nylon and UHMW tests) may improve the durability of UHMW. If larger proportions are used though, the coating integrity may suffer, as the nylon's did when PTFE particles were added. Overall UHMW was a good lubricant film which performed almost as well as the nylon. UHMW applied to stainless steel coatings may realize greater durability.

4.4.5 Surface Modification

A polymer can only act as a lubricant if it remains adhered to the coating surface. Since the surface characteristics play a crucial

role in the durability of the coating, finding the optimum topography was of great interest. It is believed the unique surface topography of the plasma sprayed coating in the as-sprayed condition allows the polymer to be retained during high contact pressure and creep wear conditions.

When polymers were applied to uncoated, machined Amsler rollers, their adhesion was very poor, with durability being less than 200 revolutions.¹⁷⁸ The polymer had nothing to hold onto, for there is no chemical bond or diffusion layer. It is believed only the microasperities and weak secondary electron bonds retained the polymer. In light of the machined finish roller's performance several surface roughening techniques were employed to attain better adhesion.¹⁷⁹ Table 3.30a and b summarized the results of various surface roughening techniques. The grit blasting had the greatest effect, from a performance standpoint, in approaching a plasma sprayed surface.

Grit blasting does not give the extreme peaks and valleys which are present on the plasma sprayed surfaces. Figure 4.15 are SEM micrographs illustrating the difference between a grit blasted surface and an as-sprayed steel coating surface. The range of peaks and valleys are much greater in the plasma sprayed coating.

Valleys in the coating surface were believed to increase the polymer adhesion. Valleys, in the form of grooves, were cut into the roller's surface using a lathe. Unfortunately, these grooves were very coarse from a microscopic view and did not provide the high density of polymer pinning points which the steel coatings did. Different groove sizes were attempted, each with about the same result. The combination of grit blasting and grooves increased the durability somewhat. By grit blasting the surface, the newly formed peaks are rounded off. This deformation may increase the pinning strength because the rounded off surface would have a more complex topography, possibly approaching that of a sprayed coating. Grinding gave the least benefit because it did the least surface damage. Grinding only slightly altered the smooth, machined surface and did

not create deep valleys. No technique was found that could simulate or mimic the inherent surface texture of a plasma sprayed steel coating.

4.4.6 Lubricated tests

Nylon / 308 L-Si stainless steel coatings were evaluated under grease and water lubricated conditions. Neither lubricant extended the life of the coatings, in fact both lubricants reduced coating durability. When water was added to the wear track the polymer film exhibited an increased degradation. It is believed water penetrated the polymer coatings and reduced its adhesion. Nylon is hydrophilic, meaning water is readily absorbed. The absorbed water, which is incompressible, could distort and tear apart the polymer film under high contact pressures. This was supported by the visual observation of a more rapid degradation in terms of decreased revolutions to polymer film removal.

In a dry test, the nylon film would slowly wear from a thin ring of exposed metal to polymer film failure over several thousand revolutions. With the addition of water, once this ring appeared, it would expand and virtually all of the polymer film would be gone in 200-400 revolutions. The water did help lubricate the steel coating on steel wear tests by maintaining a friction coefficient of $\mu=0.3$, but the water also increased the debonding frequency to 100%. It is speculated that once the polymer film 'seal' was breached, water would penetrate the steel coating and cause debonding. The debonding was a direct result of hydraulic forces acting within the coating lamellae by incompressible water.

The lubricated tests with grease displayed much the same behavior as water lubricants. The polymer coating was degraded at an accelerated rate. Once part of the polymer film was worn through the coating debonded. Unlike with water lubricant, it was not necessary for the entire polymer film to have worn off. The friction coefficient remained at $\mu=0.10$ throughout the test, regardless of

the polymer film status. Less than 5% of the applied grease actually remained in the contact zone. This suggested the grease which did remain was adhered to the polymer film surface. Overall the lubricated tests suggest the polymer / steel coating performs best in dry conditions.

4.4.7 Polymer Reapplication

Several tests were performed to evaluate the reapplication of a polymer film. Following a wear test to near failure, which varied in length due to variations in coating behavior, nylon was reapplied to the coating surface. The film did not adhere as well as on a fresh steel coating surface. The increase in coating life was around 25% nor did it increase the coating life. At onset of the test nearly all of the reapplied nylon was shed and lost from the system. Only the polymer from the previous test appeared to remain.

Neither of the surface preparation techniques could help retain the newly applied nylon. The as-worn coating surface was relatively smooth (Type I wear) and had nowhere near the texture of a freshly sprayed steel coating. The reapplied nylon had nothing to pin it to the surface. Texturing the surface had little benefit. This is a similar behavior as observed in the application of roughened, uncoated Amsler rollers. Perhaps a surfacing technique may be developed which can restore a steel coating to its original surface texture. Until then, the steel coating will have to be reapplied if the polymer is to perform up to its potential.

4.4.8 Interrupted tests.

The interrupted testing of the polymer coating allowed a detailed analysis of the degradation mechanism. Every durable polymer coating tested (nylon, UHMW, etc.) displayed the same wear behavior. Seven stages of wear were identified, and each is discussed in detail. These stages represent a trend, with the rate of polymer degradation varying between individual tests. The

identification of these stages of wear is the best way to explain how and why the polymer degrades

Stage 1 occurred within 300 revolutions, with the majority of polymer loss being within 100 revolutions. The excess polymer coating was shed and lost from the system. The initial coating thickness was on the order of 30-50 μm . The steady state lubricating film was less than 5 μm , which was the same regardless of initial polymer thickness. This mechanism was the result of shear forces during break in. The porous coating surface allowed polymer to be pinned down. The contact pressure forced polymer into the valleys of the coating surface. The excess polymer, having very low shear strength, was squeezed out of the contact zone. The bottom roller appeared shiny with no transfer of material occurring. Figures 3.34 and 3.41 illustrated the polymer removal both visually and in the SEM.

Stage 2 is steady state wear. The friction coefficient has stabilized to a value of 0.08-0.12 and remains unchanged for a short period (< 1000 revs.). The friction coefficient begins to climb at a rate of 0.007 per thousand revolutions to a value of 0.1 or 0.15 over 4-5k revolutions . The excess polymer has left the system. The bottom roller remains shiny, with no apparent material transfer. This stage occurs between 300 and 4000 revolutions. This wide range of steady state can be attributed to the post deposition quality of the lubricating polymer film.

If the polymer is fully adhered and not overheated during the spray process, the chances of it being retained in the coating is increased. Retention equated to a longer life and greater resistance to the degradation process. Nylon, for example, was easy to overheat. If overheated it became brittle, thereby decreasing its fluid flow during the break-in stage. A brittle polymer coating would not form a steady state lubricating film, and test life would be < 3000 revolutions. If nylon could not deform plastically under the contact pressure it would not adhere to the coating. In this respect UHMW was superior, as it never displayed brittle behavior.

Large nylon particles transferred to the bottom roller mark the beginning of Stage 3. The transferred material was a darker color. Small pieces of nylon were torn from the coating surface. At first the material did not adhere to the roller, but after 50 revolutions or so, a thin film started to form. The transferred material was initially in the form of 'blobs', which were quickly compressed into a thin film by the high contact pressure. This film would visually grow thicker as the test progressed to termination (Stage 7) Up to this point, the friction coefficient had been increasing at a very slow rate. The transfer of material caused a 'bump' in the friction trace, indicating a decrease in the friction coefficient. This decrease was short lived as the friction coefficient increased at a rate of 0.027 / thousand revolutions- four times greater than in stage 2. This bump provided a very predictable landmark during the wear test. It was always characterized by the initial transfer of material to the bottom roller. This stage occurred between 3k and 5k revolutions, and lasted only 50-200 revolutions. This stage marked the increased wear and degradation of the polymer film and also reduced the volume of the polymer film by 50-75%.

Stage 4 began when the transfer of material to the bottom roller has reached visual equilibrium. Stage 3 was the actual transfer of material. The film on the lower roller grew thicker (visually observed) as the test progressed. This stage occurred at 5k to 8k revolutions and lasted 2k to 3k revolutions. With a majority of the lubricating film worn away, the rate of friction coefficient increase rose to 0.06 / thousand revolutions. The greatest amount of this friction increase did not come until the last 1k revolutions of stage 4. The friction coefficient was around 0.15 at the beginning of this stage. This is a consistent value from test to test. The final friction coefficient was between 0.23 and 0.27. Figures 3.43 and 3.44a illustrated the change in surface film between stages 3 and 4. Figure 3.44b illustrated a nylon concentration adhered in a valley of the steel coating. The surrounding area was devoid of any appreciable nylon.

Stage 5 starts when the polymer film began to wear through completely. A ring formed in the center of the coating exposing the bare steel coating below. When the ring begins to form, the friction coefficient decreased, with the value being around $\mu=0.25$ just prior to this. As the ring expanded the friction coefficient continued to decrease. The value reached 0.20-0.25 and then began to rise at an increased rate. It was speculated that this decrease in friction was caused by a decrease in the contact patch area. As the ring expanded the polymer contact zone shrank. At some point the remaining polymer could not support the load and contact occurred between the steel coating and bottom roller. At this point stage 6 began and no further friction reduction was observed. Also, this was the first point on steel on steel contact. Observation estimated this to occur when 20-40% of the surface was depleted of the polymer film, i.e. the depleted ring being 1-2 mm in width.

Stage 6 marked the end of the polymer coating. At this point the ring had widened to over 50-75% of the roller surface, steel coating on steel contact was imminent. This stage could last 2k-4k revolutions, especially in the nylon / stainless steel coatings, with the friction coefficient remaining fairly constant at $\mu=0.25$. The small amount of polymer film appeared to support the load and minimized the steel coating contact.

Stage 7 occurred when the remaining polymer film was worn away. At this point steel coating contact occurred, and wear and friction increased. At this point the friction would climb to 0.46 or debond within 1000 revolutions. The film which was present on the lower roller was destroyed as steel on steel wear progressed. If any polymer film remained it was worn away and lost from the system as wear debris.

All but a few tests were terminated at the end of Stage 6. This allowed the remaining coating to be observed in the SEM. The results were all similar being that <10% of the polymer coating remained. That which was left resided in deep valleys of the steel coating's surface. Figure 3.46 illustrated the remaining coating,

the dark areas were polymer. Even when stage 7 was allowed to progress none of the coatings could be worn to the steel substrate.

The seven stages of wear gave a good understanding of how the polymer coating degraded from a visual standpoint. The consistency of degradation for each polymer supported the idea that the wear mechanism were test dependent, regarding the steel coatings and contact conditions. For example, the transfer of material would not effect an open system in the same way. It is possible a closed system accelerated the polymer failure. Polymers often display better wear resistance when worn against a hardened steel counterface, as opposed to themselves. The transferred material simulates a polymer against polymer wear condition.

Overall the interrupted tests illustrate that the polymer film has a wear life which follows a pattern of degeneration. The tests also confirm the theory that the chief mechanism of adhesion is retention within the steel coating valleys. Interrupted tests at 5% creep would predictably illustrate the same phenomena, as the friction behavior is similar. The interrupted tests were limited as they were only visual observations. No information about the polymer itself was given. To complete the picture a more analytical technique was used to characterize the structure of as-melted, as-sprayed, and as-worn nylon films.

4.4.9 Polymer Film Analysis

The polymer film analysis gave some insight as to the nature of nylon when it undergoes spray deposition and high contact pressure wear testing. The analysis required a great deal of interpretation based on experience and probable material behavior.¹⁰⁶ The two techniques ATR and SR were applied to determine if changes in structure had taken place. Both techniques complimented one another to give a good picture of the nylon structure.

One of the most significant observations was that neat, as-melted nylon and plasma sprayed nylon exhibited similar structures. Nylon was thought to degrade rapidly in the plasma plume. From a structural standpoint however, nylon was much more resistant to thermal degradation. Nylon will darken in color when overheated; the ideal coating color has always been yellow to light brown. Nylon samples were spray coated ranging from nearly transparent to black. Upon analysis, only the nylon films that were dark brown, almost black in color, indicated the structure had been destroyed. Figure 4.16 illustrates the FTIR spectra of a pyrolyzed nylon sample. None of the amide or carbonyl linkage peaks exist, indicating this sample is nothing more than random carbon atoms.¹⁰⁶

The surface of the as-sprayed nylon coating had an increased presence of C-O bonds. This is a result of atmospheric O₂ reacting with the methylene groups. Hydrogen, being very reactive, was displaced by oxygen at the high temperature coating surface. Thus, C-H bonds became C-O bonds. The surface was the most affected because it was exposed to the hot atmospheric plume for the greatest length of time. This degradation was not detected by ATR, because it only existed at the surface. This illustrated how results can be highly dependent on the analysis technique.

The nylon film also underwent some change when wear tested, specifically when the polymer material transferred to the bottom roller. The shift in the Amide II linkages (Figure 3.49) was observed when comparing the film from the worn bottom roller to an as-sprayed nylon film. This shift illustrated a change in the order of the nylon structure. When the nylon coating was wear tested the applied loads caused it to increase its crystalline order to reduce energy. The material became increasingly ordered as it approached the surface, where it was worn away yielding a new surface, and so on. Fresh, highly ordered material was constantly being exposed.

The ordering or alignment came as a result of amorphous regions yielding to the individual crystals. In the orthorhombic structure of nylon long chains can extend beyond their 'grains' and

into other 'grains'.¹⁰⁶ Between the individual crystals there exist amorphous regions. These regions will yield under load to allow individual crystal to align themselves. This alignment requires a bulk of material to generate the necessary local stresses. The random wear particles which transfer to the bottom roller never generate a thick film. Thus, the driving force is not large enough to align the highly random conglomeration of particles.

The observations and analysis of the polymer films demonstrated that the spray process had minimal effect on their structure. Not until the polymer was worn did it change, and how significant this change was is unknown. In plasma spraying the nylon was exposed to UV radiation and very high temperatures. If other, less intense, spray processes were used it is probable the polymer would behave the same.

4.4.10 Synopsis

The nylon /308 L-Si stainless steel coating was the most successful system. The durability was excellent, exceeding 13K revolutions under extreme contact conditions. The polymer system also displayed the best friction control. By having the lubricant film reside over the steel coating as opposed to being dispersed within it the nature of the wear process was changed. The polymer film survived the longest when tested dry and was not effective when reapplied. A consistent degradation behavior was observed between polymers. The nylon amide structure was not changed until it was transferred to the bottom roller during wear testing, and then only slightly. Polymer films and their wear behavior are based on empirical observations. Further analysis is necessary to understand the wear behavior at a crystalline or molecular level.

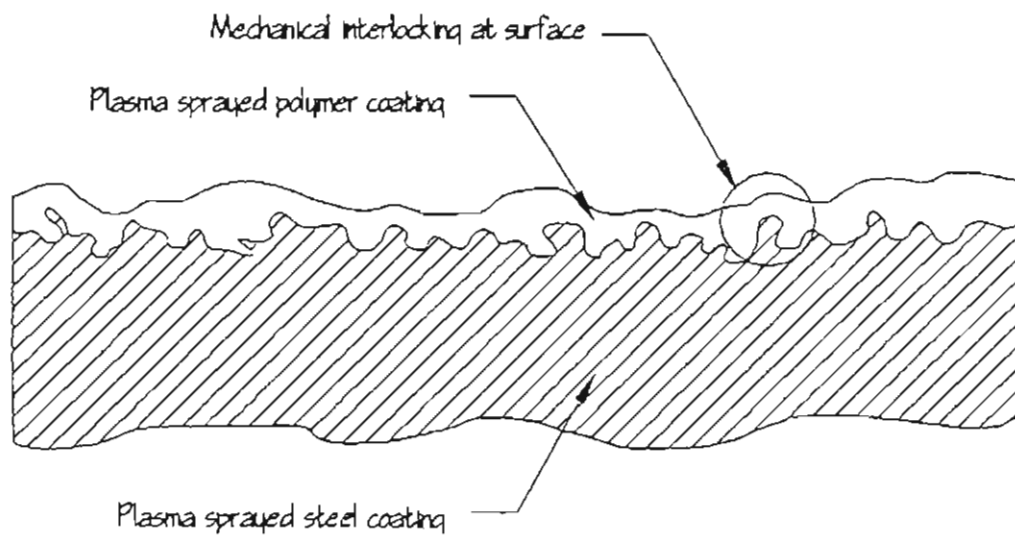


Figure 4.13. Schematic drawing showing the surface topography of a plasma sprayed steel coating.¹³⁶ The polymer coating is adhered to the surface by the peaks and troughs.

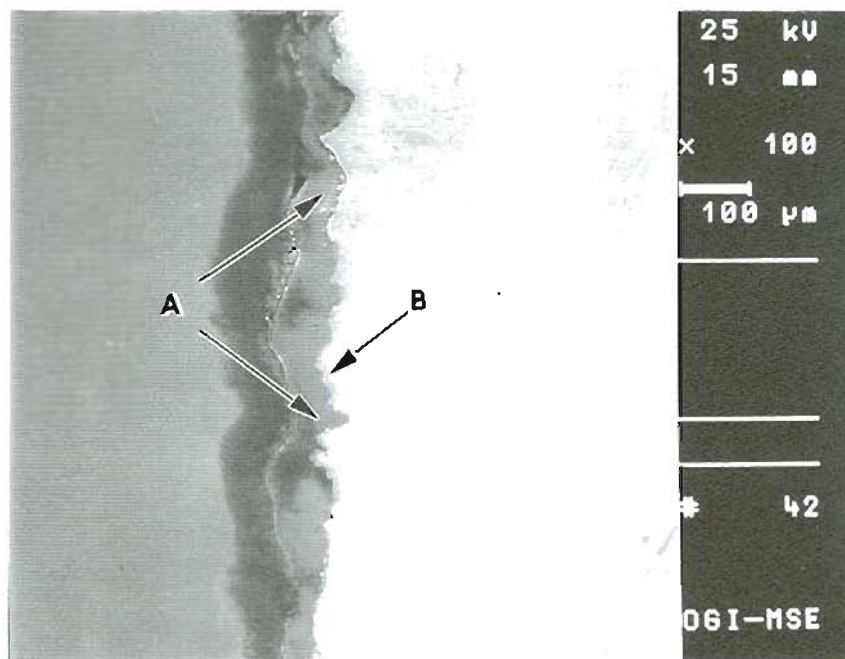
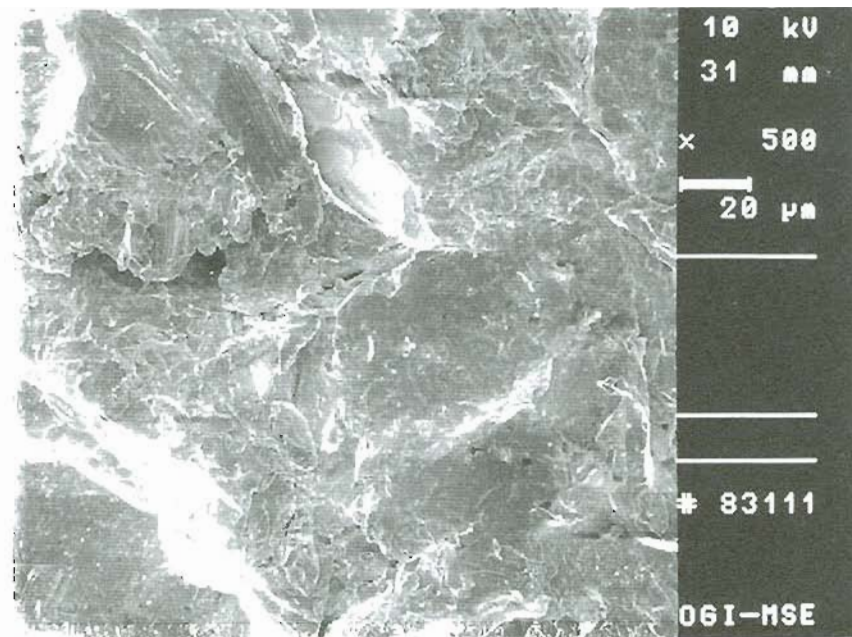
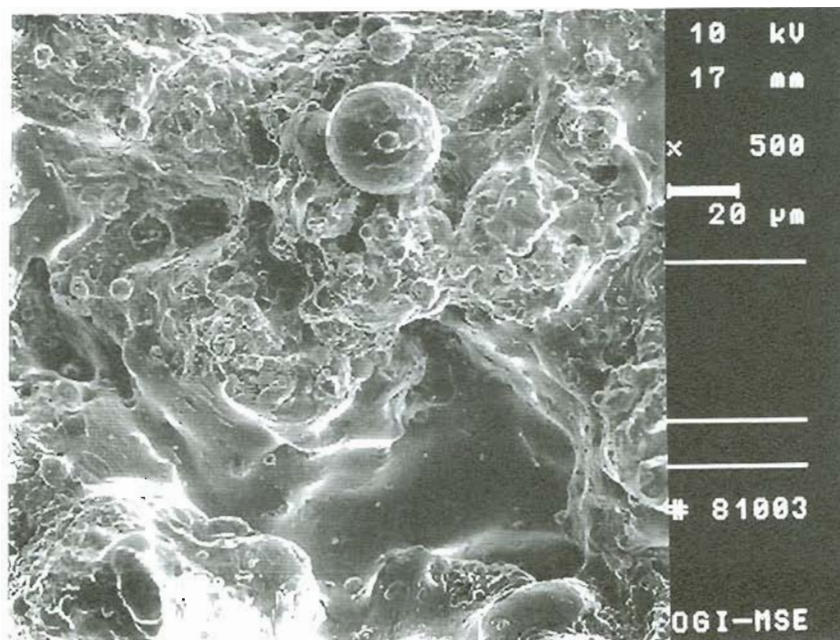


Figure 4.14. SEM photograph of nylon / 1080 steel coating showing polymer (A) and steel coating (B) interface.¹⁷⁹ Note the surface roughness of the steel coating which gives nylon its excellent adhesion.



(a)



(b)

Figure 4.15. SEM photographs illustrating two surface textures.¹⁸⁰
a) Grit blasted surface (alumina, 36 grit). b) Plasma sprayed surface. Note difference in peak to valley height for the plasma sprayed surface. 500x.

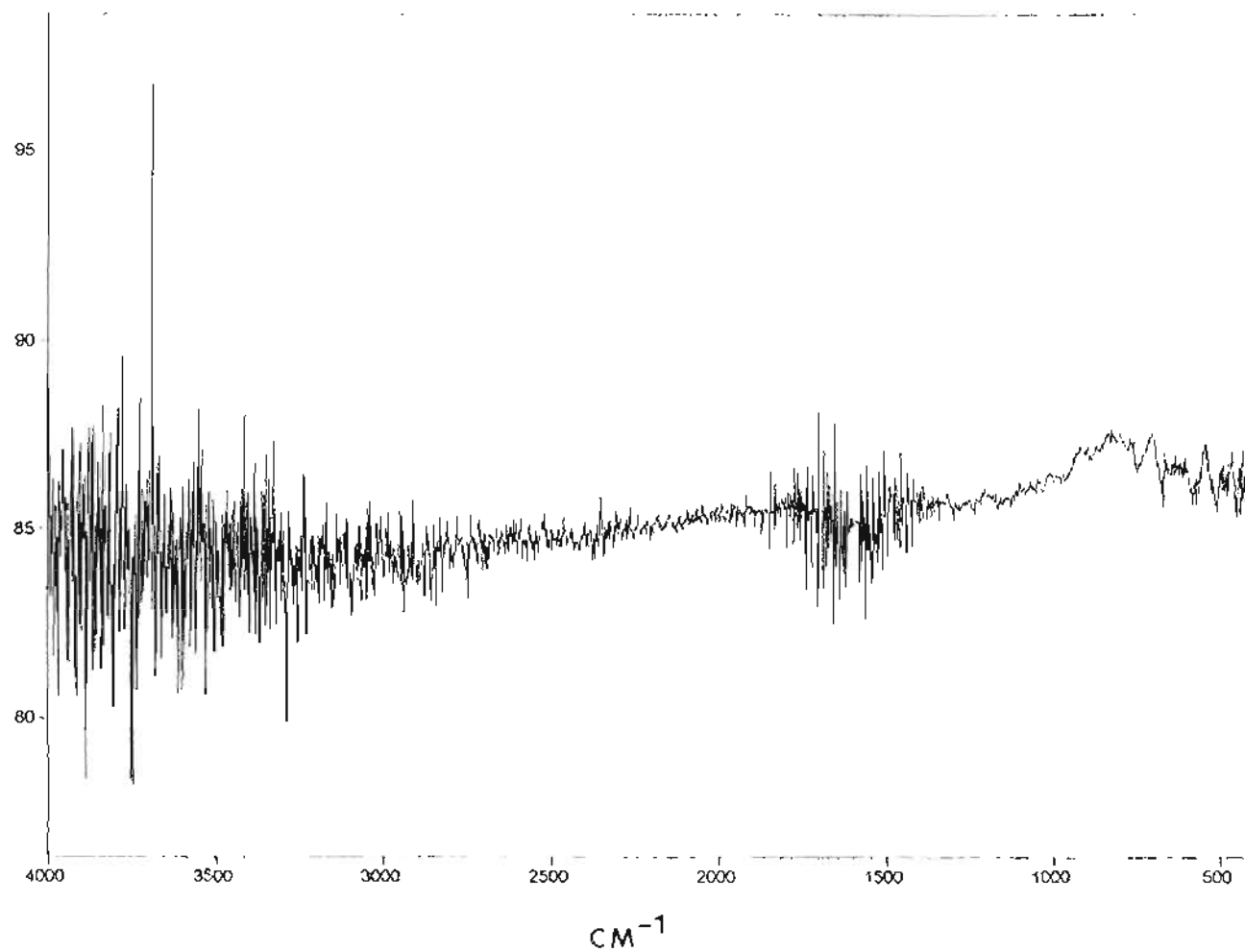


Figure 4.16. FTIR spectra of as-sprayed nylon film, using ATR. The spectra illustrates the result of massive overheating of nylon (dark brown to black in color). None of the characteristic peaks (Amide I, II, etc.) are present because the structure has been completely destroyed.

4.5 Steel Coating Deposition on Rail

The next step of developing a plasma sprayed coating on Amsler rollers was to successfully deposit it on a rail head. The coating procedure required changes in fixturing to accommodate the larger scale. Greater changes were also needed in the spraying parameters. Testing allowed the coating microstructure to be modified or optimized to accommodate the rail surface. The large scale performance of these coatings is the first test as to whether they will be practical in the field. A description of the tests utilized is given, along with a discussion of the results.

4.5.1 Parameter Optimization

The geometric difference between Amsler rollers and a rail head affected the coating's microstructure. Early track lab samples had poor performance. Metallography revealed a high volume fraction of oxide and numerous cracks within the oxide. The microstructure was not the same as an Amsler roller sprayed under similar gas parameters and working distance. Adjustments were made in each parameter to assess the individual effect on microstructure. The effect, positive or negative was determined through visual microscopy. It was believed decreasing oxide and porosity would improve coating performance. Performance tests for each parameter variation were not done as only a limited number of large scale tests were possible. Consequently, the new ideal coating parameters were based solely on SEM analysis.

The variation of parameters came as increases and decreases in the gas flow rates of nitrogen and hydrogen, and working distances. The changes were with respect to the standard 230 slpm N_2 / 30 slpm H_2 , 235 mm working distance. When nitrogen was both increased and decreased, the effect was an increased volume of porosity. The volume fraction of oxide appeared to be unchanged. Nitrogen is used to provide the primary plasma gas for the system.

When total gas flow is decreased the exit plasma has a higher enthalpy. The increased thermal energy could vaporize the smaller, ideal particles, reducing the coating's integrity. A change in working distance increased the porosity volume fraction, but had little effect on the oxide volume fraction. An increase in unmelted particles was observed when working distance was increased. This may be due to particles cooling to a semi-molten, plastic state prior to impact on the substrate.

The change in hydrogen flow rate was the most dramatic. When H₂ was eliminated from the system (flow = 0), both porosity and oxide volume fraction increased. As hydrogen increased the volume of oxide and porosity decreased. The optimum H₂ flow rate was between 50 and 100 slpm, with 75 slpm appearing to be the best. When H₂ flow rate was increased to over 100 slpm, the microstructure degraded via larger voids and larger oxide volume. Hydrogen as a secondary gas increased arc voltage and plume enthalpy. It also acted to create a reducing environment. This reducing environment would minimize oxidation. When too much hydrogen was present though, the reducing benefit was minimized. This is due to the limited amount of oxygen available to be reacted with or 'gettered'. H⁺ ions are very reactive and a surplus of them appeared to create unfriendly plume conditions.

Determining ideal plasma gun operation was strictly empirical and required extensive investigation. The additive effects of ionized plasma gas behavior, electron behavior, and particle interaction, cloud the understanding of what is taking place as a coatings is deposited. When parameters are not ideal the coating may have poor structure and/or wear performance. Determining which parameter change, if any, will improve the coating can only be found by trial and error. This experiment illustrated the need for reoptimization when the substrate geometry changes dramatically, and further illustrates how complex the plasma system can become.

4.5.2 Large Scale Testing

The three full scale tests included: the track lab, rolling load machine, and FAST implant. The track lab test consisted of a short length of track which is raised on each end. The coupons are placed in the center portion of the track. The geometry of a track lab coupon was illustrated in Figure 2.11. A four axle, 263,000 lb car runs back and forth over the coupons, at a speed of 10-15 mph. Durability was measured in cycles, which is multiplied by the load to give million gross tons (mgt).

The rolling load machine consists of a 36 inch diameter cylindrical wheel which rolls backwards and forwards over the rail head. The wheel travels over the rail, which is fixed on the machine bed, at 10 in/s. Two vertical actuators acting through the rail apply a vertical load up to 80 kips. A third actuator can apply a horizontal load and to maximize contact stresses, the rail can be tilted 45°. Tilting the rail increases contact at the gage corner, which better simulates conditions in the field.

The FAST implant test consisted of bolting a 12 foot section of coated rail onto a test loop. The train had four locomotives and 75 loaded cars, yielding 316 axles of 78 kips per train pass. The curvature of the track was 2 to 3° in the location of the FAST implant.

The track lab coupons which were spray coated with steel had poor initial performance, as shown in Table 3.35b. Sample RLM1 was 1 to 1.5 mm thick and had the unoptimized coating microstructure. The surface preparation was limited to only alumina grit shot blasting. Track Lab coupons TL1 and TL2 also had poor microstructures due to the unoptimized gas parameters. Both samples had a coating thickness greater than 1 mm. Feathering the coating thickness at the ends of the coupon in TL2 improved the durability over TL1. The coating had very little strength when a shear load was applied. The nature of the track lab test would allow side impact of the coating if the coupon was not flush with the rest

of the track. When the ends were feathered, the mismatch would be minimized.

Track Lab coupons TL3 and TL4 were sprayed using the optimized spray parameters. The surface preparation involved cleaning of the surface with alumina and texturing with steel shot. Tests have shown this yields the roughest surface and improves steel coating adhesion.¹⁸⁰ TL3 was sprayed with a 308 stainless steel as opposed to a 1080 steel, to compare performance. Stainless steel forms a very tenacious oxide layer. It was hypothesized this would improve its debonding resistance. Both TL3 and TL4 were coated with nylon to measure the durability and friction reduction of a nylon / steel coating when subjected to larger scale testing. These samples marked the reduction of coating thickness to 0.25 - 0.5 mm for improved debonding resistance.

The full scale track samples were coated in two areas to maximize testing. RLM2 through RLM5 consisted of a 1 mm and 0.5 mm 1080 steel coating overlaid with a 30-50 μm nylon coating. Table 3.35a and b summarized the test parameters and results. Both new and worn head hardened rail were used to assess the effect of substrate hardness and subtle geometric changes on coating performance. The differences in steel coating thickness allowed for a direct comparison of coating performance as a function of thickness. Both coatings had identical surface preparation, spray procedure and ambient conditions. As these coatings were deposited within a short span of each other the preparation and deposition procedure remained identical, and human inconsistencies were minimized.

The last full scale sample was a 12' rail. This sample required an interrupted spray to vary the working distance. This may have an effect as it creates a second interface. A second interface has not been shown to adversely effect a coatings performance, but it is not thought to improve it. The steel thickness was more difficult to control because of coating deposition rate fluctuations, which were caused by multiple rail head rotations and the awkward size of the

sample. In spite of this, coating thickness is estimated to be 0.25 - 0.5 mm. This FAST implanting allowed the rail will be tested on both the top and the gage face for friction and wear performance.

The full scale tests gave a good understanding to the behavior of the laboratory developed coating. The mechanisms of failure were similar to that seen when Amsler testing. The coatings debonded, and durability was reduced as the steel coating thickness increased. The polymer film appeared to wear away prior to steel coating failure. The full understanding of the failure analysis is a study onto itself, but initial results follow the pattern of laboratory observations. The large scale tests give hard data as to the success of nylon / steel coating system in transitioning from the laboratory to the field. The initial results are promising with respect to the expectations of industry. Further development is necessary before full transitioning of the coating system to the field can be accomplished.

Chapter Five Conclusions

1) Graphite / 1080 steel coatings

Nickel-coated graphite was readily retained in 1080 steel coatings. The durability was 10-15k revolutions for 0.5 mm and 0.25 mm thick coatings, when creep remained around 5%, with a contact pressure of 1220 N/mm² and below. The friction coefficient was 0.14.

The wear mechanisms consisted of particle pull-out caused by crack networks and edge effects.

Nickel-graphite volume fractions between 6-12% had the best performance. Below 3%, friction reduction was minimal and above 12%, the wear rate increased.

Certain contact conditions lessened the friction reduction ability of nickel-graphite. These included increased sliding speed between rollers (creep or RPM) and any increase in surface roughness of the bottom roller.

Severe contact conditions (35% Creep and $P_o > 1220$ N/mm²) produced rapid coating degradation.

Graphite powder was not a viable material for coating production as it was difficult to retain.

Nickel-graphite / 1080 steel coatings had excellent durability when contact condition were mild. (Creep < 8% and $P_o < 1220$ N/mm²).

2) Copper / 1080 steel coatings

Copper wire when co-deposited with 1080 steel produced large copper volume fraction (30-60%) coatings. Copper powder allowed a broader volume fraction (6%-40%) of copper to be retained.

The durability was low (>2000 revolutions), with minimal friction reduction ($\mu=0.37$) in some tests. Material transfer to the bottom roller occurred in proportion to the retained copper volume fraction.

Twin wire spraying illustrated wire interaction within the plasma plume. Interaction was minimized when wire injection distance was offset by 12 mm or more.

3) Polymer / Steel Coatings

Excellent durability at $P_o= 1220 \text{ N/mm}^2$ and 35% creep was achieved by nylon and UHMW when deposited over a 1080 steel or 308 L-Si stainless steel coating.

The best performing coating was nylon / 0.25 mm stainless steel with a durability of 12-14k revolutions, with friction increasing from 0.10 at test onset to 0.25-0.30 at test termination

Seven stages of wear were identified in the polymer system. These generally appeared to be consistent regardless of the polymer type or steel coating thickness.

The incidence of debonding was minimized by reducing steel coating thickness to 0.25 mm instead of 1 mm.

Preliminary tests of polymer / steel coatings in the field have shown some friction reduction with promising durability. Further evaluation is necessary to claim success or failure.

Chapter Six Synopsis

6.1 Future Work

The analysis of the steel coatings containing graphite, copper, or a polymer raised a windfall of questions. A separate thesis could have been dedicated to each system in order to completely understand the wear behavior. Many of the questions were academic, in that the discovery of their answer would not improve the coatings performance. Some question though, may offer some greater insight as to the behavior of the coating systems and also offer means of improving coating performance.

In the graphite / steel system, graphite was the cause of a large quantity of initiated cracks in the coating. If a tougher, more wear resistant matrix were used, would it increase the coating life? Perhaps a high strength (i.e. SAE 4340) steel or a superalloy would provide better toughness against crack propagation between graphite particles. Also, at what creepage does the graphite lose its ability to lubricate? Wear tests using creep values varying from 5% to 35% in increments of 1% could reveal the critical creep where the film ceases to lubricate. The film would probably become less and less effective, with the average friction coefficient rising, as creep was increased. In addition, a range of nickel-graphite powder (50 μm -500 μm) may yield a relationship between mean particle size and durability. Finally, further understanding of the graphite film with respect to the film's thickness and structure may offer clues to how its life may be extended.

Future work with copper as a lubricant for rolling/sliding contact could focus on the transfer of material and how it affects

durability. A closer study of the relationship between contact conditions and volume fraction may yield a better understanding of why these coatings failed. Copper / steel coatings could be tested in an open system to eliminate the buildup of transferred material. However, copper as a lubricant under these contact conditions has not shown any optimistic performance and is, in the opinion of the author, completely unsuitable for wheel/rail interaction.

The polymer / steel system could benefit the greatest from future work. Continued study of the optimum surface roughness may increase durability. Reproducing the steel coating's surface texture may eliminate the need for a metal coating. There are many types of polymers available. A broader study of polymer types could be of benefit. Increasing the steel coating durability may allow multiple redeposition of polymer. This comes under the guise that the steel coating's surface can be retextured to that of a freshly sprayed coating. Tests in the field should continue, with large sections of track being coated. Field testing will give better clues to the degradation process of the coating and may offer solutions to overcome them.

6.2 Final Comments

In a dissertation it is commonly expected that the results will yield new, discovered information. The scope being to expand on related work and in most cases break new ground. The goals in the beginning of the project were to develop a self lubricating coating using the existing 1080 steel coating matrix. This coating would have to endure high contact pressures and creepages. This left a wide envelope for possible materials and coating systems. The analysis of the three systems attempted to characterize the coatings and provide a foundation for predicting the behavior of other similar coatings.

The three specific systems: graphite, copper and polymers were decided upon because of their diverse wear behavior. In

essence if one system failed, its shortcoming would not influence the whole project. This was clearly evident with the copper / steel coating system. The failure to lubricate or illustrate friction reduction under these severe conditions did not discourage the investigation of polymers or graphite. Graphite had a completely different lubrication behavior, slip of the crystal structure. The polymers utilized their inherent low wear rate and durability.

Thermal sprayed coatings as a whole have undergone intensive investigation, but the applications have been very specific. The testing of sprayed coatings under rolling/sliding contact was uncharted territory. As a result promising leads were followed and abandoned if shown to be unsuccessful. This was balanced though by investigation of why the system failed. It was known early on that copper would not be suitable for the end use of wheel/rail interaction. Nonetheless, it was investigated so that the wear mechanisms and failure of the coating could be understood.

The industrial applications of this project focused on the railroad industry. The coating parameters and performance was tailored around rail deposition for wheel/rail contact. Even if the most suitable coating system (nylon / stainless steel) is never applied to a rail in the field, other applications may be realized. The severe environment of wheel/rail contact may have indirectly provided accelerated testing results for the coating utilized elsewhere, e.g. a high load, pure rolling bearing.

Overall these coatings were an attempt to reduce or eliminate the need for outside lubrication in a rolling wear condition. Since these conditions exist in many places, many applications can be found. This study provides the groundwork for future coatings in the diverse area of rolling / sliding contact. It also offers insight how other coatings may behave at low load sliding conditions.

Though the results were poor for some coating systems the contact conditions were about as severe as can be. Metals and some other materials under these same conditions in general, would disintegrate at a rate of 10 to 10,000 times greater!

References

1. Jamison W., "Wear of steel in combined rolling and sliding," *ASLE Transactions*, Vol. 25, No. 1, 1980, pp. 71-78.
2. *Mechanisms of Low Rail Rollover*, Videocassette, Association of American Railroads, Pueblo, CO., 1990.
3. McMurchie, D., "Development of a 1080 Steel Plasma Sprayed Coating for Slide/Roll Wear Conditions," Ph.D. Thesis, Department of Materials Science & Engineering, Oregon Graduate Institute of Science and Technology, 1996.
4. Pritchard, C., "Traction between rolling steel surfaces: a survey of railway and laboratory experiments," *Proceedings of the 7th Leeds-Lyon Symposium on Tribology: Tribology Friction and Traction*. British Railways Board, Paper VIII (i), 1981, pp. 197-206.
5. Rigney, D.A., "Plastic Deformation and Sliding Friction of Metals," *Wear*, Vol. 53, 1979, pp. 345-370.
6. Teer, D.G. and Arnell, R.D., "Friction Theories," *Principles of Tribology*, J. Halling, Ed., MacMillan Press, New York, 1978, pp.72-91.
7. Bowden, F.P. and Tabor, D., *The Friction and Lubrication of Solids*, Oxford University Press, Great Britain, 1986, pp. 85-119.

8. Brockley, C.A. and Davis, H.R., "The Time-Dependence of Static Friction," *Journal of Lubrication Technology*, Jan. 1968, pp. 35-41.
9. Johnson, K.L., "Aspects of Friction," *Proceedings of the 7th Leeds-Lyon Symposium on Tribology: Tribology Friction and Traction*. British Railways Board, Paper I (i), 1981, pp. 3-12.
10. Archard, J.F., "Elastic Deformation and the Laws of Friction," *Proceedings of the Royal Society*, London, Vol. 243, Series A, 1957, pp. 190-205.
11. Gupta, P.K. and Cook, N.H., "Junction Deformation Models for Asperities in Sliding Interactions," *Wear*, Vol. 20, 1972, pp. 73-87.
12. Burwell, J.T. and Rabinowicz, E. "The Nature of the Coefficient of Friction," *Journal of Applied Physics*, Vol. 24, 1953, pp. 136-139.
13. Bush, A.W., Gibson, R.D., and Thomas, T.R., "The Elastic Contact of a Rough Surface," *Wear*, Vol. 35, 1975, pgs. 87-111.
14. Bowden, F.P. and Tabor, D., *The Friction and Lubrication of Solids*, Oxford University Press, Great Britain, 1986, pp. 60-79.
15. Rabinowicz, E., "Compatibility Effects when Soft Metals are Used as Solid Lubricants," NBS special publication, No. 452, Washington. D.C., 1976, pp. 72-83.
16. Suh, N. P. and Sin, H.C., "The Genesis of Friction," *Wear*, Vol. 69, 1981, pp. 91-114.

17. Peterson, M.B., "Wear Testing and Approaches," *Source Book on Wear Control Technology*, D.A. Rigney and W.A. Glaeser, Ed., American Society of Metals, Ohio, 1978, pp. 40-48.
18. Eyre, T.S., "Wear Characteristics of Metals," *Source Book on Wear Control Technology*, D.A. Rigney and W.A. Glaeser, Ed., American Society of Metals, Ohio, 1978, pp.1-10.
19. Swain, M.V., "Microscopic Observations of Abrasive Wear of Polycrystalline Alumina," *Wear*, Vol. 35, 1975, pp. 185-189.
20. Dean, S.K. and Doyle, E.D., "Significance of Grit Morphology in Fine Abrasion," *Wear*, Vol. 35, 1975, pp. 123-129.
21. Hurricks, P.L., "The Fretting Wear of Mild Steel from 200° to 500° C," *Wear*, Vol. 30, 1974, pp. 189-212.
22. Waterhouse, R.B., "Fretting in Hostile Environments," *Wear*, Vol. 34, 1975, pp. 301-309.
23. Bitter, J., "A Study of Erosion Phenomena," *Wear*, Vol. 6, 1963, pp. 5-21.
24. Finnie, I., "Erosion of Surfaces by Solid Particles," *Source Book on Wear Control Technology*, D.A. Rigney and W.A. Glaeser, Ed., American Society of Metals, Ohio, 1978, pp. 220-236.
25. Blau, P.J., "Rolling Contact Wear," *Friction, Lubrication, and Wear Technology*, ASM Handbook, Vol. 18, 10th Ed., ASM International, Materials Park, Ohio, 1992, pp. 257-262.

26. Su, X., "Surface Initiated Rolling/Sliding Contact Fatigue in Pearlitic and Low Carbon Bainitic Steels," Ph.D. Thesis, Department of Materials Science & Engineering, Oregon Graduate Institute of Science and Technology, 1996.
27. Krause, H. and Poll, G., "Wear of Wheel-Rail Surfaces," *Wear*, Vol. 113, 1986, pp.103-122.
28. Hirvonen, J.P., Kauppinen, P., Andersson, P., et. al., "Elastic and Dry Sliding Characteristics of HVOF-Sprayed Al_2O_3 and Al_2O_3 - TiO_2 Coatings," *Thermal Spray Coatings: Research, Design, and Applications*, Proceedings of the 5th National Thermal Spray Conference, C.C. Berndt and T.F. Bernecki, Ed., ASM International, Materials Park, Ohio, 1993, pp. 475-485.
29. Fessenden, K.S., Zurecki, Z., Slavin, T.P., "Sliding Wear Resistance of Electric Arc Sprayed Coatings," *Thermal Spray Coatings: Properties, Processes, and Applications*, Proceedings of the 4th National Thermal Spray Conference, T.F. Bernecki, Ed., ASM International, Materials Park, Ohio, 1991, pp. 81-88.
30. Suh, N.P., *Tribophysics*, Prentice-Hall Inc., New Jersey, 1986, pp. 11-20.
31. Bowden, F.P. and Tabor, D., *The Friction and Lubrication of Solids*, Oxford University Press, Great Britain, 1986, pp. 90-119.
32. Ludema, K.C., "Sliding and Adhesive Wear" *Friction, Lubrication, and Wear Technology*, ASM Handbook, Vol. 18, 10th Ed., ASM International, Materials Park, Ohio, 1992, pp. 236-241.

33. Suh, N.P., "The Delamination Theory of Wear," *Wear*, Vol. 25, 1973, pp. 111-124.
34. Nichols, Jr., C.W., "What Happens to a Lubricant in Service," *Standard Handbook of Lubrication*, J.J. O'Connor, Ed., McGraw-Hill Inc., 1968, pp.17.1-17.11.
35. Devanathan, R., "AAR Lubrication Study, Report #2," Dept. Materials Science & Engineering, Oregon Graduate Institute of Science and Technology, 1993, pp. 1-53.
36. Bolton, P. and Clayton, P., "Rolling-Sliding Wear Damage in Rail and Tyre Steels," *Wear*, Vol. 93, 1984, pp. 145-165.
37. Rabinowicz, F., *Friction and Wear of Materials*, J. Wiley and Sons, New York, 1965, pp. 27-43.
38. Bayer, R.G., Clinton, W.C., Nelson C.W., et al., "Engineering Model for Wear," *Wear*, Vol. 5, 1962, pp. 378-391.
39. Tabor, D., "Wear- A Critical Synoptic View," *Wear of Materials-1977*, ASME, New York, 1977, pp. 1-11.
40. Jamison, W.E., "The Wear of Railroad Freight Car Wheels and Rails," *Journal of the ASLE*, Vol. 36, No. 7, 1979, pp. 401-411.
41. Beagley, T.M., "Severe Wear of Rolling/Sliding Contact," *Wear*, Vol. 36, 1976, pp. 317-335.
42. Cheng, H.S., "Introduction to Lubrication" *Friction, Lubrication, and Wear Technology*, ASM Handbook, Vol. 18, 10th Ed., ASM International, Materials Park, Ohio, 1992, pp. 79-80.

43. Fein, R.S., "Liquid Lubricants," *Friction, Lubrication, and Wear Technology*, ASM Handbook, Vol. 18, 10th Ed., ASM International, Materials Park, Ohio, 1992, pp. 81-88.
44. Hamrock, B.J. and Dowson, D., "Isothermal Elastohydrodynamic Lubrication of Point Contacts, Part III- Fully Flooded Results," *Journal of Lubrication Technology, ASME Transactions*, Vol. 99, 1977, p. 264.
45. Wills, G.J., *Lubrication Fundamentals*, Marcel Dekkar Inc., New York, 1980, pp. 60-61.
46. Campbell, W.E., "Solid Lubricants," *Standard Handbook of Lubrication*, J.J. O'Connor, Ed., McGraw-Hill Inc., New York, 1968, p. 11.13.
47. Johnson, K.L., *Contact Mechanics*, Cambridge University Press, New York, 1985, pp. 90-104.
48. Clayton, P. and Hill, D., "Rolling Contact Fatigue of Rail Steel," *Wear*, Vol. 117, 1987, pp. 319-334.
49. Kalker, J., "Wheel-Rail Rolling Contact Theory," *Wear*, Vol. 144, 1991, pp. 243-261.
50. Campbell, W.E., "Solid Lubricants," *Standard Handbook of Lubrication*, J.J. O'Connor, Ed., McGraw-Hill Inc., 1968, pp. 11.1-11.6.
51. Sliney, H.E., "Solid Lubricants," *Friction, Lubrication, and Wear Technology*, ASM Handbook, Vol. 18, 10th Ed., ASM International, Materials Park, Ohio, 1992, pp. 113-122

52. Lancaster, J.K., "Lubrication by Transferred Films of Solid Lubricants," *ASLE Transactions*, Vol. 8, 1965, pp. 146-155.
53. Stachowiak, G.W. and Batchelor, A.W., *Engineering Tribology*, Tribology Series 24, Elsevier Scientific Publishing Co., New York, 1993, p. 490.
54. Gardos, M.N., "The Synergistic Effects of Graphite on the Friction and Wear of Molybdenum Disulphide Films in Air," *Tribology Transactions*, Vol. 31, 1988, pp. 214-227.
55. Baily, A.I. and Courtney-Pratt, J.S., "Real Contact and Shear Strength of Monomolecular Layers," *Proceedings of the Royal Society*, London, Vol. 227, Series A, 1955, pp. 500-515.
56. Bowden, F.P. and Tabor, D., *Friction and Lubrication of Solids, Part 2*, Oxford University Press, 1964, pp. 120-145.
57. Deacon, R.F. and Goodman, J.F., "Lubrication by Lamellar Solids," *Proceedings of the Royal Society*, London, Vol. 243, Series A, 1958, pp. 464-482.
58. Stachowiack, G.W. and Batchelor, A.W., *Engineering Tribology*, Tribology Series 24, Elsevier Scientific Publishing Co., New York, 1993, p. 486.
59. Iliuc, I., *Tribology of Thin Layers*, Elsevier Scientific Publishing Co., New York, 1980.
60. Sargent, L.B., "Lubricants", *Tribology, Friction, Lubrication, and Wear*, A.Z. Szeri, Ed., Hemisphere Pub. Corp., New York, 1979, pp. 427-440.

61. Bryant, P.J., Gutshall, P.L., and Taylor, L.H., "A Study of Mechanisms of Graphite Friction and Wear," *Wear*, Vol. 7, 1964, pp. 118-126.
62. Campbell, W.E. and R. Kozak. "The Wear of Carbon Brushes in Dry Atmosphere," *ASME Transactions*, Vol. 70, 1948, p. 491.
63. Sliney, H.E., "Dynamics of Solid Lubrication as observed by Optical Microscopy," *ASLE Transactions*, Vol. 21, 1978, pp. 109-117.
64. Tsuya, Y., "Lubrication with Molybdenum Disulfide Film Under Various Conditions," *ASLE Transactions*, Vol. 15, 1972, pp. 225-232.
65. Farr, J.P.G., "Molybdenum Disulphide in Lubrication: A Review," *Wear*, Vol. 35, 1975, pp. 1-22.
66. Gardos, M.N., "The Synergistic Effects of Graphite on the Friction and Wear of Molybdenum Disulphide Films in Air," *Tribology Transactions*, Vol. 31, 1988, pp. 214-227.
67. Haltner, A.J. and Oliver, C.S., "Frictional Properties of Some Solid Lubricant Films under High Load," *Journal of Chemical Engineering Data*, Vol. 6, 1961, pp. 128-130.
68. Feng, I.M., "Lubricating Properties of Molybdenum Disulfide," *Lubrication Engineering*, Vol. 8, No. 6, 1952, p. 285.
69. McCain, J.W., "A Theory and Tester Measurement Correlation About Molybdenum Disulphide Dry Film Lubricant Wear," *Journal of the Society of Aerospace, Material, and Process Engineers*, Vol. 6, 1970, pp. 17-28.

70. Johnson V.R. and G.W. Vaughn. "Investigation of the Mechanism of Molybdenum Sulfide Lubrication in Vacuum," *Journal of Applied Physics*, Vol. 27, No 10, 1956, p. 1173.
71. Bartz, W.J. and Xu, J., "Wear Behaviour and Failure Mechanism of Bonded Solid Lubricants," *Lubrication Engineering*, Vol. 43, 1987, pp. 514-521.
72. Schey, J.A., *Tribology in Metalworking*, ASM International, Materials Park, Ohio, 1983, p. 43.
73. Bowden, F.P. and Tabor, D., *Friction and Lubrication of Solids*, Oxford University Press, 1977, p. 287.
74. Stachowiack, G.W. and Batchelor, A.W., *Engineering Tribology*, Tribology Series 24, Elsevier Scientific Publishing Co., New York, 1993, p. 487.
75. Stachowiack, G.W. and Batchelor, A.W., *Engineering Tribology*, Tribology Series 24, Elsevier Scientific Publishing Co., New York, 1993, p. 498.
76. Miyake, S. and Takahashi, S., "Small-Angle Oscillatory Performance of Solid-Lubricant Film-Coated Ball Bearings for Vacuum Applications," *ASLE Transactions*, Vol. 30, 1987, pp. 248-253.
77. Sliney, H.E., "The Use of Silver in Self-Lubricating Coatings for Extreme Temperatures," *ASLE Transactions*, Vol. 29, 1986, pp. 370-376.

78. Sliney, H.E., "Self-lubricating Composites of Porous Nickel and Nickel-Chromium Alloy Impregnated with Barium Fluoride Calcium Fluoride Eutectic", *ASLE Transactions*, Vol. 9, 1966, pp. 336-347.
79. Dellacorte, C. and Sliney, H.E., "Composition Optimization of Self-Lubricating Chromium-Carbide Based Composite Coatings for Use to 760° C," *ASLE Transactions*, Vol. 30, 1987, pp. 77-83.
80. Bowden, F.P. and Tabor, D., *The Friction and Lubrication of Solids.*, Oxford University Press, New York, 1954, pp. 146-153.
81. Campbell, W.E., "Studies in Boundary Lubrication ,1,". *ASME Transactions*, Vol. 61, 1939, p. 633.
82. Cocks, M., "The role of Atmospheric Oxidation in High Speed Sliding Phenomena, II," *ASLE Transactions*, Vol. 1, No. 1, 1958, p. 101.
83. Whitehead, J.R., "Surface Deformation and Friction of Metals at Light Loads," *Proceedings of the Royal Society*, London, Vol. 201, Series A, 1950, p. 109.
84. Ling, F.F., *Friction and Lubrication in Metal Processing* , ASME, New York, 1966, pp. 20-38.
85. Brick, R.M., Pense, A.W., and Gordon, R.B., *Structure and Properties of Engineering Materials*, 4th Ed., McGraw-Hill Co., New York, 1977, pp. 254-304.
86. Lancaster, J.K., "Basic Mechanisms of Friction and Wear of Polymers," *Plastics in Bearings Conference*, London, 1973, pp. 1-15.

87. Jain, V.K. and Bahadur, S., "Material Transfer in Polymer-Polymer Sliding," *Wear*, Vol. 46, 1978, pp. 177-198.
88. Blanchet, T.A., "The Mild/Severe Wear Transition of PTFE Polymers in Oscillatory Contacts," *Wear of Materials*, ASME International Conference on Wear of Materials, 1991, pp. 34-45.
89. Makinson, K.R. and Tabor, D., "The Friction and Transfer of PTFE," *Proceedings of the Royal Society*, London, Vol. 281, Series A, 1964, pp. 49-61.
90. Tanaka, K., "Structure and Properties of Polymers Important to their Wear Behavior," *Tribology in the 80's*, Proceedings of an International Conference, NASA Conference Publication 2300, Vol. 1, 1983, pp. 253-289.
91. Tanaka, K. and Kawakami, S., "Effects of Various Fillers on the Friction and Wear of Polytetrafluoroethylene-Based Composites," *Wear*, Vol. 79, 1982, pp. 221-234.
92. Low, M.B., "The Effect of the Transfer Film on the Friction and Wear of Dry Bearing Materials for a Power Plant Application," *Wear*, Vol. 52, 1979, pp. 347-363.
93. Bhushan, N.A. and Wilcock, D.F., "Frictional Behavior of Polymeric Compositions in Dry Sliding," *Proceedings of the Seventh Leeds-Lyon Symposium on Tribology*, Westbury House, IPC Business Press, England, 1981, pp. 103-113,
94. Bunn, C.W. and Howells, E.R., "Structures of Molecules and Crystals of Fluorocarbons," *Nature*, Vol. 174, 1954, pp. 549-551.

95. Buckley, D.H., *Surface Effects in Adhesion, Friction, Wear and Lubrication*, Elsevier Scientific Publishing Co., New York, 1981, pp. 134-152.
96. Gong, D., Xue, Q, and Wang, H., "ESCA Study on Tribochemical Characteristics of Filled PTFE," *Wear*, Vol. 148, 1991, pp. 161-169.
97. Makinson, K.R. and Tabor, D., "The Friction and Transfer of Polytetrafluoroethylene," *Proceedings of the Royal Society*, London, Vol. 281, Series A, 1964, pp. 58-61.
98. Pooley, C.M. and Tabor, D., "Friction and Molecular Structure: the Behaviour of some Thermoplastics," *Proceedings of the Royal Society*, London, Vol. 329, Series A, 1972, pp. 251-274.
99. Tanaka, K., *Effects of Various Fillers on the Friction and Wear of PTFE-Based Composites*, in *Composite Material Science*, K. Friedrich, Ed., Elsevier Scientific Publishing Co., New York, 1986, pp.137-174.
100. Stachowiack, G.W. and Batchelor, A.W., *Engineering Tribology*, Tribology Series 24, Elsevier Scientific Publishing Co., New York, 1993, p. 719.
101. Egelman, N., "Engineering Plastics for the Automotive Industry," *Advanced Materials & Processes*, Vol. 149, No. 5, May 1996, pp. 35-37.
102. Smith, W.F., *Principles of Materials Science and Engineering*, McGraw-Hill Inc., New York, 1986, pp. 299-361.

103. Dumbleton, J.H. and Shen, C., "The Wear Behavior of Ultrahigh Molecular Weight Polyethylene," *Wear*, Vol. 37, 1976, pp. 279-288.
104. Atkinson, J.R., Brown, K.J., and Dowson, D., "The Wear of High Molecular Weight Polyethylene, Part 1: The Wear of Isotropic Polyethylene Against Dry Stainless Steel in Unidirectional Motion," *Journal of Lubrication Technology*, ASME Trans., Vol. 100, 1978, pp. 208-218.
105. Stevens, M.P., *Polymer Chemistry: An Introduction*, 2nd Ed., Oxford University Press, New York, 1990, pp. 511-583.
106. Russell, G., Cascade Materials R & D, Inc., Private Communication, 1997.
107. Briscoe, B., "Wear of Polymers: An Essay on Fundamental Aspects," *Tribology International*, Vol. 14, 1981, pp. 231-243.
108. Tanaka, K. and Miyata, T., "Studies on the Friction and Transfer of Semi-Crystalline Polymers," *Wear*, Vol. 41, 1977, pp. 383-398.
109. Birkett, A. and Lancaster, J.K., "Counterface Effects on the Wear of a Composite Dry-Bearing Liner," *Proceedings of the JSLE Int. Tribology Conference*, Tokyo, Japan, Elsevier Scientific Publishing Co., July 1985, pp. 465-470.
110. Barrett, T.S., Stachowiak, G.W., and Batchelor, A.W., "Effects of Roughness and Sliding Speed on the Wear and Friction of Ultra-High Molecular Weight Polyethylene," *Wear*, Vol. 153, 1992, pgs. 331-350.

111. Pooley, C.M. and Tabor D., "Friction and Molecular Structure: The Behaviour of Some Thermoplastics," *Proceedings of the Royal Society*, London, Vol. 329, Series A, 1972, pp. 251-274.
112. Eiss, N.S. and Bayraktaroglu, M.M., "The Effect of Surface Roughness on the Wear of Low Density Polyethylene," *ASLE Transactions*, Vol. 23, 1980, pp. 269-278.
113. Stachowiack, G.W. and Batchelor, A.W., *Engineering Tribology*, Tribology Series 24, Elsevier Scientific Publishing Co., New York, 1993, p. 721.
114. Blanchett, T.A. and Kennedy, F.E., "The Development of Transfer Films in Ultra-High Molecular Weight Polyethylene/Stainless Steel Oscillatory Sliding," *Tribology Transactions*, Vol. 32, 1989, pp. 371-379.
115. Eiss, N.S., Wood, K.C., Herold, J.A, et al., "Model for the Transfer of Polymer to Rough, Hard Surfaces," *Transactions ASME, Journal of Lubrication Technology*, Vol. 101, 1979, pp.212-219.
116. Warren, J.H. and Eiss, N.S., "Depth of Penetration as a Predictor of the Wear of Polymers on Hard, Rough Surfaces," *Transactions ASME, Journal of Lubrication Technology*, Vol. 100, 1978, pp. 92-97.
117. Eiss, N.S. and Smyth, K.A., "The Wear of Polymers Sliding on Polymeric Films Deposited on Rough Surfaces," *Transactions ASME, Journal of Lubrication Technology*, Vol. 103, 1981, pp.266-273.
118. Stevens, M.P., *Polymer Chemistry: An Introduction*, 2nd Ed., Oxford University Press, New York, 1990, pp. 421-429.

119. Aggarwal, S.L., *Polymer Handbook*, J. Brandrup and E.H. Immergut, Ed., John Wiley & Sons, New York, 1975, pp V13-V22.
120. Campbell, I.M., *Introduction to Synthetic Polymers*, Oxford University Press, New York, 1994, pp. 128-185.
121. Koenig, J.L., *Chemical Microstructure of Polymer Chains*, John Wiley & Sons, New York, 1980, pp. 356-402.
122. Koenig, J.L., *Spectroscopy of Polymers*, American Chemical Society, Washington, DC, 1992, pp. 43-64.
123. Urban, M.W., "Fourier Transform Infrared and Fourier Transform Raman Spectroscopy of Polymers," *Structure-Property Relations in Polymers*, M.W. Urban and C.D. Craver, Ed., American Chemical Society, 1991, pp. 1-39.
124. Seymour, R.B., *Introduction to Polymer Chemistry*, McGraw-Hill Company, New York, 1971, pp. 284-303.
125. Sargent, M. and Koenig, J.L., "Fourier Transform IR Spectroscopic Analysis of the Molecular Structure of Compatible Polymer Blends," *Structure-Property Relations in Polymers*, M.W. Urban and C.D. Craver, Ed., American Chemical Society, 1991, pp. 191-219.
126. Howell, H.E. and Davis, J.R., "Qualitative Identification of Polymeric Materials Using Near-Infrared Spectroscopy," *Structure-Property Relations in Polymers*, M.W. Urban and C.D. Craver, Ed., American Chemical Society, 1991, pp. 263-285.

127. Colthup, N.B., Daly, L.H., and Wiberley, S.E., *Introduction to Infrared and Raman Spectroscopy*, 3rd Ed., Academic Press Inc., 1990, pp. 75-93.
128. Stevens, M.P., *Polymer Chemistry: An Introduction*, 2nd Ed., Oxford University Press, New York, 1990, pp. 160-180.
129. Frank, E.E., "Location of Lubricators," *Rail and Wheel Lubrication Symposium*, AAR Publication, Chicago, 1982, p. 143.
130. Clayton, P., "The Relations Between Wear Behavior and Basic Material Properties for Pearlitic Steels," *Wear*, Vol. 60, 1980, pp. 75-93.
131. Permar, R.W., "Current Rail / Flange Lubrication Practices on USA Transit Systems," *Rail and Wheel Lubrication Symposium*, AAR Publication, Chicago, 1987, pp. III-4-1.
132. Lounsberry, S.M., "The Moore and Steele Approach to Wayside Rail Lubrication," *Rail and Wheel Lubrication Symposium*, AAR Publication, Chicago, 1987, pp. IV-1-5.
133. Jia, Y., "Failure Analysis & Material Evaluation of TMP Refiner Plates," Ph.D. Thesis, Department of Materials Science & Engineering, Oregon Graduate Institute of Science and Technology, 1995, pp. 36-45.
134. Antony, K.C., Arnaut, A.D., Bhansali, K.J., et. al., "Hardfacing," *Welding, Brazing, and Soldering*, ASM Handbook, Vol. 6, 9th Ed., ASM International, Materials Park, Ohio, 1983, pp. 771-803.

135. Schmidt, R.D. and Ferriss, D.P., "New Materials Resistant to Wear and Corrosion to 1000° C," *Wear*, Vol. 32, No. 3, 1975, p. 279.
136. Scholl, M., Unpublished Work, Department of Materials Science & Engineering, Oregon Graduate Institute of Science and Technology, 1996.
137. Steffens, H.D., Babiak, Z., and Brandl, W., "Thermal Barrier Coatings: Some Aspects of Properties Design," *Thermal Spray Coatings: Properties, Processes, and Applications*, Proceedings of the 4th National Thermal Spray Conference, T.F. Bernecki, Ed., ASM International, Materials Park, Ohio, 1991, pp. 289-294.
138. Varacalle, Jr., D.J., "An Analytical Methodology to Predict the Coating Characteristics of Plasma-Sprayed Ceramic Powders," *Thermal Spray: Research and Application*, Proceedings of the 3rd National Thermal Spray Conference, T.F. Bernecki, Ed., ASM International, Materials Park, Ohio, 1990, pp. 271-283.
139. Whitfield, R.W., "New KIC™ (Kinetically Impacted Coating) Gun and Thermal Spray Coating System," *Thermal Spray: Practical Solutions for Engineering Problems*, Proceedings of the 9th National Thermal Spray Conference, C.C. Berndt Ed., ASM International, Materials Park, Ohio, 1996, p. 964.
140. Ito, H., Nakamura, R., Shiroyama, M., et al., "Post-Treatment of Plasma Sprayed WC-Co Coatings by Hot Isostatic Pressing," *Thermal Spray: Research and Application*, Proceedings of the 3rd National Thermal Spray Conference, T.F. Bernecki, Ed., ASM International, Materials Park, Ohio, 1990, pp. 233-238.

141. Murakami, K., Nakazono, S., Asako, H., et al., "Thermal Spraying as a Method of Producing Rapidly Solidified Materials," *Thermal Spray: Research and Application*, Proceedings of the 3rd National Thermal Spray Conference, T.F. Bernecki, Ed., ASM International, Materials Park, Ohio, 1990, pp. 351-355.
142. Kingswell, R., Rickerby, D.S., Scott, K.T., et al., "Comparison of the Erosive Wear Behaviour of Vacuum Plasma Sprayed and Bulk Alumina," *Thermal Spray: Research and Application*, Proceedings of the 3rd National Thermal Spray Conference, T.F. Bernecki, Ed., ASM International, Materials Park, Ohio, 1990, pp. 179-185.
143. Solonenko, O.P., Ushio, M., and Ohmori, A., "Comprehensive Investigation of 'Metal Drop-Substrate' Interaction," *Thermal Spray Coatings: Research, Design and Application*, Proceedings of the 5th National Thermal Spray Conference, C.C. Berndt and T.F. Bernecki, Ed., ASM International, Materials Park, Ohio, 1993, pp. 55-60.
144. Smith, R.W., and Mutasim, Z.Z., "Plasma Sprayed Refractory Metal Structures and Properties," *Thermal Spray: Research and Application*, Proceedings of the 3rd National Thermal Spray Conference, T.F. Bernecki, Ed., ASM International, Materials Park, Ohio, 1990, pp. 369-374.
145. Nicoll, A.R., "The Effect of Varying Plasma Gun Nozzle Diameter on the Surface Roughness; Hardness and Bond Strength of Al₂O₃ and Cr₂O₃ Coatings," *Thermal Spray Technology: New Ideas and Processes*, Proceedings of the 2nd National Thermal Spray Conference, D.L. Houck, Ed., ASM International, Materials Park, Ohio, 1988, pp. 19-25.

146. Scholl, M. and Clayton, P., "Abrasive and Erosive Wear of Some Hypervelocity Air Plasma Sprayed Coatings," *Thermal Spray: Properties, Processes and Applications*, Proceedings of the 4th National Thermal Spray Conference, T.F. Bernecki, Ed., ASM International, Materials Park, Ohio, 1991, pp. 39-52.
147. Mulheran, P.A., Harding, J.H., Kingswell, R., et al., "Modeling the Structural Development in a Plasma Sprayed Coating," *Thermal Spray: International Advances in Coatings Technology*, Proceedings of the 13th International Thermal Spray Conference, C.C. Berndt, Ed., ASM International, Materials Park, Ohio, 1992, pp. 749-753.
148. Varacalle, Jr., D.J., Hagrman, D.L., Fincke, J.R., et al., "An Experimental Study of Twin-Wire Electric Arc Sprayed Zinc and Aluminum Coatings," *Thermal Spray: Practical Solutions for Engineering Problems*, Proceedings of the 9th National Thermal Spray Conference, C.C. Berndt Ed., ASM International, Materials Park, Ohio, 1996, pp. 717-723.
149. Zhongli, Z., Weisheng, G., and Jinlin, W., "The Arc Sprayed Zn-Al Pseudo-Alloy Coating," *Thermal Spray: International Advances in Coatings Technology*, Proceedings of the 13th International Thermal Spray Conference, C.C. Berndt, Ed., ASM International, Materials Park, Ohio, 1992, pp. 399-403.
150. Tani, K., Nakahira, H., and Harada, Y., "High Velocity Flame-Sprayed Self-Fluxing Alloys," *Thermal Spray: Research and Application*, Proceedings of the 3rd National Thermal Spray Conference, T.F. Bernecki, Ed., ASM International, Materials Park, Ohio, 1990, pp. 593-598.

151. Vuoristo, P.M.J., Niemi, K.J., and Mantyla, T.A., "On the Properties of Detonation Gun Sprayed and Plasma Sprayed Ceramic Coatings," *Thermal Spray: International Advances in Coatings Technology*, Proceedings of the 13th International Thermal Spray Conference, C.C. Berndt, Ed., ASM International, Materials Park, Ohio, 1992, pp. 171-176.
152. Smith, R.W., Harzenski, E., and Robisch, T., "High Velocity Oxy-Fuel Spray Wear Resistant Coatings of TiC Composite Powders," *Thermal Spray: Research and Application*, Proceedings of the 3rd National Thermal Spray Conference, T.F. Bernecki, Ed., ASM International, Materials Park, Ohio, 1990, pp. 617-624.
153. Kreye, H., Schwetzke, R., and Zimmermann, S., "High Velocity Oxy-Fuel Flame Spraying-Process and Coating Characteristics," *Thermal Spray: Practical Solutions for Engineering Problems*, Proceedings of the 9th National Thermal Spray Conference, C.C. Berndt Ed., ASM International, Materials Park, Ohio, 1996, pp. 451-462.
154. Kaufold, R.W., Rotolico, A.J., Nerz, J., et al., "Deposition of Coatings Using a New High Velocity Combustion Spray Gun," *Thermal Spray: Research and Application*, Proceedings of the 3rd National Thermal Spray Conference, T.F. Bernecki, Ed., ASM International, Materials Park, Ohio, 1990, pp. 561-569.
155. Kubel, E.D., *Advanced Materials and Processes*, Vol. 132, No. 6, December 1987, pp. 69-80.

156. Disam, J., Lubbers, K., Neudert, U., et al., "Effect of Spraying Parameters of the LPPS Method on the Structure of Ceramic Coatings," *Thermal Spray Coatings: Research, Design and Application*, Proceedings of the 5th National Thermal Spray Conference, C.C. Berndt and T.F. Bernecki, Ed., ASM International, Materials Park, Ohio, 1993, pp. 487-491.
157. Montavon, G., Robert, B. Verdy, C, et al., "Characterization of the Tensile Properties of Vacuum Spray Copper Deposits," *Thermal Spray: Practical Solutions for Engineering Problems*, Proceedings of the 9th National Thermal Spray Conference, C.C. Berndt Ed., ASM International, Materials Park, Ohio, 1996, pp. 827-833.
158. Sampath, S. and Herman, H., "Microstructure of Vacuum Plasma Sprayed Coatings," *Thermal Spray Technology: New Ideas and Processes*, Proceedings of the 2nd National Thermal Spray Conference, D.L. Houck, Ed., ASM International, Materials Park, Ohio, 1988, pp. 1-8.
159. Jones, S.A., Auhl, J.R., and Meyer, T.N., "Particulate-Reinforced Aluminum-Base Composites Produced by Low Pressure RF Plasma Spraying," *Thermal Spray: Properties, Processes and Applications*, Proceedings of the 4th National Thermal Spray Conference, T.F. Bernecki, Ed., ASM International, Materials Park, Ohio, 1991, pp. 329-335.
160. Wang, X.W., Kudesia, R., Lou, J., et al., "Deposition of Electronic Films by Atmospheric RF Plasma Aerosol Spray Technique," *Thermal Spray: Practical Solutions for Engineering Problems*, Proceedings of the 9th National Thermal Spray Conference, C.C. Berndt Ed., ASM International, Materials Park, Ohio, 1996, pp. 567-574.

161. Hoyaux, M.F., *Solid State Plasmas*, Pion Lmtd., London, 1970, pp. 44-110.
162. Dykhuizen, R.C. and Smith, M.F., "Investigations Into the Plasma Spray Process," *Thermal Spray Technology: New Ideas and Processes*, Proceedings of the 2nd National Thermal Spray Conference, D.L. Houck, Ed., ASM International, Materials Park, Ohio, 1988, pp. 61-66.
163. Kotz, J.C. and Purcell, K.F., *Chemistry & Chemical Reactivity*, Saunders College Publishing, New York, 1987, pp. 213-343.
164. Scholl, M., "Plasma Spraying with Wire Feedstock," *Thermal Spray Industrial Applications*, Proceedings of the 7th National Thermal Spray Conference, C.C. Berndt and S. Sampath, Ed., ASM International, Materials Park, Ohio, 1988, pp. 491-496.
165. Willen, W.S., "Parametric Sensitivities of Copper-Nickel-Indium and Inconel 718 Plasma Sprayed Coatings," *Thermal Spray: Properties, Processes and Applications*, Proceedings of the 4th National Thermal Spray Conference, T.F. Bernecki, Ed., ASM International, Materials Park, Ohio, 1991, pp. 21-28.
166. Chen, S.L., Siitonen, P., and Kettunen, P., "Experimental Design and Parameter Optimization for Plasma Spraying of Alumina Coatings," *Thermal Spray: International Advances in Coatings Technology*, Proceedings of the 13th International Thermal Spray Conference, C.C. Berndt, Ed., ASM International, Materials Park, Ohio, 1992, pp. 51-56.

167. Dallaire, S., Arsenault, B., and DeSantis, A., "Investigation of Selected Plasma-Sprayed Coatings for Bonding Glass to Metal in Hermetic Seal Applications," *Thermal Spray: Properties, Processes and Applications*, Proceedings of the 4th National Thermal Spray Conference, T.F. Bernecki, Ed., ASM International, Materials Park, Ohio, 1991, pp. 417-423.
168. Durga, V., Rao, N., Rose, R.A., et al., "Metal Encapsulated Solid Lubricant Coating System," Ford Motor Company, Patent # 5,302,450, 1994.
169. Sliney, H.E., "Solid Lubricants," *Friction, Lubrication, and Wear Technology*, ASM Handbook, Vol. 18, 10th Ed., ASM International, Materials Park, Ohio, 1992, pp. 114-121.
170. Sliney, H.E., "Wide Temperature Spectrum Self-Lubricating Coatings Prepared by Plasma Spraying," *Thin Solid Films*, Vol. 64, 1979, pp. 211-213.
171. Sliney, H.E., "Self-Lubricating Composites of Porous Nickel and Nickel-Chromium Alloy Impregnated with Barium Fluoride-Calcium Fluoride Eutectic," *ASLE Transactions*, Vol. 9, 1966, pp. 336-347.
172. Sliney, H.E., "Wide Temperature Spectrum Self-Lubricating Coatings Prepared by Plasma Spraying," *Thin Solid Films*, Vol. 64, 1979, pp. 211-217.
173. Solomir, J.G., "Wear-Resistant and Self-Lubricating Plasma-Sprayed Coatings; some of their properties and performances," *7th International Metal Spraying Conference*, Vol. 1, Paper 37, Cambridge, United Kingdom, 1974, pp. 194-198.

174. McCune, Jr., R.C., Reatherford, L.V., Zaluzec, M.J., "Thermally Spraying Metal/Solid Lubricant Composites Using Wire Feedstock," Ford Motor Company, Patent # 5,194,304, 1993.
175. Ghouse, M., "Plasma Sprayed Nickel-Graphite Composite Coating Characteristics," *Metal Finishing*, Aug. 1990, pp.29-32
176. Nelson, J.A., *Metallography and Microstructures*, ASM Handbook, Vol. 9, 9th Ed., ASM International, Materials Park, Ohio, 1985, pp. 242-24.
177. Niebuhr, C., Beloved Wife, Unpublished Work, 1997.
178. Christensen, D., Unpublished Work, Department of Materials Science and Engineering, Oregon Graduate Institute of Science and Technology. 1995.
179. Singh, D., Unpublished Work, Department of Materials Science and Engineering, Oregon Graduate Institute of Science and Technology. 1996.
180. Davis, H.L., Unpublished Work, Department of Materials Science and Engineering, Oregon Graduate Institute of Science and Technology. 1996.
181. *Modern Plastics Encyclopedia*, W.A. Kaplan Ed., Vol. 72, No. 12, McGraw Hill Inc, New York, 1995. pp. B-146-206
182. Danks, D. and Clayton, P., "Comparison of the Wear Process for Eutectoid Rail Steels: Field and Laboratory Tests," *Wear*, Vol. 120, 1987, pp. 235-250.

Biographical Sketch

The author's mother, in retrospect, was quoted as saying "had he been the first, he may have been the last." She of course was referring to his mild temperament and passive nature. The youngest of four, the author was born in Redwood City, California on March 25th, 1970. Wanting to go to Cal Poly, San Luis Obispo from an early age, he entered as a freshman 2 weeks after high school graduation. Four and a half years later he emerged with a Bachelor of Science in Materials Engineering. Eighteen years of continuous education was not enough, making graduate school the only venue. A good program and strong desire to maintain a west coast zip code (and keep his new wife happy !) brought the author to OGI. With the gods smiling on him, he was chosen by Professor Paul Clayton to work on the development of a self-lubricating coating. The combination of gentle advisor prodding and a strong desire to complete his formal education and return to the land of sun and sanity, lead to completion of the degree in April 1997.

Aside from the mundane teenage jobs that often carry into college, the author's experience is limited to a brief exposure at General Electric Nuclear Materials the summer before graduation. A one week, all expense paid vacation to the National Thermal Spray Conference in scenic Cincinnati, OH in October 1996 allowed the author to present his first published paper.

Outside of school the author is possessed by a strong desire to chase a synthetic leather sphere on grass. Besides soccer, a strong interest in skiing and surfing also permeate his thoughts. Two parrots act as surrogate children until the school days are over. By the time this is published the author will be gainfully employed as a tribologist at Quantum Corporation and enjoying the California sun with his wife and family.